THESIS

FISSION PRODUCT EFFECTS IN THORIA

Submitted by: HERBERT DAVID LEIGH III

DATE: 30th July 1976

This thesis is submitted as partial fulfilment of the requirements for the degree of Doctor of Philosophy in the Department of Ceramic Engineering, School of Chemical Technology, The University of New South Wales.

This is to certify that the work described in this thesis was done by me in the School of Chemical Technology, The University of New South Wales, and has not been submitted previously for any other University degree or award.

Signed

Herbert David Leigh

TABLE OF CONTENTS

ACKNOWLEDGEMENTS

The author wishes to thank Professor E. R. McCartney of the Department of Ceramic Engineering for his helpful guidance and encouragement during this work and for his critical review of this presentation.

Special appreciation is given to Dr. K. D. Reeve and Dr. J. Wolfrey of The Australian Atomic Energy Commission for useful discussions and to Mr. E. J. Ramm who prepared thoria grinding media used in this work and Mr. B. Buykx who carried out thermal diffusivity determinations.

Further thanks are given to Mr. A. S. Malin and Mr. F. H. Scott of the Department of Metallurgy for their assistance with electron microscopic and electron microprobe examinations.

This work was sponsored by the Australian Atomic Energy Commission.

ABSTRACT

The aims of this work were: 1. to establish a technique for simulating a thoria based nuclear fuel element after high burn-up in a conceptual heavy water moderated thermal reactor enriched with two per cent $U^{233}O_2$, and 2. to determine the effect that solid fission products have on the fuel element after a simulated high burn-up.

Several techniques were employed to this end which involved isothermal and non isothermal heating of thoria alone and thoria containing fissium under various atmospheres for various times and temperatures. X-ray analysis of phases and their structure formed under the above conditions were correlated with microstructural examinations and physical and electrical property determinations.

Thoria was shown to accommodate large concentrations of foreign oxides in the fluorite structure. The most striking examples being the solid solutions developed between thoria and the divalent oxides baria and strontia. When all the typical fission products were reacted together with thoria, stable zirconate phases were formed as well as synthetic pyrochlores in a fluorite matrix. The oxygen partial pressure above the reacting compositions affected the final phases which formed, especially phases involving molybdenum and cerium. Under conditions of high thermal gradients the microstructure of the thoria compacts were similar to those observed for urania fuel elements after burn-up except that columnar grains were not developed.

Moreover, this work has shown that it is possible to simulate at least some of the physical and chemical changes which take place in a fuel element during burn-up without the use of radiation.

Also in view of the absence of columnar grain growth in thoria under high thermal gradients it is probable that the gaseous UO_3 in urania systems plays the major role in columnar grain development. Certain fission products greatly affect thoria, notably strontia, and baria which has produced translucent thoria pellets. While these systems have the highest defect concentration of any studied in this work,the mobility appears to be quite low and the enhanced densification is ascribed to the Hedvall effect rather than improved diffusion. Some systems, however, such as those containing neodymium, do show high electrical conductivity dependence on oxygen pressure even at low temperatures making them likely solid electrolyte systems.

CHAPTER I

INTRODUCTION

Interest in thoria as a nuclear fuel matrix has been increasing over the years because of a number of desirable properties. It is chemically stable at high temperatures, it can be converted into a fissile fuel and, hence, requires less enrichment with fissile uranium than to maintain a nuclear reaction with, for example, natural urania. Because of its highly stable stoichiometry, it can be fabricated without the need for atmosphere control; it appears to be less susceptible to radiation damage than urania fuels and, finally, there is a lower peak to average power ratio during burn-up than in urania fuels, leading to easier control of the reactor[1]. The present project may be broadly defined as a study of the changes caused by solid fission products in thoria based nuclear fuels, to be carried out by simulating the solid fission products that would occur after 5 per cent and 10 per cent burn-up of heavy atoms in a $(Th^{232},U^{233})O_2$ system.

The original plan of the work was to separate the investigation into five main studies: 1. sintering; 2. simulation of the fission products; 3. investigation of phase and microstructural changes; 4. the effect of a thermal gradient on the simulated system; 5. physical property determinations. These five studies have remained essentially intact, however the investigation of phase and microstructural changes of simulated fuel elements has been expanded to include binary systems of fission product oxides with thoria and experiments with reaction couples. The study of physical properties and thermal gradient effects has been severely

curtailed. Since the simulation of a fuel element after burn-up and producing a good thermal gradient proved to be much more difficult than originally anticipated, the bulk of the work was hence directed at producing simulated fuel elements and studying their microstructure rather than developing apparatus for accurate measurement of thermal and physical properties.

CHAPTER II

PREPARATION OF DENSE THORIA

2.1. Precursors of ThO_2

Many workers have shown that characterization of oxide powders is necessary to control and reproduce the densification of oxide compacts[2,3]. One important influence on the oxide powders' characteristics is the precursor used. Moorthly et al,[4] Moorehead[5] and others have shown that thorium oxalate produces a highly sinterable starting material when calcined around 600°C. The oxide derived from oxalate more readily formed dense thoria compacts than oxide from nitrates, hydroxides or tannates. The oxalate derived thoria developed a high degree of crystallinity at temperatures below 1000°C. Densities of up to 9.9 g/ml[5] have been reported, compared to the theoretical density of 10.01 g/ml[6].

2.1.1. Precipitation and Decomposition of Thorium Oxalate

Preparation of thorium oxalate is generally carried out by the addition of oxalic acid to a thorium nitrate solution. By this technique thorium oxalate hexahydrate[7], and dihydrate[8], have been obtained. The thorium oxalate appears to form a cubic crystallite at low precipitation temperatures (around 20°C) and a square plate like crystallite at higher temperatures (around 50°C)[9]. The size distribution of the crystallites precipitated at low temperatures is very narrow having its maximum around 0.8 microns while the distribution of the high temperature crystallites is broader, having its maximum around 2 microns. Generally speaking, the smaller a powder's particle size, the more reactive it is,

which indicates that a low temperature precipitation is desirable in this case. Jenkins et al[10] have confirmed thorium oxalate dihydrate to be orthorhomic with lattice parameters Ao = 10.504, Bo = 9.735 and Co = 8.506.

The mechanism of decomposition of thorium oxalate is still in dispute however, D'Eye[8] and separately, Srivastava[11] have both suggested similar reaction paths which involve the formation of a basic carbonate and, possibly, carbon monoxide which in turn form the metal oxide and CO_2. Srivastava agrees in general with the above mechanism but suggests the formation of carbon as well. In any case, the decomposition of thorium oxalate in the absence of air is characterized by two D.T.A. endotherms, one around 270°C which is generally considered to be the loss of water of hydration and a second peak around 360°C which corresponds to the decomposition of the oxalate. The decomposition of the hexahydrate was followed by Bussiere et al[12] and Moorehead[5] using D.T.A., T.G.A. and emanation power. The decomposition goes through three stages in nitrogen: the loss of free water occurs at 100°C, loss of water of hydration at 230°C and the decomposition of the oxalate occurs at 400°C. The thoria obtained in this manner is a highly reactive powder.

2.2. Characterization of Thorium Dioxide Powder

In the previous section the behaviour of oxide powders derived from the oxalate was discussed generally and the importance of a powder's history and origin was pointed out. There are many ways to characterize a powder, however, objectives are always similar. The characterization methods must be able to detect changes in parameters which will affect the response of the powder to the

fabrication process and the final properties of the compact e.g. the particle size of a powder may affect both its sinterability and the strength of the sintered compact. Given a known chemical composition, the problem reduces to the determination of particle size, morphology and crystal structure.

2.2.1. Surface Area Measurement by Gas Adsorption

The classical technique for determining particle size involves classification of particles by sieves and sedimentation; however, for very fine particles around 10 μ m and less these techniques are not entirely satisfactory for detecting minor but significant changes in particle size distribution. A useful method for determining the surface area of a powder is gas adsorption. While this technique does not give particle size, it does give a specific surface which is related to particle size and distribution. It is therefore a useful method to indicate changes in the particle size or size distribution of similar samples of oxide powder. Allred, Buxton and McBride[13] have used this method to determine the effect that precipitation temperature and calcination temperature have on ThO_2 derived from oxalate. Particle size analyses of samples of a powder calcined at 650°C and 750°C gave similar plots, the lower temperature material having particles of smaller sizes. The significance of the two distributions becomes immediately apparent, however, from a plot of specific surface versus temperature which shows the lower calcined powder to have double the specific surface of the higher calcined powder, 25 m^2/g vs 13 m^2/g. The use of specific surface also shows that the optimum precipitation temperature of the oxalate is 40°C which gives a specific surface of 32 m^2/g after calcination at 600°C. Moorehead[5] obtained a

specific surface of 21.8 m^2/g after 600°C treatment of oxide which was obtained from oxalate precipitated at 70°C as compared to 26 m^2/g obtained from a specific surface plot by Allred[13].

2.2.2. X-ray Analysis for Crystal Size

X-ray diffraction has been used to determine the crystal and crystallite size of ThO_2 prepared in a variety of ways. There appears to be a good correlation between crystallite size determined by specific surface and X-ray line broadening the relation being $S_{N_2} = S_{x\ ray}\ (\frac{1}{F})$ where S_{N_2} is the specific surface determined by nitrogen adsorption and $S_{x\ ray} = \frac{6}{\rho D}$, ρ being the density and D being the cube edge determined by X-ray line broadening. 1/F is a packing factor which is indicative of the crystallite area unavailable for nitrogen adsorption. X-ray diffraction of the crystal itself is of course a direct measure of the perfection of the crystal lattice of the powder.

2.2.3. Scanning Electron Microscopy for Particle Morphology

Transmission electron microscopy has been used to analyze ThO_2 powders with a great deal of success by Beckett and Winfield[14], Warren and Elyard[15], Moorthly[16] and others. However, there are some problems associated with the technique such as sample preparation and the fact that the particles themselves may be too thick or highly adsorbing to give a good micrograph. Scanning electron microscopy can overcome these problems and allows more detail to be observed in the surface structure. Moorehead[5] has used this technique successfully in observing particle size and shape changes during heating of ThO_2 powders. The plate like structure of thoria is clearly shown by the micrographs. During successive heat treatments, the plates became a network of spherical shaped crystallites

joined by necks with pores of comparable size. By the use of surface area, X-ray and scanning electron microscopic data, characterization of ThO_2 powders can be accomplished.

2.3. Sintering and Densification of Thoria

It is not the purpose of this work to study in detail sintering mechanisms of ceramic powders; however, it is necessary to understand the basic mechanisms of the process especially with regard to ThO_2. In general, the sintering process refers to material transport mechanisms which occur below the melting point of a compact whereby a dense integral mass is obtained. A completely dense compact with no porosity is rarely obtained. It is the degree to which a compact has densified and the reasons for such densification or lack thereof which is of primary importance to any sintering study.

2.3.1. Micro and Macro Sintering

Micro sintering is a term coined by Moorehead[5] which refers to processes occurring during nucleation and growth of crystallites within a particle or pseudomorph relic created upon decomposition of some precursor. The microsintering processes are those which occur well below temperatures normally associated with densification of compacts. Allred, Buxton and McBride[13], who were studying the properties of ThO_2 derived from the oxalate, found that the growth of ThO_2 crystallites an equation of the form $D = t^x c^{A-B/T}$. D being the average crystallite diameter, t being time, x, A and B being constants and T being temperature. B is the activation constant for the process $\Delta H/R$, ΔH being the activation energy which was found to be 10.97 Kcal/mole. They conclude that this low value is in accordance with growth taking place only among well

ordered groups of crystallites. Other workers[14,15,17] have confirmed that the size and shape of ThO_2 crystallites depends on the original thorium compound decomposed and the heat treatment after decomposition.

Macrosintering deals with the processes involved in the densification of compacts made of polycrystalline grains. Sintering is generally divided into three separate stages: 1. the initial 2. the intermediate, and 3. the final. In all of the sintering stages, the driving force for material transport is an overall lowering of free energy. In the initial stage, sintering occurs by the coalescence of contact points of particles. At and around the contacts, a neck is formed which expands in such a way to decrease its curvature. During this stage, overall shrinkage of the compact is low, 2 to 3 per cent. During the intermediate stage pore shrinkage and grain growth occur. The final stage of sintering occurs at the transition from continuous to discontinuous porosity. It is in the final stage of sintering when the compact develops strength and uniformity of structure. There are four general processes by which mass transport during sintering occurs. These are: 1. Plastic flow, 2. vapour transport, 3. surface diffusion, and 4. bulk diffusion. Several models have been devised to describe the sintering of spheres during the initial and intermediate stages of sintering and to relate the various mass transport processes to them; however, it is beyond the scope of this work to discuss them further.

2.3.2. Final Stage Sintering and Secondary Recrystallization

The final stage of sintering is technologically the most interesting stage for ceramic applications and it is also the most complex to model quantitatively. The elimination of pores and

consequent increase in sintering occurs through diffusion processes, both grain boundary diffusion and lattice diffusion. Work by Alexander and Balluffi[21], Coble[22], Burke[23] and others has shown the influence grain boundary movement has on the densification of sintered materials during the intermediate and final stages of sintering. The grain boundary is a continuous lattice imperfection, which exists between crystals, consisting of a disruption of the lattice periodicity, usually a few atoms wide. Grain boundaries can contribute to the elimination of defects from grains e.g. pore removal is assisted by vacancy annihilation at the grain boundary while impurities may concentrate in its vicinity. Sintering and, therefore, densification proceeds readily while the mobility of vacancies or vacancy clusters is maintained at a high level, facilitating migration to grain boundaries. As the size of a grain increases, so does the difficulty for vacancies to reach the grain boundary and the rate of densification slows. Also Westbrook[24] has pointed out that vacancies and solutions may exist as a solute vacancy complex which produces charged grain boundaries as the vacancy is annihilated and the solute forms a concentration gradient about the boundary. Elimination of vacancies then ceases when the electrostatic repulsion of the grain boundary equals the diffusional driving force of the solute vacancy complex.

Exaggerated grain growth is a term which refers to the development of grains having an abnormally large size compared to the bulk of grains. The occurrence of exaggerated grain growth is undesirable in that further densification ceases. Burke[25] has shown the process occurs in several ways. First as density approaches 92 to 98 per cent of theoretical for a pure oxide, the likelihood increases of producing a grain having more than six sides which

requires it to have concave grain boundaries. It is this fact and that grain boundaries move to lower their area which produces the exaggerated grain growth of the large grains at the expense of the smaller grains. Coble[26] and Jorgensen[27] have shown that the onset of exaggerated grain growth can be postponed or prevented by the use of a second additive. Burke[25] states that an exaggerated grain growth may be inhibited by an addition that decreases grain boundary mobility, even though the addition need not completely prevent grain growth.

2.3.3. Densification Aids for Thoria

The effect of starting materials on the densification has already been discussed and was shown to be very important. From the preceding section, it is also clear that the prevention of exaggerated grain growth is an important factor. Laha[28] and Jorgensen[29] have both observed that CaO additions to ThO_2 enhanced sintering and the final density which was obtained. Laha however concluded that the increase was due to an increase in diffusion due to an increase in vacancy concentration created by introducing a +2 valency cation to a +4 valency matrix while Jorgensen explained the increase in sintering in terms of grain boundary mobility. The inhibition of grain boundary mobility appears to be the correct explanation for the increase in sintering since the increase in vacancy concentration does not account for the prevention of exaggerated grain growth. In fact an increase in vacancy concentration would tend to increase grain boundary mobility.

Bennett[30] claims that densification is enhanced by sintering ThO_2 activated by a glow discharge device. Cleaning the surface

producing an increased surface energy, and an enhanced diffusion rate are the reasons given for the increase in sintered density. The atmosphere over the compact during sintering also contributes to the density. Im and Wadsworth[31] discuss use of N_2 and H_2 atmosphere to enhance the sintering of ThO_2 compacts and Moorehead showed that vacuum sintering increased the density and lowered the porosity of ThO_2.

2.3.4. Densification Inhibitors

Recently, Graham and Caplan[32] noted that unexplained voids were forming in NiO layers formed upon the oxidation of Ni. The existence of CO_2 at the temperatures up to 1270°C during oxidation of the Ni surface is startling; however, Gallagher[33] has found, by Mossbauer spectroscopy, chemisorbed CO_2 to exist on iron oxide films up to 1000°C. In a study on ZrO_2 used in an electroyte, Thompson[34] detected CO_2 by I.R. spectroscopy at temperatures up to at least 800°C. The existence of chemisorbed CO_2 at high temperatures raises the question of density inhibition by a lowering of the surface energy available for sintering. This subject has not been fully investigated to date.

CHAPTER III

CHANGES IN A FUEL ELEMENT DURING FISSION

A nuclear fuel used in a fission reactor is one which contains fissile atoms, which upon capture of a neutron will fission, usually into two new atoms of different masses. A fertile atom is one which upon capture of a neutron produces a fissile atom. In thermal reactors the ratio of fissile to fertile atoms is approximately 1 to 50 while in a fast reactor it is approximately 1 to 5. The terms thermal and fast are derived from the energy of the neutron responsible for fission which, of course, is dependent upon the degree of moderation. Fast neutrons have very high kinetic energies of the order of 1 Mev, slow neutrons about 2 to 3 ev and thermal neutrons about .025 ev. When fission occurs, the fission fragments are produced and energy is released, about 200 Mev per fission, approximately 80 per cent of which is kinetic energy of the fission fragments. The fuel element undergoes gross changes as burn-up proceeds due to the new chemical species produced, damage to the original crystal structure and the heat produced by the energy released upon fission.

3.1. Microstructural Damage During Burn-up

The damage or alteration of the fuel element occurs on both micro- and macro-structural scale and depends on the degree of burn-up which has occurred and the temperature of the fuel during burn-up. On a micro-structural scale, point defects in the crystal caused by energetic particles disrupt the lattice as does the accumulation of fission products. The energetic fission fragments travel through the lattice and displace atoms in normal lattice positions, primary knock-ons, and may either take up the lattice

position or form an interstitial position leaving a vacancy. Secondary knock-ons, produced by the ejected atom, may continue until the energy of the atom decreases to 100 ev or less, the energy for producing a lattice vacancy. The macrostructural changes occur by the temperature distribution in the fuel element which creates cracks in the fuel due to thermal stress.

3.1.1. Swelling in Fuel Elements during Burn-up

The causes of swelling of a fuel element during burn-up can be divided into three general groups, point defect concentration, accumulation of fission products and thermal expansion. Fox et al[35] and Roberts[36] observed increases in unit cell size with burn-up of UO_2. Both single crystal and polycrystalline UO_2 were studied and both showed an increase up to a certain exposure and then a decrease which levelled off to a value still higher than that for unaffected UO_2. Other workers found similar results (Berman et al[37], Bleiburg[38] and Bales et al[39]) as long as temperatures did not exceed 400°C. Fox et al[35] were also able to show partial recovery could be obtained by post irradiation annealing. The explanation for the recovery of the lattice parameter of UO_2 after a critical exposure level was given as growth of defect clusters. Olsen et al[40] studying a thoria diluted urania fuel found an increase in the lattice parameter with increasing exposure up to a critical level but a decrease in lattice parameter below the original value at further exposure. No explanation for this effect was given. Ross[41] found that an increase in exposure decreased the thermal conductivity but, instead of obtaining a minimum he observed a saturation level. This is consistent with clusters of point defects forming pores in the urania at high exposures. It would be expected that solution of fission products in the matrix of a

fuel would permanently change the lattice parameter of the fuel. However, the overall decrease or increase would be difficult to predict since some would tend to increase the unit cell and some would decrease it. A more detailed study of the effect of fission product reaction with the fuel will be given later.

Swelling of the fuel due to gaseous fission products also occurs since a large amount of xenon and krypton gases is produced during fission. Generally, these gases are contained in the porosity of the fuel and do not constitute any real problem for fuel stability but upon release can lead to cladding failure. It is therefore desirable to keep these products confined to the porosity of the fuel. Gaseous fission products are not of real interest to this thesis and will not be discussed further.

Solid fission product inclusions have been found by various workers in fuel elements after burn-up (Bradbury[42], Frost and Wait[43]). These included phases, made up of oxides less dense than the original fissile fuel, can cause expansion of the fuel element. The overall effect is quite low compared to the other effects mentioned above.

3.1.2. Thermal Gradient Effects in a Fuel Element

The heat produced during fission is very large and, due to the relatively low thermal conductivity of the fuel element, the heat produced cannot be removed quickly enough to prevent large thermal gradients in the fuel from being produced. The power density obtained from the fuel element determines the severity of thermal gradient. At low power densities the cylindrical fuel develops radial cracks which are created by thermal stress. If the thermal gradient exceeds $2P(1-\mu)/E\alpha$ where P = modulus of rupture,

μ = Poisson's ratio, E = Young's modulus and α = coefficient of linear thermal expansion, then radial cracks are expected to occur.

The microstructure of fuel elements after high burn-up has been observed to consist of 3 to 4 distinct zones. (Bain[44], DeHalas and Horn[45], O'Boyle, Brown and Sanecki[46]). There is always an outer ring of unaffected fuel material followed by a ring of equiaxed grain and then a region of columnar grain growth and, if the temperature developed has been sufficient, an inner central zone of core melting. The unaffected area remains unchanged except for stress cracking. The equiaxed region generally occurs in a narrow band about the centre and is characterized by large grains. Columnar grain make up an extensive region stretching from the equiaxed region to the centre or region of centre melting. It has been proposed by MacEwan and Hawson[47] that the columnar grains are thought to form by a vaporization and condensation mechanism of material in voids which form lenticular porosity and leaves long radial grain as the voids move up the thermal gradient toward the centre. The degree of grain formation depends on initial porosity and no doubt many other factors as well. Bain[44] has observed that columnar grains are replaced by broad grains as the initial porosity drops from 5 to 2 per cent. Columnar grains have also been observed without lenticular voids so there is probably at least one other mechanism operating in the formation of columnar grain. Deduction of previous temperatures from microstructure in irradiated fuels is not a straightforward process. Robertson[48] has shown that irradiated samples can be sintered at temperatures as low as 800°C to a density comparable with that of unirradiated samples which require 1500°C.

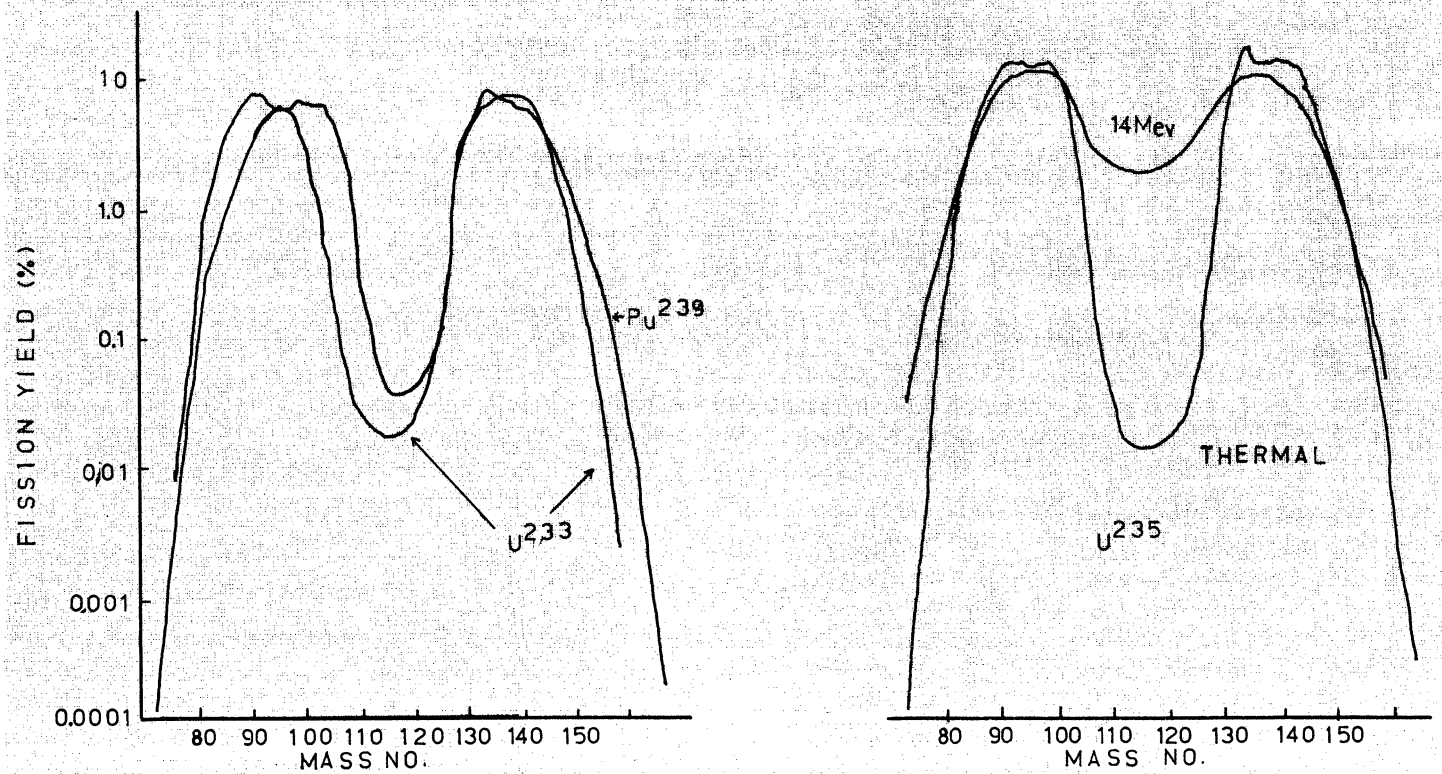

FIGURE 3.1
DISTRIBUTION OF FISSION PRODUCT MASSES FOR U^{233}, U^{235}, Th^{232}, Pu^{239}
AFTER KATCOFF (REF. 51)

The production of separate regions in the fuel, cracks and rearrangement of grains, lowers the thermal conductivity of the fuel, which increases the thermal gradient which, in turn, accelerates the deleterious effects. Rand and Markin[49] have shown also that under a thermal gradient $UO_{3(g)}$ is favoured at low temperatures and is transported away from the centre of the fuel pin thereby enriching the hotter central portion of the fuel, which, in turn, further accentuates the thermal gradient produced. The thermal gradients encountered in nuclear fuels can be on the order of $10^3 C^\circ/cm$ or higher and central temperatures higher than the melting point of UO_2 or ThO_2 have been encountered. Temperatures of $4000^\circ C$ have been suggested by Field et al[50].

3.2. Production of Fission Products

The production and accumulation of fission products in a fuel during burn-up proceeds with length of exposure time. When neutron flux stops, the production of new fission fragments stops; however, those already produced decay to form stable isotopes. The calculation of the concentration and composition of the fission products is very complicated and depends on the energy spectrum of the neutron flux, the target nucleaus, time of exposure, the total burn-up which has occurred and the cool down time. Katcoff[51] has determined fission yield, the per cent probability per fission of forming a given nuclide by radiochemistry, for various targets under thermal neutron flux and fast neutron flux. The typical fission yield versus mass number plot forms a bimodal distribution with maxima occurring around mass numbers 90 and 140. Figure 3.1 shows these distributions. With increasing neutron energy, the tendency toward symmetric fission increases. However, the maxima positions remain relatively constant. The isotopes thus produced follow their particular series

TABLE 3.1

Distribution of Fission Products

Fission Product	Atoms per 100 atoms fissioned	
	5% Burn-up	10% Burn-up
Zirconium	32.9	32.9
Neodymium (Nd,Pm Pr,Sm)*	23.7	24.5
Molybdenum	19.5	20.4
Cerium	16.6	15.1
Strontium	13.0	12.3
Ruthenium	7.6	7.2
Barium	6.3	6.4
Yttrium	6.2	6.2
Lanthanum	4.2	5.9
Rhenium (Tc)*	4.7	4.3
Tellurium	3.6	3.6
Palladium	1.3	1.8
Rhodium	0.9	0.6
Niobium	0.8	0.4

* Atoms being represented in total

of decays in a "chain" until they attain stability. A calculation for the fission product distribution for a conceptual heavy water moderated thermal reactor using urania^{233} enriched ThO_2 fuel after 5 and 10 per cent burn-up and one day cooling has been made by Gemmell, Clancy and Reeve[52]. The concentrations of solid fission products are shown in Table 3.1. Concentrations less than 10^{-9} atoms/100 atoms fissioned have been ignored as have volatile fissium including Cs. In a stoichiometric fuel, (oxygen to metal ratio 2:1) for each 100 atoms fissioned there will be 200 atoms of oxygen available for reaction with the solid fission products. The oxides produced may form separate phases or solid solutions with the fuel matrix. When the oxygen has been used up other fission products must exist in elemental form. The aspects of these conditions are discussed below.

3.2.1. Oxygen Conservation in Fuel Elements

Thoria is a stoichiometric oxide and, as such, tends to maintain an oxygen to metal ratio of 2.00; urania on the other hand may become hyper- or hypo-stoichiometric depending on the atmospheric conditions. For a fuel containing ThO_2 as the diluent, the number of oxygens produced per 100 atoms fissioned would be 200 especially at the high burn-up. These oxygen atoms may either dissolve into the fluorite structure as interstitial oxygen, or they may react with the urania to form a hyperstoichiometric phase, or they may react with solid fission products to form oxides. If the oxygen goes to form oxides with the fission products then a further reaction may occur between the oxides to form stable oxide compounds. When equilibrium of the total system has been achieved, that is the fuel matrix and fission products, the total free energy of the system will be a minimum. In Argonne National Laboratory Report

TABLE 3.2

Probable Forms of Fission Products per 100 Atoms Fissioned Listed in Order of Decreasing Free Energy of Formation

5% Burn-up	Remaining Oxygen Atoms	10% Burn-up	Remaining Oxygen Atoms
$Zr_{32.9}$ $O_{65.8}$	134.2	$Zr_{32.9}$ $O_{65.8}$	134.2
$Ce_{16.6}$ $O_{33.2}$	101.0	$Ce_{15.1}$ $O_{30.2}$	104.0
$Nb_{2.0}$ $O_{2.0}$	99	$Nb_{0.4}$ $O_{1.0}$	103.0
$Nd_{23.7}$ $O_{35.5}$	63.5	$Nd_{24.5}$ $O_{36.8}$	66.2
$La_{4.2}$ $O_{6.3}$	57.2	$La_{5.9}$ $O_{9.5}$	56.7
$Y_{6.2}$ $O_{9.3}$	47.9	$Y_{6.2}$ $O_{9.3}$	47.4
$Sr_{13.0}$ $O_{13.0}$	34.9	$Sr_{12.3}$ $O_{12.3}$	35.1
$Ba_{6.3}$ $O_{6.3}$	28.6	$Ba_{6.3}$ $O_{6.3}$	28.8
$Mo_{14.3}$ $O_{28.6}$	0	$Mo_{14.4}$ $O_{28.8}$	0
$Mo_{5.2}$	0	$Mo_{6.2}$	0
$Re_{4.7}$	0	$Re_{4.3}$	0
$Te_{3.6}$	0	$Te_{3.6}$	0
$Pd_{1.3}$	0	$Pd_{1.3}$	0
$Rh_{0.9}$	0	$Rh_{0.4}$	0

ANL-5750 Glassner[53] reports the free energy of formation of various oxides versus temperature. Using this data, stable oxides that were predicted are shown in Table 3.2. In making these predictions, no compound formation was considered due to lack of necessary thermodynamic information. As long as sufficient oxygen is present to oxidize the fission product elements completely, the free energy used is based on the free energy equivalent of cation. However, when there is insufficient oxygen, the free energy is based on one equivalent of oxygen combined. From the Table we see that the fission products are divided into three groups. Those that form stable oxides, molybdenum which is only partially oxidized, and those which remain as elements. The molybdenum being only partially oxidized, may control the oxygen partial pressure over the fuel through the equlibrium reaction $Mo + O_2 \rightleftharpoons MoO_2$. Theoretical implications of this atmosphere control by molybdenum have been made by Rand and Markin[49] for a $(U,Pu)O_{2+x}$ system. The overall oxygen to metal ratio of the fuel may be stoichiometric or hyperstoichiometric depending on the original state of the fuel system.

The oxygen potential for Mo/MoO_2 is very close to that for $U_{0.85}Pu_{0.15}O_{2.00}$ and, therefore, if the original fuel is hypostoichiometric it will oxidize until it reaches and oxygen to metal ratio close to 2.00, at which point Mo will then oxidize. No further oxidation of the fuel will occur until the Mo has been oxidized. One further complication to the oxygen balance is the possibility that the cladding case may oxidize. This reaction will take oxygen out of the system and change the oxygen partial

pressure above the fuel. Rand and Markin report the oxygen potential of the stainless steel to be equivalent to a CO_2/CO ratio of 10^{-3} as opposed to $\approx 10^{-1}$ for MoO_2/Mo.

3.2.2. Development of Oxide Fission Product Phases

The fission product oxides will differ in their solid solubility in the host matrix. When this solubility is exceeded, a second phase will form. If there is compound formation, the solubility of the compound will control the formation of a second phase. Difficulties arise in analyzing real fuel elements due to the radioactivity of the "hot" fission products. Usually one must wait until the radioactivity level has decreased before handling the fuel and, even then, heavy shielding must be used. The cool down time itself means that oxides whose isotopes are unstable will disappear while others may be formed. Cool down times may be as long as one to several years. To circumvent this problem, one of two techniques may be employed: 1. The sample may be reduced by grinding to a size where radioactivity levels are at an acceptable level; 2. Analysis and handling equipment may be heavily shielded so that analysis may proceed with minimum danger to operators. Obviously the former technique may introduce a problem of sampling, that is the sample selected may not be representative of the whole system. The latter method is cumbersome and requires compensation for the radiation activity of the sample in analyses such as electron probe microscopy.

Bradbury et al[42] and Jeffery[54] analyzed an urania fuel element which had undergone 4.6 per cent burn-up with an estimated centre temperature of 1500°C. Bradbury used the first method described for analyzing the samples as did Jeffery but in a different laboratory. Investigation of the low activity

sample showed two types of inclusions, barium free and barium containing. Two analyses were made on sections .01 inches apart; the first of these was a cursory study and the second a detailed study. In the first study, the Ba containing inclusions were devoid of Mo and associated with traces of Ce; however, in the second study both types of inclusions contained Mo. The Ba free inclusions, which appear as white particles, were believed to be elemental compositions; these will be discussed in the next section. The barium containing inclusions were found to contain zirconium and, in some cases, Sr and Ce. An analysis of the matrix was made and only Nd was detected at a 1 w/o level. Bradbury et al conclude that the zirconia found with baria indicated formation of $BaZrO_3$. Jeffery received a similar sample from the AERE Harwell and used the heavy shielding technique for analysis. Jeffery found a few barium inclusions with Mo which contained Rh, Ru, and Tc associated with the Mo. Also detected in the inclusion were Ce, Nd, Zr and Sr. The inclusions of barium without Mo contained Ce, Nd, Zr, Sr. Rh, Ru and Tc were not detected, however a very small amount of Mo was recorded. The matrix was nearly always found to contain Zr, Ce, Nd, La and Pr. Nd, La and Pr were homogeneously distributed throughout the matrix but, in certain areas, there were enrichments of Ba, Zr and Ce.

Other workers have found inclusions in $(U,Pu)O_2$ mixed oxide fuels. O'Boyle, Brown and Sanecki[46] investigated a 20 per cent Pu enriched urania fuel after 2.7 per cent burn-up. They found a grey phase which contained Sr, Ba and Ce also metallic inclusions, as have all the above workers, and in the matrix Zr, Ba, La, Ce, Nd and Pr. These results are similar to those of Bradbury[42],

however Ba containing inclusions were not analyzed for Mo or Zr so an accurate comparison cannot be made. The grey phase was found to be separated from the elemental phase, the former residing in the equiaxed region and the latter in the columnar grain region. It appears that this fuel element had been reacted at a much higher temperature, 2300°C, than that studied by Bradbury, 1500°C. In a study on plutonium fuels for fast reactors, Frost and Wait[43] found by X-ray diffraction on irradiated UO_2 a systematic decrease in unit cell size with increasing burn-up and hence inferred that rare earth, Y and Zr, which have small ionic radii, go into solid solution with UO_2 while Ba and Sr, which have larger radii, do not.

3.2.3. Development of Elemental Fission Product Phases

Elemental phases occur in nuclear fuels because there is insufficient oxygen present for them to form stable oxides. Metallic phases have been detected by Bradbury et al, Jeffery, and O'Boyle who have found Mo, Ru, Rh, Tc together as a white rounded inclusion. O'Boyle, Brown and Sanecki have studied extensively the inclusion found in columnar grains of a $(U,Pu)O_2$ mixed oxide fuel. They found the metallic inclusions associated with small voids along the columnar grain boundaries from the equiaxed grain region to the central void. The chemical composition of these inclusions were studied as a function of radial distance from the centre. As one moves from the equiaxed region toward the centre, the concentrations of Ru and Mo are inversely related to the Mo concentration decreasing with increasing temperature. Tc was considered to be generally constant. Rh and Pd were not studied due to the low concentration. The ratio of Mo to Ru was calculated to be 0.59 at mid-length of the columnar grains. In calculating the oxygen balance, they suggested that this ratio inferred formation of

LaO_2-type lanthanide oxides since the oxygen available to Mo, assuming that the rare earths each took 2 instead of 1.5 atoms of oxygen, would leave enough Mo unoxidized to give a Mo/Ru ratio of 0.58. Cotton and Wilkinson[55] point out, however, that the +4 state for the lanthanides is not as stable as the +3 and in fact even treatment of Nd_2O_3 with atomic oxygen gives no Nd^{+4}. Praseodymium can form some degree of hyperstoichiometry, however PrO_2 is a highly oxidizing agent and in fact will oxidize water itself. A more reasonable explanation would be that the urania is being oxidized to a hyperstoichiometric state to maintain electroneutrality with the +3 rare earths which go into solid solution with the matrix. As pointed out before, the amount of Mo oxidized would thus depend on the original stoichiometry of the (U,Pu)Ox mixed oxide fuel.

CHAPTER IV

STUDIES ON SIMULATED FUEL ELEMENTS

The most striking observation made during the search for studies on simulated fission products in fuel elements is the lack of published work on the subject. There is considerable literature on simple chemical systems and phase equilibria between various oxides which make up the fission products; this is discussed in Chapter V. A simulation of a fuel element with fission products is desirable for two reasons: to determine thermal properties such as thermal conductivity, thermal shock resistance and melting temperature of a fuel after burn-up, and to identify chemical reactions which affect the stoichiometry of the fuel or are involved in interaction with the cladding can material. Simulation of a fuel element may be divided into two basic studies: (1) The development of chemical phases by reaction between fission products and the fuel matrix and (2) The establishment of a thermal gradient comparable to that to which fuel elements in service are subjected.

4.1. Simulation of the Chemical Composition of a Fuel Element After Burn-up

In Chapter III, the composition of the fission products in a ThO_2 based fuel was discussed and prediction of the stable oxides which might form was made. The manner in which the fission products are added, the temperature at which the reaction takes place and the atmosphere above the reactants, all influence the final system and determine the phase or phases which will develop.

4.1.1. Method of Adding Fissium to the Matrix

In a real fuel element, the fission products are developed on an atomic scale and, as such, react and diffuse initially as discrete atoms or ions until they eventually form stable phases or solid solutions. Obviously, this initial situation cannot be simulated; however, a uniform mixture of finely divided fission products can be made. The requirement for a true simulation is a uniform mixture which can be obtained by conventional ball milling or chemical precipitation. The state of the added fission products is also important; that is, whether the fissium are added as elements, single oxides or mixed oxides. Schmitz[56], in a study on a simulated $(U,Pu)O_2$ fuel after 2 per cent burn-up, added fission products to the $(U,Pu)O_2$ matrix as metals or metal hydrides. Koizumi, Satoh and Noro[57], studying a particular aspect of phase development in urania based fuels, chose to add oxides of Ba, Sr and Zr to the fuel matrix. No information about the uniformity of mixing was given; however, equilibrium was assumed to have been reached due to the prolonged time that the samples were held at temperature. No other information on studies directly related to simulated oxide fuel elements after burn-up have been found by the author.

4.1.2. Reactions and Phase Development in Simulated Fuel Elements

Schmitz[56] reacted a simulated urania-plutonia fuel at various temperatures, up to 1750°C, for as long as 72 h. The samples were hermetically sealed in iridium tubes. It is assumed that the enclosed atmosphere was inert since iridium is brittle and can only be worked in inert atmospheres. Microstructural examination of the reacted compacts revealed a grey matrix with white inclusions and, in "rare" cases, grey inclusions. The white

inclusions were found to be alloys of Mo, Pd, and Rh. Rhenium was also found in the pure state. The matrix was found to contain rare earths and zirconium in addition to urania and plutonium. The grey inclusion was found to contain barium, uranium and plutonium which were thought to make up an oxide of the type $(U,Pu)BaO_{4-x}$. No zirconium was observed associated with barium. In order for oxides to be formed in this system, the $(U,Pu)O_2$ fuel must be reduced to $(U,Pu)O_{2-x}$. At temperatures below 2000°C, urania cannot be reduced below a valency of +4 and Pu will not be oxidized above +4; consequently, the oxygen obtained by the fission products must be made available from the plutonia and urania solid solution. From the thermodynamic treatment of a $(U_{1-x}Pu_x)O_y$ fuel element by Rand and Martin[48] it can be seen that, at temperatures below 2000°C at an initial stoichiometry of 1.96, Mo will still be partially oxidized to MoO_2; (approximately 49 per cent). In this case, the fuel would be oxidized to an oxygen to metal ratio close to 2.00. In the experimental results obtained by Schmitz[56] by lattice parameter measurement, the oxygen to metal ratio was found to be 1.979. This coupled with the fact that the compositions of the metallic inclusions, analyzed by Schmitz, were highly variable, indicates that equilibrium was not obtained in the simulated samples. By comparison, a relatively constant metallic composition was found[46] in a real $(U,Pu)O_2$ fuel element after 5.6×10^{24} fissions/cm^3. In fact, the metallic inclusions observed in the micrographs are probably alloys of the metallic constituents which were in close proximity in the pressed state. It is felt that the method of adding metal powders to an oxide fuel is not a satisfactory simulation technique.

The formation of barium and strontium zirconates has been deduced by several workers based on electron-microprobe analysis of nuclear fuels after burn-up. Koizmi et al[57] conducted a phase study to observe the behaviour of baria, strontia and zirconia in a urania matrix. The simulated fission product oxides were mixed with urania and reacted at temperatures up to 2000°C. The high temperature X-ray analysis of the compact agreed quite well with experimental examinations on urania fuel elements. At a temperature of 1500°C just below the temperature of formation of equiaxed grain growth, three components were in equilibrium; (Ba,Sr) ZrO_3 with a small amount of U, (Ba,Sr)UO_3 with a small amount of Zr, and UO_2; at 2000°C, just about the start of the formation of columnar grain, only the (Ba,Sr)ZrO_3 phase and UO_2 were found in equilibrium. The (Ba,Sr)UO_3 phase was found to decompose almost completely to mixed oxides by 1800°C. This work shows that barium and strontium zirconates are stable at least in the cool zone of the columnar grains and that (Ba,Sr)UO_3 is stable in the cool region of the equiaxed zone of a fuel element. In a thermal gradient, these phases may tend to diffuse toward the cool regions of the fuel.

So far, little has been said about the highly volatile and corrosive fission products such as Cs, I and Mo. In the work by Schmitz[56] these sorts of fissium were contained by the iridium crucible. No mention of any attack of the cladding was made; however, Cs and I are extremely corrosive to convential cladding materials. Molybdenum, even though stable as the element or the dioxide, has relatively high vapor pressures at elevated temperatures and a simulated composition will change if loss occurs. Any simulation method must take these factors into account.

4.2. Simulation of High Thermal Gradients

Thermal gradients encountered in a nuclear fuel element are generally the highest known to ceramic technologists and simulating such gradients in the laboratory is usually difficult. Freund and Sari[58] describe an apparatus which has achieved such thermal gradients by direct electrical heating. Their device consists of an external heat source, a power controlled thyristor circuit, stainless steel or tantalum electrodes and a stack of UO_2 pellets. The external heat source is used to heat the stack of pellets to 200-400°C at which time direct electrical heating is used to develop the final temperature desired. Centre core melting, columnar grains and equiaxed grains were reported to develop. Doping urania with Mo or Ru did not appear to affect the growth and migration of lenticular voids; however, near the centre an annulus of Mo and Ru was observed between an area depleted of the metals and an area where they were statistically distributed.

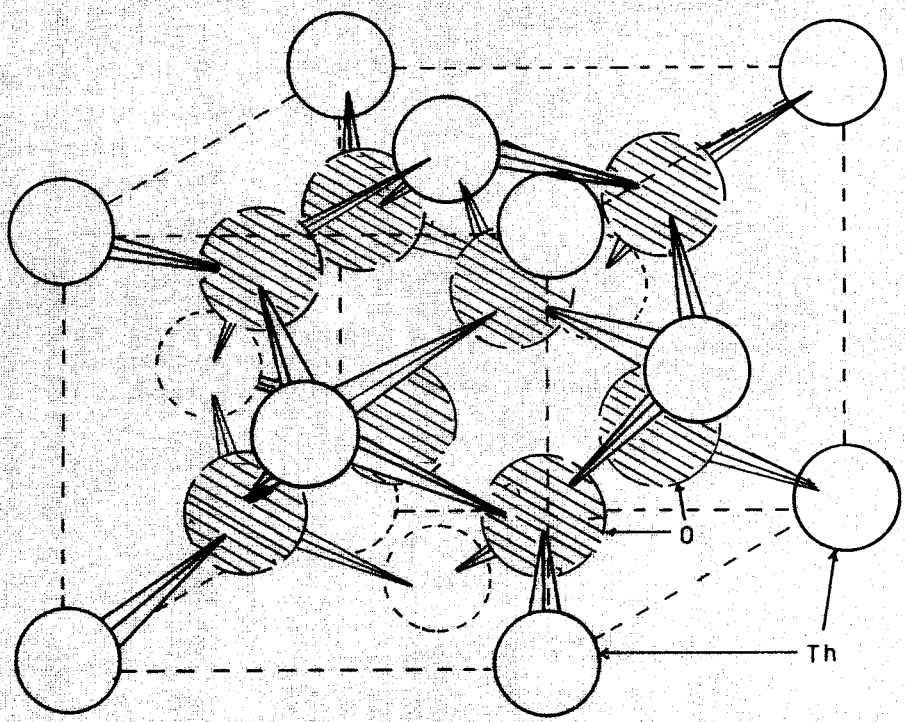

A
FLUORITE STRUCTURE OF ThO_2

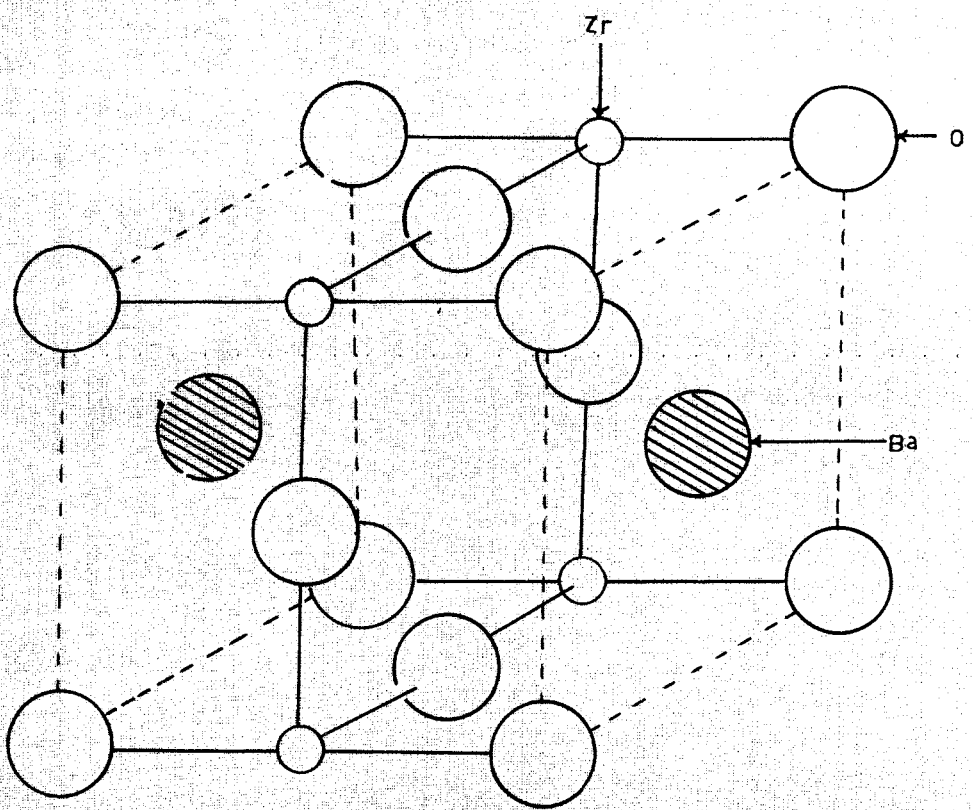

B
PEROVSKITE STRUCTURE OF $BaZrO_3$

FIGURE 5.1

CHAPTER V

PHASE EQUILIBRIA OF CHEMICAL SYSTEMS WITH ThO_2

5.1. The Crystal Structure of the Fluorite System

The fluorite structure is unusual among the oxide crystal structures in that the f.c.c. lattice consists of cations rather than anions. The normal oxygen positions are in all the tetrahedral sites of the cation lattice as shown in Figure 5.1 . There exists a large 12 sided polygon in the centre of the unit cell. Since oxygen must reside in tetrahedral sites, the cations are really not close packed because the oxygen ions are larger than the cations which forces the cations apart. It is this openness of the fluorite structure which enables it to accommodate a variety of foreign cations and interstitial anions in the lattice. The effect which various cations have on the structure will be discussed in detail in following sections.

5.1.1. The System of ThO_2 and UO_2

Both ThO_2 and UO_2 exist in the fluorite structure and, as would be expected, they form a series of almost perfect solid solutions which obey Vegards Law over the entire compositional range. These solid solutions may be obtained by reacting UO_2 and ThO_2 together in an inert or reducing atmosphere or under vacuum. However if reacted in air, the UO_2 oxidizes to form U_3O_8 which is orthorhombic and the expansion which occurs at temperatures below that at which good bonding takes place, deteriorates the compact. Handwerk, Abernathy and Bach[59] found that solid solutions of urania and thoria of the form $(U,Th)O_{2+x}$ could be obtained by reacting U_3O_8 with ThO_2 in air; however, above 60 per cent urania, some U_3O_8 appeared to remain undissolved.

Karkhanavala and Momin[60] have shown that the probable mechanism for the formation of the solid solution upon reaction of U_3O_8 and ThO_2 depends on the gas reaction of $UO_3(g)$ with $ThO_2(s)$ rather than the solid state reaction. Loosely packed powders reacted to form complete solid solutions after only a few minutes while densely packed compacts took up to one hour to obtain the same degree of solid solution. Heating a sintered ThO_2 pellet over a platinum boat which contained powdered U_3O_8 revealed that solid solution occurred on the ThO_2 exposed to the $UO_3(g)$ vapour within five minutes at 1400°C. Similar gas phase reaction between Y_2O_3 and U_3O_8 has been shown by Felton and Aitken[61].

5.1.2. Oxygen to Metal Ratio in ThO_2 and UO_2

The oxygen to metal ratio of solid solutions of UO_2 and ThO_2 is essentially 2 when oxygen is not available to the system; however, under the influence of oxygen or di and trivalent cations the situation changes dramatically. Anderson et al[62] conducted a systematic study of the oxidation of the solid solutions and complementary work on the chemisorption of O_2 on UO_2 and urania-thoria solid solution was conducted by Roberts[63]. The latter found that oxygen rapidly chemisorpted at temperatures of -183°C on the surface of urania-thoria mixed crystals and at temperatures, at and above 0°C, oxygen began penetrating into the lattice. Furthermore, the surface of the mixed crystal appeared to be thoria enriched. Anderson[62] found that, in thoria-urania solid solutions, oxygen was taken up, oxidizing urania and forming oxygen anion interstitials. The increased absorption of oxygen decreased the unit cell size of the crystal until urania reached a valency of +5, at which point the cell began to expand. The contraction can be explained by the decreased ionic size of the +5 ion as compared to

the +4. The expansion as some atoms become hexavalent would mean that hexavalent urania is formed by ion groups such as $(UO_2)^{++}$ which can occur along the diagonals of the (110) planes.

The fluorite structure remained stable at high temperatures in air however, at urania concentrations, higher than 80 mole %, other crystalline phases form until a pseudo U_3O_3 phase appears. At temperatures below 200°C, the fluorite structure is stable for all compositions. Under high pressure oxygen and high temperature, solid solutions containing 66 per cent urania lose the cubic structure while, at 50 per cent urania, the fluorite cubic phase is stable under any oxidation conditions. The oxidation of the solid solutions reaches a limit in O_2/metal ratio between 2.32-2.34, irrespective of the average uranium valency. The composition limit tends to increase as the urania content decreases from 100 per cent to 66 per cent. These facts imply a dependence on the geometry of the structure. The highest valency reached by urania is 5.46 which occurs at 15 per cent urania content. At lower urania content, the valency actually decreases. At low urania contents, the proportion of O_2 cannot be limited by geometry but by the magnitude of the free energy change of oxygen transferred from the gas phase to the solid phase which, in turn, is dependent on the particular uranium ion configuration in the solid.

Besides oxygen take-up by urania in the urania thoria solid solution, the oxygen to metal (O/M), ratio may be affected by solution of di- and trivalent cations which can cause oxygen vacancies. Frost and Wait[43] pointed out that, in urania fuels, the fate of rare earth, Ba, and Sr oxides determines the O/M ratio. If these oxides form separate oxide phases only 1.5 and 1 oxygen

atoms are taken up respectively for each tri and divalent ion; however, upon formation of solid solution with urania, two oxygen atoms are taken up for each impurity atom by the adjustment of uranium's valency. The case of a ThO_2-UO_2 matrix which is predominantly ThO_2, differs from the above case in that ThO_2 cannot change its valency so that upon complete oxidation of urania, oxygen vacancies occur with the further addition of impurity ions. Vacancies however may occur before uranium is fully oxidized, the limit probably depending on geometrical considerations as in the Th-U-O system discussed above.

5.2. Phase Relations of ThO_2 and Single Oxides

The binary systems of ThO_2 and oxides of typical fission products have been partially studied and will be discussed below. Systems of tetra-, tri- and divalent ions with ThO_2 will be considered separately.

5.2.1. Studies of ThO_2 with Tetra Valent Cations

Foreign tetravalent cations may be substituted for thorium cations in the fluorite crystal without disturbing the basic structure or introducing lattice defects. The consequences of foreign tetravalent cations randomly distributed in the ThO_2 lattice is an enlargement or contraction of the unit cell depending on the ionic ratio of the two cations. The solubility limit of foreign cations into ThO_2 is the concentration above which a new phase is formed; that is, the foreign cations no longer distribute themselves randomly on normal thorium positions but form a differently ordered phase. Drewey and Loh[64] found in the system zirconia-thoria that the solubility limit was quite low and two solid solutions occur over almost the entire composition range. At temperatures below

900°C, there exist a monoclinic ZrO_2 solid solution and a ThO_2 solid solution and, above 900°C, corresponding tetragonal solid solutions. A similar study for ThO_2 and CeO_2 has not been made but, since CeO_2 exists as a cubic fluorite crystal it should form a complete series of solid solutions with ThO_2. Ceria may change its valency and is known to have several hypostoichiometric defect structures as well as forming hexagonal Ce_2O_3. Tetravalent cations substituting for thorium in thoria should have no effect on the defect concentrations present except for the case of ceria under low oxygen partial pressure. Molybdenum, which may also be tetravalent, will be treated as a special case in a later section.

5.2.2. Studies of ThO_2 with the Trivalent Cations

There are several trivalent cations produced during fission, most of which are rare earths. Y_2O_3, La_2O_3, Nd_2O_3 are typical oxides of these trivalent atoms and are used in this study to represent all of the trivalent atoms in a fuel element after burn-up. All three of these oxides have a cubic crystal structure but Campbell[65] reports La_2O_3 and Nd_2O_3 to have a hexagonal form also. Keller et al[66] extensively studied the phase equilibria of thoria-rare earth systems and found that, in the high ThO_2 regions, complete solubility of $R_EO_{1.5}$ into ThO_2 occurred. The extent of the solubility of the rare earth into ThO_2 was dependent on the difference between the ionic radii, i.e. $r_{Th^{+4}} - r_{RE^{+3}}$. The solubility of Nd_2O_3 in ThO_2, 60 per cent at 1600°C, was the highest of all the rare earths. The solubility limit of all the rare earths in ThO_2 was much greater than would exist in a fuel element even after 10 per cent burn-up. In order to maintain electroneutrality in the fluorite lattice when +3 RE ions replace +4 Th ions, oxygen vacancies must be produced. An oxygen vacancy would be produced

for every two +3 ions. Yittria, which is not a rare earth oxide, was found by Subbarao et al[67] to form solid solutions with thoria with a solubility limit of 40 per cent at 1600°C. Unlike the case of the rare earth oxides, in which compound formation occurred above the solubility limit, two solid solutions co-exist to high Y_2O_3 concentration, when only an yittria solid solution exists. ThO_2-Y_2O_3 solid solutions have been used as solid electrolytes for sensing low oxygen partial pressures.

5.2.3. Studies of ThO_2 with the Divalent Cations

The two important divalent cationic fission products are Sr and Ba which may react with Th^{+4} to form solid solutions or perovskite compounds of the form M ThO_3. There is some controversy about the formation of these perovskite structures; however, not a great deal of work on these systems has been done. The system SrO-ThO_2 will be considered first.

Naray-Szabo[68] reported the formation of the perovskite compound $SrThO_3$ in 1947 and Coffeen[69] in 1953. In more recent work, by Smith and Welch[70], no formation of $SrThO_3$ was found. The latter also conclude that the X-ray data of Naray-Szabo correspond better to the patterns of the two component oxides. In more recent work by Fava et al[71], substitutional solid solution of SrO in ThO_2 was found, electroneutrality being maintained by formation of oxygen vacancies; $Th_{1-x}Sr_xO_{2-x}$. Based on lattice parameter determination of the mixture of SrO and ThO_2 fired to 2000°C, a solubility limit of 13 per cent SrO in ThO_2 was found. Furthermore, after reheating to temperatures below 1600°C the solid solutions dissociated to SrO and ThO_2. No mention was made of the atmosphere used during the initial firing or reheating nor

of the particle size of powders or the mixing technique. A eutectic was found to exist under an atmosphere of oxygen at high SrO content, $62SrO.38ThO_2$. The melting point of this eutectic composition was depressed 30°C under an atmosphere of argon. As reported by Smith and Welch[70], no perovskite $SrThO_3$ compound was found.

The system $BaO-ThO_2$ has been studied by all of the above mentioned authors but only in the stoichiometric ratio for a perovskite compound. All authors have reported formation of $BaThO_3$ even at temperatures as low as 1150°C. Hoffmann[72] reported that $BaThO_3$ is slowly decomposed by atmospheric CO_2 to form $BaCO_3$ and ThO_2. This effect was also observed by Smith and Welch[70]. No further information on mixtures of ThO_2 with low BaO content appears to exist.

5.3. Studies of the Fluorite Structure with MoOx

Molybdenum is of great importance to any study of fission products in fuel elements because of its abundance and its ability to control the oxygen partial pressure above the reacting oxide phases. Little work has been done on thoria-molybdena systems partly because of the difficulty in containing molybdenum oxides especially at high temperatures. The fact that Mo and its oxides are extremely volatile has precluded the accumulation of reliable phase relation data; however, Phillips and Chang[73] have developed a sealed-capsule technique which adequately preserves metal-metal oxide compositions at temperatures as high as 1700°C. Four stable phases were found; MoO_2, MoO_3, Mo_4O_{11}, Mo_9O_{26}, of which only MoO_2 was stable above 1000°C. MoO_2 was found to remain a stable phase up to 1700°C, the highest temperature obtained in the study.

In studies in the systems ThO_2-MoO_3, and ThO_2-WO_3, Trunov and Kouba[74] found $Th(MoO_4)_2$ and $Th(WO_4)_2$ respectively. In later work by Maayer et al[75], $Th(WO_4)_2$ was found to melt at 1640°C which is somewhat higher than the temperature reported by Spitsyn et al[76], 1380°C. No mention has been made of solid solution of W or Mo oxides in the ThO_2 structure. No additional information is available on compositions containing low concentration of MoO_3 or MoO_2 in ThO_2; however, it may be reasoned that stable Mo^{+6} would be less likely than Mo^{+4} to enter the fluorite structure due to its significantly smaller size compared to the Th^{4+} ion.

5.4. Formation of Mixed Oxide Phases Among Fission Products

Stable oxide phases involving typical fission products are well known. The particular phases which in fact occur in a nuclear fuel depend on the total free energy of the system. Unfortunately, the thermodynamic information required to make an accurate prediction about compound formation in a fuel element does not exist nor is the fuel element ever in thermodynamic equilibrium. In the following discussions, phases which are known to exist are examined and the likelihood of their formation in a thoria matrix considered.

5.4.1. Formation of ABO_3 Phases

The most important compounds of the perovskite type which may form are the zirconates simply because of the relative abundance of zirconium in the fission product yield. Both barium and strontium form zirconates. The perovskite structure is made from a cubic close packed lattice of oxygens and divalent metal ions, for example Ba or Sr, with the tetravalent cation lying in 1/4 of the octahedral sites (see Figure 5.1). According to Swanson et al[77], barium zirconate is cubic O^1_h-Pm3m with a lattice parameter

of 4.193. Strontium zirconate according to Traverse and Foex[78] forms cubic perovskite at high temperatures (2000°C), but at room temperature according to the X-ray index 10-268 $SrZrO_3$ forms an orthorhombic D_{2H}^{16}-P crystal with lattice parameters Ao = 5.814, Bo = 8.196, and Co = 5.792. Other compounds forming the ABO_3 structure are barium and strontium cerates and recently discovered molybdates. The molybdates will be discussed in more detail in a later section since other stable structures exist besides the ABO_3 structure in those systems. The cerates of strontium and barium were originally thought to be cubic; however, recent work by Mastromonaco et al[79] indicates that both compounds are actually orthorhombic with the lattice parameters of the respective compounds being Ao = 8.584, Bo = 6.011, Co = 6.155 and Ao = 8.779, Bo = 6.214 Co = 6.236. As in the case of $SrZrO_3$ these structures may form cubic perovskite at high temperatures. Since Ce may take on either +3 or +4 valency, formation of a defect cerate structure is possible under reducing conditions by the formation of anion vacancies.

5.4.2. Formation of $A_2B_2O_7$ Phases

The most important of these compounds are $Nd_2Zr_2O_7$ and $Ce_2Zr_2O_4$. Both form cubic Fd3 synthetic pyrochlore structures with lattice parameters Ao = 10.648 and Ao = 10.70 respectively. Other +3 valency cations may form similar structures with Zr such as La, Pr and Y. It is interesting to note that another cubic structure $Ce_2Y_2O_7$ has been reported[80] which is also cubic but exists as a fluorite structure with a lattice parameter Ao = 5.36.

$Nd_2Zr_2O_7$ is the only congruently melting compound in the ZrO_2-Nd_2O_3 system. There is an area of solid solubility in the $Nd_2Zr_2O_7$ phase which extends from 82 to 40 mole per cent of zirconia. For concentrations of ZrO_2 higher than 82 per cent,

$Nd_2Zr_2O_7$ coexists with a tetragonal ZrO_2 solid solution, while, for concentrations lower than 40 per cent, it coexists with a Nd_2O_3 solid solution. The $Ce_2Zr_2O_7$ phase is reported by Casey[81]; however, in the phase diagram by Duwez and Odell[82], no such compound formation is shown; only a vaguely bounded area of tetragonal and cubic solid solutions from 20 per cent to 80 per cent CeO_2 is shown.

The formation of these $A_2B_2O_7$ phases of large lattice parameters in a matrix of ThO_2 would certainly cause stresses in the lattice or expansion of the matrix.

5.4.3. Formation of Barium and Strontium Molybdates

As mentioned earlier, the molybdates of barium and strontium will be discussed as a special case due to the complexity of structures which may form. McCarthy and Gooden[83], while studying the Sr-MoO system, found three compounds to form inside the compositional triangle; Sr_3MoO_6, $SrMoO_4$ and $SrMoO_3$. As previously reported (Baly and Plietti[84]), stable phase Sr_2MoO_4 was not prepared and the stable phases of the bulk composition of Sr_2MoO_4 was found to be (Sr_3MoO_6+Mo). At 1200°C all three compounds form a compatibility triangle. Mo metal was found to coexist with SrO and MoO_2 as well as the three ternary compounds. Of the three stable compounds, in only $SrMoO_3$, which forms a cubic perovskite structure, is Mo stabilized in the +4 valency state. The absence of the stable phase Sr_2MoO_4 was considered surprising since this structure is K_2NiF_4 type which is a layer structure made up of perovskite and rock salt units alternating in the C direction. McCarthy has noted in other papers[85,86,87] the structural control of valence state and apparently only a small change in structural

energy is required to destabilize Mo^{4+}. It has been pointed out by McCarthy[85], that, when considering structures involving variable valency ions, not only ion size, charge and polarizability must be considered to determine stable structures but also a thermodynamic parameter.

An analogous study of the Ba-Mo-O system is not available. Since these ions are quite similar chemically it is assumed that essentially the same phase relations will exist.

Brixner[88] has studied $BaMoO_3$ and $SrMoO_3$ compounds fired up to 1500°C and found complete solid solubility of Ba and Sr in the perovskite structure. Vegard's Law was obeyed. While studying the electrical conductivity of these compounds, it was found that they exhibited resistivities in the range 10-100 Ω-cm with a positive temperature coefficient much like the tungsten bronzes. Like McCarthy[85], Brixner[88] found no evidence for non-stoichiometric phases of the form $Sr_xMoO_3 (X<1)$.

While there are other combinations of fission products which can form unique compounds, the ones discussed in the foregoing treatment are considered the most important and the ones which may be expected to form during the high temperature heat treatment of fission products in a nuclear fuel matrix.

CHAPTER VI

LITERATURE CRITIQUE

In previous Chapters, information about thoria and nuclear fuels has been set down. It is the purpose of this chapter to give a short critique of the available information dealing with fission product effects on nuclear fuels and the methods by which these effects have been studied. Furthermore, the objectives of this thesis are set down as well as the basis for the selection of the approach used to study the effects of fission products on thoria based nuclear fuels.

6.1. Critique

Investigations, of fuel elements which have undergone burn-up show that high thermal gradients exist across the fuel element during fission and that swelling due to solid and gaseous fission products occurs. Besides thermal gradients, oxygen gradients may occur across the fuel element as in the case of urania and plutonia fuel elements. These affect the chemical state of variable valency ions. Inclusions of metallic and non-metallic constituents occur in fuel elements during burn-up and these inclusions appear to occur in various temperature regions of the fuel element. The microstructure of the fuel element varies with the temperature and, in general, four distinct regions are known and are typified by centre core melting, columnar grains, equiaxed grains and unaffected or pre-irradiated microstructure.

The above facts have been noted by all workers investigating fuel elements after burn-up; however, disagreement among workers occurs mainly about the composition of the inclusions which are formed during burn-up. As pointed out earlier, Bradbury et al.[42]

and Jeffery[54], studying fuel elements of identical chemical composition and irradiation treatment, found different types and concentrations of inclusions and Bradbury et al.[42] obtained different results on samples from the same batch during two separate investigations.

Bradbury found barium containing and barium free inclusions. In his first study, molybdenum was absent from barium containing inclusions; however, in the second study, molybdenum was found in both inclusions. Zirconium and, sometimes, strontium and cerium were found with barium. Jefferey found only a few barium containing inclusions which contained molybdenum. Only those which contained molybdenum also contained Re, Rh and Tc. All the barium inclusions contained cerium, zirconium, neodymium, and strontium.

The inconsistencies in results can easily be rationalized. First, a fuel element is never in equilibrium, either thermal or chemical. This fact alone may explain the variable results obtained, but also the radioactivity of the sample requires either long cool down times before analysis begins or sufficiently well shielded analysis equipment. Size reduction of samples may also reduce the radioactivity to an acceptable level to enable normal analysis techniques to be used but the sample may be too small to be representative of the larger sample. Secondly, the total concentration of solid fission products in a fuel element after 10 per cent burn-up is of the order of two weight per cent. Such low concentrations of impurities are difficult to analyze unless they are segregated as well defined inclusions. Bradbury et al. used the sample thinning technique as did Jefferey in analysis of the specimens. The fact that Bradbury obtained results of two studies in conflict indicates that the sample preparation and/or area selection may have had a

large affect on his results. In view of this, it is not surprising that Jefferey obtained different results in his study. Furthermore, the inclusions analyzed were approximately 5μm in diameter and, since the resolution of the actual inclusions would be affected by the spreading of the microprobe beam in the sample, Bradbury asserts that the diffused electrons were on the order of 5 to 10μm in diameter, there is some question whether the analyzed elements actually resided wholly in the inclusions being studied.

The advantages of simulation of fuel elements after various degrees of burn-up and analysis of the resultant compacts are self-evident; however, the difficulties in obtaining accurate analogues to fuel elements after burn-up are great. None of the reported simulation studies of oxide fuel elements after burn-up has managed to produce a completely satisfactory analogue to a real system. In the study by Schmitz[56] in which $(U,Pu)O_2$ and fissium metal or metal hydrides were heated in sealed capsules for up to 72 h at 1750°C, two discrepancies appear. The metal phases analyzed were not of uniform composition; this fact implies that equilibrium was not achieved and is at variance with results obtained by O'Boyle et al.[46], who found relatively constant metallic compositions in zones of constant temperature. The simulation study of Koizumi et al.[57] in which oxide mixtures of Ba, Sr, Zr and U were reacted isothermally at temperatures from 1000°C to 2000°C yielded information about phases formed among these specific fissium and urania which was generally in good agreement with results obtained on fuel elements; however, neither the effect of a thermal gradient nor atmosphere was considered and both may affect the phases which may form when considering volatile or variable valency constituents.

Freund and Sari[58] used the method of direct electrical heating of a UO_2 fuel which shows great promise as a simulation technique in that a thermal gradient similar to that experienced in a nuclear reactor can be obtained and the corresponding microstructure achieved. Some stable fission products were added to the UO_2 as dopants but an extensive study was not conducted to determine phase formation or development of inclusions.

6.2. Objective

The aim of this thesis is to develop a suitable simulation technique to study the effects of fission products in thoria based nuclear fuels and compare the similarities or dissimilarities to UO_2 based fuels. A unique simulation technique may not be sufficient to determine the effects which occur in a real fuel element, therefore, the approach is based on the following criteria.

Prior to heat treatment the fissium must be oxidized to the theoretical extent determined by fission yield and free energy of formation of particular oxides. Hence the fissium will be added as oxides since controlled oxidation of elemental compacts is considered too difficult. In addition, the effect of a thermal gradient must be considered since oxygen gradients co-exist with temperature gradients and the chemical equilibrium of oxides is influenced by the oxygen partial pressure. The overall oxygen potential must also be considered in view of the influence of cladding can material and oxygen controlling reactions such as $Mo + O_2 \rightleftharpoons MoO_2$. Finally, not only are the chemical constituents forming inclusion to be determined but also the crystalline phases which are formed are to be identified.

6.3. Experimental Approach

Isothermal studies are to be conducted to determine phases which occur between fissium and thoria and among fissium oxides themselves. Sealed and unsealed samples containing fissium elements and oxides are to be studied under isothermal conditions since volatile fission products are likely to be control phase formation. Diffusion couple experiments may be used to determine the influence of oxygen partial pressure on formation of stable phases involving variable valent ions. Finally, the electrical conduction technique based on the work of Freund and Sari[58] is to be used to achieve the chemical and thermal simulation of a thoria based fuel element after 10 per cent burn-up.

CHAPTER VII

EXPERIMENTAL PART

7.1. Reagents and Materials Used

The reagents used in this work are listed in Table 7.1. In some cases, which are covered in the following sections, these reagents were precursors for materials which were ultimately used in sintered compacts with ThO_2. The starting reagents were A.R. grade in all cases.

7.2. Preparation of Starting Materials

Highly reactive thoria was obtained by calcination of the oxalate which was derived, in turn, from a nitrate solution. A quantity of thorium oxide from Departmental stocks, having total impurities of .007 per cent, was used in initial sintering studies. Due to the poor results obtained with this material all subsequent work was conducted using freshly prepared thoria as described later.

Some typical fission product oxides were used as received, while others were prepared from oxalate precursors in a similar way to thoria. The preparations of these oxides from oxalates was done to facilitate mixing of the final compositions with thoria rather than to enhance the sintering and reaction rates, although the latter effect was pronounced in certain cases. Coprecipitation was not used in this work, since the conditions of precipitation of the individual oxalates were varied and constant compositional ratios could not therefore be ensured. Metallic reagents were received in sealed capsules and care was taken to prevent oxidation of these materials during mixing.

TABLE 7.1

Reagent	Supplier	Purity
Ultra pure thorium nitrate	Roc Ric Sun Valley	99.95
Barium nitrate	Mallenckrodt	99.90
Barium oxide	Roc Ric	99
Cerous nitrate	Uni Lab	99
Cerium oxide	Koch-Light	99.9
Lanthanum oxide	Townson & Mercer	99.99
Molybdenum trioxide	Koch-Light	99.9
Molybdenum metal	Rocky Mountain Research	99.99
Neodymium nitrade	Rhone	99.9
Neodymium oxide	Koch-Light	99.5
Palladium metal	Alfa Inorganics	-
Rhenium metal	Alfa Inorganics	-
Ruthenium metal	Alfa Inorganics	-
Strontium nitrate	Uni Lab	99
Tellurium metal	Alfa Inorganics	-
Yttrium oxide	Koch-Light	99.99
Zirconium oxide	Koch-Light	99.8

The dioxide of molybdenum was prepared by partial reduction of molybdenum trioxide.

7.2.1. Preparation of Thoria

Thorium dioxide was prepared by means of calcination of thorium oxalate at 600°C for one hour in air. The oxalate was precipitated by adding oxalic acid to thorium nitrate solutions at various temperatures. Three oxalates were formed; thorium oxalate, thorium oxalate dihydrate,and hexahydrate. Thorium oxalate, $Th(C_2O_4)_2.2H_2O$, was formed by adding 0.4 molar solution oxalic acid to 0.2 molar thorium nitrate solution at 21°C and allowing to stand 24 hours. The supernaught was poured off and the precipitate washed by stirring in distilled water and allowing to stand for 24 hours. This procedure was repeated three times whereupon the precipitate was dried in an air oven at 110°C. The oxide formed after calcination was well crystalline and fully converted. The thoria was stored in sealed glass jars.

7.2.2. Preparation of Fission Product Oxides

The typical fission product oxides used in this work were either as received oxide powders or were prepared from precipitates. Soluble salts of the metal concerned were dissolved in water and were precipitated as oxalates. The precipitates were washed and dried and finally calcined to produce the metal oxides or, as in the case of barium and strontium, the carbonates. Zirconium tetrachloride and zirconium nitrate were both used as soluble salts for the precipitation of zirconium oxalate. For all others, only nitrates were used. Nitrate solutions of yttrium and lanthanum were prepared by digesting the oxides in 7.5 N nitric acid until the solution pH was approximately 6.5 whereupon precipitation of the oxalate was carried out by the addition of oxalic acid.

7.2.3. Formation of MoO_2 by Reduction of MoO_3

While MoO_3 is the stable oxide form during oxidation of Mo metal in air, MoO_2 is the stable oxide at high temperature under controlled atmospheres. MoO_2 was prepared by reducing MoO_3 to MoO_2. The overall reaction,

$$MoO_3 - \tfrac{1}{2}O_2 \rightleftharpoons MoO_2 \qquad 7.1$$

may be obtained by subtracting equation 7.3 from 7.2.

$$Mo + O_2 \rightleftharpoons MoO_2;\ \Delta G_1^o \qquad 7.2$$

$$Mo + 3/2\ O_2 \rightleftharpoons MoO_3;\ \Delta G_2^o \qquad 7.3$$

$$\Delta G_I = \Delta G_1^o - \Delta G_2^o = -\tfrac{1}{2}O_2 \rightleftharpoons MoO_2 - MoO_3 \qquad 7.1$$

The free energy of each reaction is shown in Table 7.2 and was taken from the U.S. Bureau of Mines Bulletin 542[89]. The free energy change corresponding to equation 7.1 may be calculated assuming the vapour pressure of MoO_3 at 1003°K is equal to 1.316×10^{-3} [90].

$$\Delta G_I = -2.158\times10^4\ cal(g.mole)^{-1}(K)^{-1} = -RT \ln K;\ K = \frac{(P_{O_2})^{\frac{1}{2}}}{(P_{MoO_3})}$$

$$(P_{O_2})_I = 4.402\times10^3$$

The CO_2/CO ratio giving this partial pressure of oxygen may be obtained by solving equation 7.6.

$$C + \tfrac{1}{2}O_2 \rightleftharpoons CO\ ;\Delta G_3^o \qquad 7.4$$

$$-\ C - O_2 \rightleftharpoons -\ CO_2\ ;\Delta G_4^o \qquad 7.5$$

$$\tfrac{1}{2}O_2 + CO \rightleftharpoons CO_2\ ;\Delta G_{II} \qquad 7.6$$

The ΔG_{II} for reaction 7.6 is

$$\Delta G_{II} = \Delta G_4^o - \Delta G_3^o = 4.649\times10^4\ cal(g.mole)^{-1}(K)^{-1}$$

the partial pressure ratio of gases may be obtained as follows:

TABLE 7.2

Reaction	Temperature Range of Validity	Δ Ho	2.303a	b	c	I
$C_{(graphite)} + \frac{1}{2}O_{2(g)} = CO_{(g)}$	(298.16 - 2000°K)	-25,400	+2.05	+ .27	-1.095	-28.79
$C_{(graphite)} + O_{2(g)} = CO_{2(g)}$	(298.16 - 1048°K)	-93,690	-4.60	-	-	+92.84
$Mo_{(C)} + \frac{3}{2}O_{2(g)} = MoO_{3(C)}$	(298.16 - 1068°K)	-183,650	-8.86	-1.55	+1.54	+90.07
$Mo_{(i)} + O_{2(g)} = MoO_{2(C)}$	(298.16 - 2000°K)	-132,910	-3.91	-	-	+47.42

$$\Delta G^{o} = \Delta Ho + 2.303a\ T\ Log\ T + b \times 10^{-3}T^{2} + C \times 10^{5}T^{-1} + I\ T$$

$$\Delta G_I = -RT \ln K \; ; \quad K = \frac{(P_{CO_2})}{(P_{CO})(P_{O_2})^{\frac{1}{2}}}$$

Solving the $\frac{P_{CO_2}}{P_{CO}}$ ratio as a function of (P_{O_2})

$$1.352 \times 10^{10} \, (P_{O_2})^{\frac{1}{2}} = \frac{P_{CO_2}}{P_{CO}}$$

For a $(P_{O_2}) = 4.402 \times 10^{3}$, corresponding to the O_2 pressure required in equation 7.1, the $\frac{P_{CO_2}}{P_{CO}}$ ratio is

$$\frac{P_{CO_2}}{P_{CO}} = 8.970 \times 10^{11}$$

This is of the order of magnitude of CO impurity in medical grade CO_2 gas. Reduction of MoO_3 did not occur when subjected to CO_2 gas at 1003°K for 24 hours. Other CO_2/CO mixtures were tried and at a ratio of 2, which corresponds to (P_{O_2}) of 2.19×10^{-20}, well developed MoO_2 was formed without metal or lower oxides. Obviously there is some kinetic barrier which prevents the reaction occurring at high CO_2 ratios. Why Mo metal was not formed under the low oxygen partial pressure of 10^{-20} may be seen by looking at equation 7.2.

The partial pressure of oxygen in this reaction is given by the following equation:

$-\frac{\Delta G}{RT} = \ln (P_{O_2})^{-\frac{1}{2}}$; the vapour pressure of MoO_2 and Mo being neglected

$$P_{O_2} = 6.47 \times 10^{-22}$$

The CO_2/CO ratio corresponding to this oxygen pressure is 0.344. A similar treatment for equation 7.3 gives an equilibrium oxygen

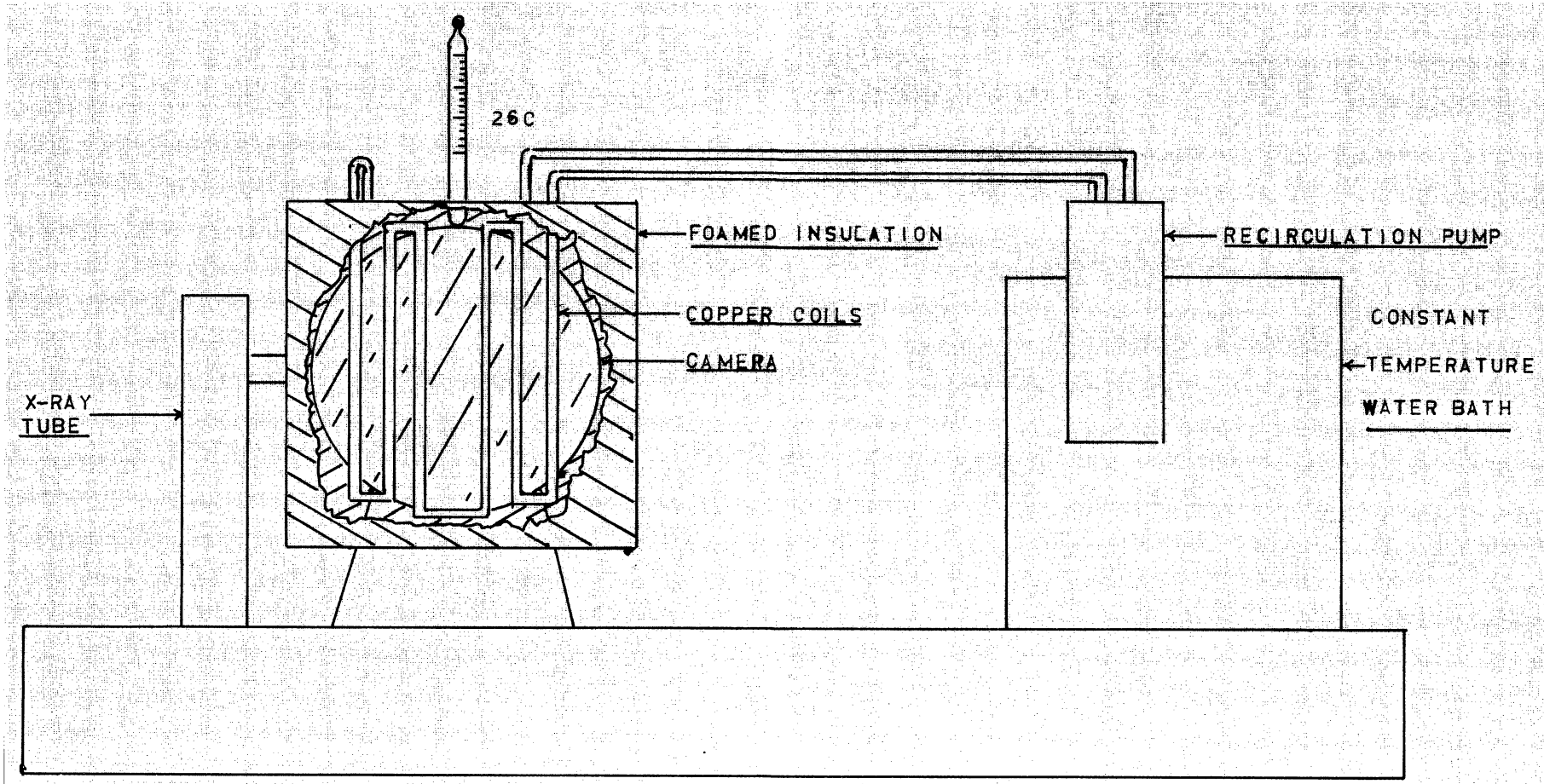

FIGURE 7.1

ARRANGEMENT FOR THE DETERMINATION OF PRECISE LATTICE PARAMETERS

partial pressure of 5.37×10^{-22} which corresponds to a CO_2/CO ratio of 0.313. The reduction of MoO_3 to MoO_2 is obviously more complicated than indicated by equation 7.1; however, well crystallized and fully converted MoO_2 free of Mo metal may be formed by heating MoO_3 under an oxygen partial pressure of 2.19×10^{-20} at 1003°K. Lower oxides begin to form when the partial pressure reaches 5.3×10^{-21}. Table 7.3 shows the X-ray data for MoO_3, MoO_2 and molybdenum oxides formed during reduction treatments.

7.3. Characterization of Raw Materials

As pointed out earlier, characterization of powders used in solid state reactions is necessary to prevent variations in the physical, thermal and chemical properties of similarly prepared sintered compacts. Several techniques were used to characterize the materials used in this work, each of which is described in one of the following sections.

7.3.1. Identification by X-ray Diffraction

A Philips X-ray diffractometer Model PW 1140 was used for identification of samples using the following conditions:

Diffractometer slits 1°/.1 mm/1°, Target Cu, Filter Ni, kV = 40, mA = 40, chart speed 20 mm/min

Scan rate 2°/min 2θ.

Detector Proportional Model No. PW 1965/50, time constant 1, attenuation 2^3.

For determination of precise lattice parameters, a Debye Scherrer camera type PW 1024/20, diameter 114.6 mm was used. Temperature control of 26°C ± .1 was effected by surrounding the camera with cooling coils which were supplied by a constant temperature water bath. Ambient temperature was held close to 25°C

TABLE 7.3

X-Ray 'd' Spacing for MoOx Oxides

File No. 4-809	5-452	5-508	CO/CO_2 Ratios During Preparation			
Mo	MoO_2	MoO_3	0/1	1/2	2/1	2.5/1
2.225	4.78	6.93	6.94	4.80	3.43	3.56
1.574	3.41	3.81	3.79	3.41	2.59	2.68
1.285	2.80	3.46	3.43	2.79	2.37	2.48
1.113	2.433	3.26	3.24	2.43	2.28	2.43
0.9952	2.420	3.006	3.00	2.41	1.75	2.34
0.9085	2.405	2.707	2.75	-	1.709	1.780
0.8411	2.397	2.655	-	2.39		1.743
	2.176	2.607	-	2.176		
	2.171	2.527	2.55			
	2.147	2.332	-	2.146		
	1.833	2.309	2.303	1.835		
	1.718	2.271	2.265	1.719		
	1.704	2.131		1.705		
	1.692	1.996		1.692		
	1.597	1.982		1.600		
	1.540	1.960				
	1.530	1.849				

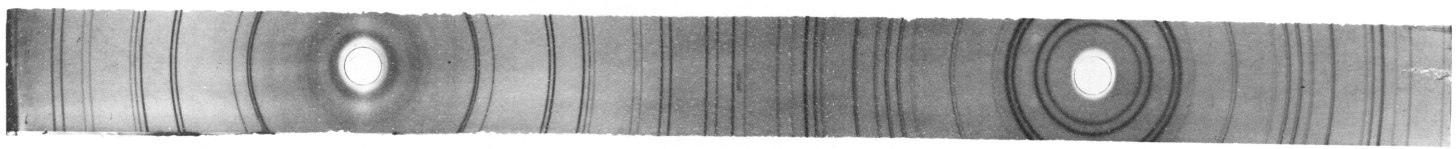

Forward Reflection

Back Reflection

Figure 7.2. Typical X-Ray Film of Thoria with CaF_2 Standard

Figure 7.3. Surface Area Measurement Apparatus

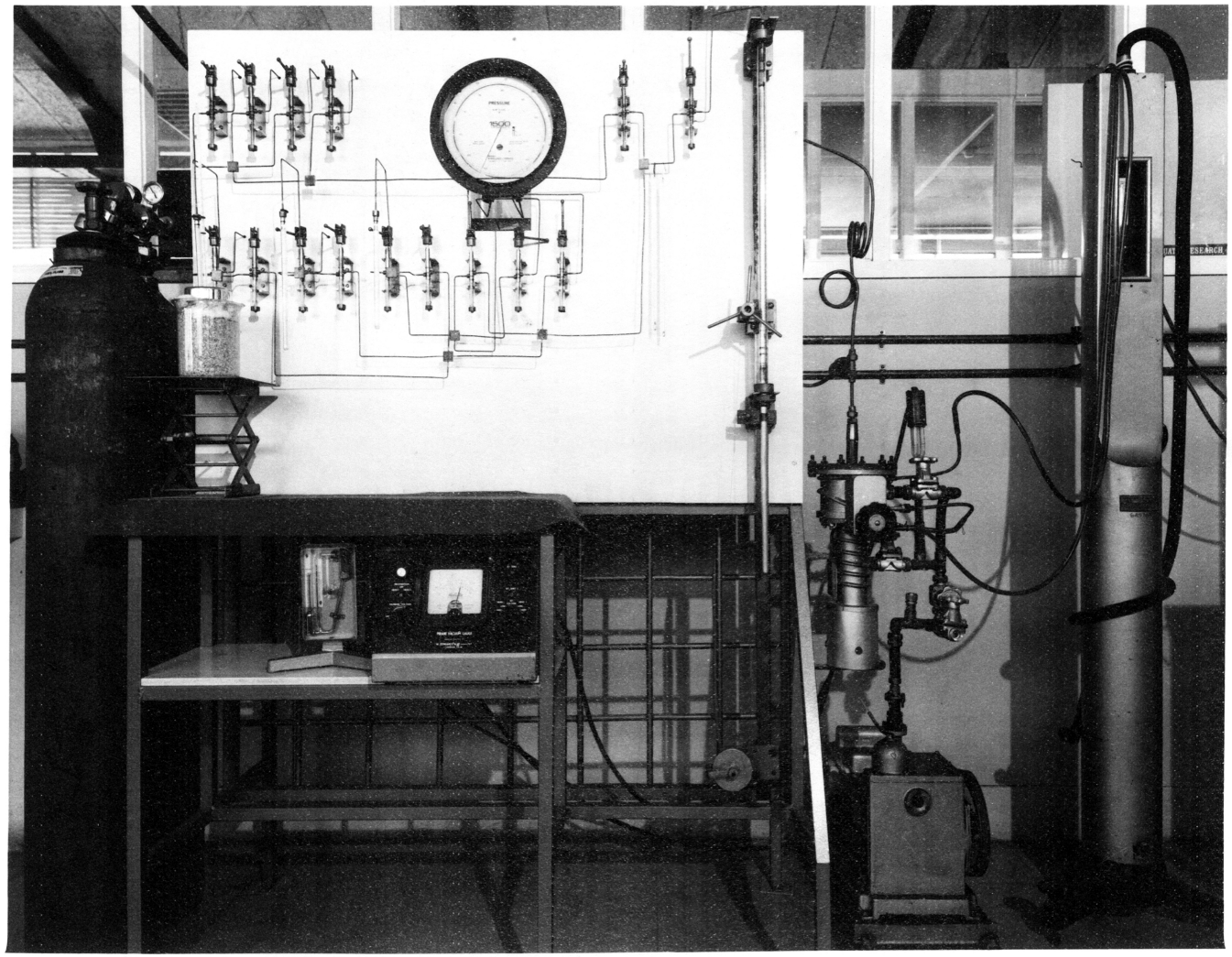

by the room air conditioner. The setup is shown in Figure 7.1.

Sample preparation. For precise lattice parameter determinations samples were crushed to -325 mesh and mixed with calcium fluoride. The mixture was placed in 0.3 mm lithium borate glass capillary tubes supplied by Philips. Satisfactory exposure was obtained after two hours. A typical film is shown in Figure 7.2. Two instruments were used to index the x-ray films: a Joyce Loebl microdensitometer and a Philips type 520220 film reader. The Joyce Loebl microdensitometer enabled determination of the line position as well as the line intensity; however, the line position had to be read from a chart which limited the absolute accuracy of the line position. The Philips film reader had the advantage of providing accurate line position to within 0.005 cm or 0.05° 2θ.

7.3.2. Surface Area Measurements by the B.E.T. Method

The surface area of powders was determined by nitrogen adsorption. The B.E.T. apparatus is shown in Figure 7.3. This instrument was built at the University of New South Wales and essentially varies from the normal B.E.T. measurement system only in that volume changes of adsorbed gases are measured as a function of specified pressures rather than both volumes and pressures. The pressure gauge used is a series 1500 type 62A-4A-X015X Wallace and Tiernqn Hi-Performance gauge. In this work samples were evacuated to pressures of 10^{-4} torr at temperatures up to $300^{\circ}C$ overnight. Dead space determinations were made using helium at liquid nitrogen temperatures. Calibration of the instrument was carried out using standard non-porous carbon black obtained from the National Physical Laboratory, Teddington, Middlesex. The surface area of the standard carbon black was quoted as 11.1 ± 0.8 m^2/g . This value compared well to the 11.26 m^2/g determined on two separate runs.

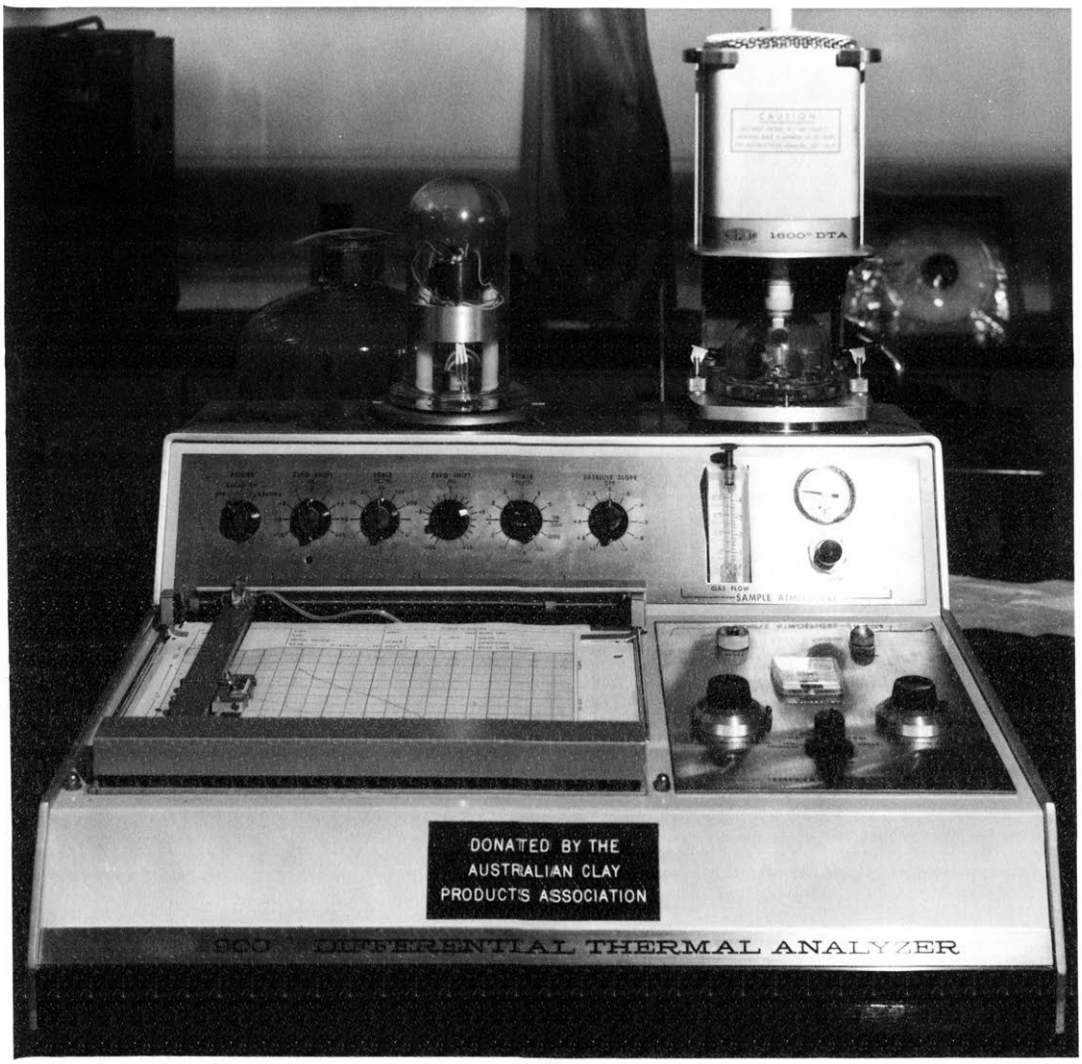

Figure 7.4. Du Pont Differential Thermal Analyzer

7.3.3. Differential Thermal Analysis

A Dupont type 900 D.T.A. shown in Figure 7.4 was used to characterize starting materials and to investigate phase changes. In all work, the high temperature cell (20-1600°C) was used. The low temperature cell was used in initial decomposition studies of oxalates but it was found that its sample configuration prevented complete oxidation of the oxalates producing endothermic rather than exothermic peaks during decomposition. The following operating conditions were used for decomposition runs:

Sample: diluted 1:1 with Al_2O_3

Reference material: Al_2O_3

Heating rate: 10°C/min and 20°C/min

Sensitivity: T (a) .8°C and 2°C per inch

Atmosphere: 101 kPa air.

The D.T.A. was useful in studying decomposition reactions; however, it was of limited value for phase work on the thoria composites due to the sluggishness of the reactions involved.

7.3.4. Scanning Electron Microscopy

The J.S.M. U3 scanning electron microscope, see Figure 7.5, with an "EDAX" attachment was used for high magnification studies. Sample holders of two different sizes were used, the 9.53 mm cylinders and the 25.4 mm cylinders. These sample holders were normally used for the 13 and 32 mm working distance respectively. An accelerating voltage of 25 KVa was used in all cases. Magnifications up to 10,000x were used. Photographs were taken using Polaroid positive/negative films type 55 and 105.

Sample Preparation

(1) Powder samples: Powder samples were dispersed in butanol,

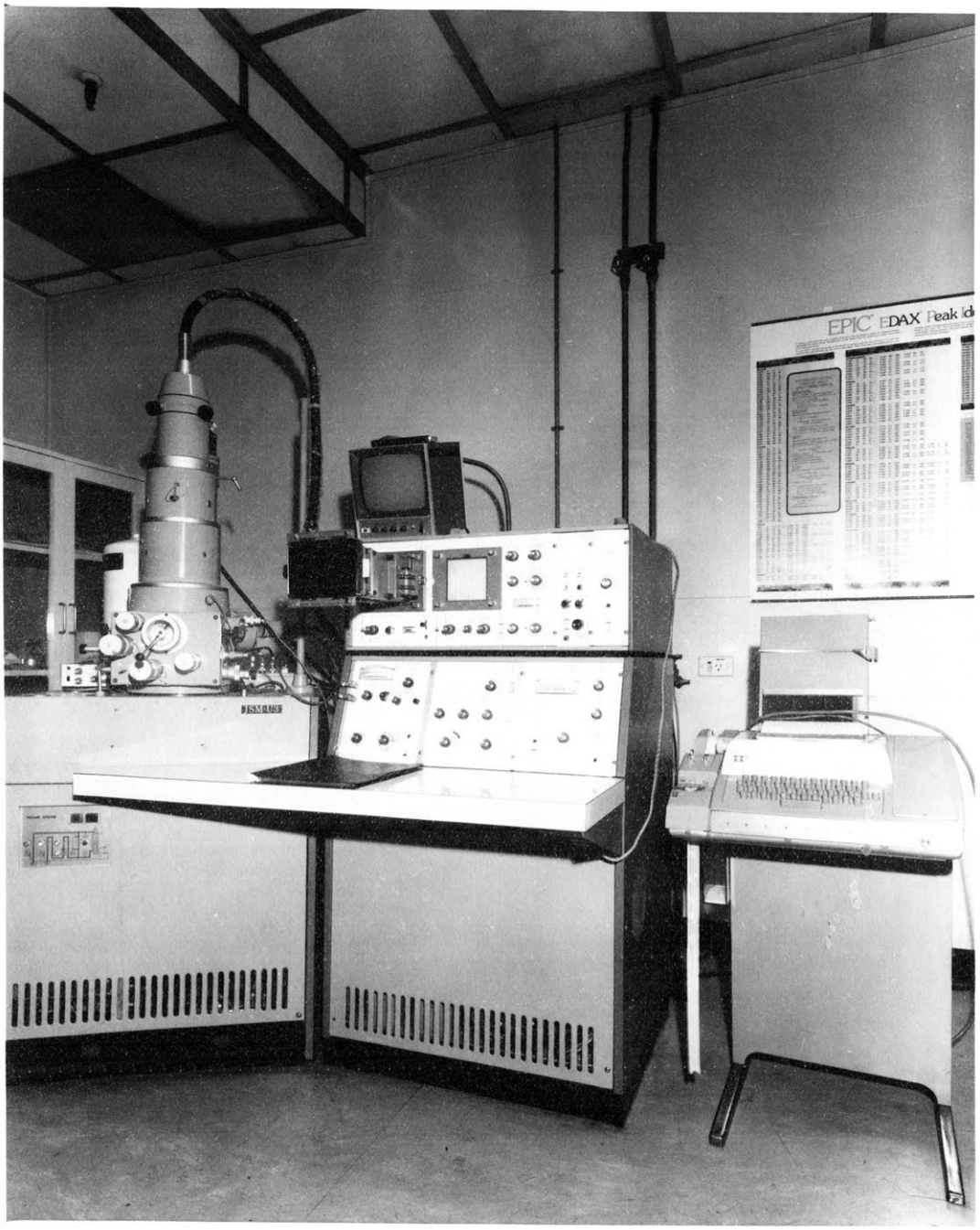

Figure 7.5. J.S.M.U3 Scanning Electron Microscope

a drop of this suspension was placed on a piece of glass cover slip which was glued to an aluminium sample holder, 9.53 mm diameter cylinder. After evaporation of the butanol, the sample was vacuum coated with gold approximately 200 Å thick.

(2) Fracture surfaces: Fracture surfaces were prepared in the following manner. Sintered compacts were broken and a broken piece was mounted on top of an aluminium cylinder by means of "dag" silver paste. As near as possible a fracture surface was aligned parallel to the top of the sample holder surface. The prepared samples were then coated with gold by vacuum deposition. In several cases, the gold coating on fracture surfaces was made much greater than 200 Å, since insufficient coating of the porous surfaces caused localized charging of the sample by the electron beam of the scanning microscope which in turn prevented detailed observations.

(3) Polished, etched and unetched samples: Polished sections were made by mounting samples in epoxy and in thermosetting Buehler No. 20-3340 AB diallyl phthalate and bakelite. The samples thus mounted were polished then coated with gold and in some cases carbon. Some were etched by immersion in boiling orthophosphoric acid for up to two minutes. It was found then only the diallyl phthalate satisfactorily withstood this treatment. The etched samples were then coated as before and examined.

7.3.5. Optical Microscopy

Two optical microscopes were used in this work: a Wild modified M-12 with both dark and light field attachments and a Union inverted stage microscope. The powders were dispersed in Gurr's Depex mounting medium and then mounted between a standard microscope slide and a cover slip. Only low magnification was

Figure 7.6. A.R.L. Probe Microanalyzer Model E.M.X.

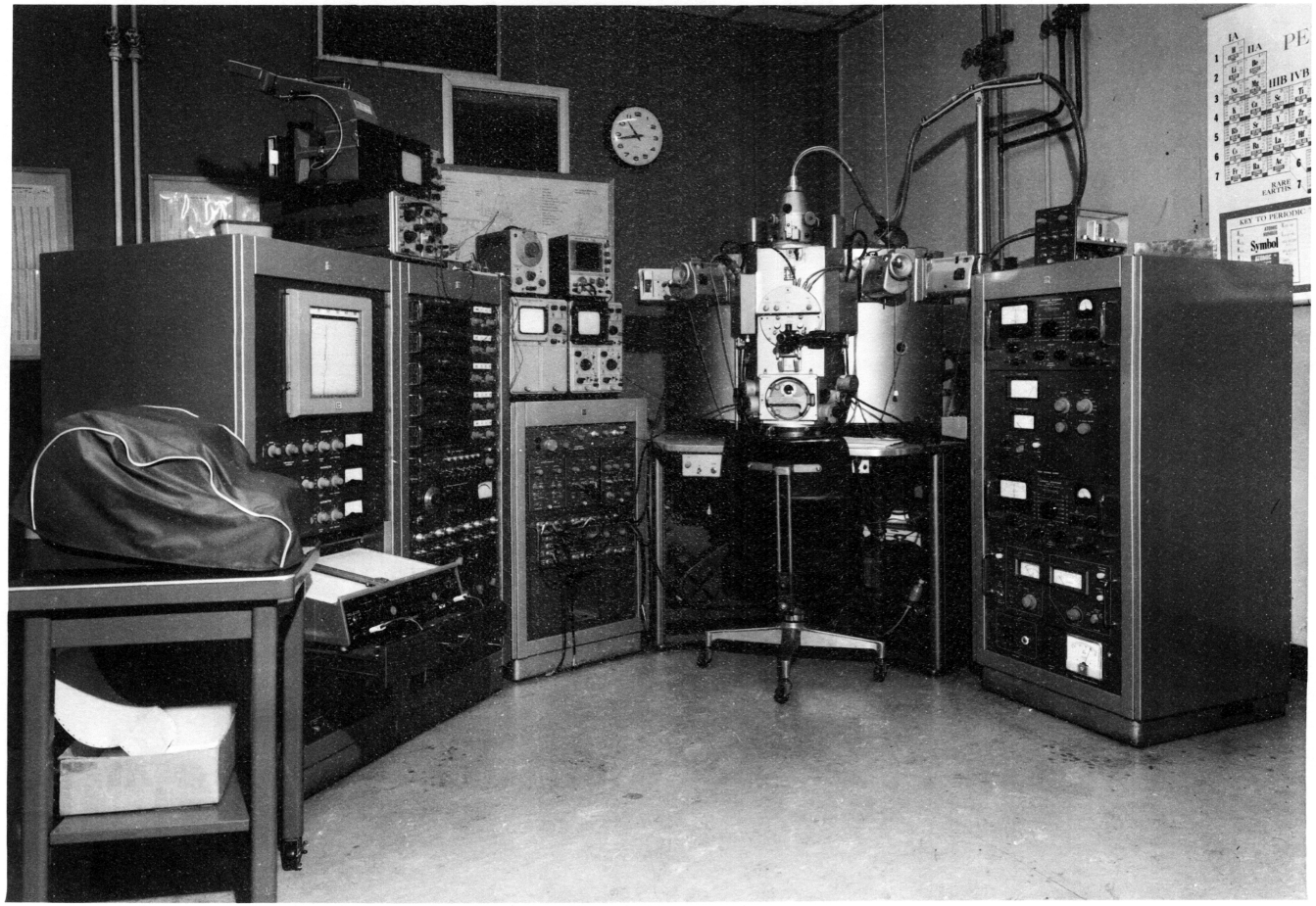

used for polished section work since high magnification was more easily done on the scanning electron microscope. Transmission microscopy was used to study powders and powder mixtures.

7.4. Phase Identification

Besides X-ray diffraction, previously described, other techniques were used to identify phases formed with ThO_2. X-ray diffraction of course is the most convenient method for identifying crystalline phases; however, other methods were used to identify implicitly phases present in low concentrations when this was not possible with X-ray deffraction.

7.4.1. Electron Microprobe Analyses

Electron microprobe analysis was carried out on an A.R.L. probe microanalyzer model EMX, see Figure 7.6. Polished sections were carbon coated prior to analysis. Standards of elements to be analyzed were used to set the wavelengths of each detector prior to analysis. The optical low magnification of the probe was 22X and high magnification was 200X which proved insufficient for viewing many specimens. Area scans were employed to analyze samples containing thoria and simulated fission products which produced relatively satisfactory results. Photographs of the resulting area scans were compared to provide information regarding chemical species found together. The sensitivity for the elements concerned was approximately 0.1%. The low concentration of elements other than thoria required long exposure times, up to 20 minutes, which degraded the resolution somewhat. When studying diffusion gradients of elements, the detector output was recorded on an X-Y recorder as a function of diffusion distance. Because of the porosity of the sample surface, a smooth curve was not obtained. Irregularities were superimposed on the general gradient obtained on analysis of diffusion couples.

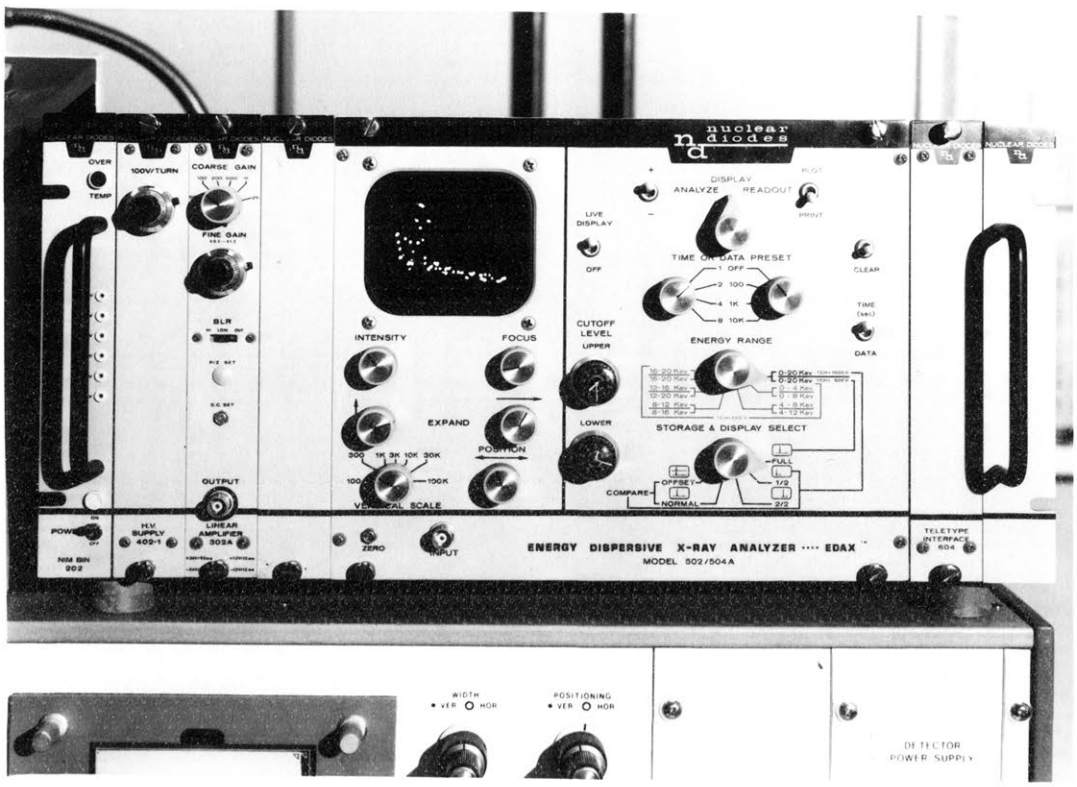

Figure 7.7. "EDAX" UNIT

7.4.2. E.D.A.X. (Energy Dispersive X-ray Analyzer) Analyses

The E.D.A.X. system shown in Figure 7.7 was used in conjunction with the scanning electron microscope. The E.D.A.X. system analyzed the X-radiation emitted from the elements exposed to the electron beam. The radiation spectrum was then analyzed for peaks associated with the elements. The E.D.A.X. system combined with the scanning electron microscope, permitted analysis of areas observed at high magnification. This was a clear advantage over the probe; however, the E.D.A.X. system had poorer resolution than the probe. Results from the E.D.A.X. analysis were printed by a teletype and plotted on an X-Y recorder. The plotted peaks were then compared to the characteristic wavelength energy for K. L. and M radiation of elements sought.

7.5. Sintering Experiments

Previous work on thoria by Moorehead[5] showed that thoria derived from the oxalate was a highly sinterable material. The present work was aimed at studying the effects of simulated fission products on thoria and, consequently, the sintering behaviour of thoria with these fission products was studied.

7.5.1. Fabrication and Firing

Powders of thoria or thoria based mixtures, obtained by calcining mixed oxalate precipitates or by ball milling mixed oxides, were transferred to a mortar and pestle and thoroughly mixed with a two per cent stearic acid-acetone solution. The air dried powder was then transferred to a hardened steel die and pressed at 7.6×10^4 KPa. The pressure was gradually released and then reapplied to minimise the frictional effects of the die walls.

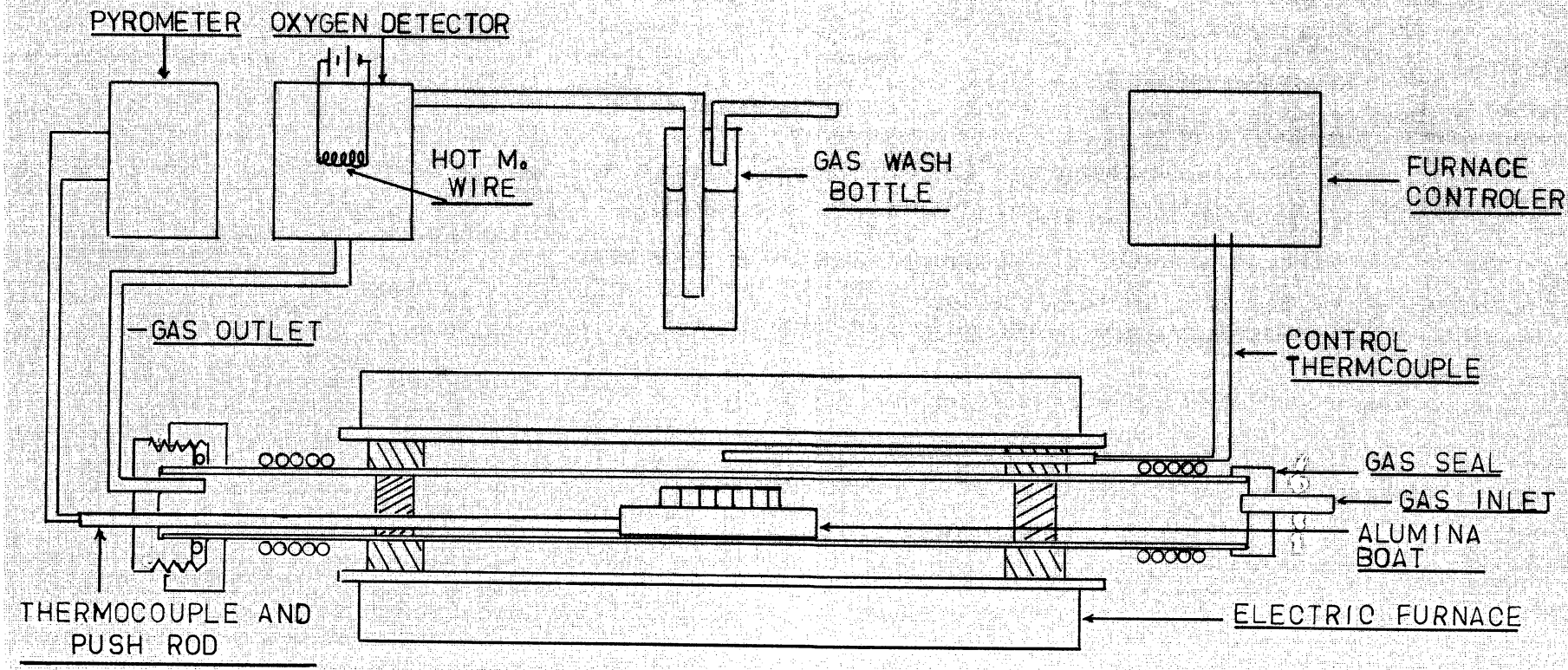

FIGURE 7.8
SET-UP FOR FIRING

Compacted pellets of several sizes were used in this work; in the majority of cases, the pellets were 9.5 mm in diameter. Care was taken to ensure that the pellets were not heated prior to firing. Stearic acid melts at 70.1°C and boils around 365°C which had the following effects; 1. if the pellets were dried in an air oven prior to measurement of green density the stearic acid first melted then crystallized forming stresses in the pellet upon further heating cracks would develop in the pellet. When the pellets were left in the air oven overnight the pellets cracked while cooling to room temperature. 2. The binder was eliminated by heating in a flowing inert atmosphere at temperatures well below the original calcination temperature of the oxide powders which eliminated any concern about binder effect on the sintering character of the pellets. Stearic acid was a good lubricant and prevented die release problems and, being hydrophobic, should have retarded hydration of oxides such as barium and strontium.

At various stages of the research, firing was conducted in five types of tube furnaces. 1. A platinum wound Stanton Redcroft 1700°C furnace, 2. A rhodium wound Hereaus furnace, 3. A molybdenum wound furnace, 4. A crystalon SiC furnace and 5. A modified gas fired tangential furnace. In the latter case, the samples were fully protected from combustion products. In all cases, the samples were placed in an alumina boat and were slowly introduced to the hot zone under flowing N_2, so that no oxygen would be present during the firing. See Figure 7.8 for a schematic diagram of the firing technique. The pellets were raised to 400° within 15 minutes and held at this temperature for 15 minutes to ensure complete loss of binder. The pellets were then raised to the final soaking temperature at 50°/min from 400°C to 800°C and 100°/min from 800°C to soak.

7.5.2. Density Measurements

The density of the sample pellets was measured in several ways which are enumerated below.

1) Measured density: Green and fired densities of the pellets were determined by weighing the specimens to the nearest 10^{-4} gram and measuring the diameter and thickness to the nearest 10^{-4} cm. Variation of the fired specimens from right cylinders led to lower measured densities than those obtained by fluid displacement.

2) Fluid displacement method: Density, porosity and apparent specific gravity values for sintered samples were obtained by standard boiling and evacuation techniques, using distilled water as the displacement fluid. Many of the oxides used in this work, however, had a tendency to hydrate and an alternative method had to be used. Displacement of mercury was tried but quickly discarded due to high variability in results obtained and also because porosity and apparent specific gravity values could not be obtained. Toluene and kerosine were both used, following the evacuation method: Samples were weighed dry to the nearest 10^{-4} gram, then immersed into the measuring fluid and evacuated for one hour. The samples were then suspended in the fluid and weighed and, finally, weighed saturated with the fluid in air. For the saturated weight determination the surface was wiped dry with a cloth slightly dampened with the measuring fluid to ensure only the fluid inside the pores of the sample was being measured. Table 7.4 shows the density values obtained for the measuring fluids used. The density, porosity and apparent specific gravity values were determined from equations shown below:

TABLE 7.4

Density, Porosity and Apparent Specific Gravity Determination Using Various Measuring Fluids

Measuring fluid	Sample No.	Bulk Density	Apparent Porosity	Apparent Specific Gravity
Water	1	7.72	15.40	9.13
	2	7.73	20.17	9.68
	3	7.78	17.67	9.45
	4	7.57	17.41	9.17
	Av.	7.70	17.66	9.36
Toluene	1	8.29	14.47	9.70
	2	7.98	17.16	9.63
	3	8.03	16.75	9.65
	4	7.97	17.92	9.71
	Av.	8.07	16.58	9.67
Kerosine	1	8.23	17.90	10.03
	2	8.02	19.89	10.02
	3	8.14	18.85	10.04
	4	8.11	18.36	9.93
	Av.	8.13	18.75	10.01

$$\text{Bulk Density} = \frac{(W_1)(S)}{(W_2-W_3)} \quad ; \quad 7.7$$

$$\text{Apparent Porosity} = \frac{(W_2-W_1)}{(W_2-W_3)} \times 100 \quad ; \quad 7.8$$

$$\text{Apparent Specific Gravity} = \frac{\text{Bulk Density}}{(1-\text{Porosity}/100)} \quad ; \quad 7.9$$

where

W_1 = Dry weight

W_2 = Saturated weight

W_3 = Suspended weight

S = Specific Gravity of measuring fluid.

The specific gravity of the measuring fluid was determined at various temperatures by means of specific gravity bottle measurements on evacuated fluid.

Of these three fluids (see Table 7.4), kerosine was chosen as the standard fluid for density measurements. Water was not a satisfactory measuring fluid for small samples in that small air bubbles often collected unnoticed on the suspending wire or sample. This lowered the suspended weight and also the saturated weight was difficult to determine accurately due to errors produced by surface drying techniques. Toluene was a good fluid for penetrating the pores of the sample and not producing air bubbles on the suspended sample but the evaporation rate was too high for precise measurements. Kerosine was most satisfactory and no problems with its use were encountered.

7.5.3. Grain Growth

Grain growth of samples was determined on polished sections which had been mounted in diallyl phthalate and etched in boiling phosphoric acid. Grain size determinations were made by the intersecting line technique. No fewer than 100 grains were measured for each determination. Polishing was accomplished by wet grinding on successively finer grades of silicon carbide paper to 600 mesh then polishing on a 4-6 micron diamond lap.

7.6. Physical Property Measurements

The amount of work involved in other aspects of this project made it necessary to be selective in the range of physical property testing undertaken. Originally it was planned to complete a full range of physical property tests on fuel elements after a simulated 5 per cent and 10% burn-up; however, the simulation work and analysis of phase development in the complicated system was more involved than originally expected.

The properties which were determined are discussed in the following sections.

7.6.1. Microhardness Determinations

Strength measurements by the diametral compression test were conducted on some samples using a type TT-O 89 KN Instron mechanical testing machine. However, the variation in the data made comparison of strengths between different types of specimen impossible. Vickers hardness tests on samples, however, gave much more reliable data and permitted a comparison of samples receiving different treatments. Hardness tests were conducted on a "Miniload" Leitz hardness tester. The hardness value was based on an average of four indentations per sample.

7.6.2. Thermal Conductivity Determinations

Apparent thermal diffusivity measurements were conducted on selected specimens using a carbon arc flash device which was constructed by the Australian Atomic Energy Commission. The temperature rise rate of the sample side opposite the flash is measured from the time of the flash. From the diffusivity determinations the thermal conductivity was determined by the equation

$$K = \alpha Cp\rho \quad ; \quad K = \text{Thermal conductivity}$$

$$\alpha = \text{Thermal diffusivity}$$

$$Cp = \text{heat capacity}$$

$$\rho = \text{density}$$

The results from the preliminary work were disappointing due mainly to the high thermal contact resistance and the uneven energy distribution across the face of the sample disc. In view of these problems further planned work on thermal conductivity of the samples was discontinued.

7.6.3. Electrical Conductivity Measurements

It is known that ThO_2, like ZrO_2, may become an electrical conductor at high temperatures. Electrical conductivity measurements of ThO_2 and of ThO_2 plus typical fission product oxides were conducted as a function of temperature and atmosphere under D.C. conditions. A Keithley type 610 B Electrometer was used to determine the conductivity. Sample discs were polished on each face and electroded with platinum paste which was fired at 600°C. The conductivity was measured by the two terminal method. The intention was to produce conductivity data which could be correlated with the type and degree of crystal defect of the particular ThO_2 fission product system. In all cases, oxygen vacancies were expected as the

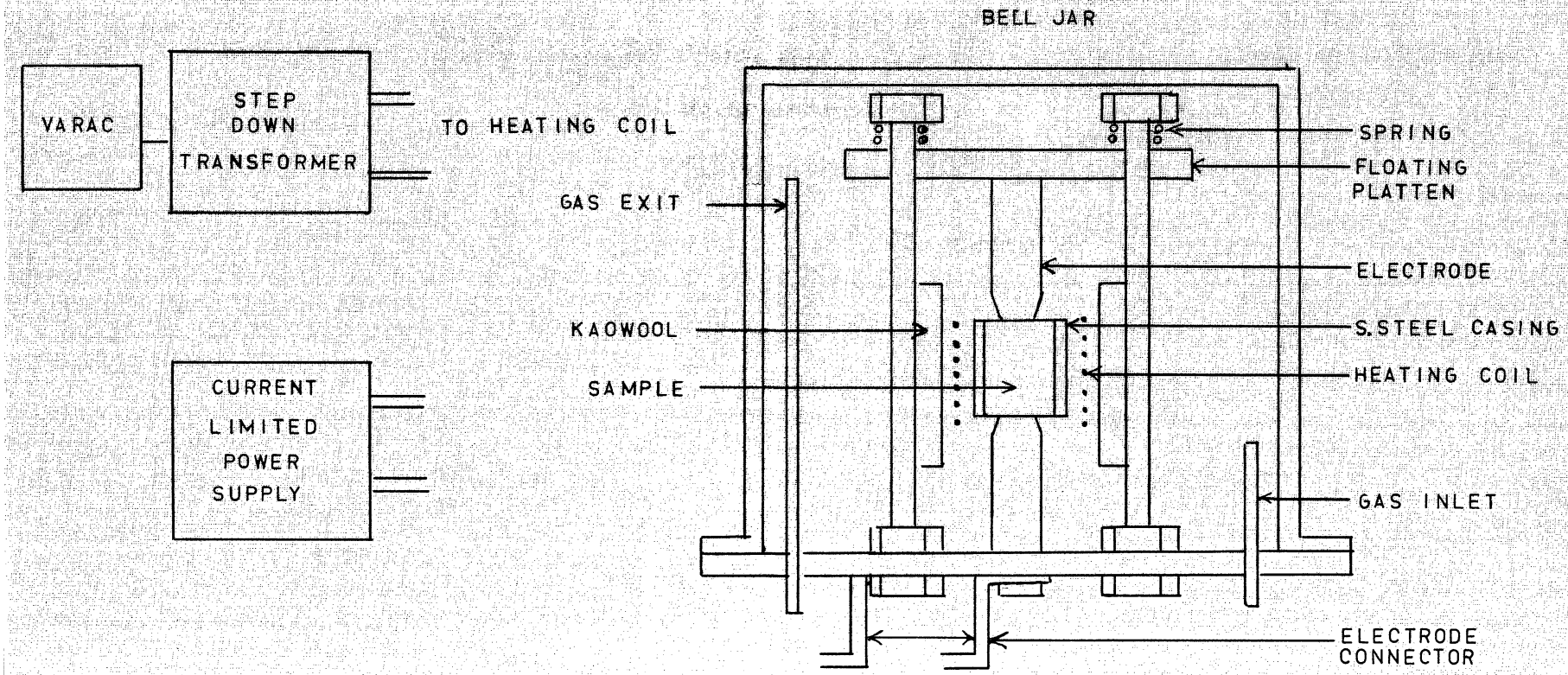

FIGURE 7.9
THERMAL GRADIENT RIG

major conductivity carrier. Under reducing conditions, the temperature versus conductivity plot was limited to 1000°C.

7.7. High Thermal Gradient Development

The study of the simulation of a fuel element would not be complete without considering the effect that a high thermal gradient has on a fuel element. The approach that was used in this work was to induce heating of the ThO_2 based samples by electrical conduction. This heating method allows a temperature build-up in the centre of the sample while the outside may be cooled. Temperatures sufficient to melt the centre of the ThO_2 based fuel elements were achieved. The microstructure of these elements as well as phase formation after the treatment have been studied.

7.7.1. Thermal Gradient Rig

The thermal gradient rig shown in Figure 7.9 consists of two electrodes which were spring loaded, an external heating coil to raise the temperature of the sample sufficiently to begin self conduction, and a glass enclosure to permit atmosphere control. Both D.C. and A.C. conduction were used, since the conductivity of ceramic conductors generally increases with temperature, it was necessary to use current limiting devices with the ThO_2 element. The D.C. current controller was a BWD type 245 dual transistor power supply. The A.C. current limits consisted of a series circuit of the sample and an external variable power resistor. The power resistor and the sample had reciprocal conductivity dependence on temperature which controlled the current of the circuit.

7.7.2. Sample Preparation

The thoria samples were fired in an inert atmosphere to produce a dense cylindrical sample. These samples were mounted in a stainless steel ring which held the pellets together during the

thermal gradient run. The mounting was achieved by heating the stainless steel to 1000°C and then pressing it over the thoria sample. The faces of the encased sample were then coated with platinum paste on each end and refired to 600°C. The electroded sample was then set into the thermal gradient rig and purged with the desired atmosphere overnight prior to the thermal gradient run.

CHAPTER VIII

RESULTS AND DISCUSSION

This work was begun to study the feasibility of simulating the conditions after high burn-up in nuclear fuels based on a urania enriched thoria system. Measurements on such a system could provide information which is difficult to obtain on a real fuel because of the intense radioactivity. The work can thus be divided into two broad stages (1) the development of a simulated fuel element in which the distribution and chemical state of the fission products and the microstructure accurately represents the situation in the real fuel element and (2) the measurements of the resulting properties. The greater part of the effort in the work reported here was directed to the first stage.

Briefly the problems associated with simulation of a fuel element after 10 per cent burn-up may be summarized as follows. First, a real fuel element is in constant change, both physically and chemically, and therefore a simulated element only approximates the real system at a specific point in time. Second, the property measurements to be made on a simulated fuel element are only meaningful if they take into account the inhomogeneity of the real fuel system. For example, thermal conductivity may be obtained for a homogeneous sample of a specific grain size, porosity and of constant chemical composition; however, across the diameter of a real fuel element at least three distinct zones of grain size with differing porosity are known to exist. In addition to the microstructural changes, macrostructural defects exist such as radial and circumferential cracks, which are developed under the specific conditions of high thermal gradient and physical confinement. In addition to these physical effects, the distribution of chemical

species changes substantially across the diameter of fuel element. A simulation of the various actions of the fuel by isothermal heat treatment was envisaged which would allow property measurements and an approximate profile of a real fuel to be made; however, some sections of a fuel only develops under the influence of a thermal gradient, e.g. the columnar grain region near the centre of the fuel pin.

Third, the concentration of fission products in a fuel after even high burn-up is relatively small, approximately 7.5 weight per cent for a 10 per cent burn-up, and the number of fission products is relatively large, approximately twenty chemical species make up 99 per cent of the normal fission products, which makes study of chemical changes in the fuel extremely difficult.

The aims of this work may be broadly summarized as:

(1) To determine the influence of typical fission products on the physical and structural character of thoria.

(2) To assemble these typical fission products with thoria and determine stable phases which develop in the composite sample.

(3) To relate these effects to the findings made on other simulated and real fuel elements.

The presentation has been divided into four sections which are:-

8.1. Characterization of Powders

The reactivity of ceramic powders is greatly dependent on their particle size and size distribution and, hence, on their surface area. It is therefore obvious that a knowledge of the starting powders used is necessary to relate studies of sintering, solid state reaction, and phase formation to each other where these studies are conducted separately. In a later section, the importance of this knowledge will be demonstrated by results on simulated fuel elements. Since the powders used in this work were, for the most part prepared from chemical precipitates, information about them will cover decomposition of the precipitated oxalate, X-ray identification of the precipitate and the calcined oxide powder, surface area determinations and microscopic studies of particle size.

8.1.1. Decomposition of Oxalates

The actual mechanism of decompositions of oxalates appears to be greatly disputed[5,8,9,14]. It is not the purpose of this work to delve deeply into the reactions occurring upon decomposition of oxalates, however a few observations will be pointed out. The observed decompositions of thorium oxalate has been discussed in detail previously in Chapter V and it only needs to be mentioned that conclusive evidence about the formation of intermediate carbonates or the direct decomposition by CO_2 or CO loss is not available since data to indicate both paths exist[5,8,9,14]. It has been observed that the atmosphere above the samples during decomposition affects the results obtained[5,12]. With these facts in mind, thermal decomposition of the thorium oxalate powders was carried out in air using the D.T.A. The first run resulted in exothermic peaks instead of the endothermic peaks reported by previous studies[5,8,9,12,14].

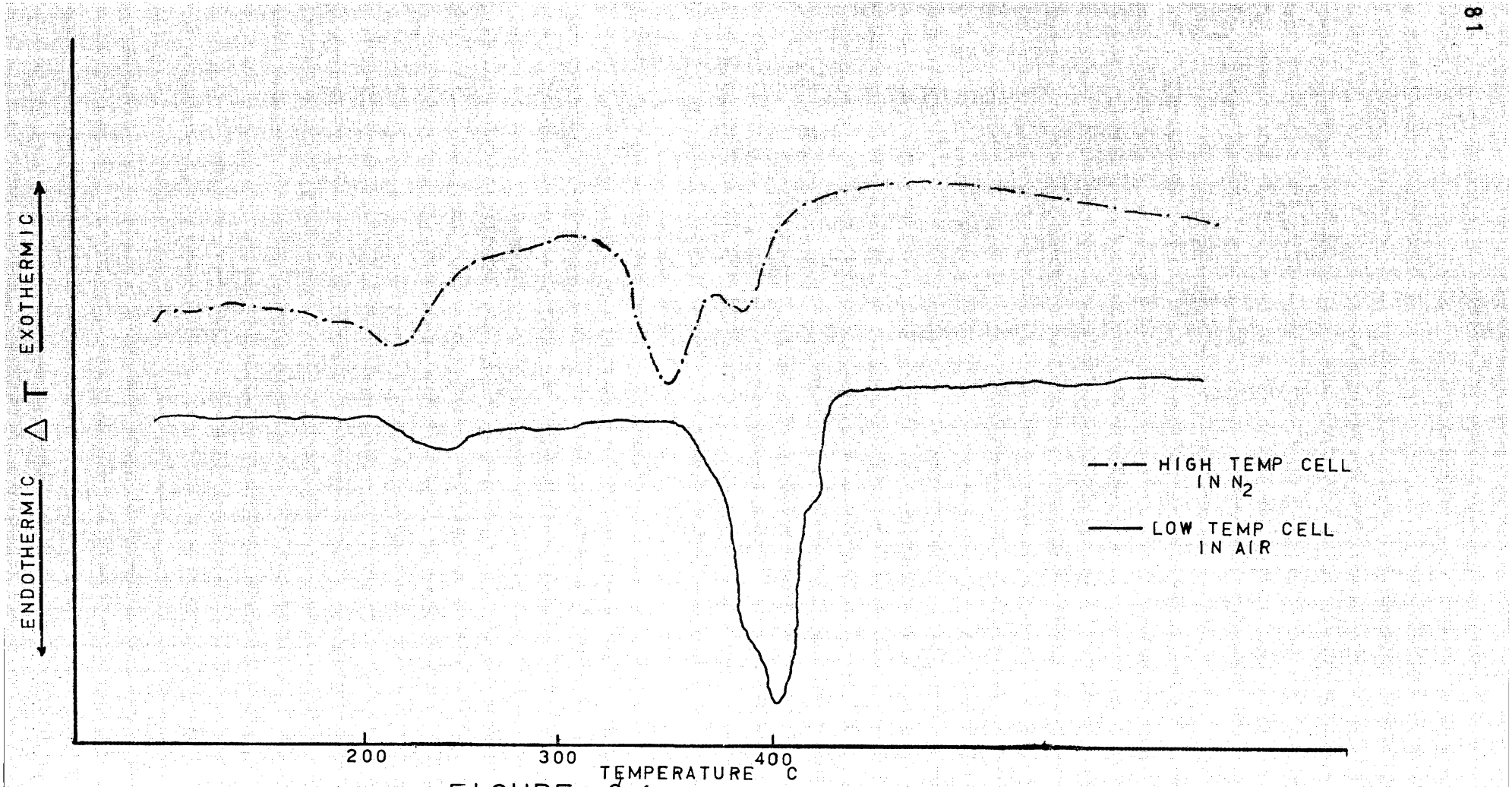

FIGURE 8.1
D.T.A. CURVES FOR THORIUM OXALATE

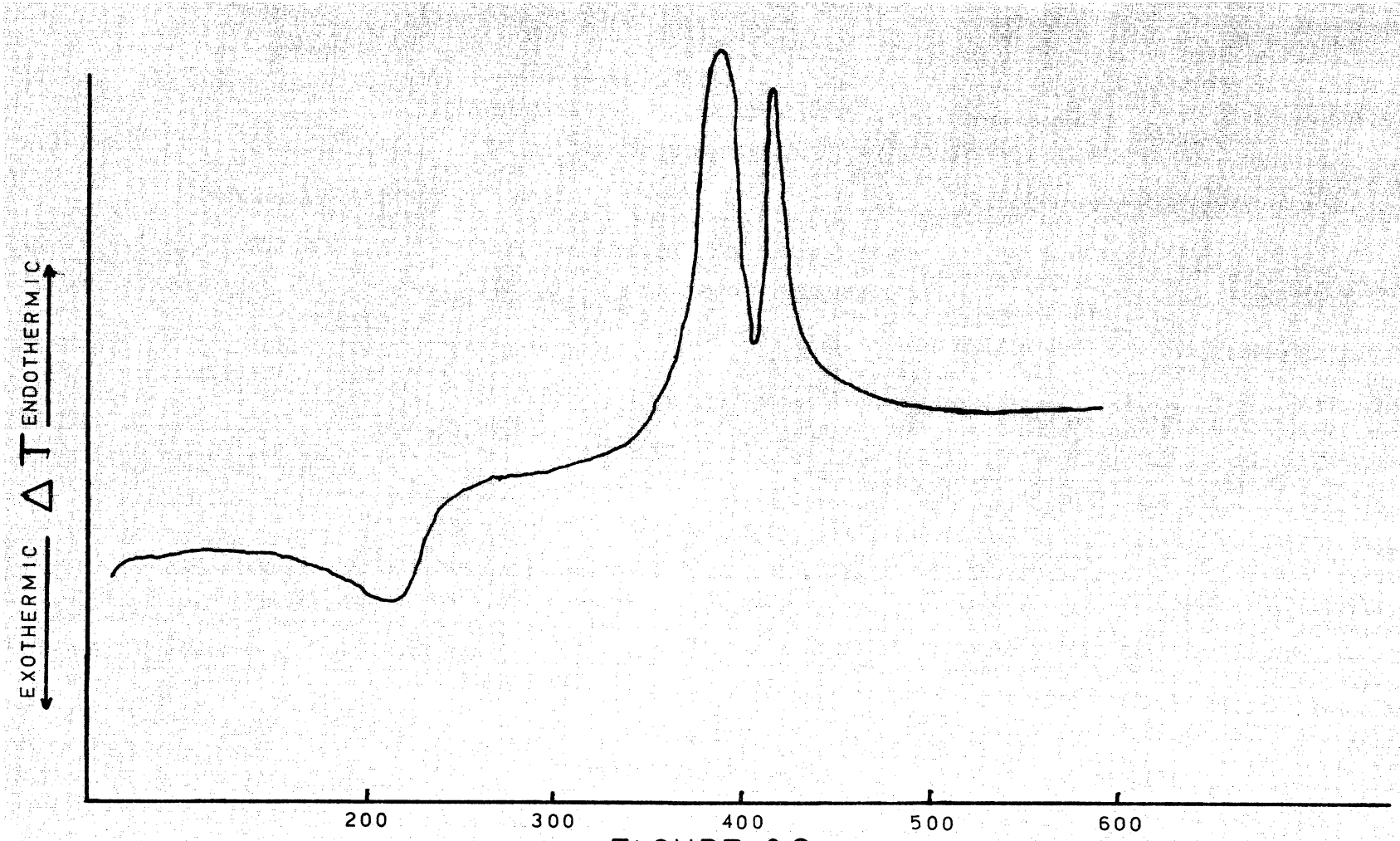

FIGURE 8.2
D.T.A. CURVE FOR THORIUM OXALATE IN HIGH TEMP. CELL IN AIR

Decomposition runs were made using both the high and low temperature cells, and under oxidizing and neutral atmospheres, flowing and still air and nitrogen. The results of these studies are shown in Figures 8.1 and 8.2 and indicate that the conditions under which decomposition occurs significantly affect the results obtained. Figure 8.1 shows the decomposition of thorium oxalate in nitrogen using the high temperature cell and in air using the low temperature cell over the same temperature range. The low temperature cell consists of a silver block in which cylindrical sample holders are embedded. The low temperature cell is generally used for sensitive work where uniform temperature during heat-up is ensured. The runs under nitrogen in the high temperature cell show three endothermic peaks which are similar to those shown in the literature but displaced somewhat from the reported temperatures. The run in air using the low temperature cell also showed one major endothermic peak with two depressions which may be small endothermic peaks. Apparently the geometry of the low temperature sample holder restricted the access of air to the sample.

In Figure 8.2 using the high temperature cell under an atmosphere of air one endothermic peak and two exothermic peaks are clearly shown. The low temperature endothermic peak, 225°C, corresponds to the water loss reaction; the exothermic peaks correspond to oxidation reactions. In one run in air a very small depression just prior to the first exothermic peak was observed which may, in fact, be an endothermic peak indicating an initial step in the decomposition prior to oxidation. Srivastava[11] suggested a complicated decomposition probably involving intermediate carbonates, however in view of the discrepancy between the exothermic peaks found in the present work and the endothermic peaks reported for decomposition in air by Srivastava, the suggested steps of the

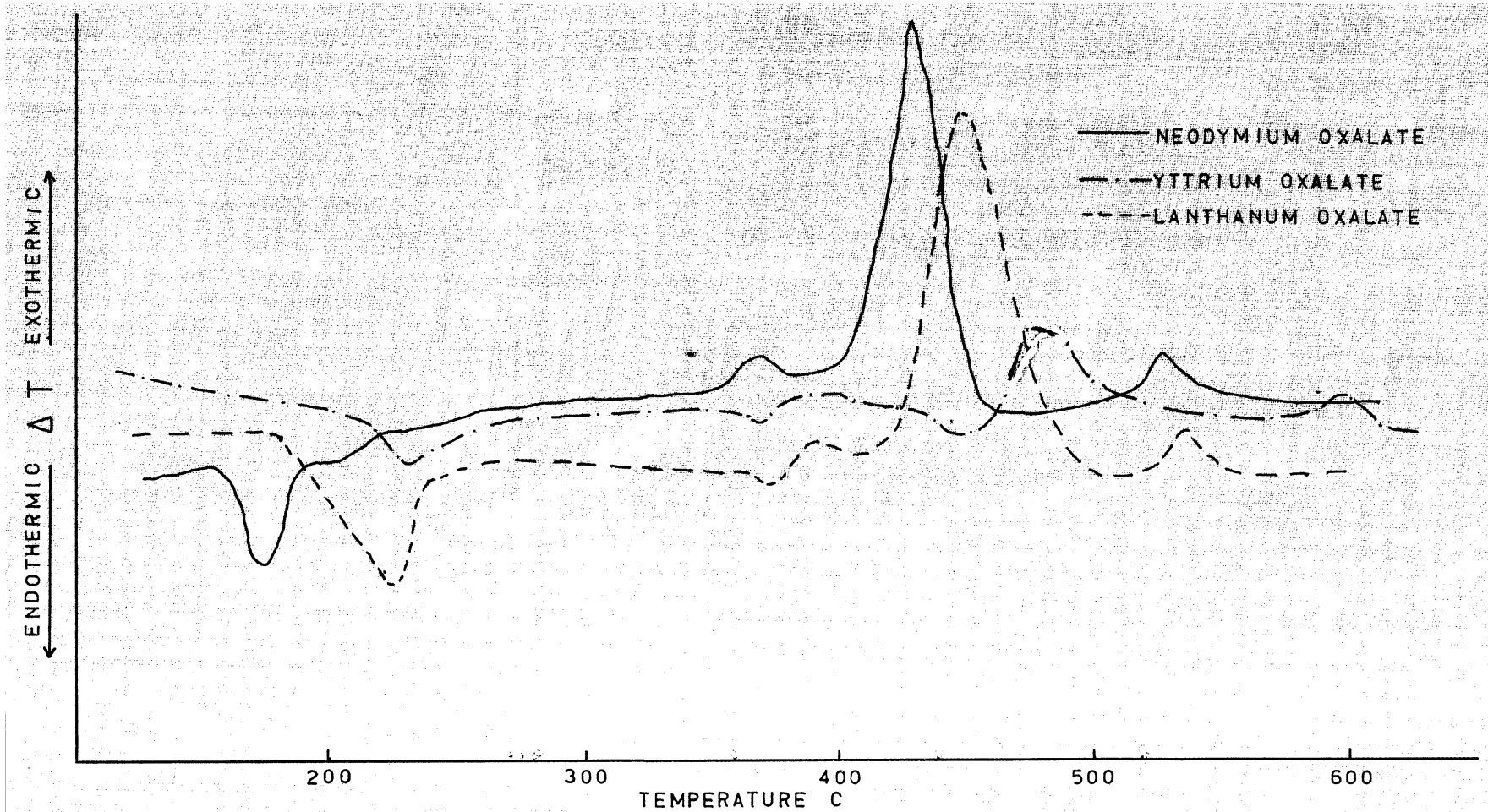

FIGURE 8.3

D.T.A. CURVES FOR Nd, Y, La OXALATES IN HIGH TEMP. CELL IN AIR

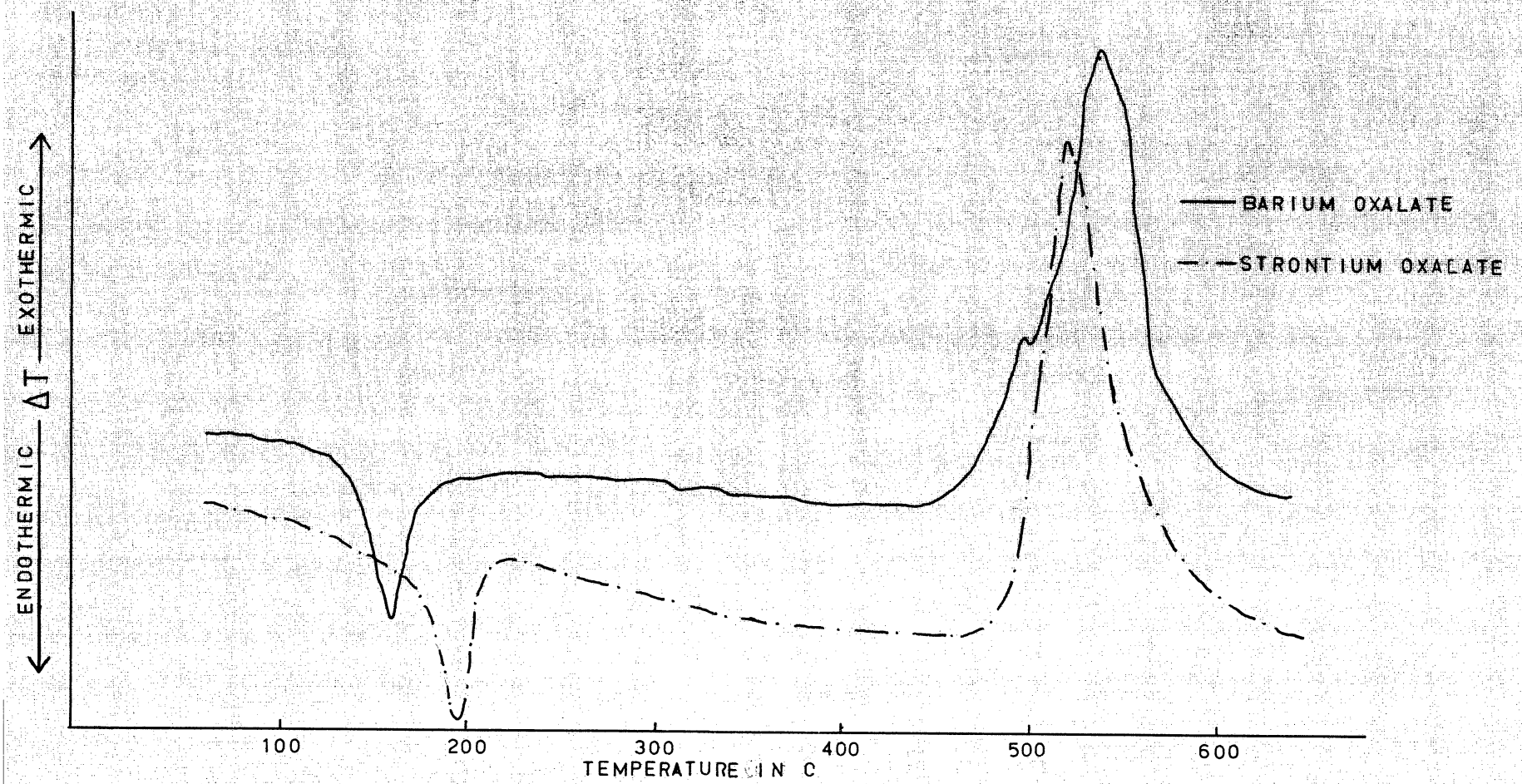

FIGURE 8.4

DTA CURVES FOR Ba,Sr OXALATES IN HIGH TEMP. CELL IN AIR

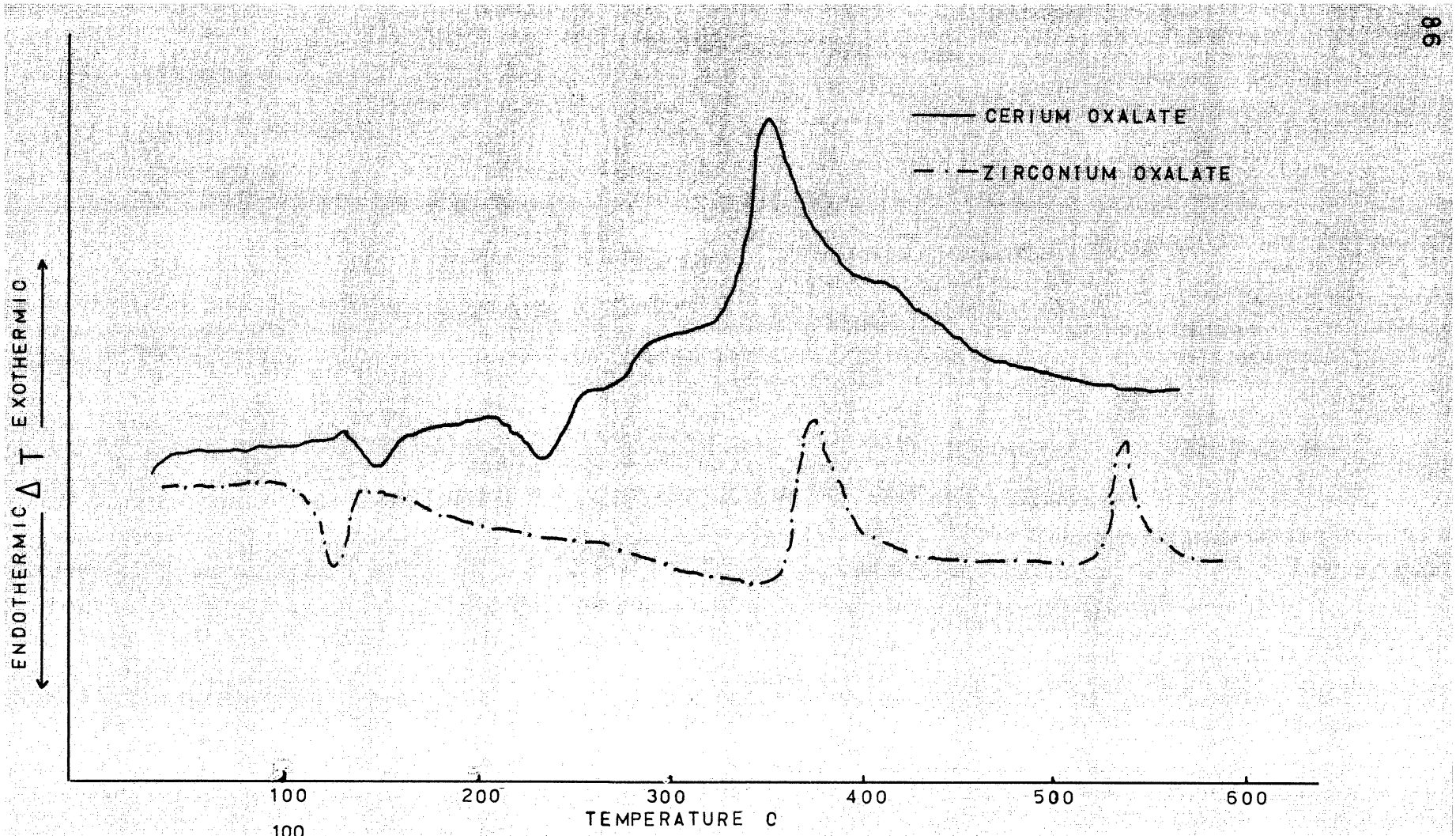

FIGURE 8.5

D.T.A. CURVES FOR Zr, Ce OXALATES IN HIGH TEMP CELL IN AIR

decomposition are questioned. It is apparent that the decomposition studies on thorium oxalate in air showing no exothermic peaks were simply made on samples which were not effectively oxidized. That the sample holder or sample preparation may affect the results of decomposition is clearly shown by the D.T.A. run mentioned above, comparing results from the low temperature cell and high temperature cell. Whether or not the decomposition takes place through intermediate carbonates or directly through CO_2 and CO loss is a question which needs further investigation but is not within the scope of this work. What is important, however, is that the oxalate is completely decomposed by 450°C.

Decomposition of the oxalates of typical fission product oxides were carried out as part of the characterization of powders. These decomposition runs are shown in Figures 8.3, 8.4 and 8.5. All of the oxalates characteristically have a low temperature endotherm indicating water loss which occurs between 130°C to 240°C. The oxalates have been divided into three categories, those of trivalent cations, divalent cations and tetravalent cations. This classification appears generally a good one in view of the similarity of the decomposition curves of the respective oxalates. The oxalates of the first type all appeared to have three exothermic peaks. For neodymium, the major peak occurs at 430° while, for yttrium, it occurs at 465°C and for lanthanum at 446°C. Strontium and barium oxalates both had a well defined endothermic peak at 199°C and 167°C, respectively. Strontium had one major peak at 520°C while barium appeared to have a doublet peak with the major peak occurring at 528°C. Zirconium oxalate is characterized by two exothermic peaks occurring at 377°C and 528°C, while cerium appeared to have only one exothermic peak occurring at 361°C and two small endothermic

peaks at 145°C and 239°C. These results indicate that the decomposition of the oxalates should be relatively simple reactions involving loss of water of hydration and oxidation reactions. Where the oxidation reactions probably involve the oxidation of carbon or CO, thermal gravimetric analysis may be useful in determination of the actual reaction or reactions involved.

8.1.2. Surface Area Measurement

Surface area determinations were made using the B.E.T. method of nitrogen adsorption to correlate with the microscopic analysis of the oxide powders. Plots of the surface area data yielded excellent straight lines and the results are set out in Table 8.1.

TABLE 8.1

Surface Area of Fission Product Powders after Calcination of the Oxalate at 600°C

	Specific Surface m^2/g	Correlation Coefficient
$BaCO_3$	2.43	.9937
$SrCO_3$	0.64	.9998
ZrO_2	13.63	.9999
CeO_2	20.88	.9999
Y_2O_3	8.53	.9999
La_2O_3	17.55	.9999
Nd_2O_3	13.15	.9999
MoO_2	8.36	.9999

As described previously, samples were thoroughly baked out prior to the actual adsorption run. Moorehead[5] has shown that outgassing temperatures up to 400°C for one hour are effective for cleaning the powders surface but, above 400°C, sintering commences which tends to lower the surface area of the powder. To prevent the sintering effect, lower temperatures and longer times were used

for outgassing. The value of surface area for thoria was found to be 26.98 m^2/g immediately after calcination at 600°C for one hour which compared to the value 22.3 m^2/g obtained by Moorehead[5] and 26 m^2/g by other workers[13,94]. Assuming that the particles of thoria are in the shape of square plates having an edge to thickness ratio of 10 to 1, an approximate size may be calculated by the following equation:-

$$S = \frac{2.4\ D^2}{0.1\ D^3 \rho} \qquad (8.1)$$

where S = specific surface in m^2/g

D = edge length in 10^{-3} mm

ρ = density in g/ml

Based on equation 8.1 this thoria powder should have an edge length of approximately 0.09 microns. During this work it was noted that densities obtained on firing thoria pellets from a known source dropped with storing age of the powder. It was felt at the time that chemisorbed gases, especially CO_2, could account for the decrease in sintering. As shown previously, CO_2 has been known to remain on powders up to 800°C which, in the case of thoria that begins sintering at temperatures as low as 400°C, would impede the initial stage of sintering with the result of lowering the ultimate bulk density which can be obtained. Table 8.2 shows the specific surface of ThO_2 after exposure to CO_2 for various times.

TABLE 8.2

Effect of CO_2 Adsorption on Surface Area of Thoria

Run	Hours exposed to CO_2	Specific Surface m^2/g	Correlation Coefficient
1	0	26.98	.9998
2	24	24.34	.9999
3	48	24.93	.9998
4	72	24.92	.9999

After the first surface area determination, the sample was baked-out at 120°C for 24 hours under vacuum; after the second run, the bake-out temperature was increased to 250°C. Further increase in bake-out temperature below 400°C had no effect. Obviously, a decrease in the surface area of approximately 2 m^2/g is significant representing 7.5 per cent. However, since this decrease in surface area is associated with the presence of a tenaciously adsorbed layer of CO_2, the reactivity of the particles is probably affected much more than would normally be expected from this change. For example, neck formation between particles and grain growth may be impeded.

8.1.3. Microscopic Characterization of Powders

In order to correlate the surface area determinations to particle morphology, scanning electron microscopy was used. Samples of the powders were prepared as described previously and photographed under high magnification. The following figures show each oxalate and the respective oxide after calcination at 600°C. By using the observed particle shape of the calcined powder, the observed size may be correlated to the surface area determined by nitrogen adsorption. The calculated values of particle size by surface area and micrographs are shown in Table 8.3.

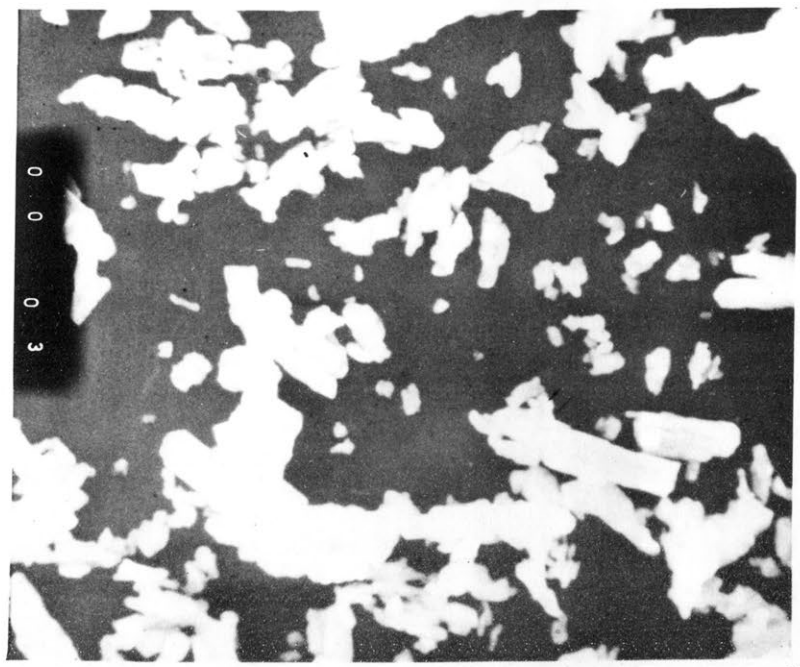

(A)

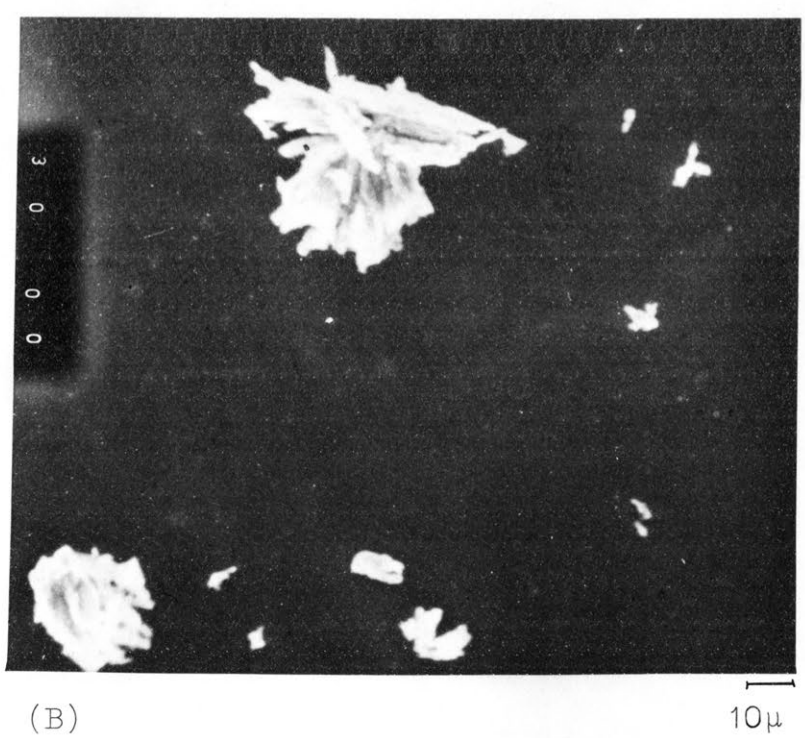

(B)

Figure 8.6. Scanning Electron Micrographs of
(A) Barium Oxalate
(B) Barium Carbonate

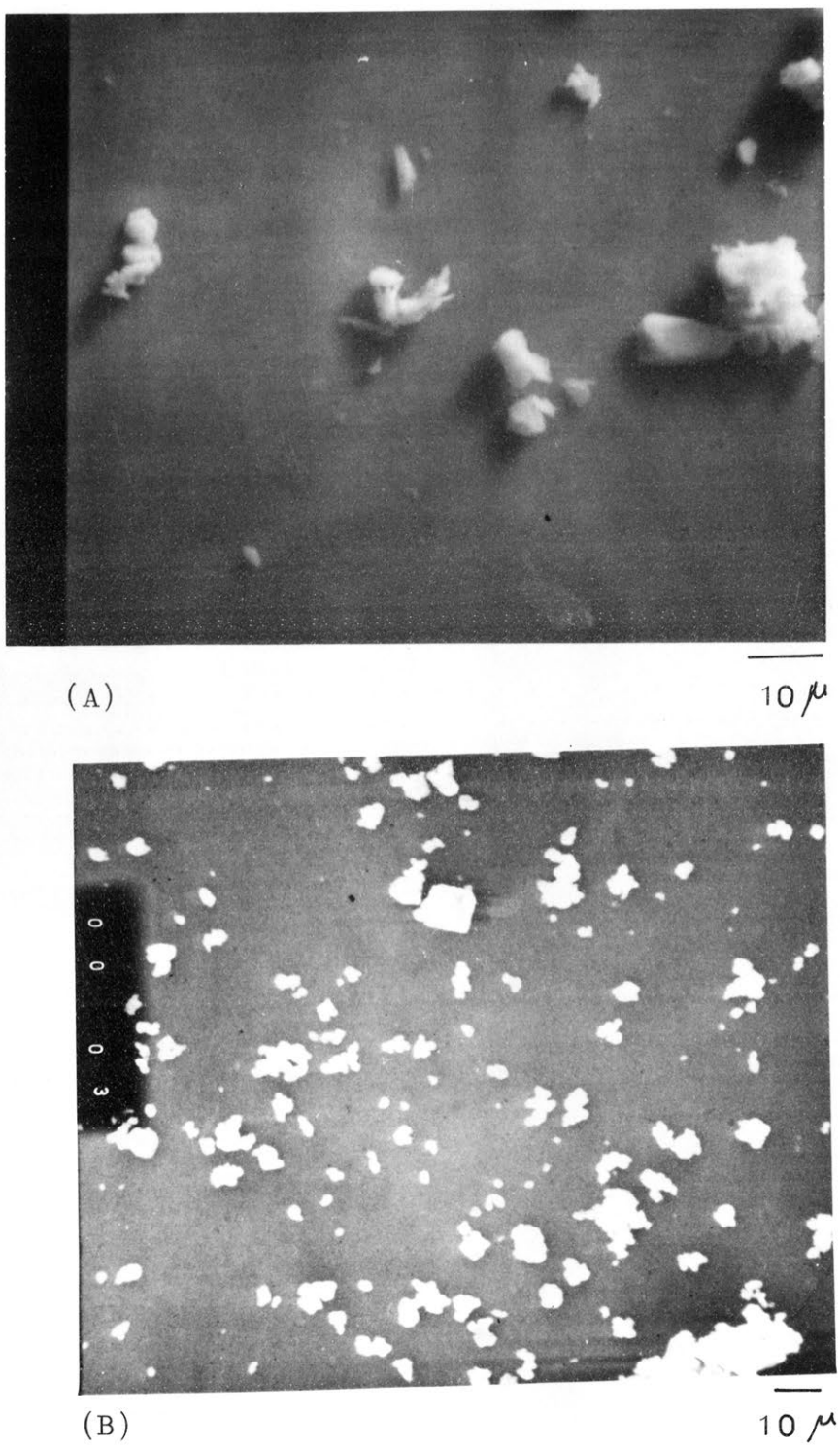

Figure 8.7. Scanner Electron Micrographs o:

(A) Strontium Oxalate

(B) Strontium Carbonate

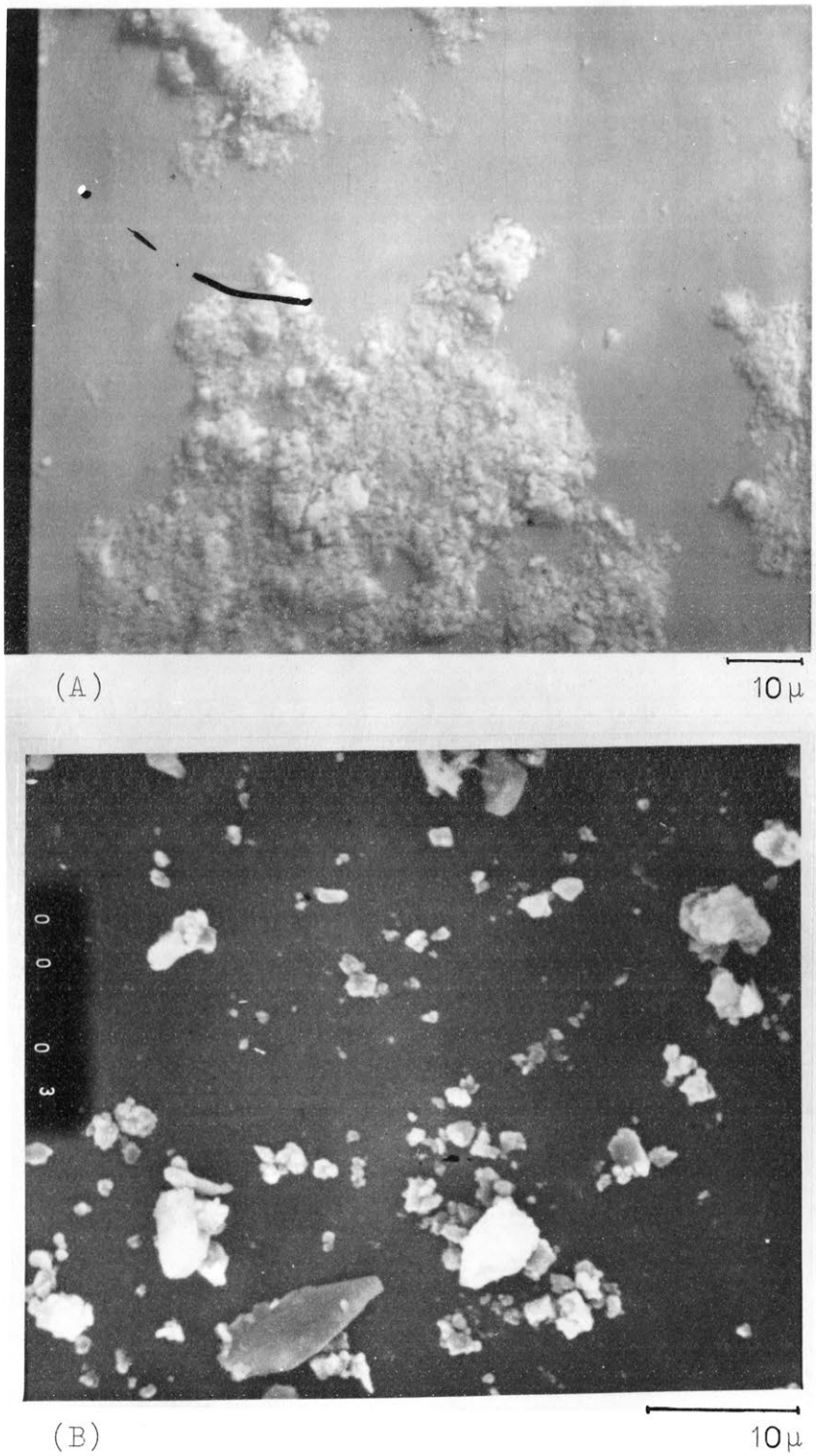

Figure 8.8. Scanning Electron Micrographs of
(A) Yttrium Oxalate
(B) Yttrium Oxide

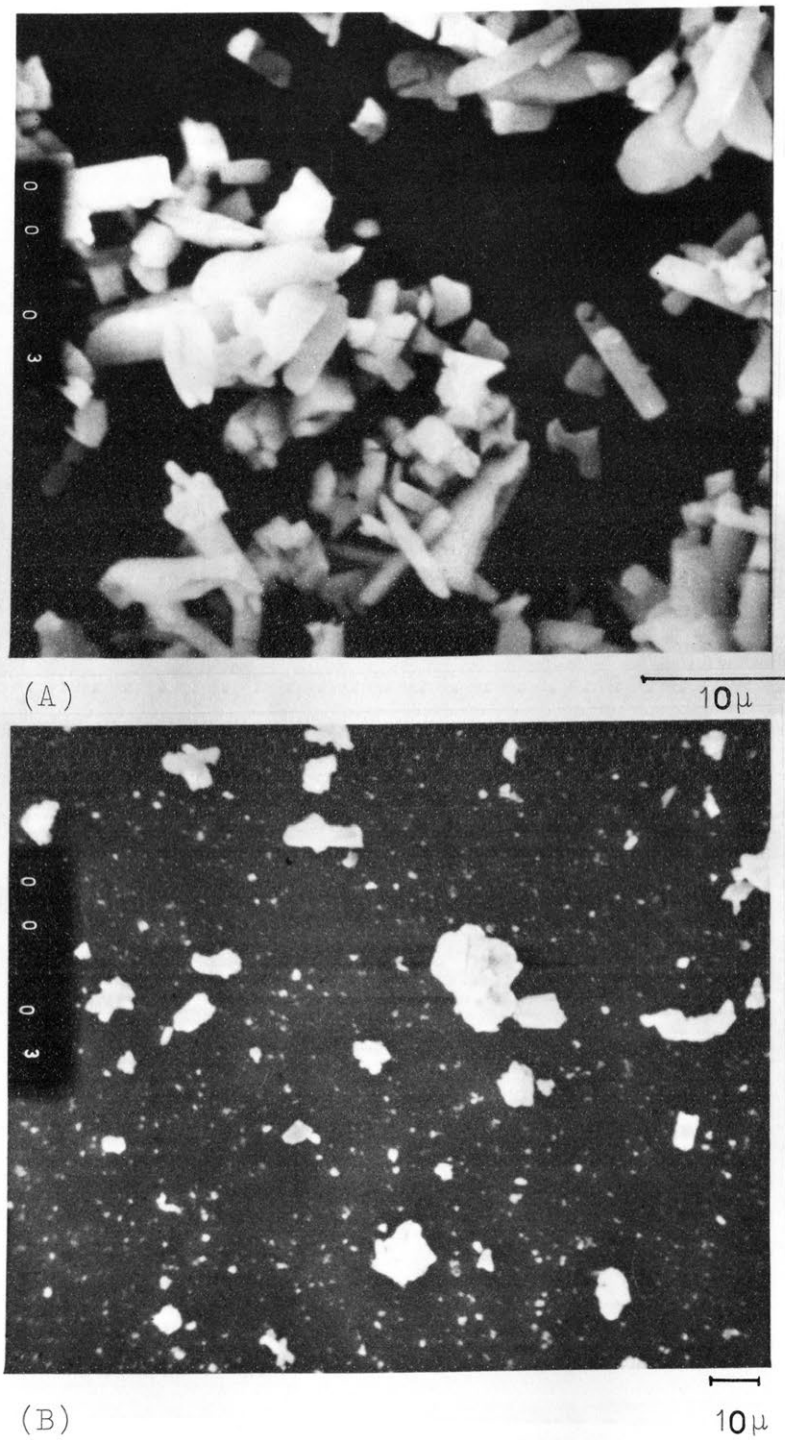

Figure 8.9. Scanning Electron Micrographs of
(A) Lanthanum Oxalate
(B) Lanthanum Oxide

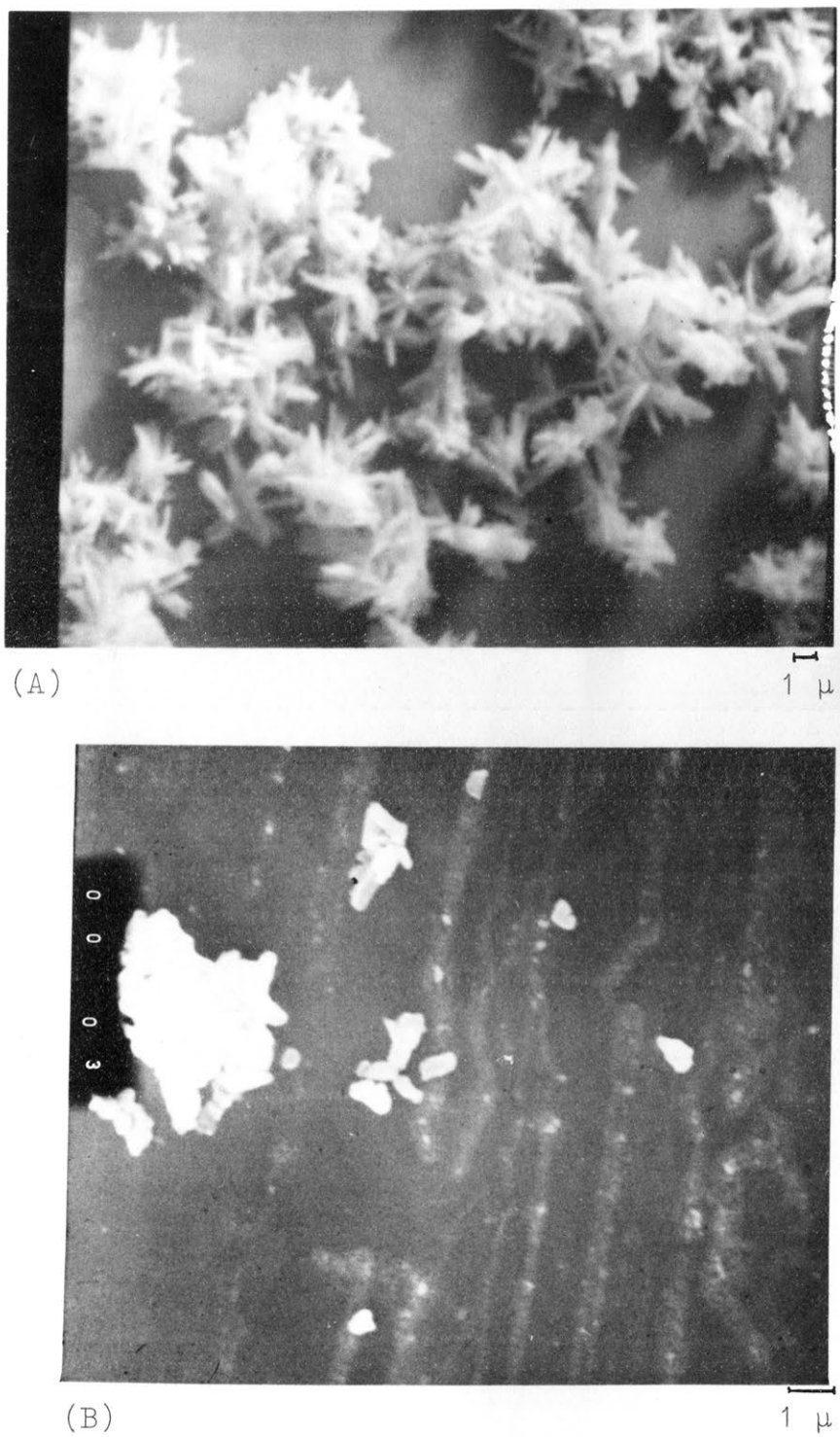

Figure 8.10. Scanning Electron Micrographs of
(A) Neodymium Oxalate
(B) Neodymium Oxide

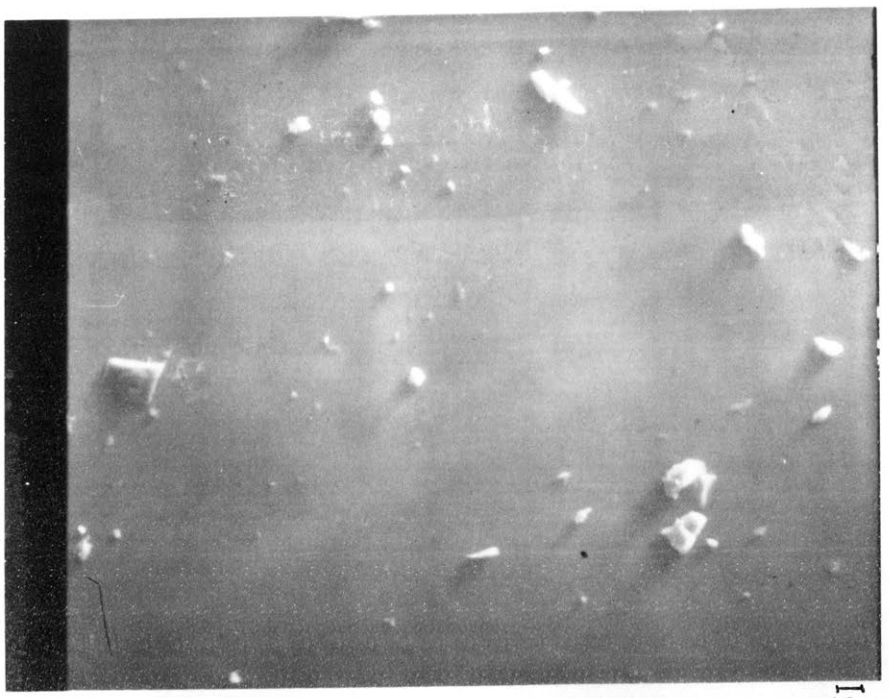

(A) 10 μ

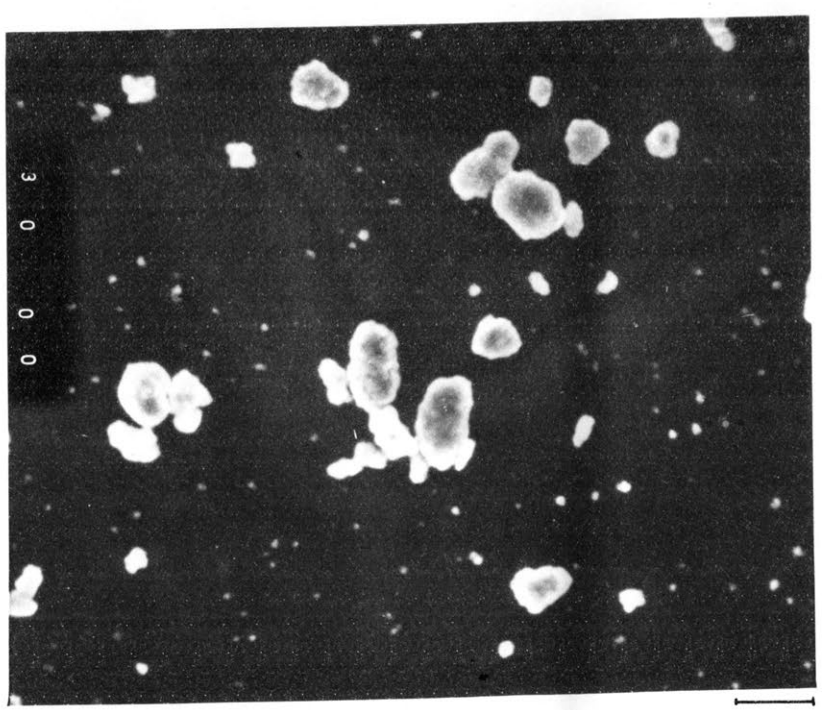

(B) 10 μ

Figure 8.11. Scanning Electron Micrographs of

(A) Zirconium Oxalate

(B) Zirconium Oxide

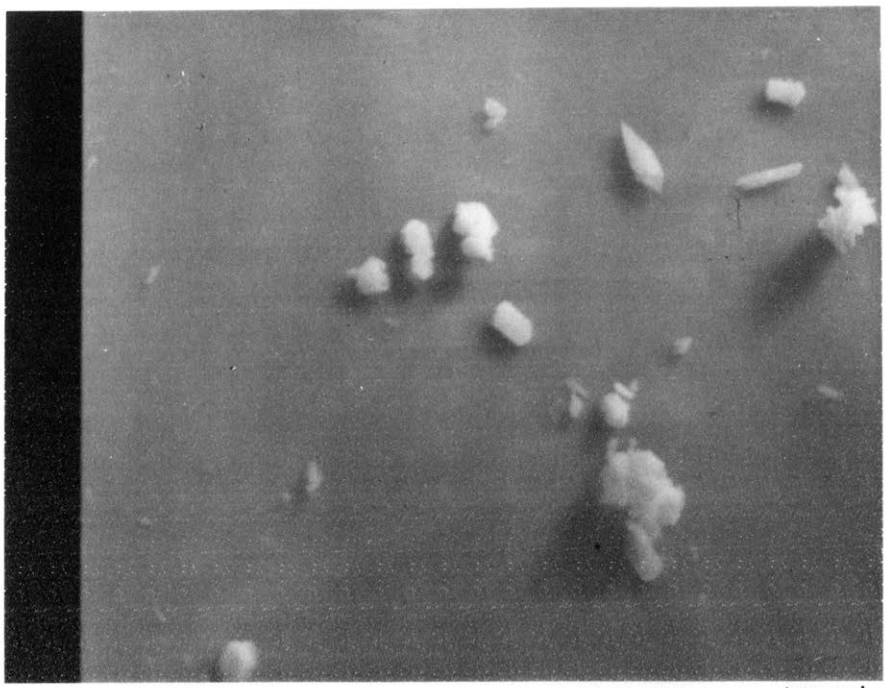

(A)

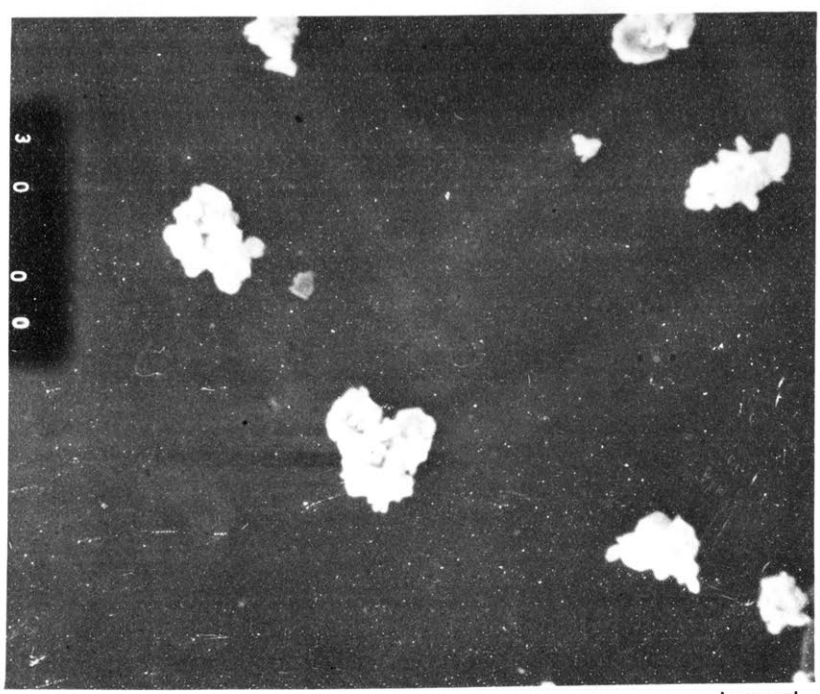

(B)

Figure 8.12. Scanning Electron Micrographs of

(A) Cerium Oxalate

(B) Cerium Oxide

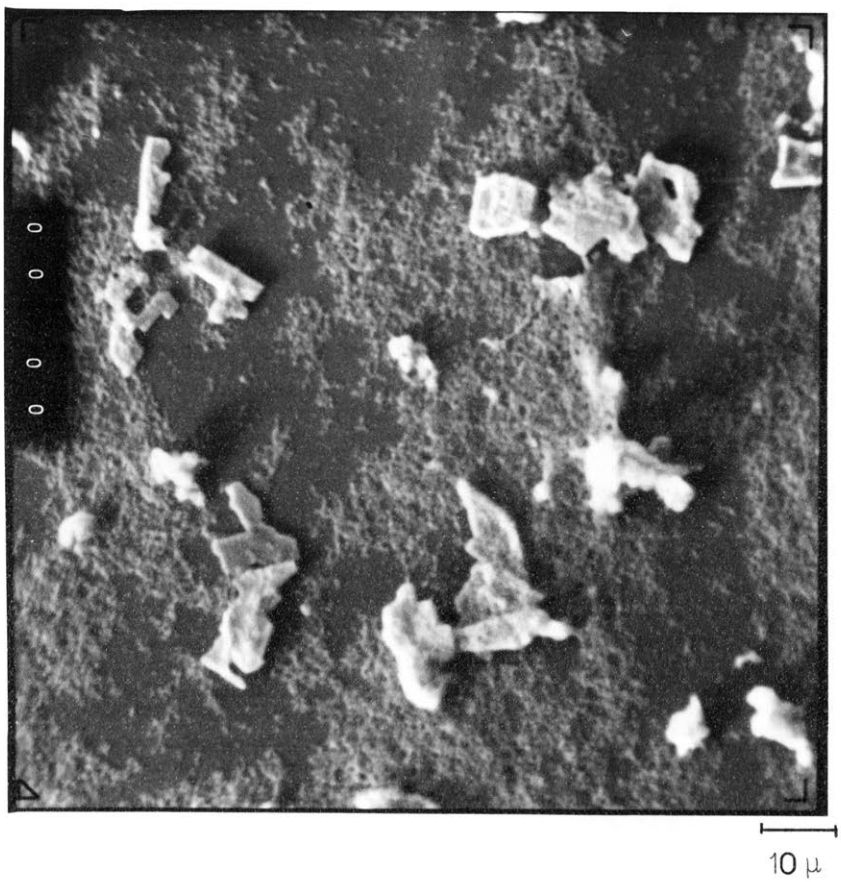

Figure 8.13. Scanning Electron Micrographs of MoO_2

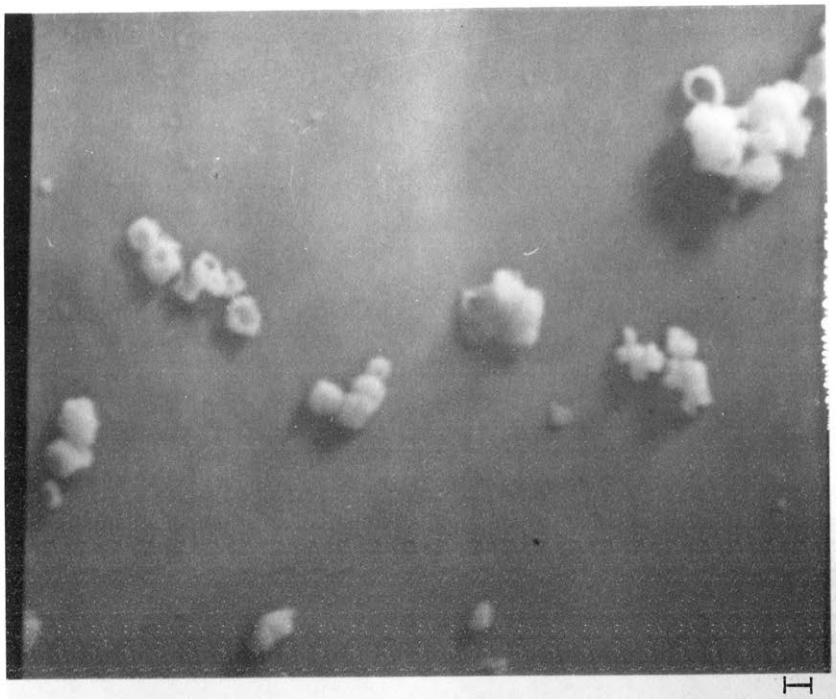

(A) 1 μ

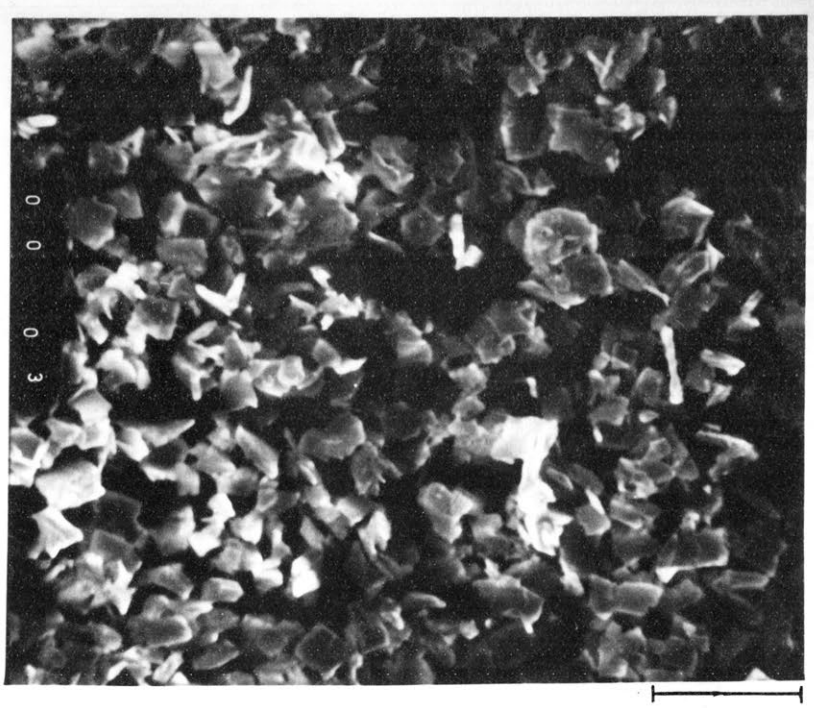

(B) 1 μ

Figure 8.14. Scanning Electron Micrographs of

(A) Thorium Oxalate

(B) Thorium Oxide

TABLE 8.3

Correlation Between Particle Size Determined from B.E.T. and S.E.M.

Powder	Based on B.E.T. Surface Area		Based on Scanning Electron Microscopy in Micrometers
	Equivalent Spherical Diameter in micrometers	Equivalent Plate Edge Length in Micrometers	
$BaCO_3$	0.557	2.229	0.7-50.0
$SrCO_3$	1.995	7.979	1.0-20.0
Y_2O_3	0.140	0.562	0.2-6.5
La_2O_3	0.053	0.210	0.3-23.3
Nd_2O_3	0.063	0.252	0.2-1.7
ZrO_2	0.079	0.314	0.2-10.0
CeO_2	0.040	0.161	1.0-14.0
MoO_2	0.111	0.444	2.0-10.0
ThO_2	-	0.089	0.1-0.3

Not all of the oxalates nor the calcined products had a well defined shape or size. Moorehead[5] had shown that the thorium oxide which is formed upon decomposition occurs in a relic of the oxalate. Of the additional oxides studied in this work only cerium appeared to have this behaviour and, even then, it is not as pronounced as for thorium. Since the size of particles for these powders was not uniform, an observed particle size range is given for the microscopic examination. The size of the particle determined from surface area measurements may be found using equation 8.1 or equation 8.2 which is shown below and is the equivalent spherical diameter.

$$D = \frac{6}{S\rho} \qquad (8.2)$$

where S is specific surface, ρ is density.

Since the particle shape may not be defined by either a sphere or platelet, correlation may not necessarily be expected. Correlation between the B.E.T. measurements and microscopically determined size may be considered relatively good for all powders except CeO_2 and MoO_2. Also the assumption of plate-like morphology gave better agreement between the two methods. Thoria was the powder which gave best correlation between the two methods which is undoubtedly due to the uniform size and shape of the powders.

8.2. Microstructure of Sintered ThO_2 Based Compositions

The sintering of thoria has been studied by many workers who have suggested various mechanisms for achieving high density thoria compacts containing small additions of metal oxides. In their study of calcium additions to thoria Jorgensen and Schmidt[29] observed that the density of the compact was much greater than for thoria alone. The suggestion was made[29] that the cause of the increased density is dislocation pinning which thereby prevents exaggerated grain growth from occurring. Other workers proposed[28] that the real reason for the increased sintering was increased oxygen vacancy diffusion produced upon the introduction of the divalent calcium into the tetravalency lattice of thorium. While it was not the ultimate goal of this thesis to answer this question, studies conducted during the work has shed some light on the dilemma. These results will be discussed in the following sections.

8.2.1. The Effect of Oxalate Precipitation Method on Sintered Density of Thoria

The precipitation method used to prepare the oxalate of thorium has an influence on many properties of the resultant powder which, one would expect would, in turn, have an effect on

Acid to Nitrate Ratio

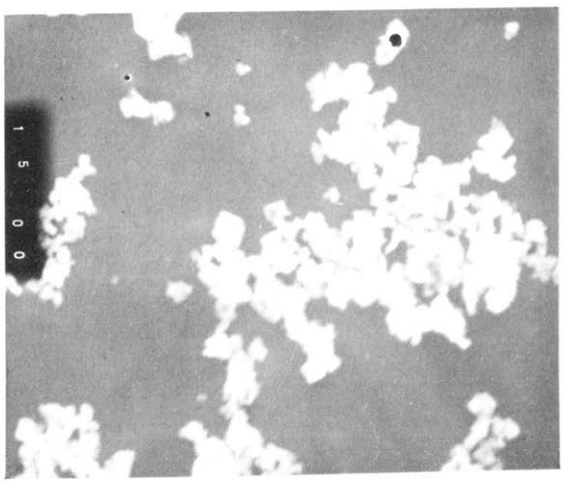

5:4

(A)

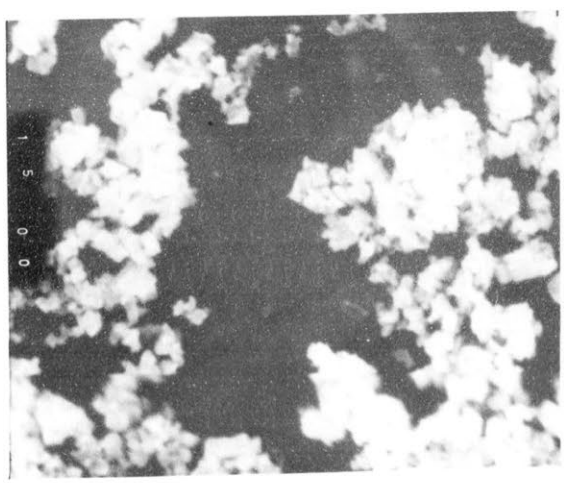

8:4

(B)

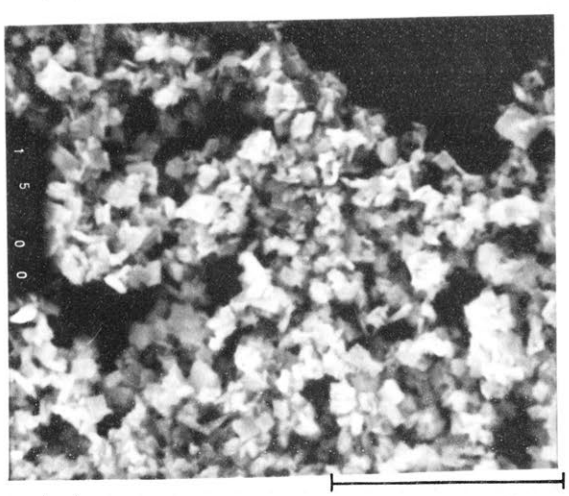

12:4

(C)

Figure 8.15. Scanning Electron Micrographs of Thorium Oxide Derived from the Oxalate Precipitated at 26 C

Acid to Nitrate Ratio

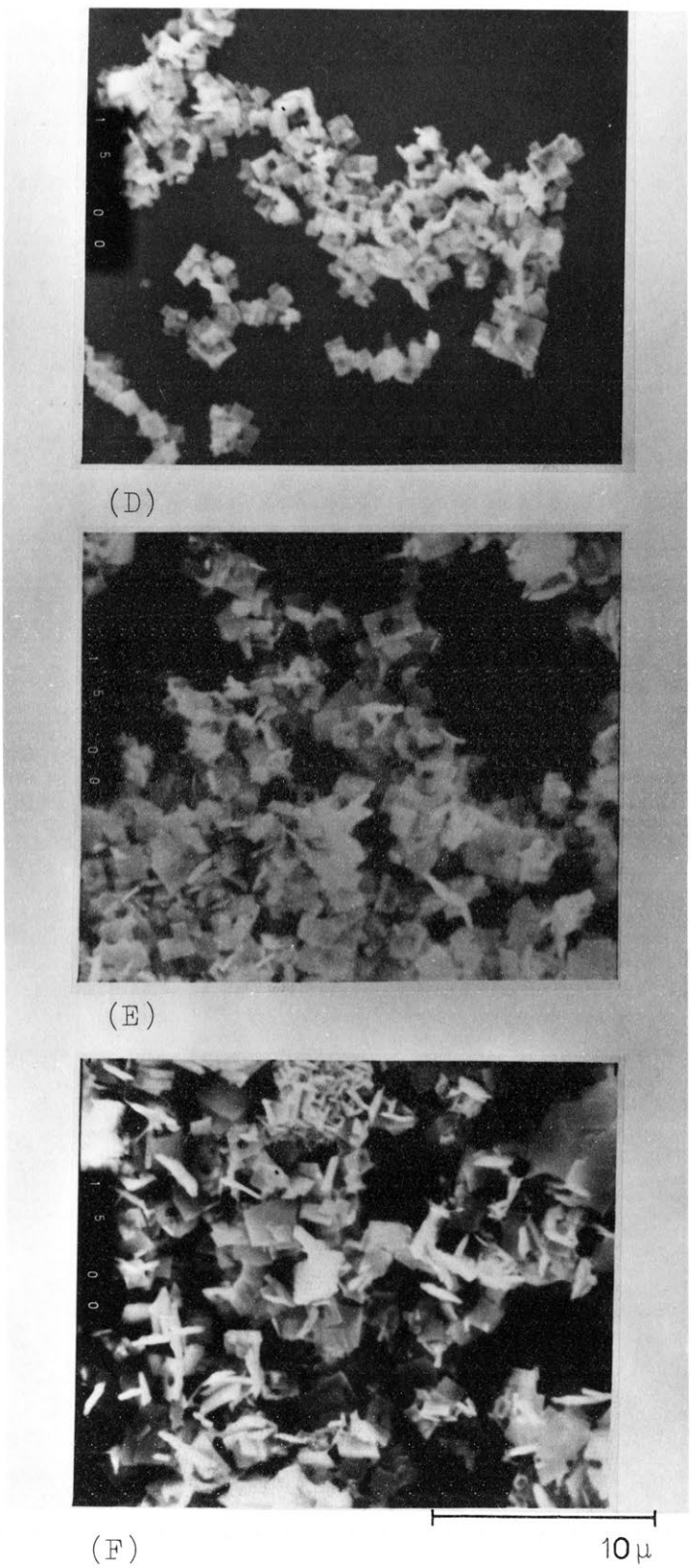

5:4

8:4

12:4

Figure 8.15. Scanning Electron Micrographs of Thorium Oxide Derived from the Oxalate Precipitated at 70 C

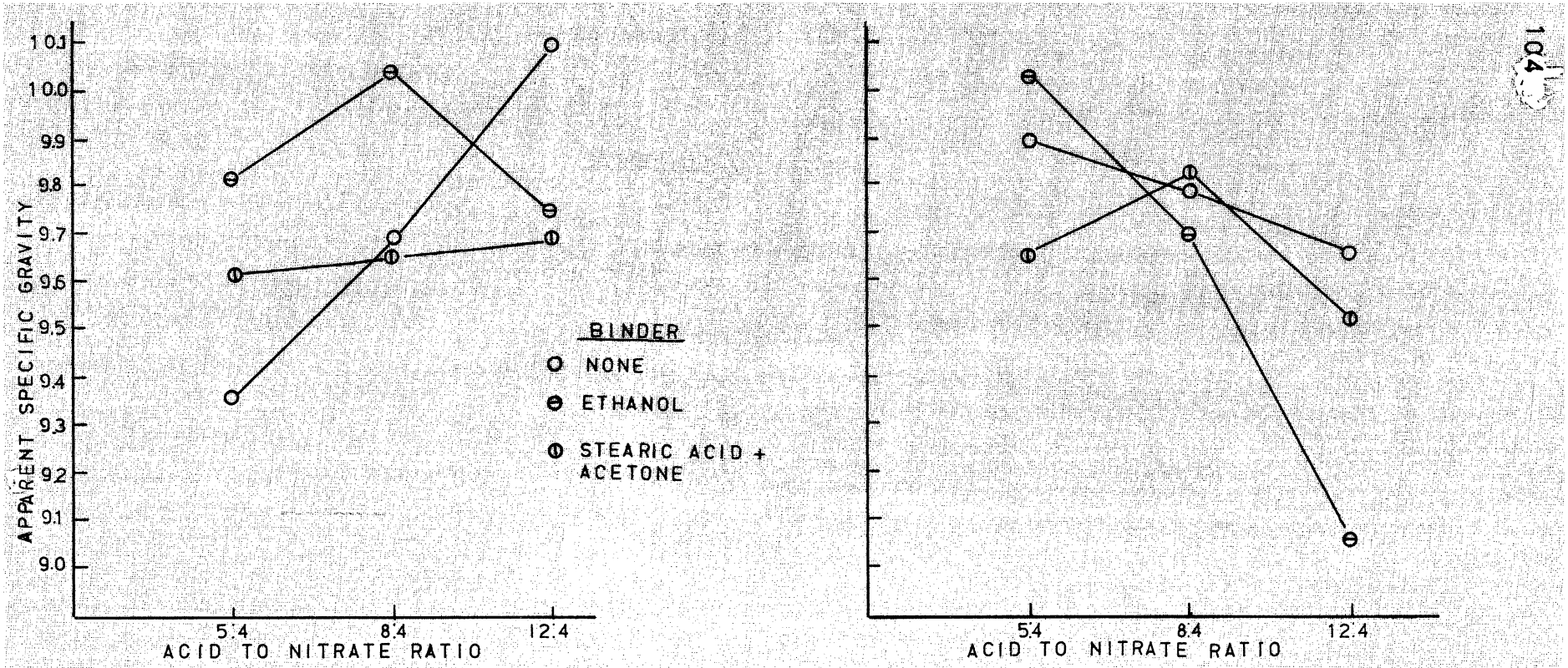

FIGURE 8.16

APPARENT SPECIFIC GRAVITY OF THORIA COMPACTS SINTERED AT 1600 C FOR 8H VS PRECIPITATION CONDITIONS OF THE OXALATE

the sintering rate and, therefore, the final density of the thoria compacts. The two variables in the precipitation of thorium oxalate which were studied, were the temperature and pH of the precipitating solutions. Previous work[5] has suggested that a molar ratio of 5 to 4 of oxalic acid to thorium nitrate produces well defined and formed thorium oxalate of fairly large size. This ratio, however, is not large enough to precipitate all of the thorium in solution. The pH should therefore affect first the particle size. It has also been shown that the size of thorium oxalate crystals tends to decrease with decreasing precipitating temperature so the lower temperature precipitated oxalate should produce a calcine of greater reactivity than that precipitated at a higher temperature. For convenience two temperatures were selected, 70°C and 26°C, and three ratios of oxalic acid to thorium nitrate were used, 5:4, 8:4, 12:4. After the preparation of the precipitate and calcination, pellets were pressed at 76.8 MPa and fired at 1600°C for eight hours. The results of this firing are shown in Table 8.5. The precipitation treatment had a marked effect on the morphology of the thoria powder as seen by the scanning micrographs in Figure 8.15 A through F which show oxide powder derived from oxalates prepared under the six respective conditions. Figures 8.16 A and B show the specific gravity results of these pellets fired using no binding, ethanol and a solution of stearic acid in acetone.

The most notable difference among the precipitations during preparation was the rate of settling of the precipitate. The precipitate made with excess oxalic acid and stoichiometric oxalic acid addition settled within two hours so completely that the supernaught could easily be poured off, while the precipitate of

insufficient oxalic acid was not completely separated after 24 hours. The pH of the precipitate suspension after the addition of the oxalic acid is shown below in Table 8.4.

TABLE 8.4

The Effect of Precipitation Parameters on the Yield and Size of Thorium Oxalate Crystallites

Precipitation Temperature	26°C			70°C		
Moles Oxalic Acid / Moles Thorium Nitrate	5:4	8:4	12:4	5:4	8:4	12:4
pH of Suspension	0.84	0.94	1.35	0.62	0.70	0.95
Yield %	56.5	95.7	100	52.0	93.6	100
Maximum Crystallite Size (μ)	0.25	0.33	0.42	0.5	0.8	1.25

Figures 8.15 A-F show that both the increase in precipitation temperature and the increase of oxalic acid increases the size of the platelets. The apparent specific gravity of the oxides prepared from each precipitate showed that there was an increase with oxalic acid concentration for low temperature precipitation. This trend however, reversed for the high temperature precipitation.

8.2.2. Calcination of Thorium Oxalate

Previously we have shown that the decomposition of the oxalate is affected dramatically by the conditions under which calcination takes place. Because of this a series of calcination treatments was conducted to determine the effect that calcination in air and in oxygen had on the final density of fired pellets. The weight loss was determined on each powder following the calcination treatment in a tube furnace. Table 8.5 shows the results of the study and the treament. Treatment 3 consisted of one

TABLE 8.5

Effect on Calcination Treatment of Th — Oxalate on Fired ThO_2

	Treatment 1	Treatment 2	Treatment 3	Treatment 4
Calcination atmosphere	O_2	Air	O_2	Air
Cool down atmosphere	O_2	Air	Air	Air
Temperature °C	600	600	600	700
Time hours	1	1	1	1
Weight loss %	39.9	40.3	40.2	-
Sintering temperature °C	1600	1600	1600	1600
Pellets density g/ml	8.03	8.02	8.23 *	-
Porosity %	18.36	17.25	14.53	-
A.S.G.	9.87	9.70	9.62	9.50

* Pressed pellets were placed in vacuum furnace for two hours at 400°C prior to firing.

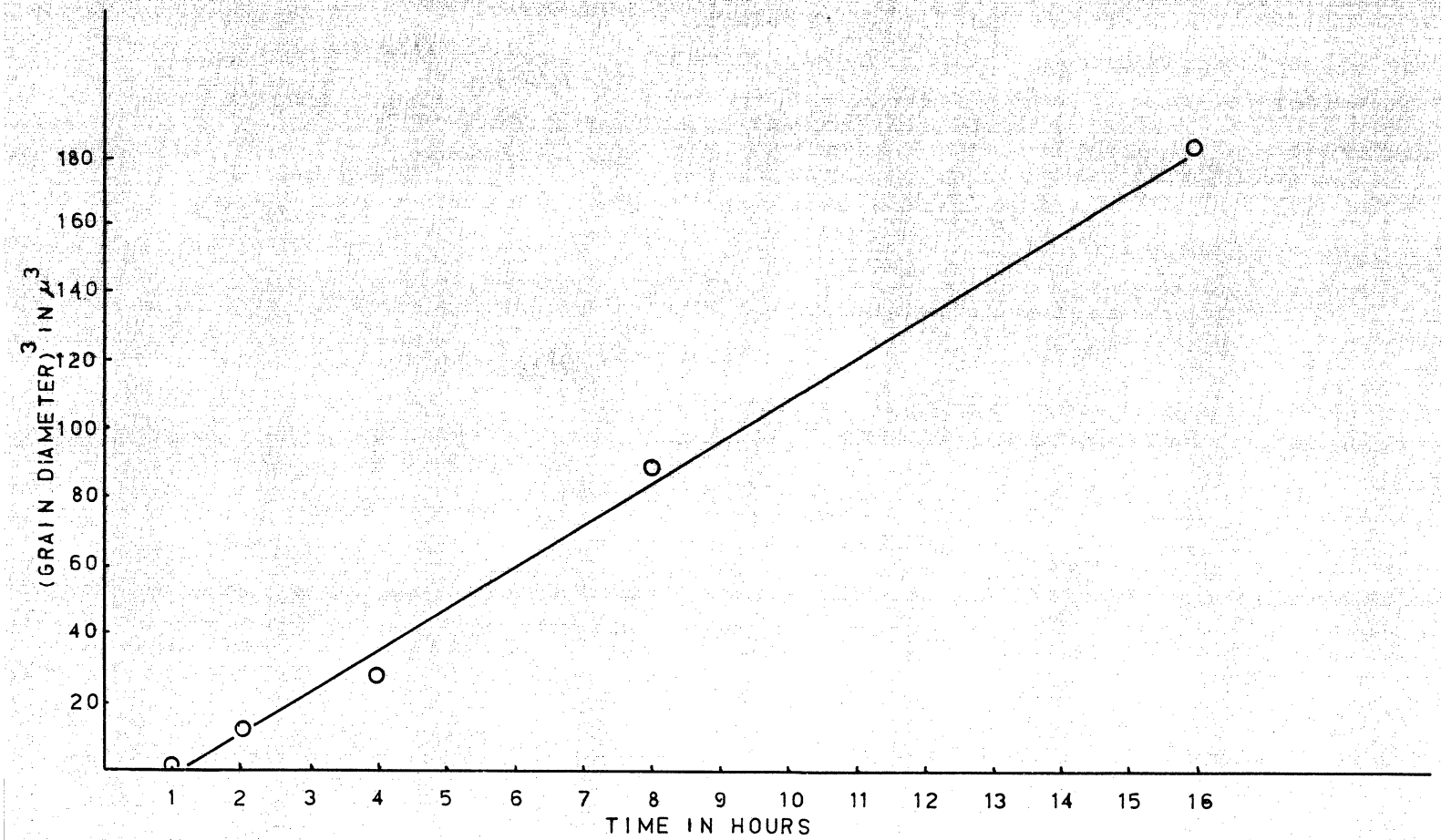

FIGURE 8.17

GRAIN DIAMETER CUBED VS TIME

additional step in that a vacuum treatment was carried out on the pellets at 400 degrees for two hours just prior to firing. The weight loss of the powders during the three calcination treatments was greatest for the calcination in air but the difference was fairly small. In addition to the 600°C treatment a 700°C calcination temperature was made in air which lowered the apparent specific gravity. The trend in these results is similar to that obtained by Moorehead[5] who found that a 600°-800°C calcination temperature produced an optimum in specific gravity of fired thoria compacts. Since the decomposition of the oxalates is completed by 600°C, as seen by the D.T.A. results, the standard calcination treatment of 600°C in air for one hour was adopted for all powders.

8.2.3. Grain Growth of Thoria

The grain growth of thoria has been investigated as a function of time and temperature by various workers[28,29]. Moorehead[5], who studied the grain growth as a function of time at 1600°C, found that the cube of mean grain diameter varied as the function

$$G^3 - G_o^3 = At \qquad (8.3)$$

where G = the mean grain diameter

t = time

A = change of diameter with time.

In that work, the constant A was calculated to be 16.67 x (10^{-12}cm^3/hour). In Figure 8.17 a plot has been made for values of grain size of thoria after 1, 2, 4, 8 and 16 hours respectively at 1600°C. The points may be assumed to be along a straight line of slope 12.11x(10^{-12}cm^3/hour). The values of mean grain diameter for the various firing times is shown in Table 8.6.

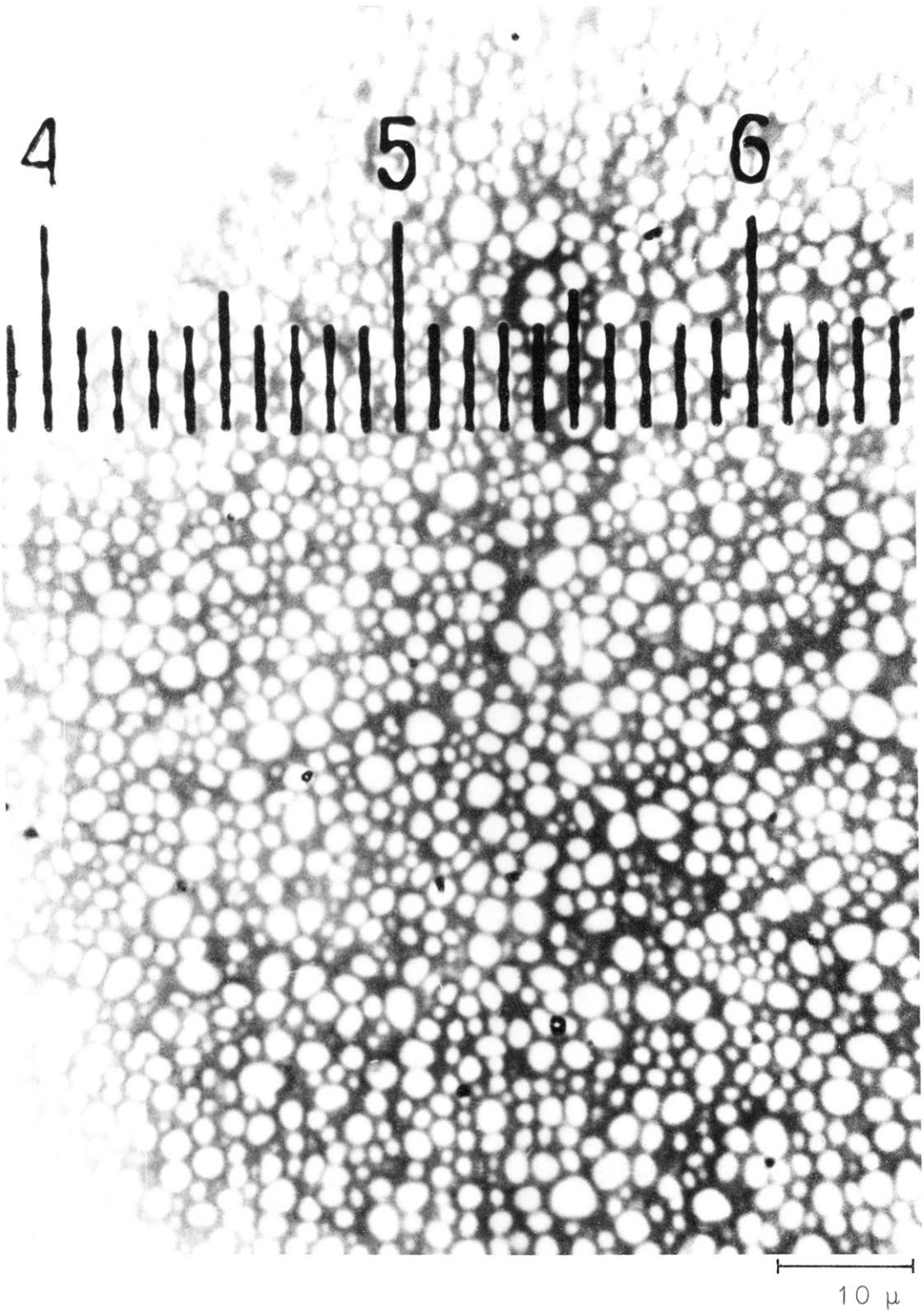

Figure 8.18. A. Polished Surface of Thoria After 1 Hour at 1600 C

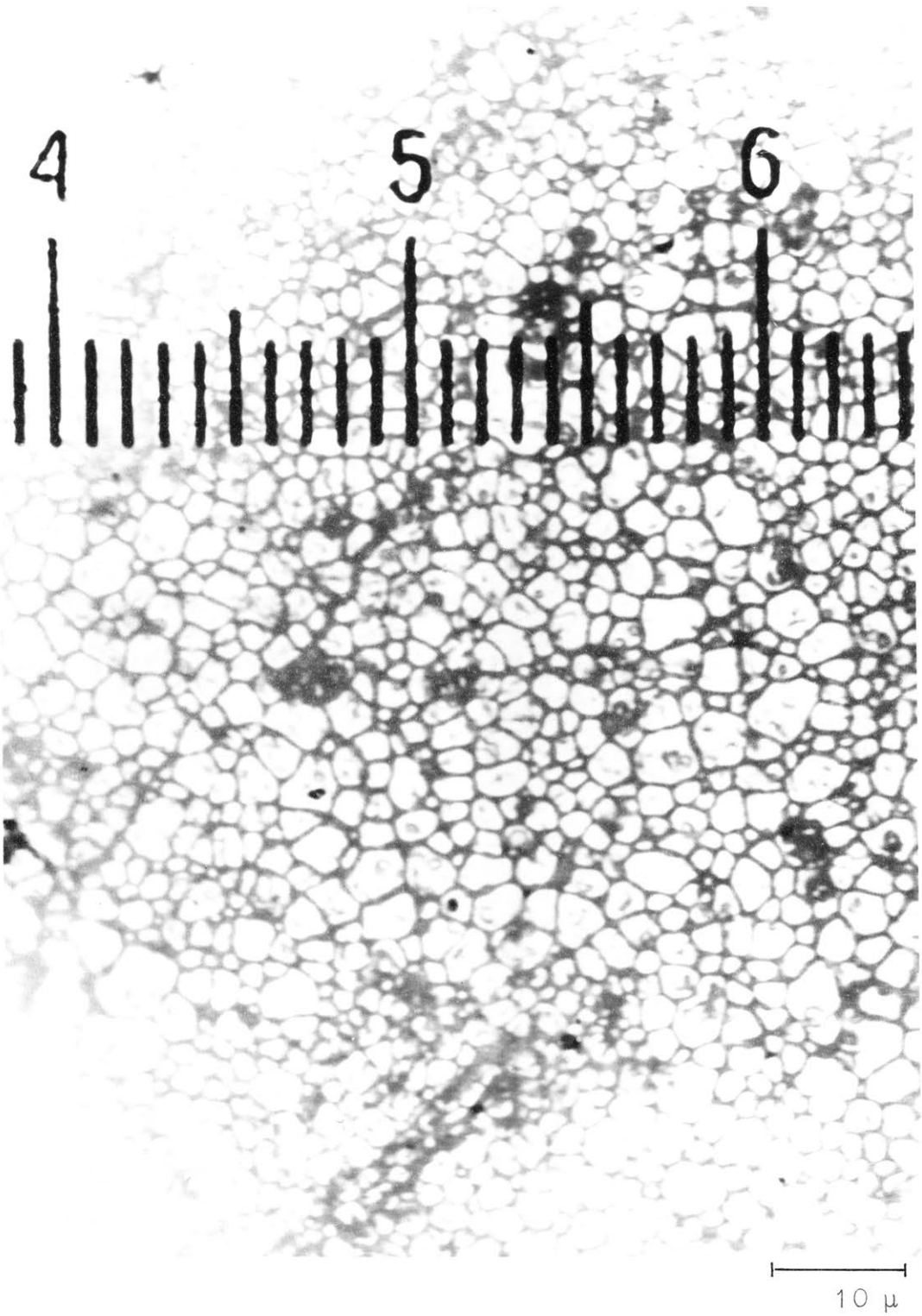

Figure 8.18. B. Polished Surface of Thoria After 2 Hours at 1600 C

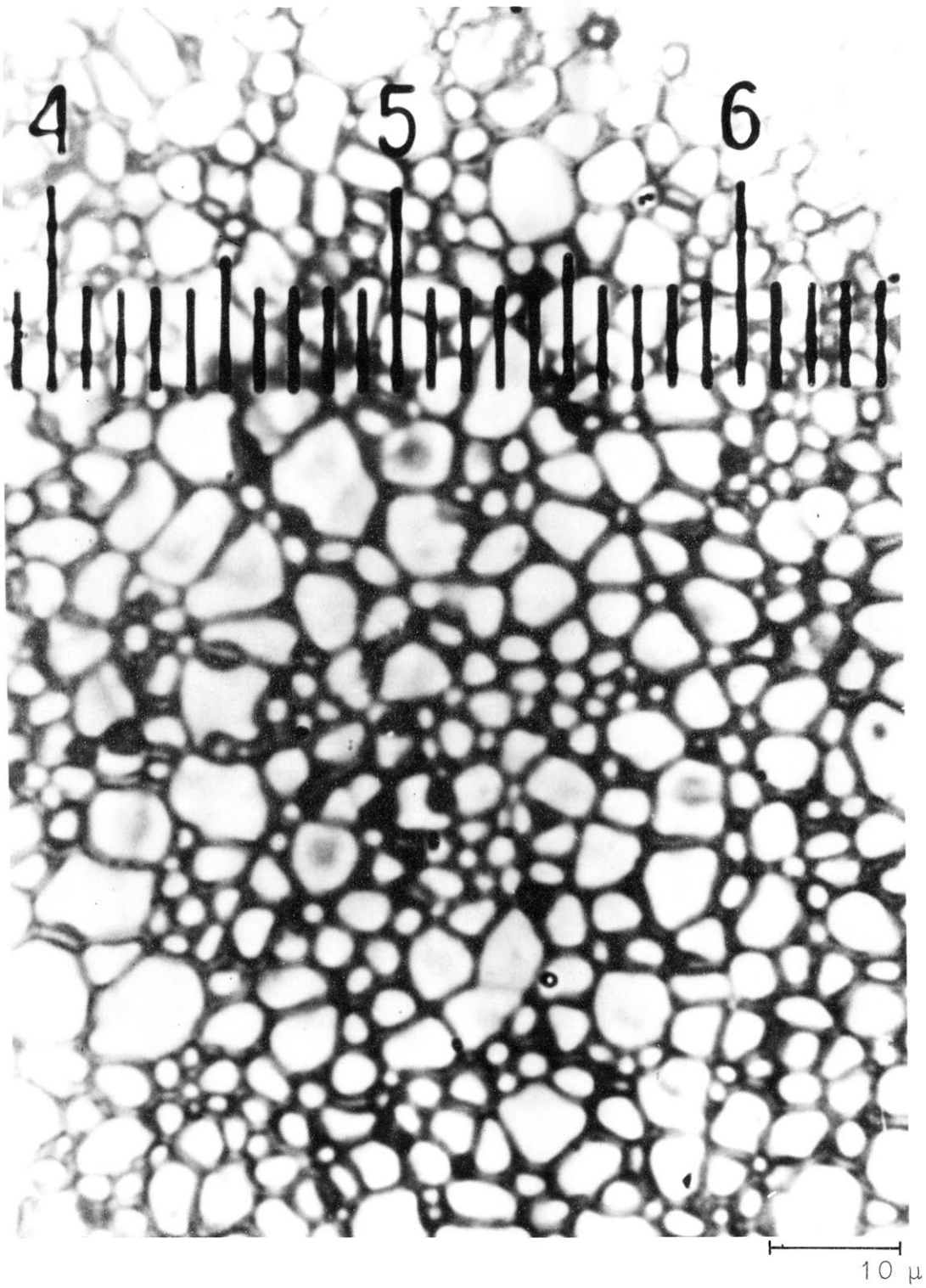

Figure 8.18. C. Polished Surface of Thoria After 4 Hours at 1600 C

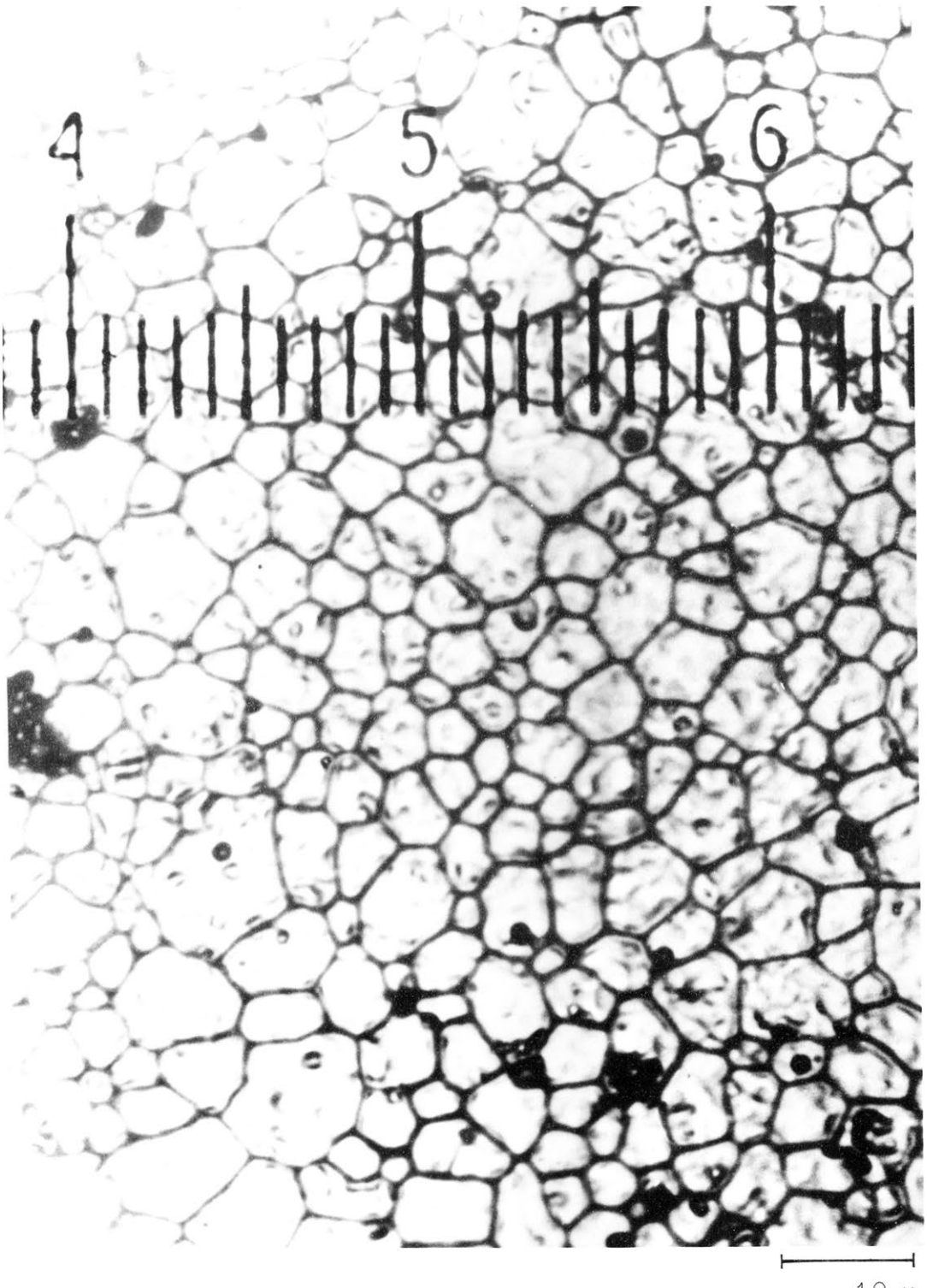

Figure 8.18. D. Polished Surface of Thoria After 8 Hours at 1600 C

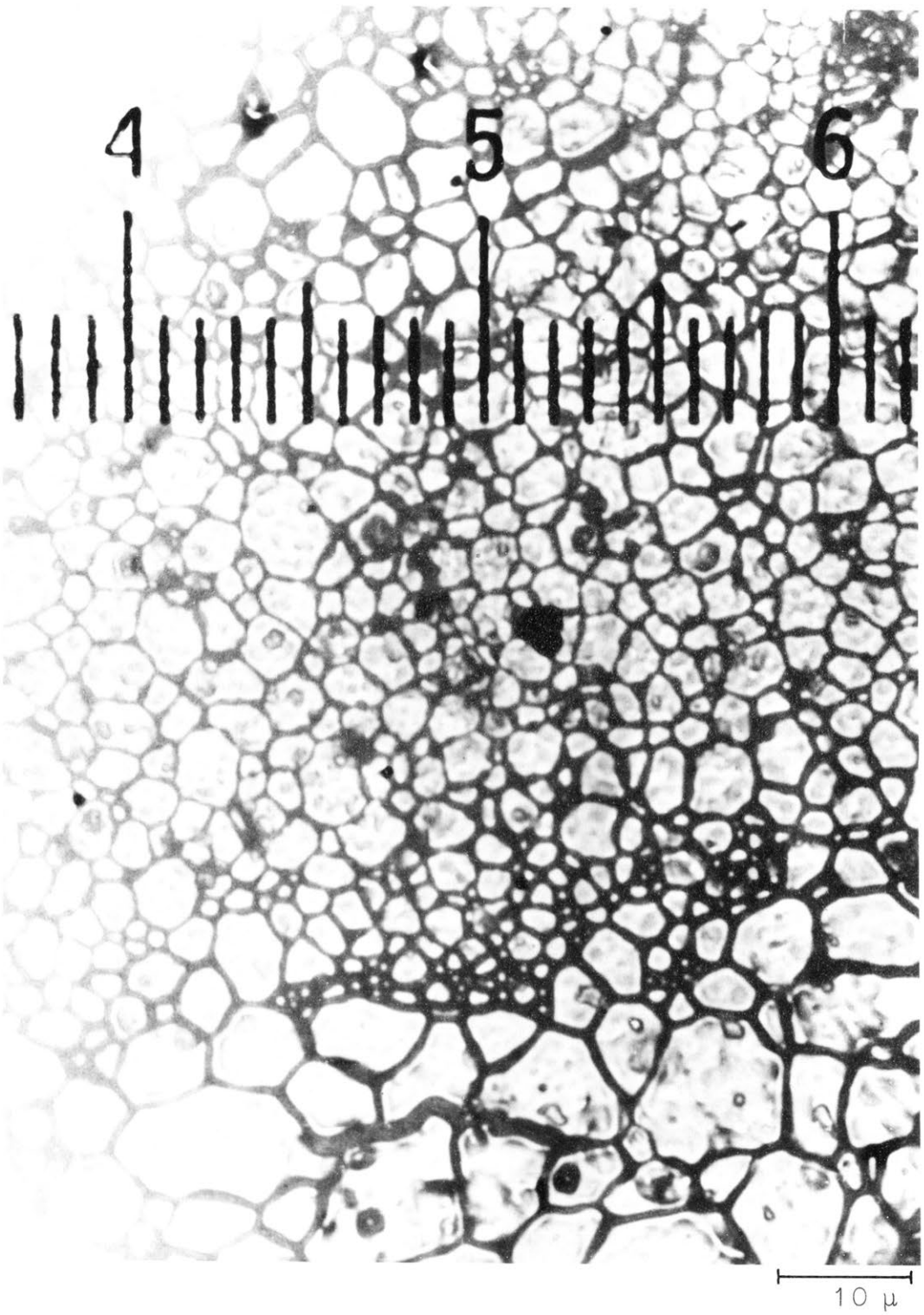

Figure 8.18. E. Polished Surface of Thoria After 16 Hours at 1600 C

(A)

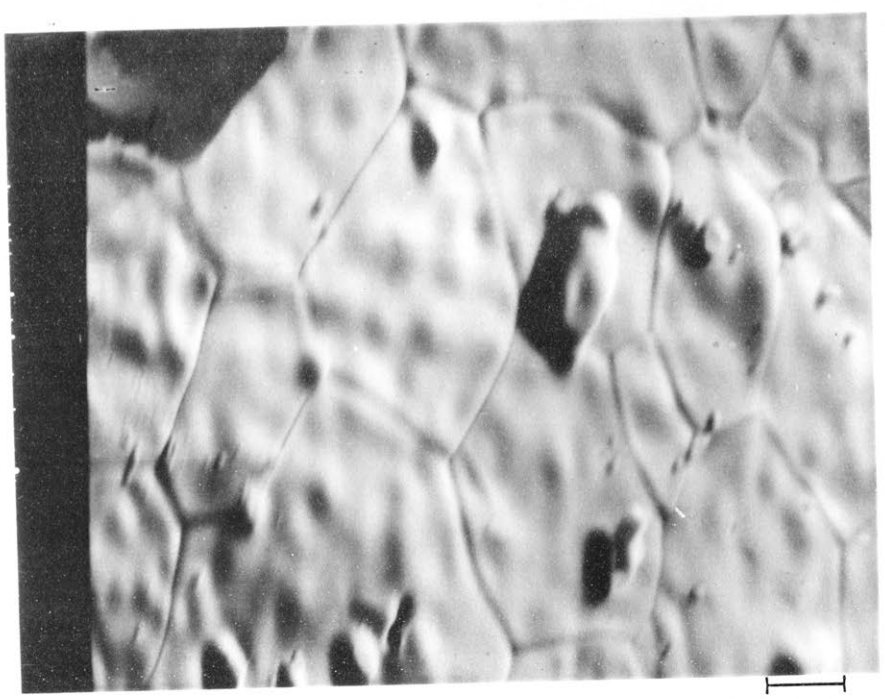

(B)

Figure 8.19. Scanning Micrographs of Thoria After 8 Hours at 1600 C
(A) Fractured Surface (B) Pressed Fac

TABLE 8.6

Effect of Time on Grain Size of Thoria

Hours at 1600°C	Average Grain Size
1	1.16
2	2.30
4	3.03
8	4.45
16	5.66

Figures 8.18 A-E show the optical micrographs of the polished and etched thoria pellets fired for the respective times. Scanning electron micrograph Figure 8.19 shows the surface of the thoria pellet fired to 1600°C for eight hours. The grain size estimated by this photograph was found to be 4.76 micrometers which compares to 4.45 micrometers determined by optical microscopy and 5.16 micrometers found by Moorehead. It is apparent that exaggerated grain growth begins after eight hours and appears well developed by sixteen hours firing. The effect of dopant oxide addition on the microstructure will be discussed in a later section.

8.2.4. Sintered Densities of Thoria Combined with Single Fission Product Oxides

As mentioned earlier, the addition of calcium oxide to thoria has been studied by other workers[28,29]. A series of eight binary systems with thoria were studied in molar concentrations up to 20 per cent. The average values of density, porosity and apparent specific gravity of these systems are tabulated in Table 8.7. Of all the systems studied, the divalent oxides, strontia and baria, were outstanding in that density of thoria containing these oxides

TABLE 8.7

Effect of Oxide Additions on the Density of Thoria Pellets

Fired to 1400 C and 1600 C for 16 hours under Dry N_2

Oxide Addition %	Oxide	1400 C Bulk Density	1400 C Apparent Porosity	1400 C Apparent Specific Gravity	1600 C Bulk Density	1600 C Apparent Porosity	1600 C Apparent Specific Gravity
5	ZrO_2	7.14	29.79	10.18	9.73	1.36	9.86
10	ZrO_2	6.33	36.09	9.90	9.53	2.95	9.82
20	ZrO_2	5.96	38.63	9.71	9.29	4.12	9.63
1	CeO_2	7.55	24.35	9.98	9.15	5.68	9.71
5	CeO_2	6.67	32.80	9.93	8.02	21.14	10.17
10	CeO_2	7.06	27.84	9.79	8.34	16.46	9.98
20	CeO_2	6.39	32.44	9.49	6.39	34.72	9.81
5	Nd_2O_3	8.27	18.11	10.10	-	-	-
10	Nd_2O_3	7.03	25.32	9.47	8.62	0	8.62
20	Nd_2O_3	6.72	22.24	8.62	7.47	13.29	8.61
5	La_2O_3	5.73	41.08	9.71	-	-	-
10	La_2O_3	5.39	42.27	9.35	6.71	27.10	9.21
20	La_2O_3	-	-	-	6.97	16.86	8.38
5	Y_2O_3	6.98	27.67	9.65	7.85	24.28	10.25
10	Y_2O_3	7.43	25.19	9.93	8.28	16.46	9.92
20	Y_2O_3	6.45	28.30	9.00	8.11	5.09	8.55
1	BaO	7.54	27.09	10.35	9.46	2.03	9.69
5	BaO	-	-	-	9.74	0	9.74
10	BaO	-	-	-	9.60	0	9.60
20	BaO	-	-	-	9.07	2.01	9.26
1	SrO	8.02	19.70	9.99	8.93	5.70	9.48
5	SrO	10.03	2.63	10.07	9.57	2.53	9.82
10	SrO	-	-	-	9.29	1.98	9.48
20	SrO	-	-	-	-	-	-

TABLE 8.7. (Cont'd)

5	MoO_2	7.21	29.84	10.37	9.01	4.86	9.47
10	MoO_2	6.28	38.42	10.21	8.06	20.01	10.07
20	MoO_2	5.92	42.24	10.25	7.67	22.28	9.85

increased dramatically. As one would expect, density increased while porosity decreased with firing temperature. In most cases, the apparent specific gravity decreased with an increase in firing temperature, indicating development of closed porosity. The question whether or not the increase in density was a result of increased diffusion or was caused by grain boundary pinning will be discussed later. Generally, the density results may be discussed in terms of the type of oxide in combination with thoria, that is divalent, trivalent or tetravalent. The binary systems producing generally the highest density and the lowest porosity as a class were those containing divalent oxide of barium and strontium. Of the trivalent oxides, yittrium and neodymium appeared to improve density the most. Of the tetravalent oxides, zirconium formed the most dense composites. Generally speaking, the pellets fired at 1400°C were much softer and weaker than those fired at 1600°C. The only systems in which hydration problems were encountered were lanthanum, strontium and barium. In fact, some of these systems completely disintegrated before density data could be obtained. The strontia and baria systems were of particular interest due to their tendency toward translucency. Strontia samples fired at 1400°C were highly translucent, almost transparent, while pellets fired to 1600°C were poorer in these optical properties. Photographs of the translucent pellets are not available due to hydration or attack by CO_2 of the samples. Of the binary systems with thoria and tetravalent oxides, those containing zirconia appeared to be most dense.

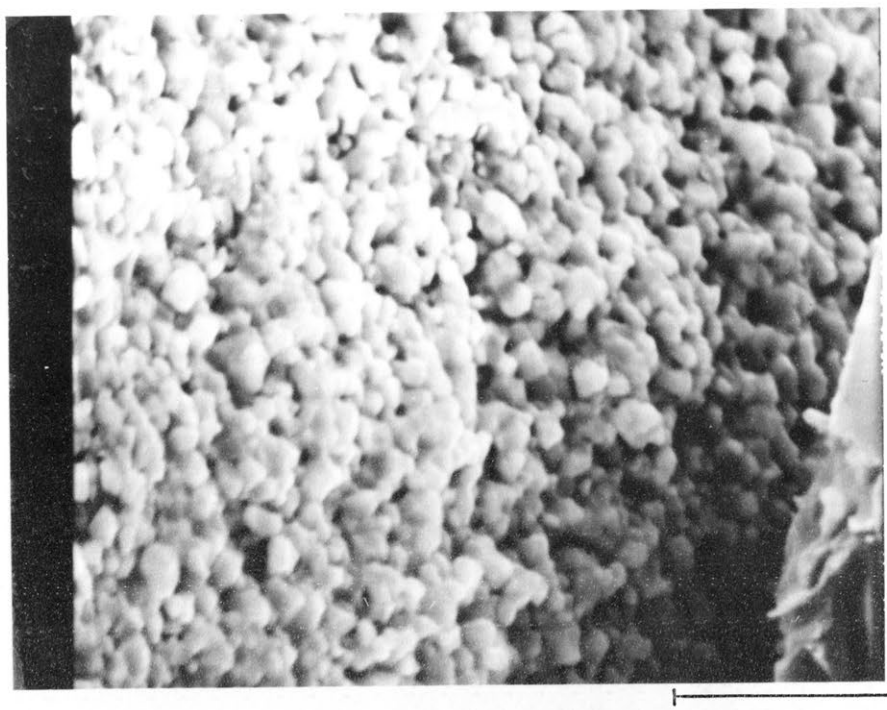

1% Strontia
16 hours
1400 C

(A) 10 μ

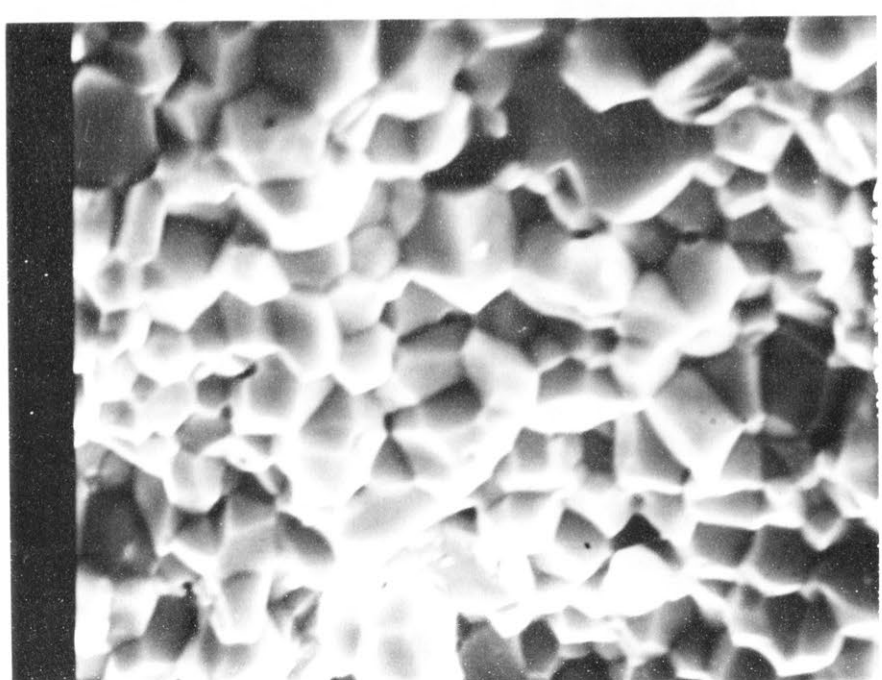

5% Strontia
16 hours
1400 C

(B) 10 μ

Figure 8.20. Scanning Electron Micrographs of Thoria Containing Strontia (A) and (B)

10% Strontia
16 hours
1400 C

(C) 10 μ

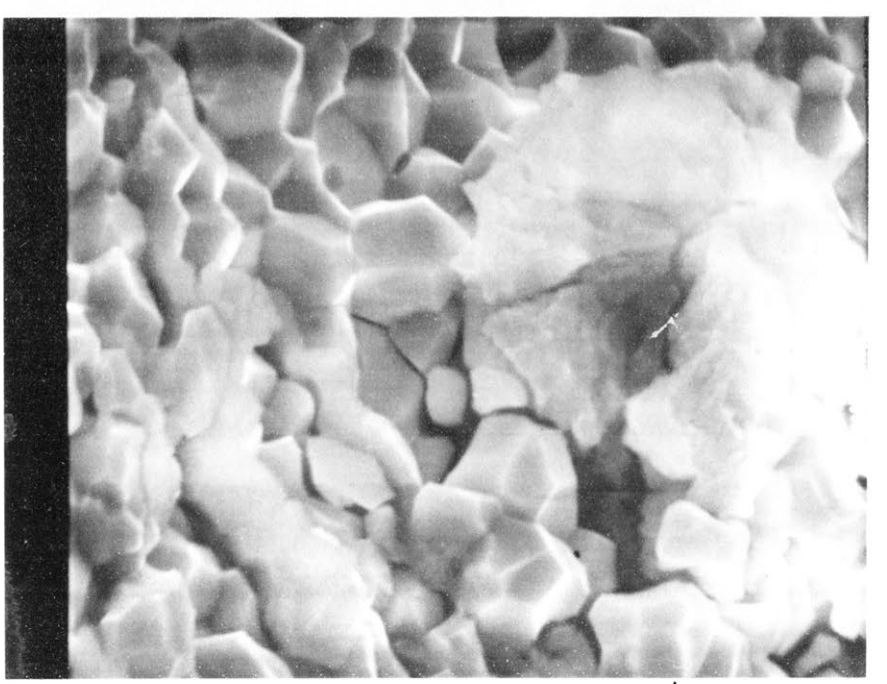

20% Strontia
16 hours
1400 C

(D) 10 μ

Figure 8.20. (C) and (D) Scanning Electron Micrographs of Thoria Containing Strontia

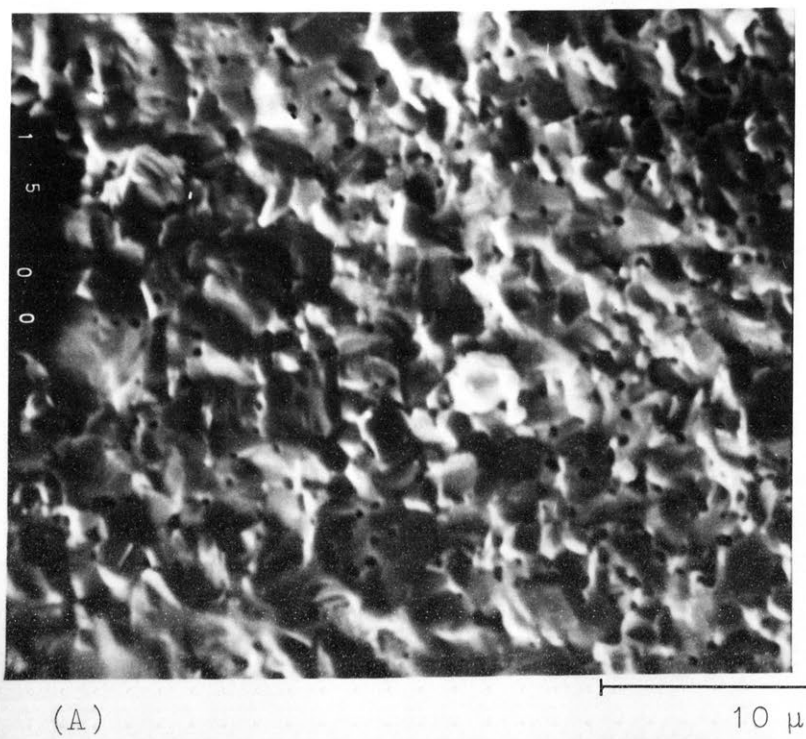

1% Strontia
16 hours
1600 C

(A)

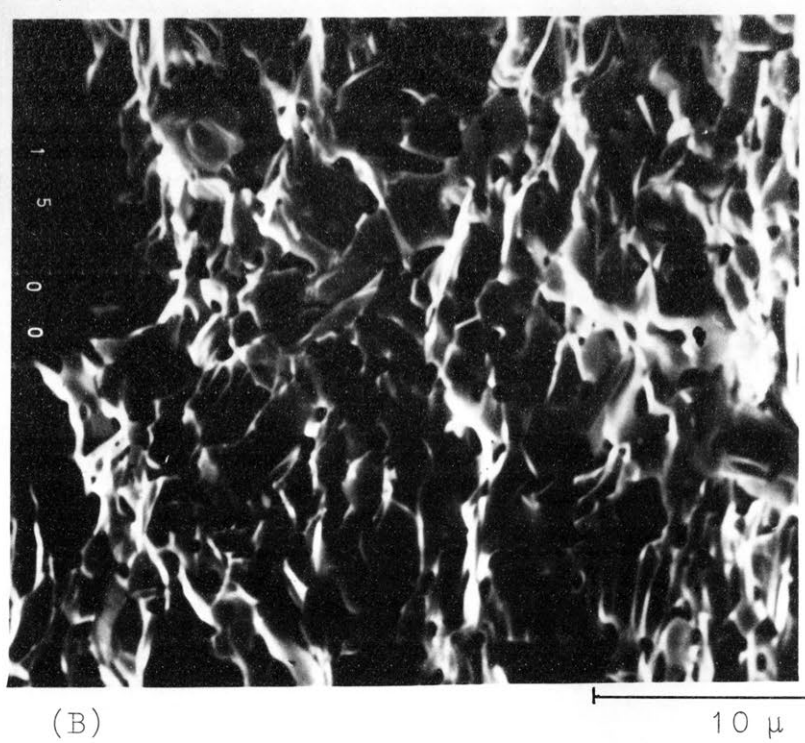

5% Strontia
16 hours
1600 C

(B)

Figure 8.21. Scanning Electron Micrograph of Thoria Containing Strontia

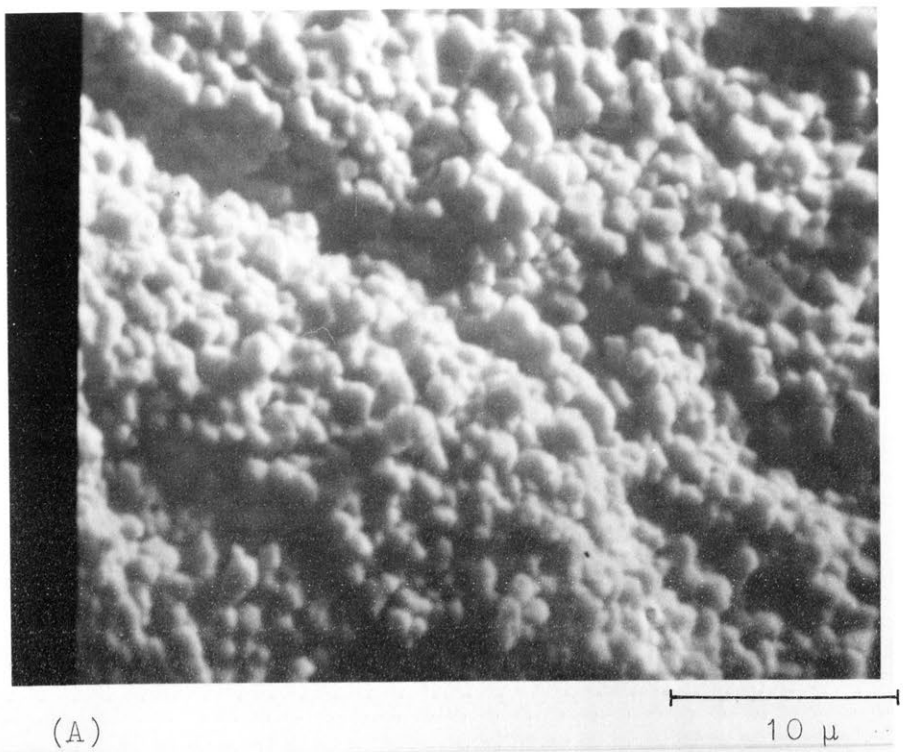

1% Baria
16 hours
1400 C

(A) 10 μ

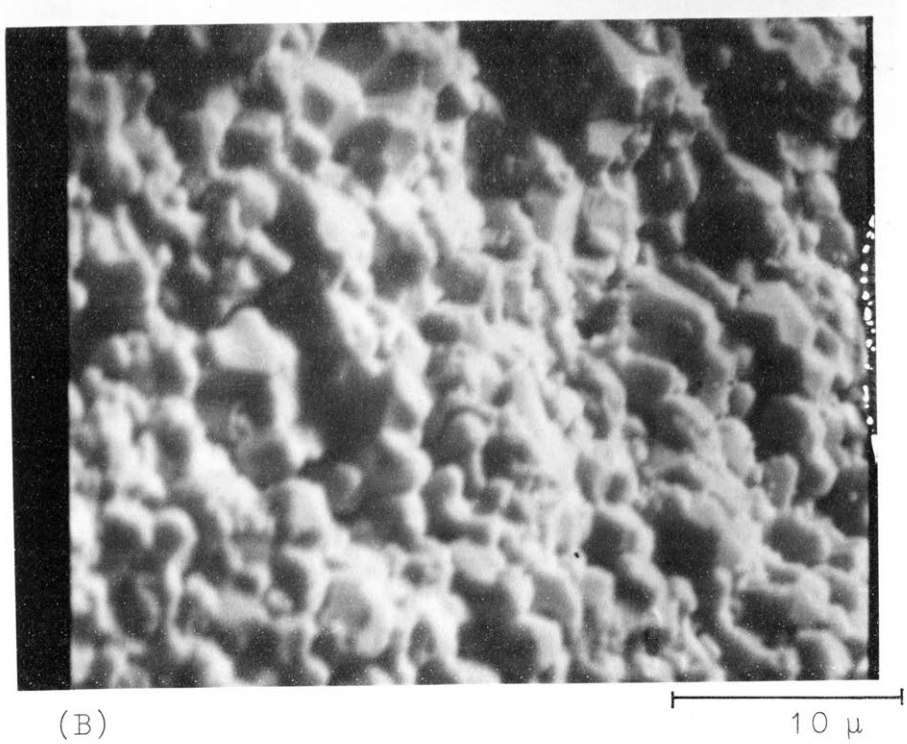

5% Baria
16 hours
1400 C

(B) 10 μ

Figure 8.22. (A) and (B) Scanning Electron Micrograph of Thoria Containing Baria

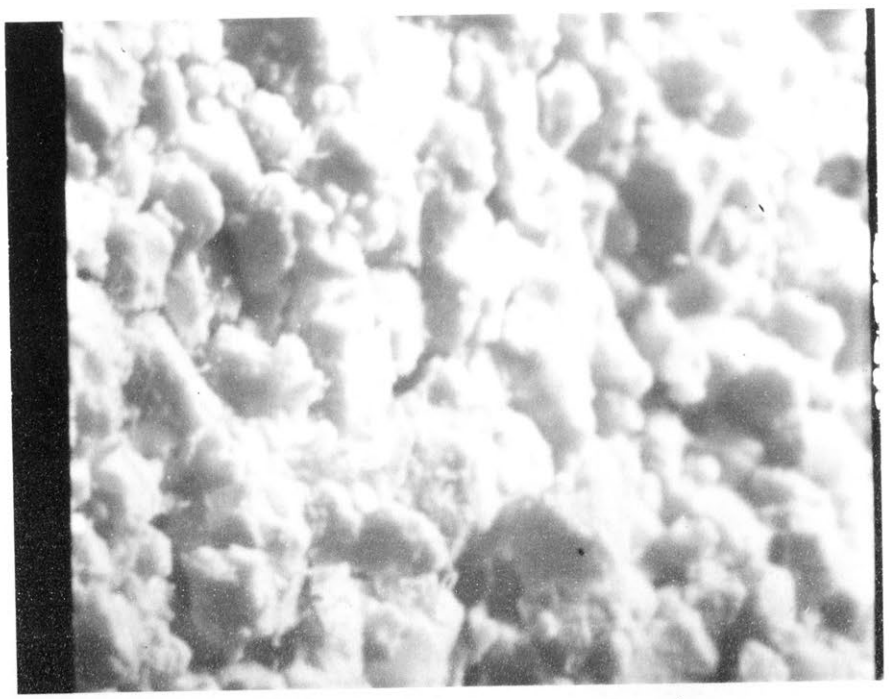

10% Baria
16 hours
1400 C

(C)

10 μ

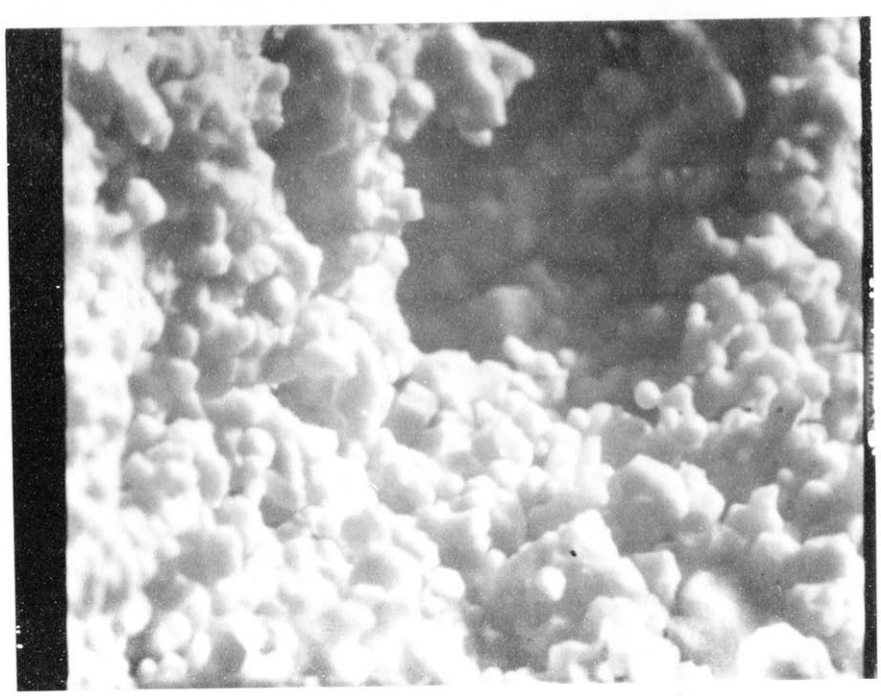

20% Baria
16 hours
1400 C

(D)

10 μ

Figure 8.22. (C) and (D) Scanning Electron Micrograph of Thoria Containing Baria

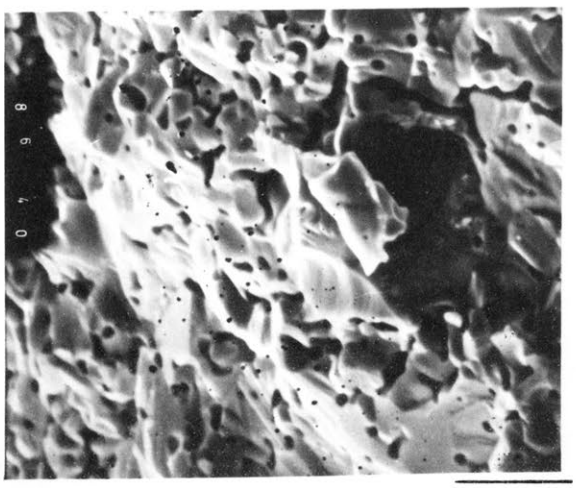

1% Baria
16 hours
1600 C

(A) 10 μ

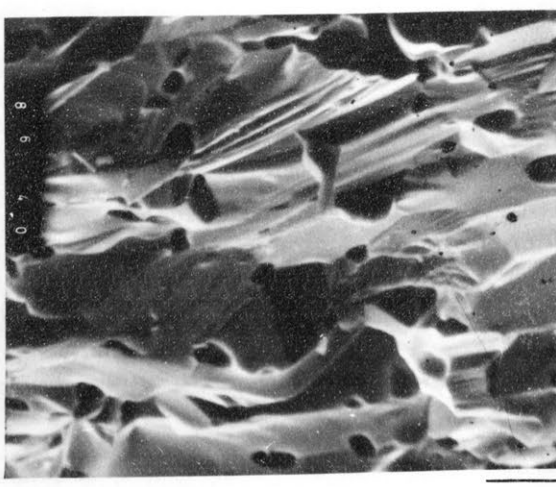

5% Baria
16 hours
1600 C

(B) 10 μ

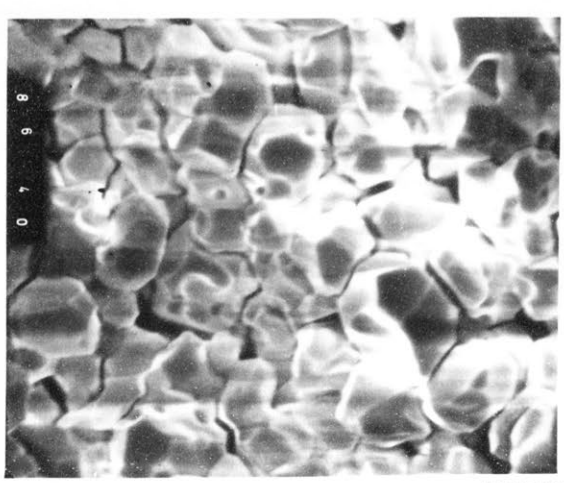

10% Baria
16 hours
1600 C

(C) 10 μ

Figure 8.23. (A)(B)(C) Scanning Electron Micrograph of Thoria Containing Baria

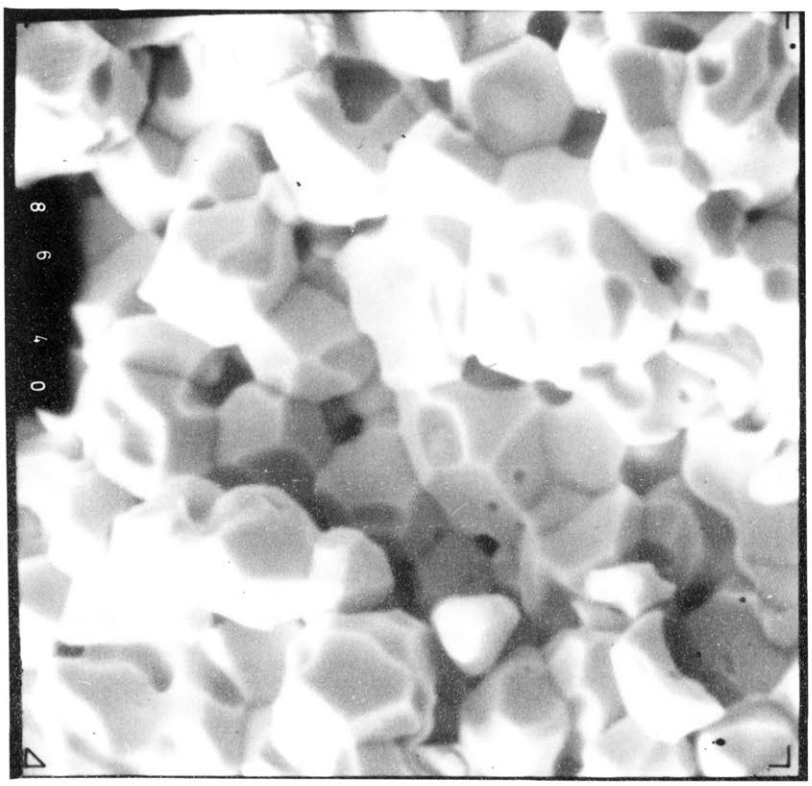

20% Baria
16 hours
1600 C

(D)

10 μ

Figure 8.23(D). Scanning Electron Micrograph of Thoria Containing Baria

8.2.5. Microstructure of Thoria and Binary Systems with Thoria

The microstructure of binary systems with thoria was studied by means of the scanning electron microscope. Polished sections of the samples were not sufficiently good for thorough optical microscopy. The scanning electron micrographs confirmed the results obtained from density measurements. The systems containing strontia and baria are shown in Figures 8.20 through 8.23. The structure of the specimen containing strontia was found to be quite regular consisting of well shaped dodecahedrons bonded together at the flat sides forming a uniform and apparently well bonded matrix. There was very little observable porosity in the 1400°C samples; however, those fired to 1600°C showed relatively a great deal of porosity and generally a less well developed grain but perhaps more strongly bonded matrix. Of particular interest was the system containing ten per cent strontium which was fired to 1400°C. The surface of the fractured specimen showed a small area which had been affected between the time of fracture and analysis of the specimen. The outcropping may have been formed either by the hydration of strontia in the thoria matrix or a strontia carbonate formed by the mechanism of CO_2 attack similar to that suggested by Hoffmann[72] when studying $BaThO_4$ perovskites. The former condition suggests free strontia which was not confirmed by X-ray diffraction while the latter behaviour could occur without free strontia. It appears likely that the artifact may be a carbonate of strontia. The systems containing baria were generally similar to those containing strontia except that the grain growth appeared to be somewhat less. The ThO_2-BaO sample, fired to 1400°C, also showed the effect

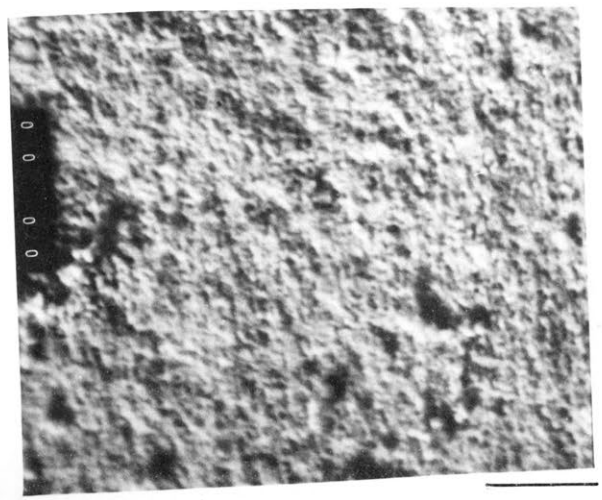

5% Neodymia
16 hours
1400 C

(A) 10 μ

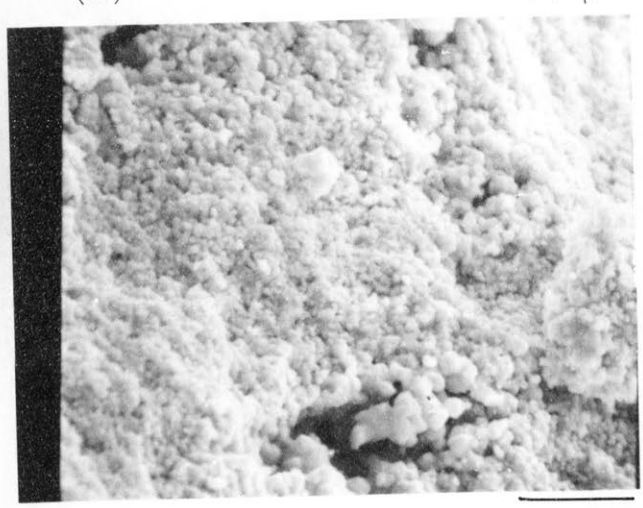

10% Neodymia
16 hours
1400 C

(B) 10 μ

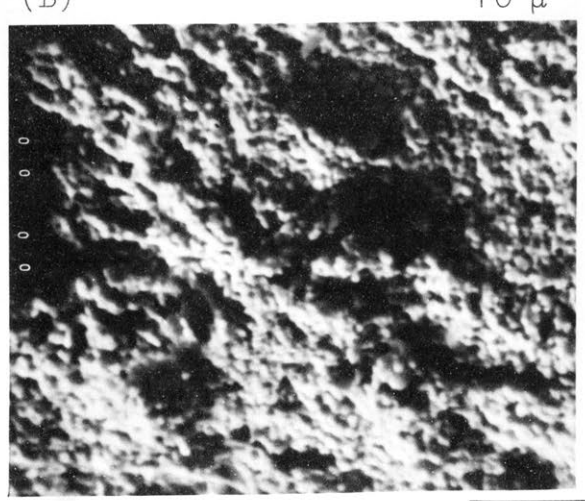

20% Neodymia
16 hours
1400 C

(C) 10 μ

Figure 8.24. (A)(B)(C) Scanning Electron Micrograph of Thoria Containing Neodymia

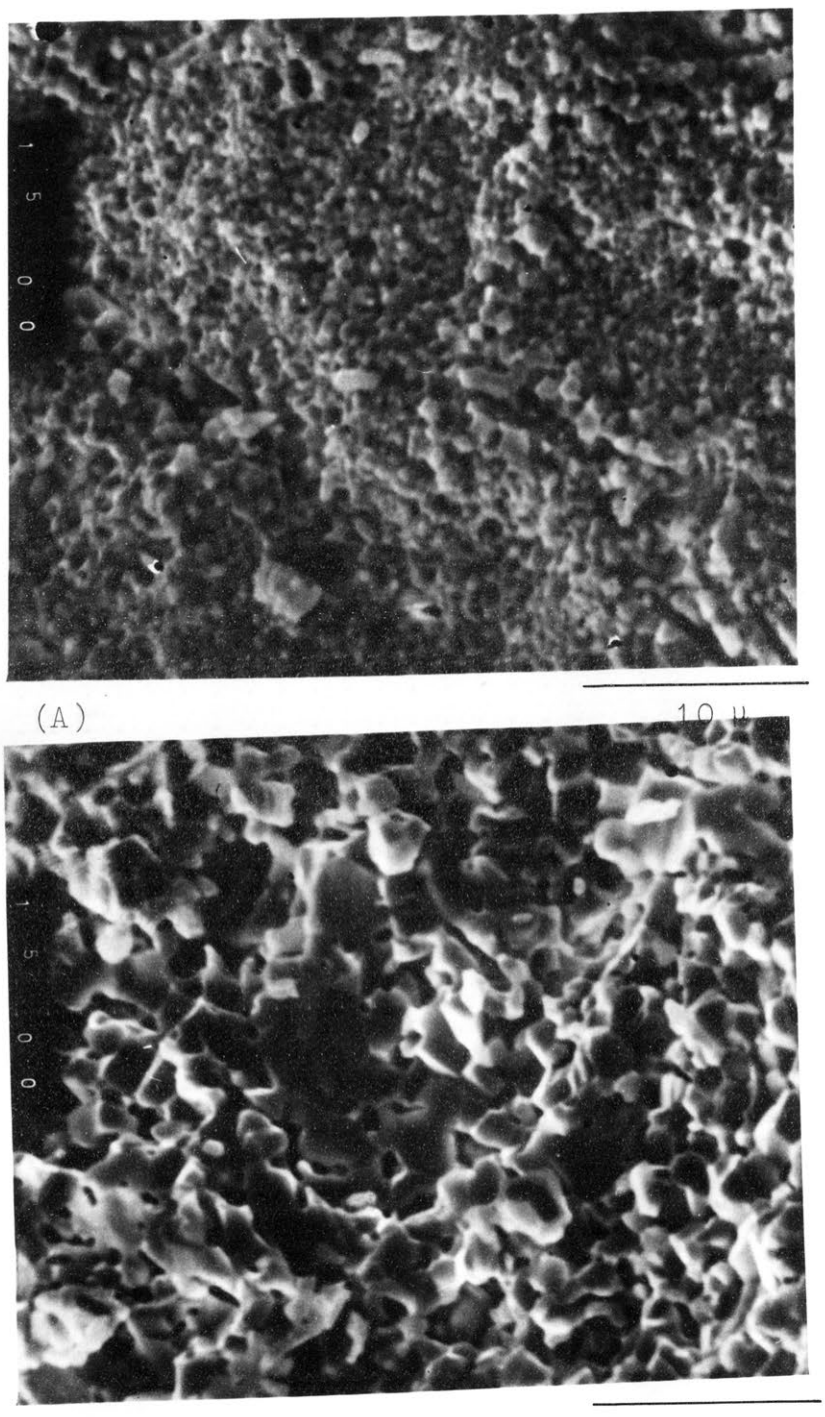

Figure 8.25. Scanning Electron Micrograph of Thoria Containing Neodymia
(A) 10% Neodymia, 16 hours, 1600 (
(B) 20% Neodymia, 16 hours, 1600 (

(A)

10 μ

5% Lanthana
16 hours
1400 C

(B)

10 μ

10% Lanthana
16 hours
1400 C

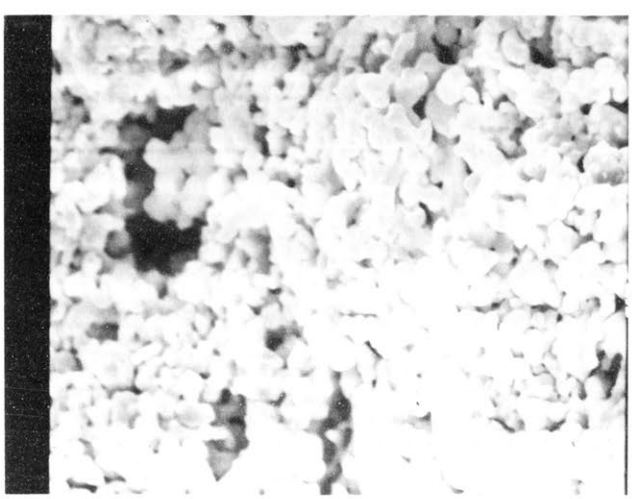

(C)

10 μ

20% Lanthana
16 hours
1400 C

Figure 8.26. (A)(B)(C) Scanning Electron Micrographs of Thoria Containing Lanthana

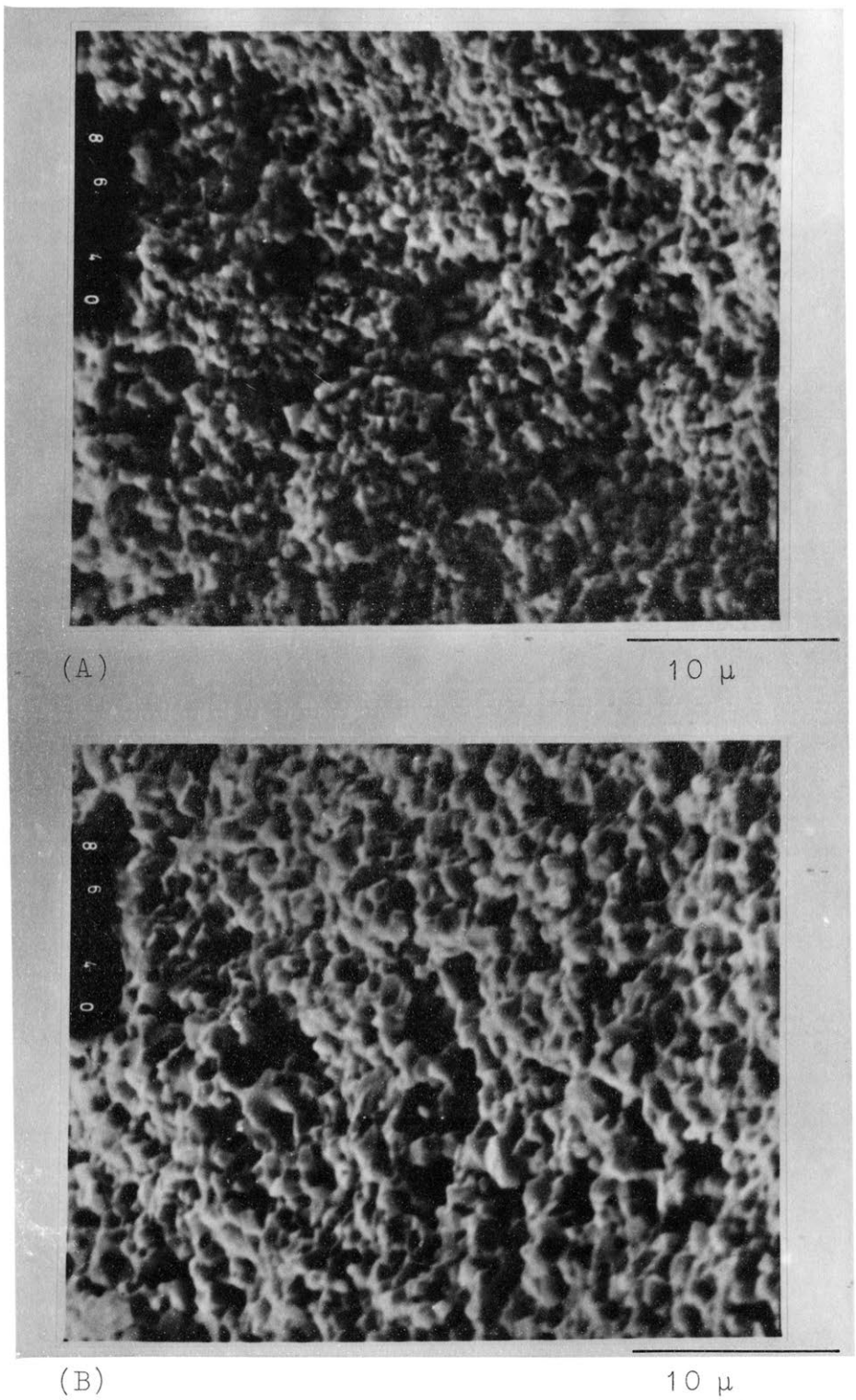

Figure 8.27. Scanning Electron Micrograph of Thoria Containing Lanthana
(A) 10% Lanthana, 16 hours, 1600 C
(B) 20% Lanthana, 16 hours, 1600 C

5% Yttria
16 hours
1400 C

(A) 10 μ

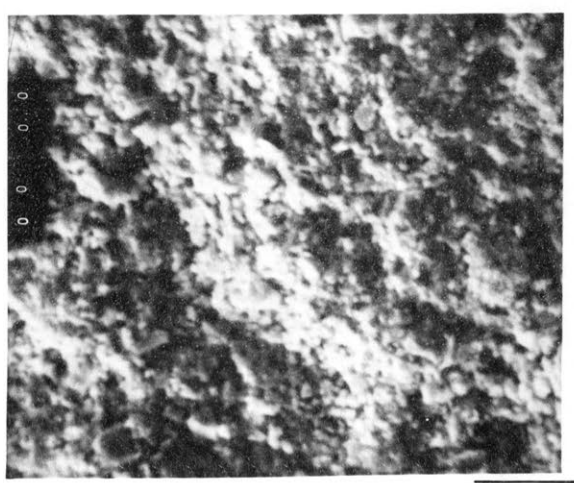

10% Yttria
16 hours
1400 C

(B) 10 μ

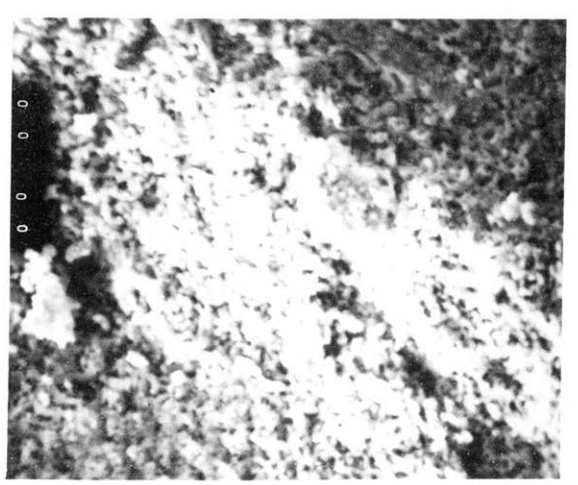

20% Yttria
16 hours
1400 C

(C) 10 μ

Figure 8.28. (A)(B)(C) Scanning Electron Micrographs of Thoria Containing Yttria

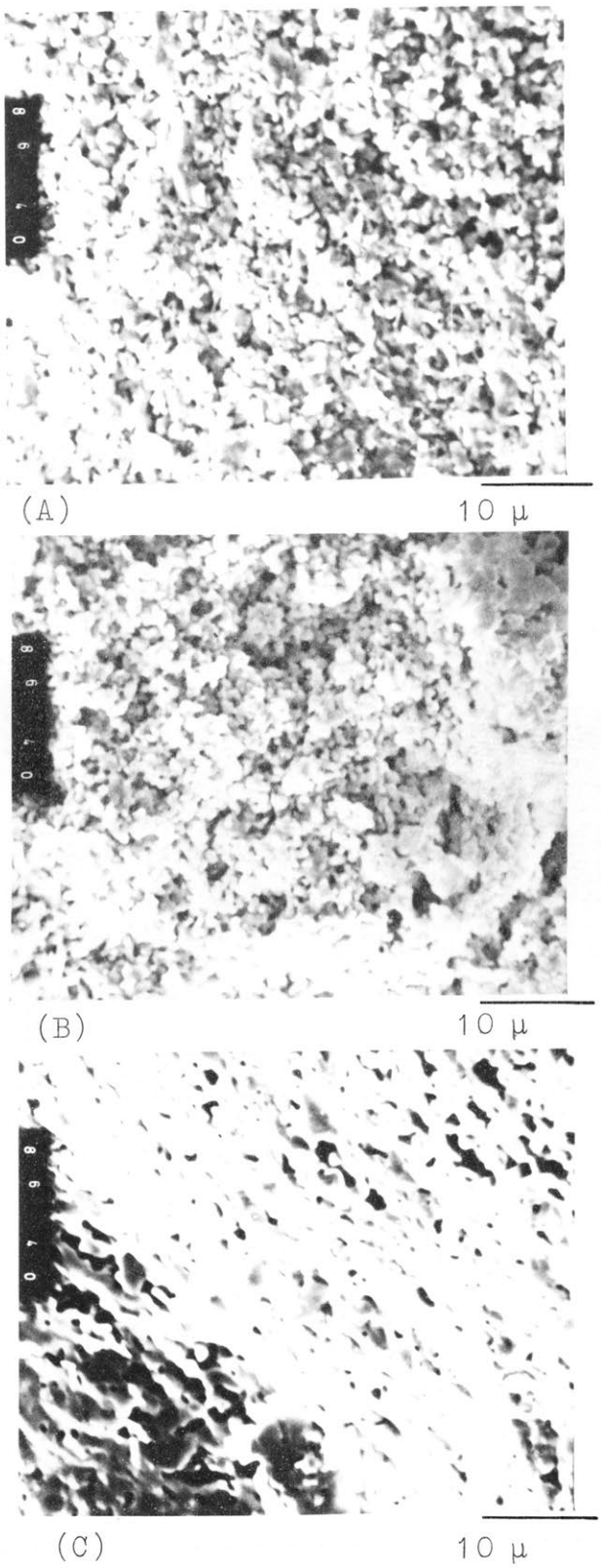

Figure 8.29. Scanning Electron Micrographs of Thoria (A)(B)(C) Containing Yttria

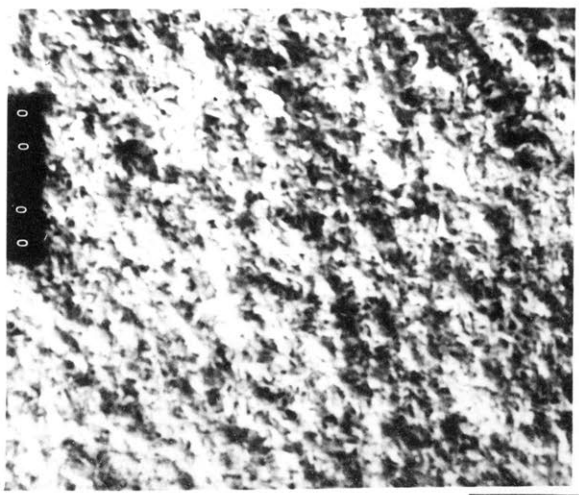

5% Zirconia
16 hours
1400 C

(A) 10 μ

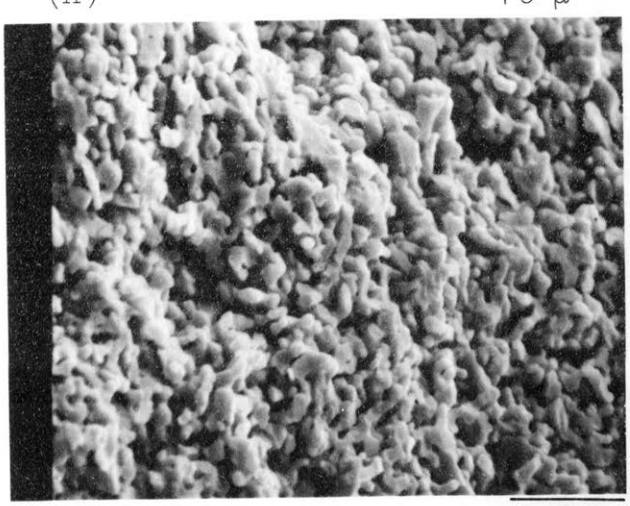

10% Zirconia
16 hours
1400 C

(B) 10 μ

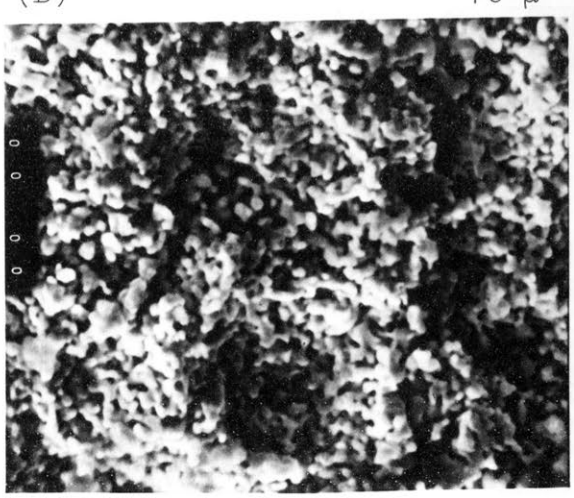

20% Zirconia
16 hours
1400 C

(C) 10 μ

Figure 8.30. (A)(B)(C) Scanning Electron Micrographs of Thoria Containing Zirconia

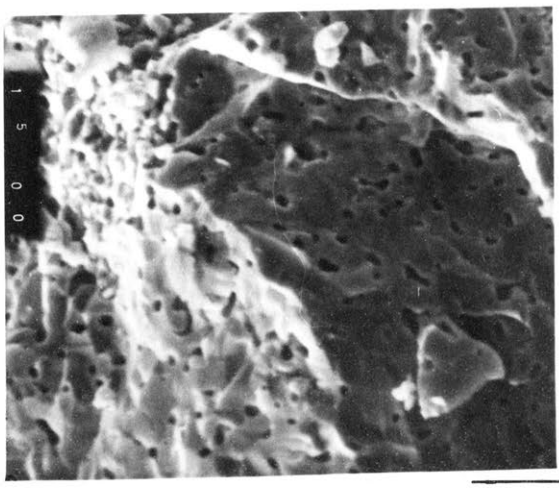

5% Zirconia
16 hours
1600 C

(A) 10 μ

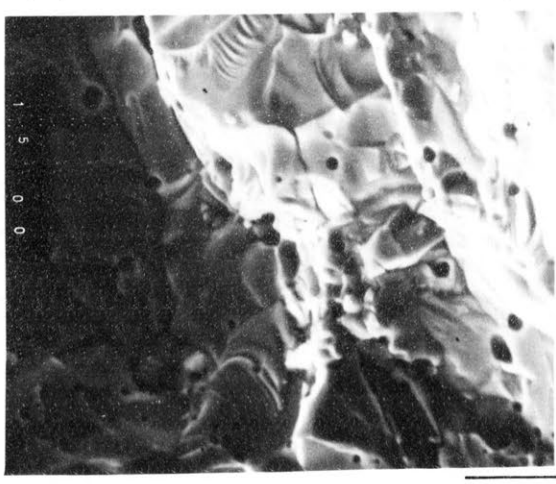

10% Zirconia
16 hours
1600 C

(B) 10 μ

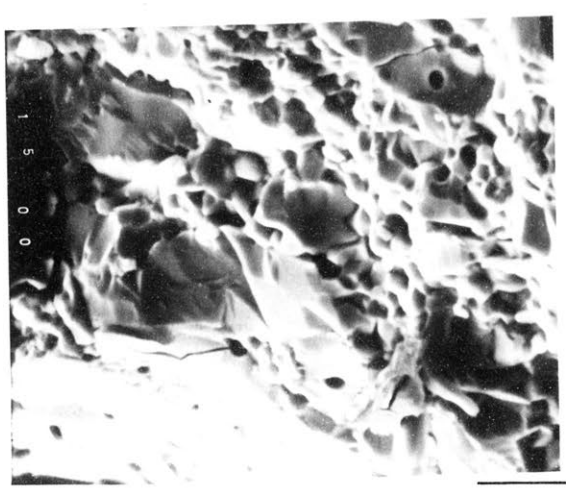

20% Zirconia
16 hours
1600 C

(C) 10 μ

Figure 8.31. (A)(B)(C) Scanning Electron Micrographs of Thoria Containing Zirconia

of exposure to atmosphere, however, the outcroppings were more uniformly distributed and less well developed than in the case of strontia.

The systems containing trivalent oxides were very porous and poorly developed when compared to the previous two systems. Figures 8.24 and 8.25 show the systems containing neodymium after firing to 1400° and 1600°C respectively. Some grain growth occurred with increased firing temperatures but there was still a high proportion of unnecked grain. Samples containing 20 mole per cent began to develop a dense matrix after 1600°C firing but significant porosity still existed, as evidenced by the density results. Similar effects occurred for both lanthana and yittria systems as shown by Figures 8.26 through 8.29. Attention is drawn to the Figure 8.29 in particular which shows the 20 per cent yittria system. The structure appears relatively dense and generally comparable to the corresponding neodymia system. However, there appears to be a large degree of closed porosity. This observation confirms what was found for this system in density measurements. The tetravalent systems containing respectively zirconium, molybdenum, have generally dense microstructures. The zirconia systems fired to 1400°C and 1600°C appeared to have the most dense microstructures of the tetravalent systems. As seen in Figures 8.30 and 8.31 the zirconia system forms a dense matrix with little apparent closed porosity. Systems fired to 1600°C showed an extremely dense surface where grain structure is difficult to distinguish.

Molybdenum systems were not as well bonded as the zirconium systems. The grain structure could easily be distinguished. The molybdenum systems fired to 1400°C were very unusual as seen in Figure 8.32. The grains appear spherical with some sort of glazing

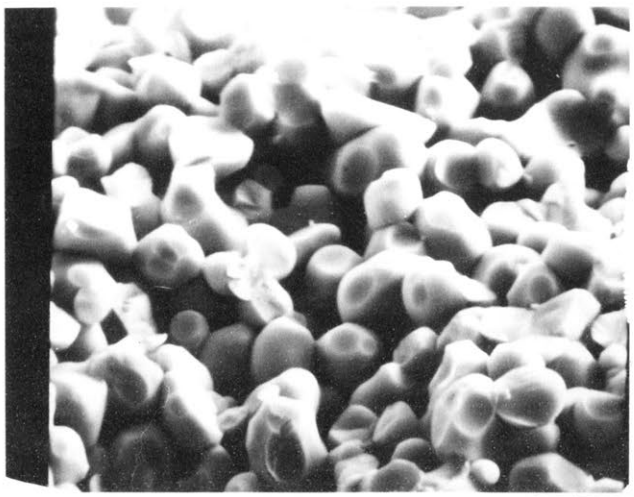

5% Molybdena
16 hours
1400 C

(A) 10 μ

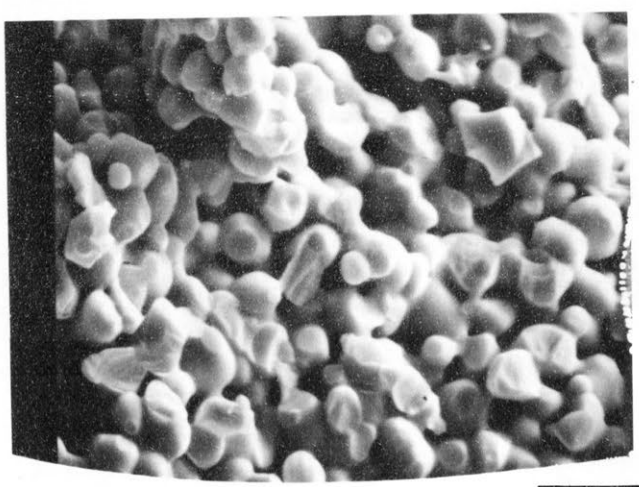

10% Molybdena
16 hours
1400 C

(B) 10 μ

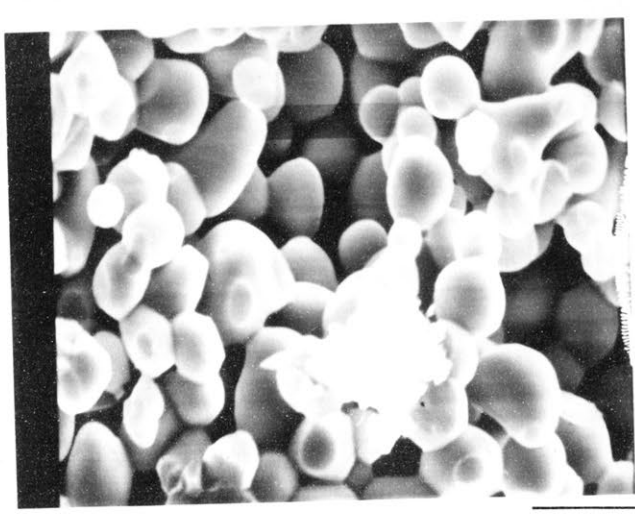

20% Molybdena
16 hours
1400 C

(C) 10 μ

Figure 8.32. (A)(B)(C) Scanning Electron Micrographs of Thoria Containing Molybdena

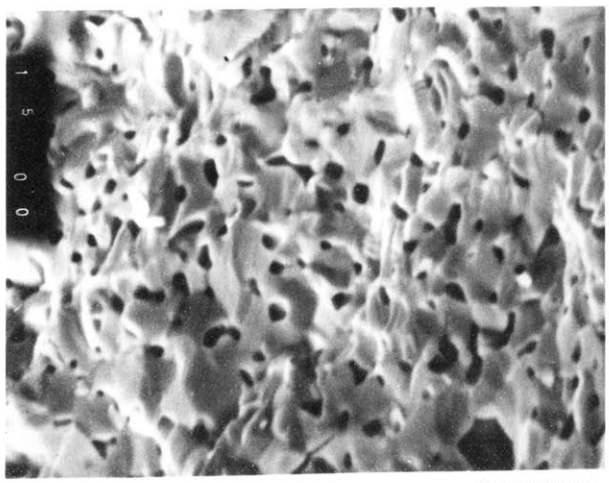

5% Molybdena
16 hours
1600 C

(A) 10 μ

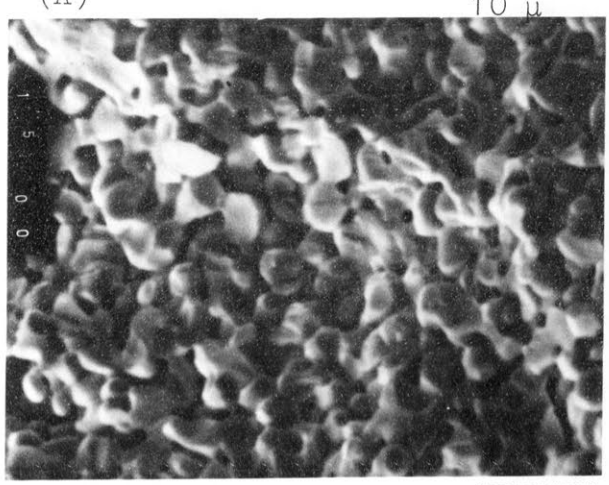

10% Molybdena
16 hours
1600 C

(B) 10 μ

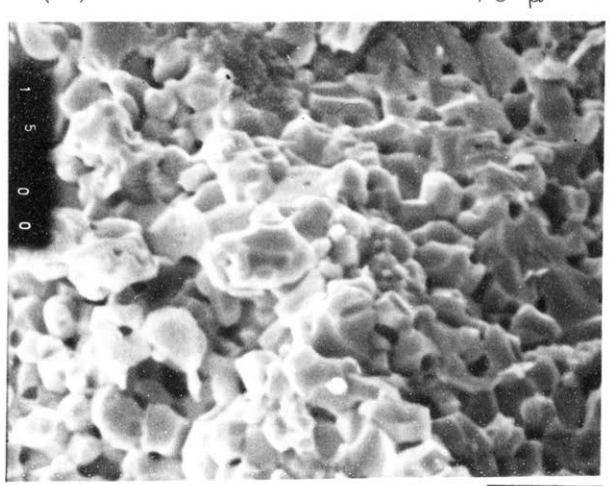

20% Molybdena
16 hours
1600 C

(C) 10 μ

Figure 8.33. (A)(B)(C) Scanning Electron Micrographs of Thoria Containing Molybdena

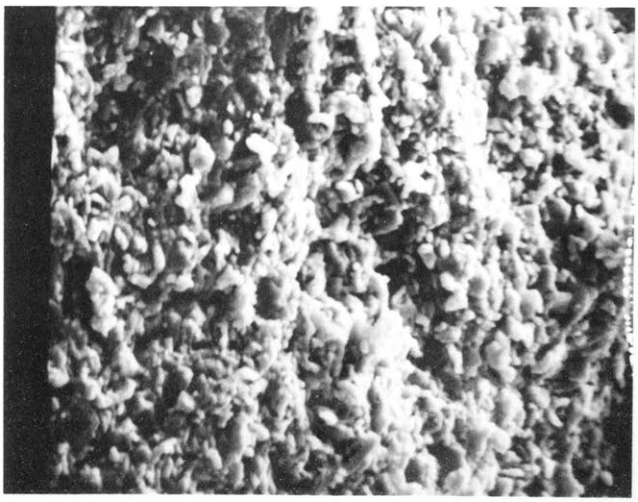

1% Ceria
16 hours
1400 C

(A) 10 μ

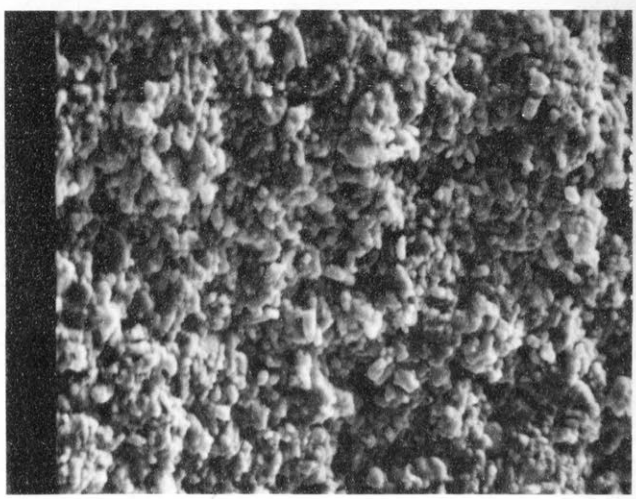

5% Ceria
16 hours
1400 C

(B) 10 μ

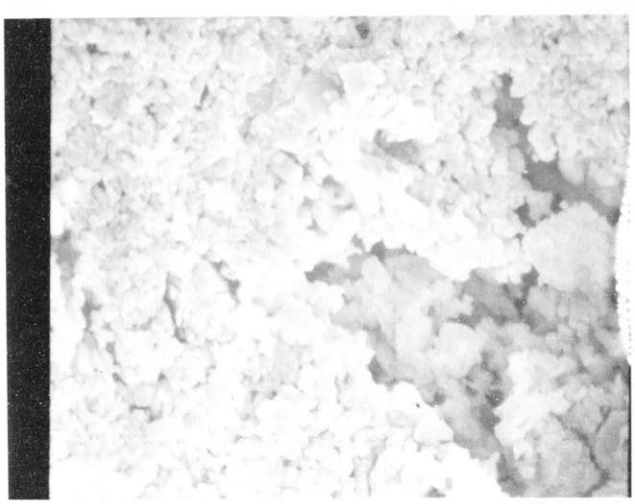

10% Ceria
16 hours
1400 C

(C) 10 μ

Figure 8.34. Scanning Electron Micrographs of Thoria (A)(B)(C) Containing Ceria

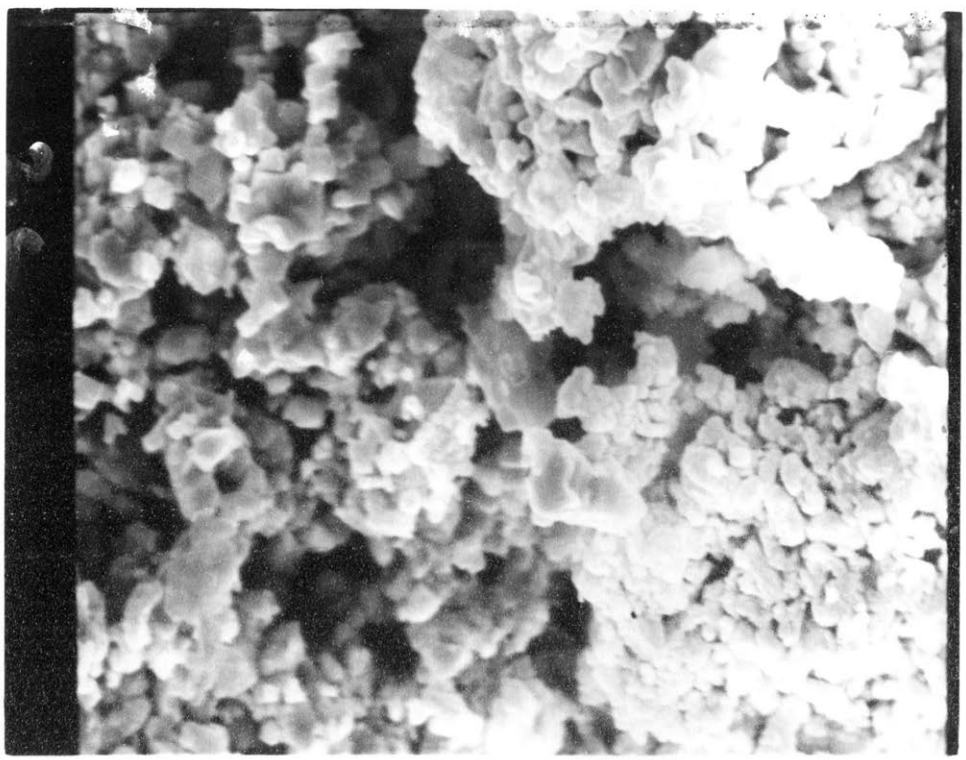

(D) 10 μ

Figure 8.34 (D). Scanning Electron Micrographs of Thoria Containing Ceria
20% Ceria, 16 hours, 1400 C

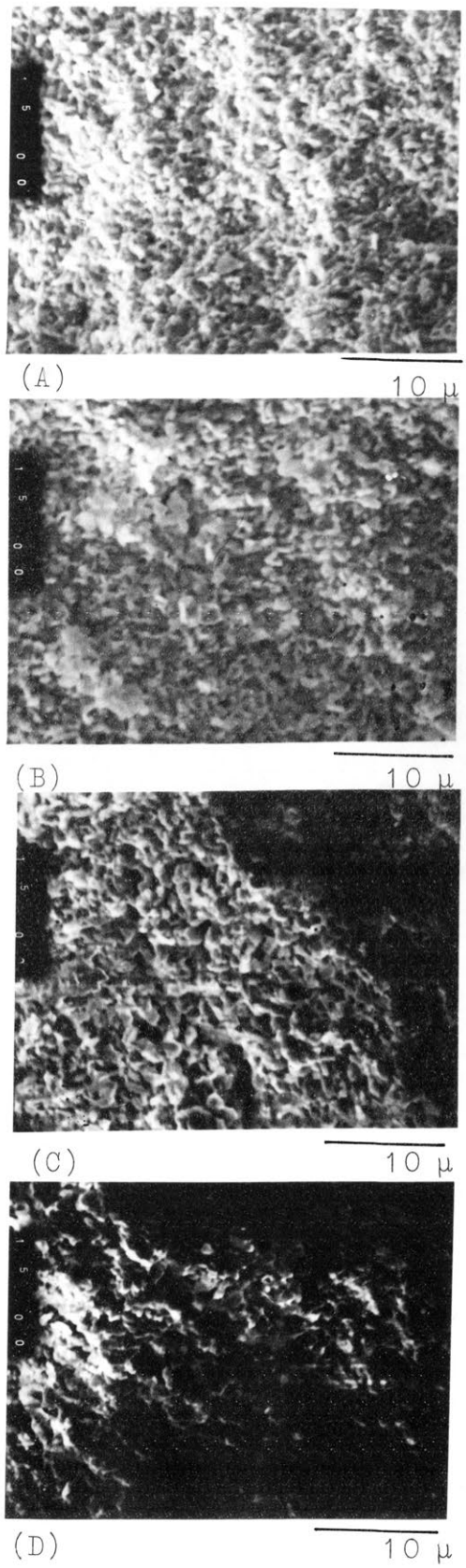

Figure 8.35. (A)(B)(C)(D) Scanning Electron Micrographs of Thoria Containing Ceria

(A) 10 μ

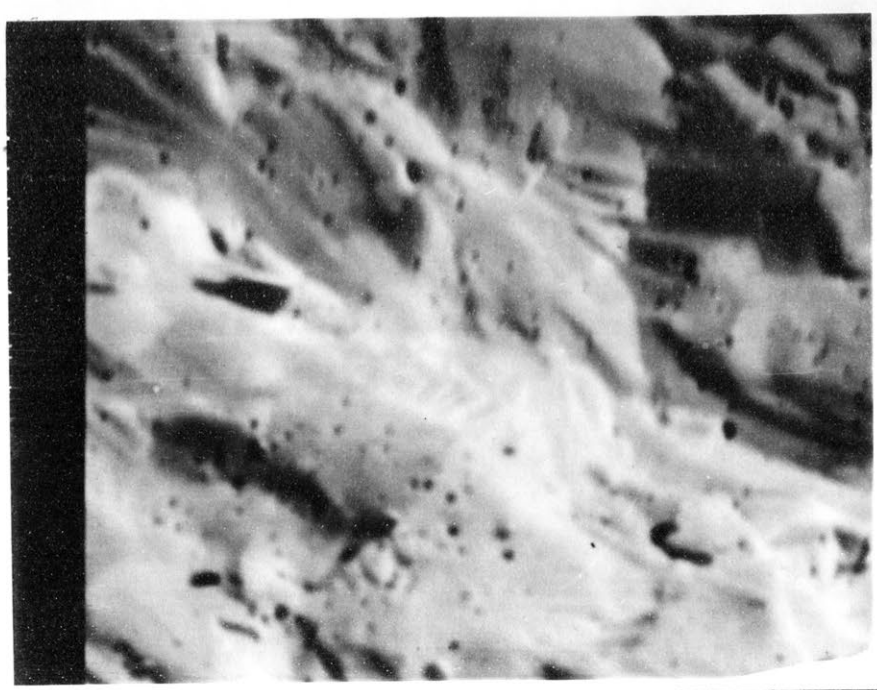

(B) 10 μ

Figure 8.36. Scanning Electron Micrographs of Thoria
(A) Fired 16 hours at 1400 C
(B) Fired 16 hours at 1600 C

effect. The high temperature systems shown in Figure 8.33 generally retained the grain nature of the lower temperature but the glazing was not evident. Also the necking which was developing in the low temperature stages has proceeded but sintering has obviously not been completed.

The ceria systems shown in Figures 8.34 and 8.35 have the least dense microstructure of all the tetravalent systems. Sintering had hardly begun even after 1600°C. The grain size of this system was apparently quite small, on the order of 1 micron for the low temperature system and approximately 2 microns for the high temperature systems.

Figures 8.36 A and B show pure thoria after 1400° and 1600°C firing respectively. From these microstructures it is obvious that with the exception of zirconium, strontium and barium, all fission product oxides impede grain growth and sintering of thoria.

8.2.6. Microhardness

Microhardness determinations were made on pellets composed of thoria and typical fission product oxides as a function of firing temperature and composition. The results of the measurements are shown in Table 8.8. As one would expect, the hardness of samples increased as the firing temperature increased. Of the pellets studied and fired to 1400°C, only those containing ten per cent strontia and five per cent neodymia had greater hardness than the pure thoria pellets. Of these two types, the pellets containing strontia were particularly hard, having a Vickers hardness three times that of thoria. The neodymia containing pellets were only slightly harder than pure thoria and dropped in hardness with increasing concentration of neodymia. For pellets fired to 1600°C

TABLE 8.8

Micro Hardness of Binary Systems of Thoria and Oxide Additions

Mole % of Oxide Addition		Vickers Hardness in kg/mm^2	
		1400 Firing Temperature	1600 Firing Temperature
5	Y	72.2	426.1
10	Y	144.8	565.2
20	Y	154.9	3645.3
5	Nd	447.4	-
10	Nd	141.6	1318.2
20	Nd	194.1	-
5	La	26.0	-
10	La	19.3	806.3
20	La	109.2	1743.4
1	Sr	-	5903.0
5	Sr	-	8541.3
10	Sr	953.3	-
20	Sr	-	-
1	Ba	42.8	-
5	Ba	-	-
10	Ba	-	-
20	Ba	-	-
5	Zr	187.9	6344.0
10	Zr	103.2	2792.0
20	Zr	63.5	2425.2
5	Mo	150.4	3623.6
10	Mo	63.4	2812.6
20	Mo	50.8	2510.5
1	Ce	305.6	4807.0
5	Ce	94.6	2368.0
10	Ce	161.3	3318.6
20	Ce	59.6	647.7
0	-	307	8059.0

only those containing five per cent strontia were equivalent to pure thoria pellets in hardness. Pellets containing ten per cent strontia were not tested as these had disintegrated and it is not known whether these pellets would have had a hardness greater than pure thoria; however, judging from the general trend between pellets containing one per cent and five per cent strontia it is likely that those containing ten per cent would have been harder.

A correlation was sought between hardness and composition of the pellets. The pellets were found to be of two types; those whose hardness decreased with decreasing thoria content and those whose hardness increased with decreasing thoria content. Pellets of the first type were those containing neodymia, zirconia, molybdenia and ceria. The pellets containing baria had disintegrated before sufficient microhardness data could be obtained to establish any trends. Pellets containing the remaining oxides were of the second type. The only correlation which could be made between the microhardness measurements among the samples was that, as the porosity of pellets containing thoria and one addition oxide decreased, the microhardness increased. This correlation of course is only a qualitative one; however, when one realizes that the microhardness determination is a measure of the energy required to displace material, the correlation between porosity and microhardness for a particular composition is expected.

8.2.7. Effect of Aging of Calcined Oxide on Sintered Density

It was briefly pointed out earlier that variability in sintered density was found in thoria specimens prepared from the same material but fired at different times. Besides the obvious possibility of improper temperature control, other information[34]

indicates that exposure to atmospheric CO_2, could account for the variation in fired density of pellets made from the same material. The first two columns of Table 8.9 compare the densities after firing to 1400°C, of pellets produced from freshly calcined oxide and those produced from oxide which had been stored under air. The third and fourth columns give similar results on two sets of pellets, the first of which were fired immediately after pressing freshly calcined oxide, the second of which were fired after storage under dry CO_2.

TABLE 8.9

Density of ThO_2 Pellets made from Aged and Unaged Powders

	Firing Temperatures			
	1400°C		1400°C	
	Unaged	Aged in dry air	Unaged	Aged in CO_2
Density (av) g/ml	7.70	7.28	7.83	7.59
Porosity (av) %	17.99	26.71	23.35	25.03
Apparent specific gravity (av)	9.56	9.90	10.14	10.25

These results show the effect that indiscriminate storage may have on the sinterability of very fine powders. Because this effect was recognized, thoria powder used in this work was made by calcining the oxalate just prior to, or within a few days of use. The ageing mechanism which caused the decrease in fired density is not completely understood; however, it can be said that the adsorption of CO_2 on the powder prior to firing is one factor that affects the ultimate density.

8.2.8. Thermal and Electrical Property Measurements

Thermal diffusivity measurements were carried out on several thoria-fission product oxide binaries by the Australian Atomic Energy Commission. Table 8.10 shows the results obtained.

TABLE 8.10

Thermal Diffusivity of Fired Thoria Compositions

Room Temperature Oxide Added to Thoria	Mole Per Cent of Added Oxide	Apparent Thermal Diffusivity cm^2/sec
Strontia	5	0.0085
Strontia *	5	0.0121
Ceria	5	0.0131
None		0.0130

* Fired to 1600°C, all others fired to 1400°C

The thermal conductivity may be calculated using equation

$$k = \alpha C_p \rho \; ; \qquad (8.2)$$

k = Thermal conductivity

α = Thermal diffusivity

C_p = Heat capacity

ρ = Bulk density

This equation involves determination of both heat capacity and density. Since the samples were relatively porous, a porosity correction would also have to be made. The values of thermal diffusivity are somewhat in question due to two problems encountered during the run. First the thermal contact resistance was apparently quite high and second the energy distribution across the sample was uneven. The second problem has been overcome recently by the installation of an impulse laser. In view of the problems associated with determination of heat capacities and the inherent problems with the thermal diffusivity measurements no further work was planned along these lines.

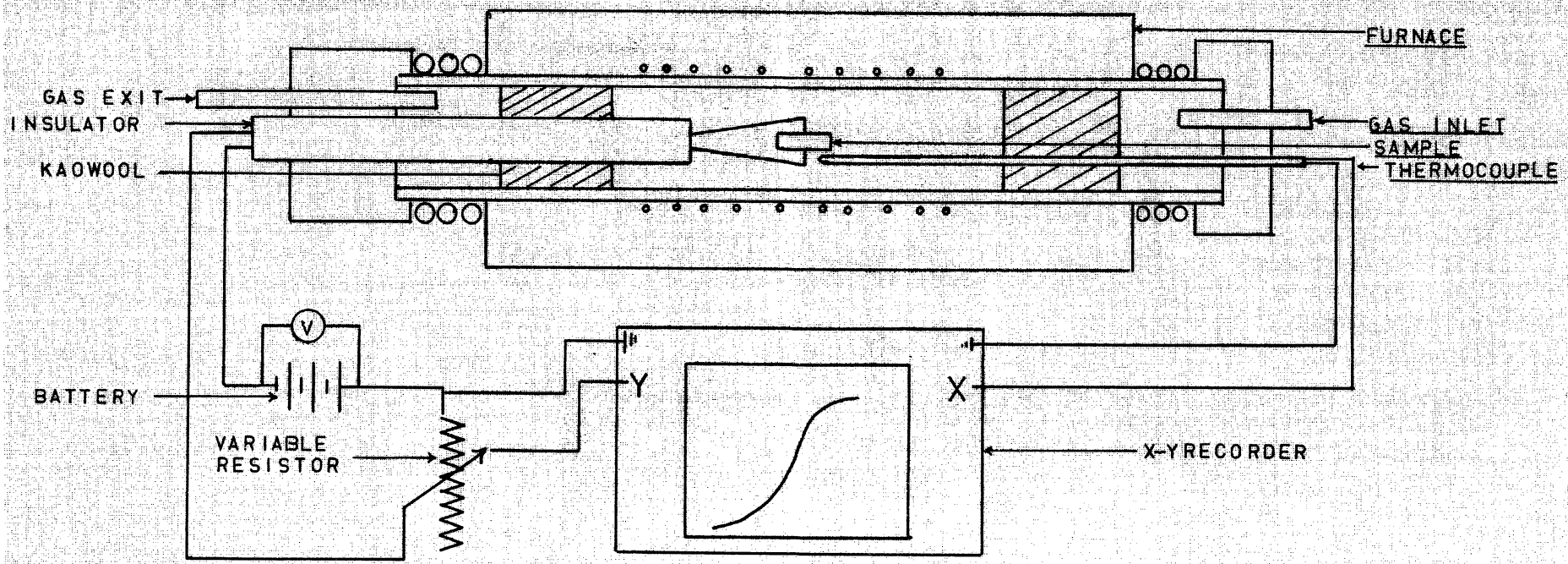

FIGURE 8.37

D.C. ELECTRICAL CONDUCTIVITY APPARATUS

The electrical conductivity measurements of the binaries were carried out on representative samples using D.C. current according to the experimental circuit shown in Figure 8.37. The two-electrode measurements were carried out up to 1000°C under oxygen and in some cases nitrogen. Nitrogen was used to determine what the effect of lowering oxygen partial pressure would have on the conductivity of the specimen. Since all were expected to be ionic conductors the oxygen partial pressure should have a large effect on the conductivity. Figure 8.38 shows plots of ln σ versus 1/T for the various binaries. Work has been reported by Subbarao et al.[67] on the conductivity of thoria-yttria solid solutions in the range of compositions used in this work. In their work, A.C. conductivity was determined at 1000 Hz as a function of temperature in air and oxygen. The findings of this work were that increasing the oxygen partial pressure increased the conductivity and that the conductivity was essentially ionic. At five per cent yttria, the activation energy for conduction was 1.0 ev, at 2 per cent, 1.1 ev and, at one per cent, 1.3 ev. Extrapolating the activation energy to ten per cent which is the concentration of yttria used with thoria in this work a value of 0.53 ev is obtained. The value of the activation energy obtained for the yttria-thoria solid solution in oxygen in this work was 0.56 ev and in nitrogen was 0.45 ev. The total conductivity obtained in this work was less than that previously reported. However this undoubtedly is due to the A.C. versus D.C. measuring technique. In Table 8.11 the activation energies for electrical conduction are shown for the binaries under oxygen and nitrogen. In the binary solid solutions two regions were noted which appeared to have different activation energies. These regions will be termed

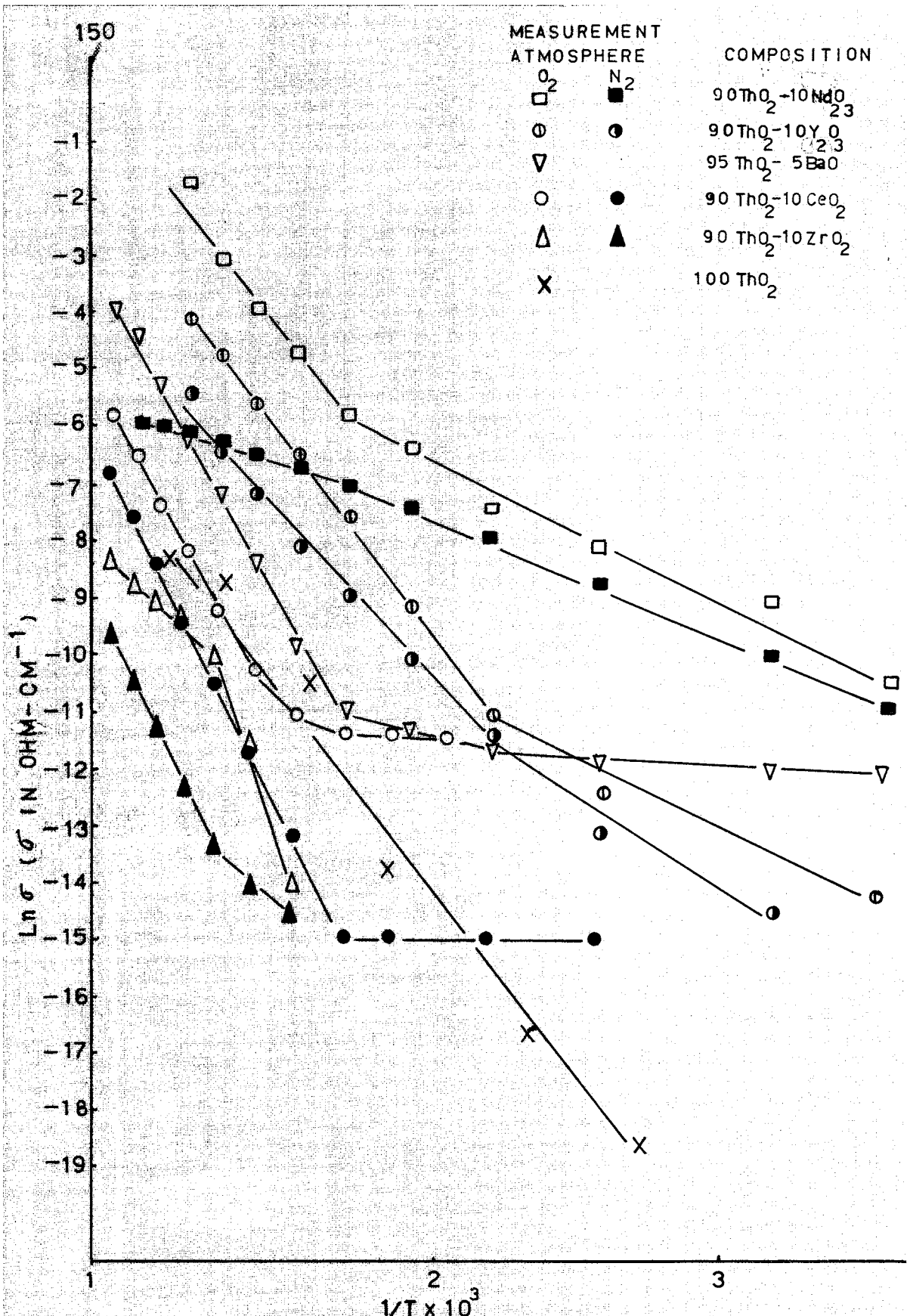

FIGURE 8.38

CONDUCTIVITY VS $1/T \times 10^3$ C

the high temperature region and the low temperature region. This character was not seen for pure thoria. In every case but one, the activation energy in the high temperature region was significantly greater than that for the low temperature. The exception was the binary system with zirconia. In all cases, the conductivity under nitrogen was lower than under oxygen. Data available are not adequate to understand exactly the mechanisms involved but it appears in the case of binaries of +4 valency ions the energy to activate conduction sites is greater under conditions of low oxygen partial pressure which accounts for the low conductivity, while for the binaries containing +3 valency ions the activation energy for conduction in atmospheres of low oxygen partial pressure is lower but the number of carriers is also lower hence the decrease in conduction. The reason for the extraordinarily large increase in activation energy for conduction from high temperatures to low temperatures in oxygen for the zirconia system is not understood.

TABLE 8.11

Activation Energy for Electrical Conduction of Binary Systems with ThO_2

Measuring Atmosphere Temperature Range	Activation Energy in ev			
	O_2		N_2	
	High	Low	High	Low
% Oxide Addition to ThO_2				
10 Zr 10	0.41	1.53	0.88	0.40
10 Ce 10	0.81	0.04	0.83	0.01
10 Y 10	0.56	0.06	0.45	0.30
10 Nd 10	0.52	0.22	0.13	0.16
5 Ba 5	0.81	0.12		
100 Th 100	0.63	0.63		

8.3. Structure and Composition of Phases in the Binary Systems of Thoria and Fissium

Major effects that fission products have on thoria are the change of structure of the thoria fluorite lattice and the formation of second phases in the thoria matrix. To study these structural effects, their basic studies were undertaken which are discussed in the following sections. These include lattice parameter change of thoria with single fission product oxide addition, diffusion gradients across reaction couples, and formation of new phases between several fission products oxides and thoria. These studies were to be used to predict changes which could occur in the simulated thoria based fuel element.

8.3.1. Effect of Added Oxides on the Crystal Structure of Thoria

Thoria is a stable dioxide with little tendency toward non-stoichiometry. While it is known to accommodate large quantities of impurities, the limit of solubility of the various added oxides used in this work was expected to occur below the 20 mole per cent addition, in view of evidence suggesting that calcia was soluble in thoria only up to five per cent or less[29]. There were also large disparities between the sizes and valencies of the added ions and those of thorium.

Originally, an X-ray diffractometer was used to study the crystal structure of the binary systems with thoria but only thoria lines were detected. Film was then used in an effort to see second phases which might not be detected by the diffractometer. Sample dilution was also tried in an effort to identify any separate phases in the thoria matrix. In no case was a second

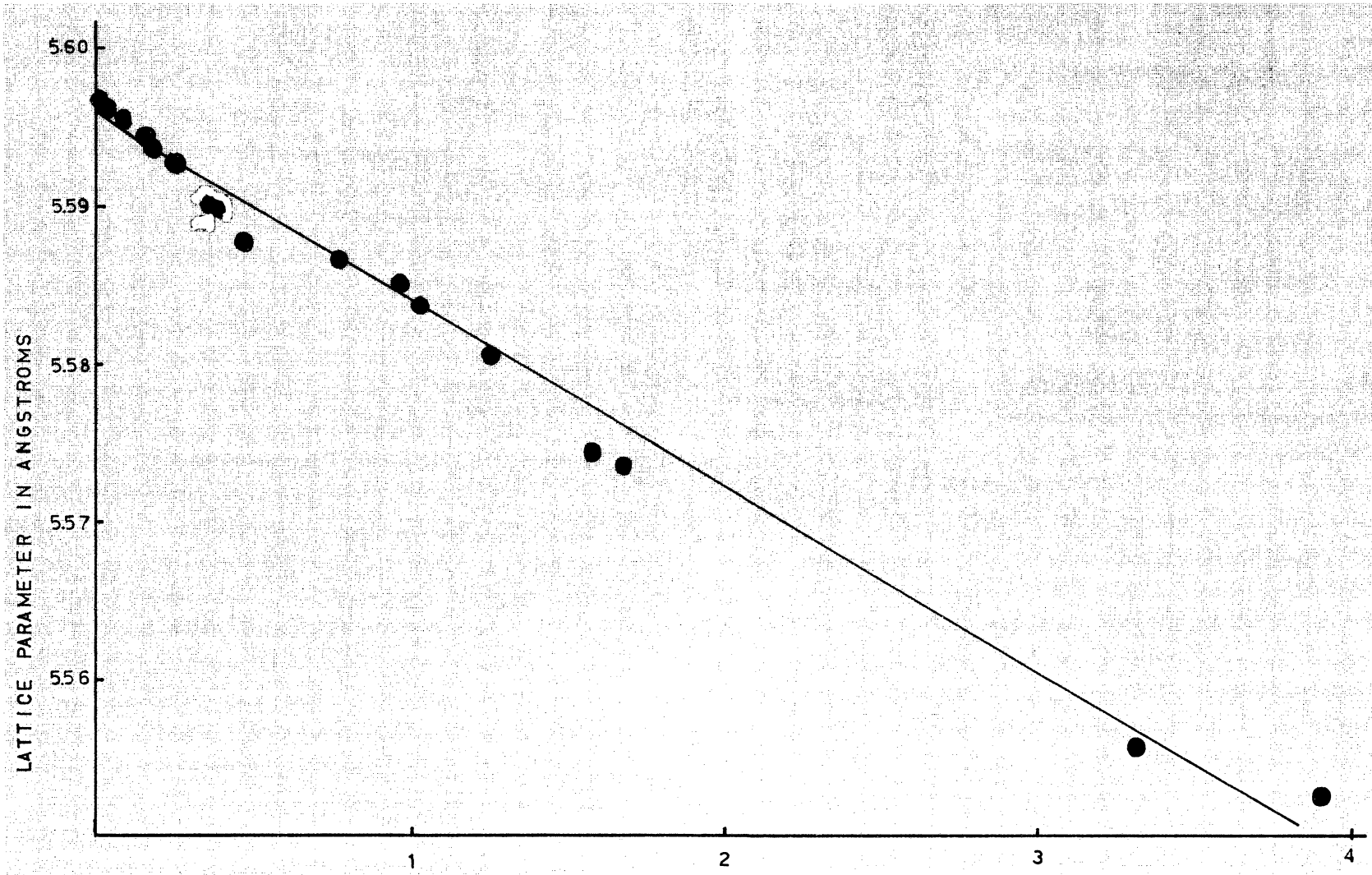

FIGURE 8.39
LATTICE PARAMETER VS $1/2[\cos^2\theta/\sin\theta + \cos^2\theta/\theta]$

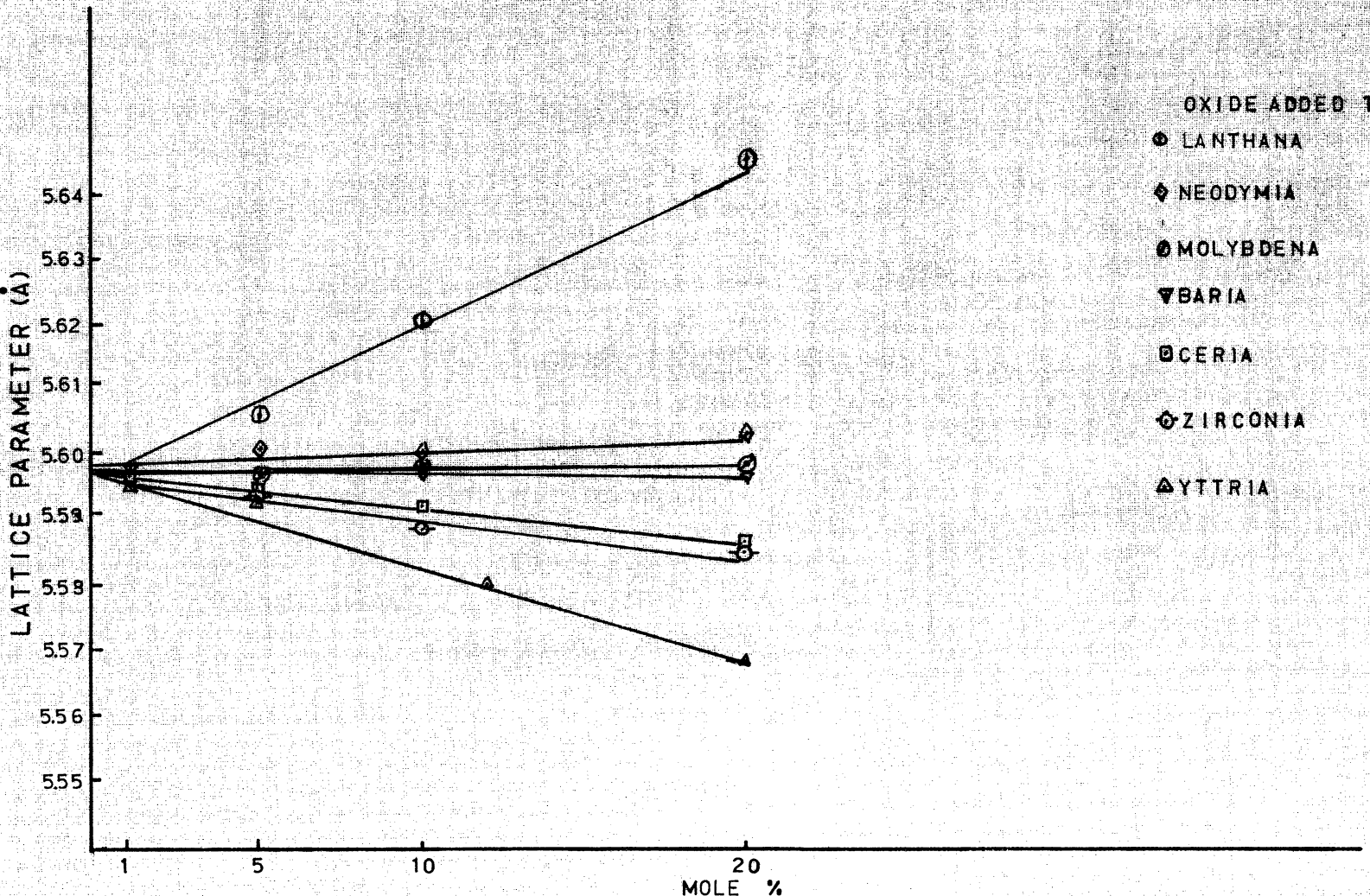

FIGURE 8.40

LATTICE PARAMETER VS COMPOSITION OF BINARY SYSTEMS ThO_2-RO_x

phase found; only thoria lines were observed for all binary systems studied in this work up to 20 mole per cent. Great care was taken to ensure the maximum sensitivity. In Figure 7.2 a typical film is reproduced and shows the clarity and fineness of the lines on the film. The back reflections were easily seen and therefore improved the accuracy of the lattice parameter determinations. Lattice parameter determination of pure thoria was made. The crystal structure is cubic belonging to the space group $O_h^3(Fm3m)$. The lattice parameter determined for thoria fired in dry nitrogen at 1700°C for 72 hours was 5.5957. This indicates a smaller unit cell than the 5.5997 which is given by Swanson and Tatge[91]. The raw data were corrected using two methods; the first involved plotting the raw lattice parameter against a plotting function involving θ, as seen in Figure 8.39. The second method involved determining the lattice parameter of calcium fluoride which was used as an internal standard and adjusting the raw Ao values for thoria accordingly. The two correction methods gave a value of 5.5958 Å and 5.5957 Å respectively. X-ray diffraction patterns of binary systems studied in this work were indexed according to the above mentioned method and the resulting lattice parameters are shown in Figure 8.40. Although Vegard's law assumes several conditions which are not met in the formation of these solid solutions, the lattice parameters tend to vary linearly with composition at least up to 20 per cent. Over large compositional ranges Subbarao et al.[67] and Keller et al.[66] have shown that large deviations from Vegard's law are found.

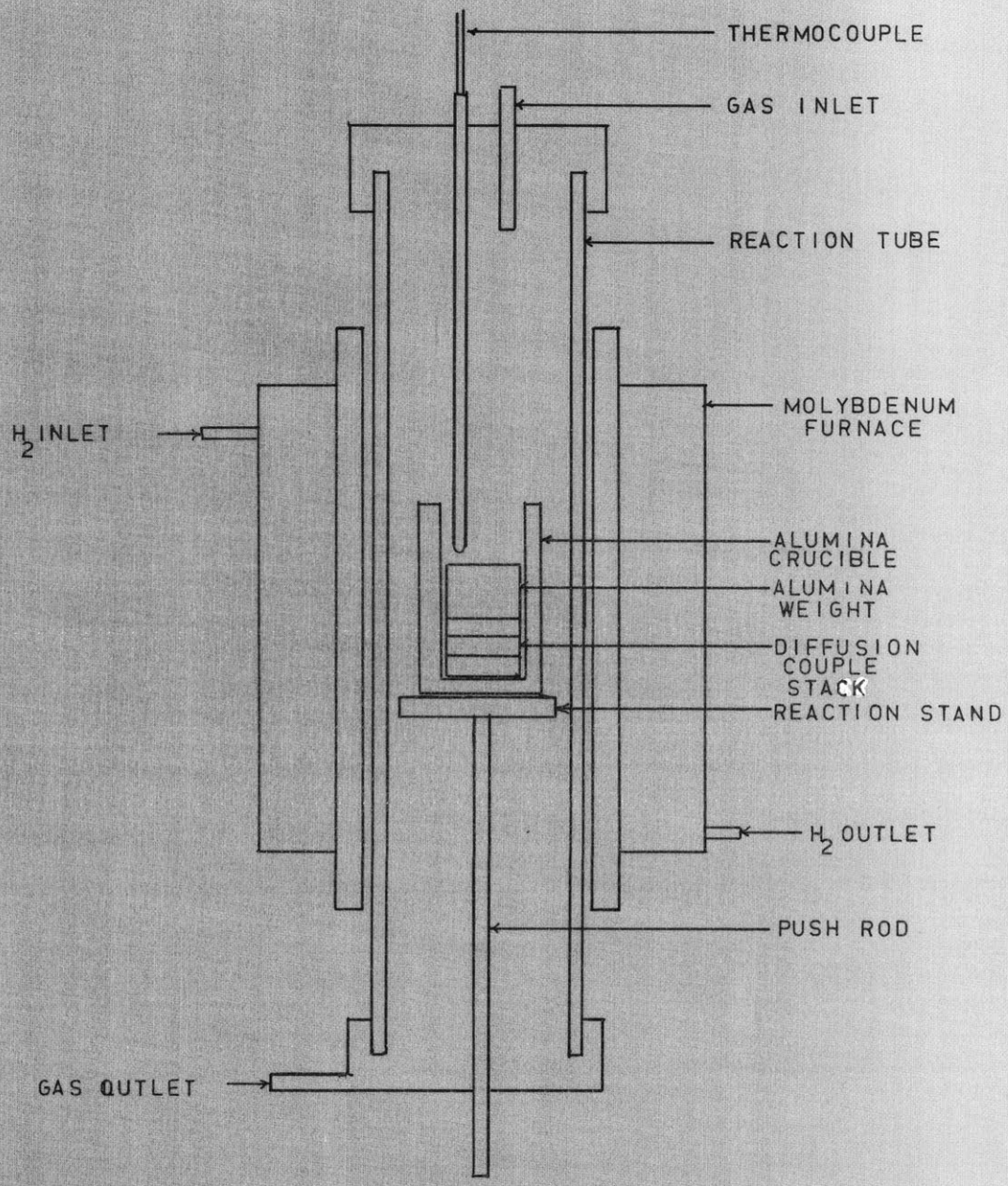

FIGURE 8,41

DIFFUSION COUPLE REACTION FURNACE

8.3.2. Diffusion and Reaction Occurring between Thoria and Fission Product Oxides

A series of diffusion couples was planned to be fired to determine the effect of temperature and atmosphere on the distribution of fission products among themselves and thoria. In another study of a simulated fuel element after high burn-up, the results of which are discussed in detail in Section 8.43, a stable pyrochlore phase of the type $Nd_2Zr_2O_7$ was found with which cerium became associated under reducing conditions but not under neutral conditions. In order to determine the validity of that finding the initial diffusion couple study was made on a system consisting of the three pellets ThO_2, CeO_2, and $Nd_2Zr_2O_7$. The configuration of the pellets are shown in Figure 8.41. The pellets were prefired to relatively high densities shown in Table 8.12.

TABLE 8.12

	Density g/ml	Porosity %	A.S.G.
ThO_2	9.22	2.59	9.46
CeO_2	6.95	1.77	7.076
$Nd_2Zr_2O_7$	5.22	5.36	5.55

The pellets were polished prior to stacking in the alumina crucible and fired for 6000 minutes at 1460°C under oxygen or under five per cent H_2 in N_2. The reaction between these pellets was very slight and, in fact, the pellets separated upon handling. X-ray diffraction was carried out on the surface of the pellets and, in all cases, ceria was found at the interface indicating that cerium was the principal diffusing species. The couple was

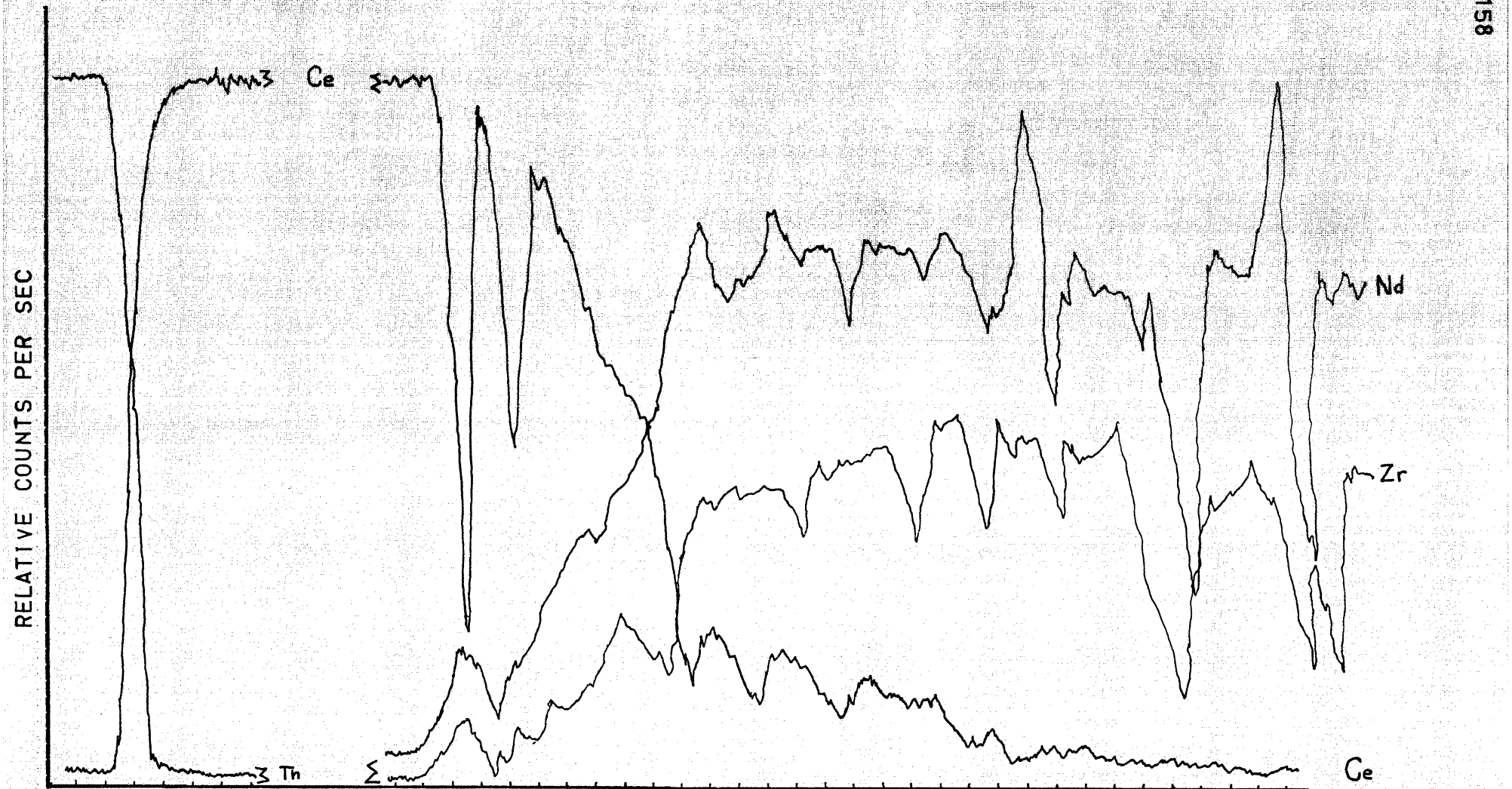

FIGURE 8.42
PROBE TRACE ON OXIDIZED DIFFUSION COUPLE

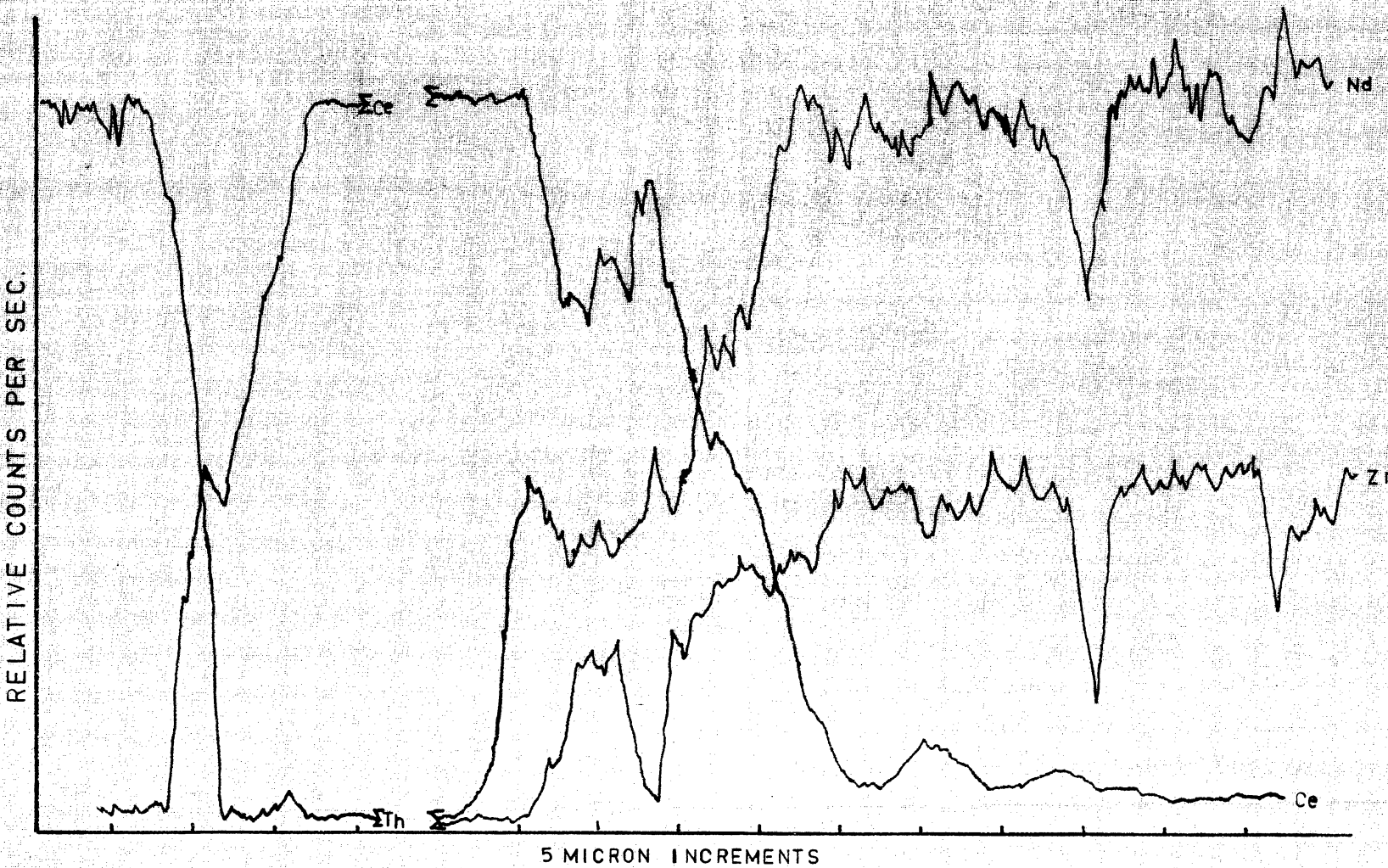

FIGURE 8.43
PROBE TRACE ON REDUCED DIFFUSION COUPLE

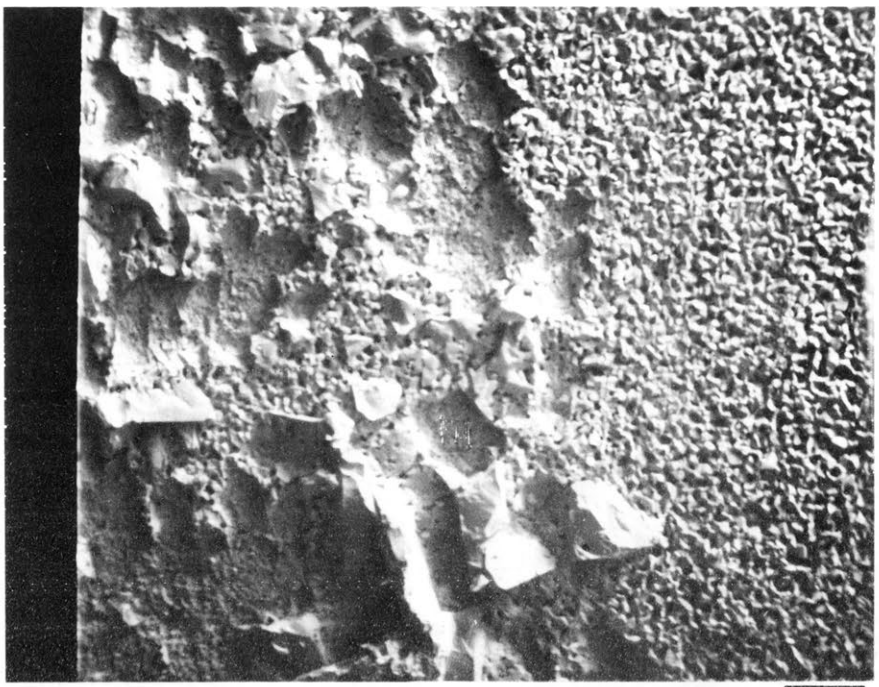

(A) 100 μ

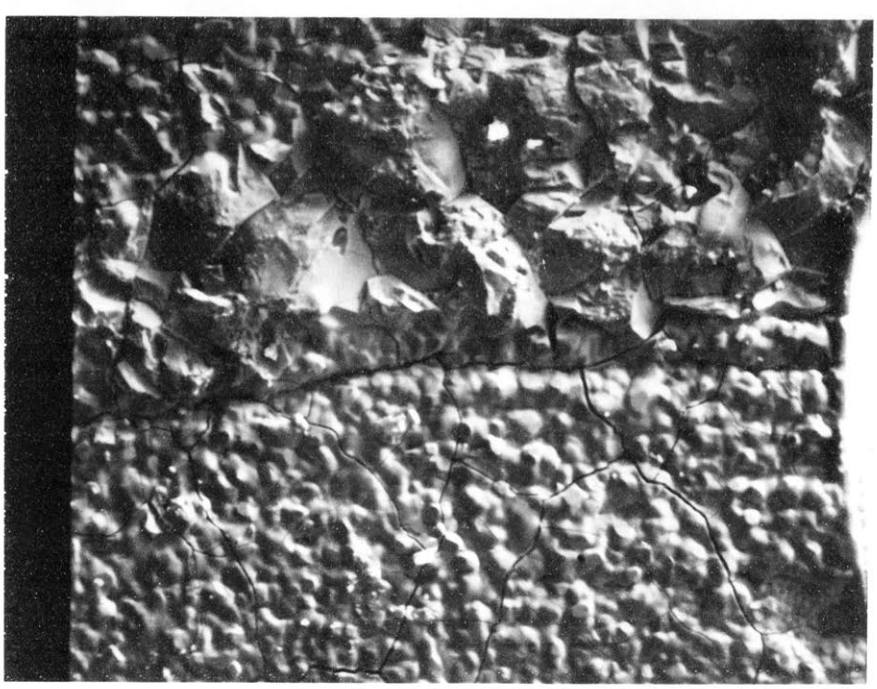

(B) 100 μ

Figure 8.44. Scanning Electron Micrographs of the Surface of Diffusion Couple Interfaces Reacted under Reducing Conditions
(A) $Nd_2Zr_2O_7$-Ce_2O_3 Interface
(B) ThO_2-Ce_2O_3 Interface

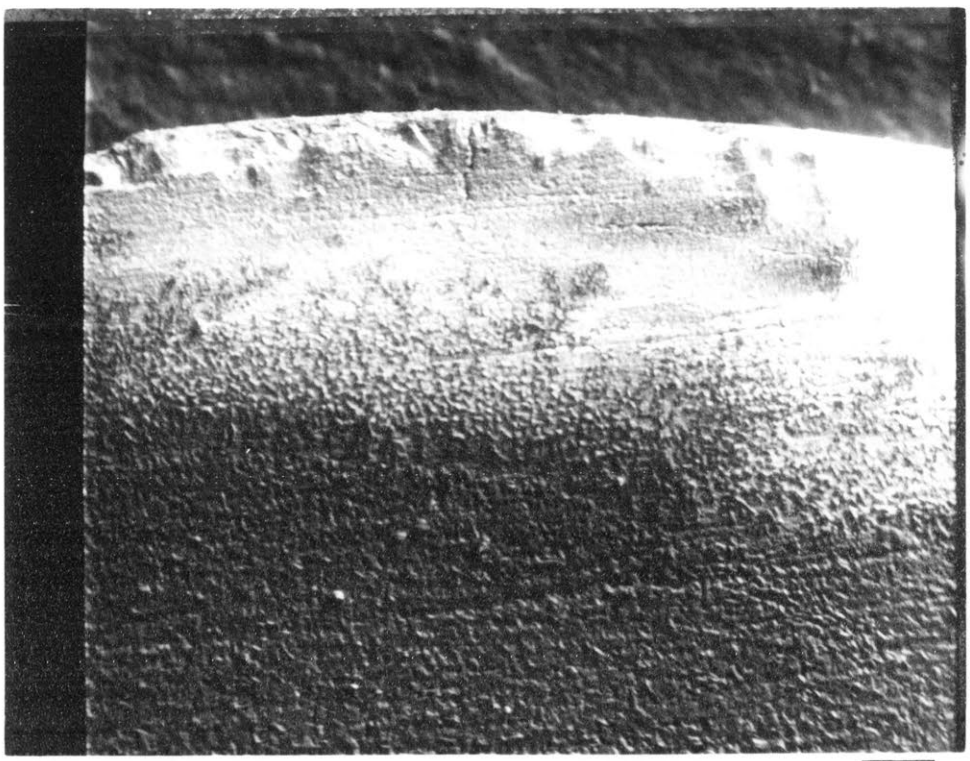

Figure 8.45. Scanning Electron Micrograph of the Thoria Ceria Interface near the Edge of the Thoria Pellet

mounted and polished so that both reaction interfaces were exposed and an electron microprobe trace was made across the interfaces. Resulting traces are shown in Figure 8.42 for the oxidizing conditions and in Figure 8.43 for the reducing conditions. The extent of reaction between the couples was very low. Ce appeared to be the only diffusing species, which confirms the X-ray diffraction results, penetrating only 120 and 60 microns into the $Zr_2Nd_2O_7$ pellets under oxidizing and reducing conditions respectively and only about 5 microns into thoria. Second, the porosity of the reacting pellets made microanalysis difficult in that voids were not easily distinguishable from ion concentration minima. Third, since the pellets were not firmly stuck together, location of the exact position of the interface btween reacting pellets was not possible. Scanning micrographs of the interfaces show that the ceria has a marked effect on the microstructure of the pellets. Figure 8.44 shows the $Nd_2Zr_2O_7$ and ThO_2 surfaces in contact with ceria reacted under reducing conditions. The unevenness of reaction may indicate that the contact between the pellets during the reaction was not good. It is interesting to note that these micrographs were made on uncoated samples which indicates that traces of ceria in the +3 state make these oxides sufficiently conducting to prevent charging under the influence of the electron beam. Similar pictures of the oxidized samples could not be made. Figure 8.45 shows again the thoria surface at lower magnification where charging occurs near the edge of the pellet where ceria was not in contact.

An attempt to reduce the porosity of the pellets, which adversely affected the microprobe analysis, was made by hot pressing compacts of the ceria and the neodymia zirconia solid solution.

Hot pressing was conducted at the Australian Atomic Energy Research Establishment using an induction heater and graphite dies. After the hot pressing was completed the $Nd_2Zr_2O_7$ pellet was found to be poorly densified and the ceria pellet had been converted to Ce_2O_3 which had occurred in the original couple work in reducing conditions. The neodymia pellet crumbled after a few days. Crumbling of neodymia compounds,which was attributed to hydration, has been noted by Fullam and Mitchell[93] in work done on hot pressing of rare earth oxides. The explanation by a hydration mechanism is not entirely satisfactory in that samples containing Nd_2O_3 fired in air and N_2 in this work have remained stable for, in some cases, up to two years. While there is not sufficient evidence available to confirm or deny the hydration theory, a possible explanation may be CO_2 attack found by Hoffmann[72] in the $BaThO_4$ system. The reaction of the neodymia at high temperature in a carbon atmosphere may sufficiently deplete the structure of oxygen to allow the Hoffmann mechanism to occur. Of course, a completely different mechanism of deterioration involving reoxidation of the reduced specimen could also occur. By reduced specimen it is meant that the equilibrium concentration of oxygen vacancies is increased, not necessarily that the valency state of Nd^{+3} or Zr^{+4} has been grossly changed since both are rather stable.

8.3.3. Stable Mixed Oxide Phases with Thoria

In order to determine the stable phases formed between typical fission product oxides and thoria, a study similar to that reported by Koizumi and Satoh[57] was carried out. In their study Koizumi and Satoh analyzed phases formed between the oxides of Ba, Sr, Zr and U at various temperatures using high temperature X-ray

techniques. The results of that investigation were compared to results reported on the analysis of real urania based fuel elements.

In this study, the phases formed between the fission product oxides of +2, +3 and +4 valency cations and thoria were analyzed by X-ray diffraction at room temperature on pellets fired at 1400°C and 1600°C under an inert and reducing atmosphere. The neutral atomosphere was obtained by admitting flowing argon while the reducing atmosphere was obtained by a flowing mixture of five per cent H_2 and ninety-five per cent N_2. The five compositions studied are shown in Table 8.13. Pellets of each composition were pressed and fired under the above mentioned conditions for 24 hours.

TABLE 8.13

Compositions of Oxides used in the Study of Stable Mixed Oxide Phases with Thoria

Powder	Composition
1	BaO, Nd_2O_3, ThO_2, ZrO_2
2	BaO, Y_2O_3, ThO_2, ZrO_2
3	BaO, La_2O_3, ThO_2, ZrO_2
4	BaO, Nd_2O_3, CeO_2, ThO_2, ZrO_2
5	BaO, Nd_2O_3, CeO_2, ThO_2

Phases which were identified in pellets of composition (1) were thoria, barium zirconate and a pyrochlore of the type $Nd_2Zr_3O_7$. Under reducing condition at 1600°C the thoria lattice had become distorted which was indicated by the diffraction peaks which were broadened and less intense. In pellets of composition (2) in

which the neodymium was replaced by yttria, barium zirconate was detected for all firing conditions. At 1400°C, both yttria and thoria phases were detected but there was no indication of the formation of a pyrochlore of the type $Y_2Zr_2O_7$. At high temperatures the thoria phase disappeared while another phase, which will be called phase X_1, appeared. This phase X_1 could not be unquestionably identified. The X-ray pattern for it was however similar to that for $Ce_2Y_2O_7$ as given in the X-ray file 9-286 and may be $Th_2Y_2O_7$.

Pellets from composition (3), in which lanthanum was substituted for yttrium, and fired to 1600°C, contained only two phases; a thoria phase and barium zirconate. These two phases probably both contain amounts of dissolved lanthanum oxide. The low temperature fired pellets crumbled before a diffraction pattern could be made which indicated free lanthanum oxides was present which readily hydrated. There was no indication of a pyrochlore phase between lanthana and either thoria or zirconia.

The first three compositions were designed to show the effect on the stable phases between the three oxides of Ba, Th and Zr and the three different sesquioxides of Nd, Y, and La. The fourth and fifth compositions were designed to study what effect ceria had on the stable phases formed in the first composition in two situations respectively; 1) when it is added to the four oxides of composition, and, 2) when it is substituted for zirconia. The pellets of composition (4) fired under neutral conditions were composed of two thoria phases (ThO_2 phase 1 and ThO_2 phase 2) and a barium zirconate phase. The major thoria phase had a smaller lattice parameter than pure thoria which was indicated by the shift of thoria diffraction pattern peaks to

higher angles. The second thoria phase gave a very weak diffraction pattern which was only slightly displaced from that for pure thoria. The major thoria phase is probably a ceria thoria solid solution with dissolved neodymia. There was no indication of the $Nd_2Zr_2O_7$ type phase seen in composition (1). Under reducing conditions, the three phases which were detected were: 1) a thoria rich phase; 2) a barium zirconate phase; and 3) a pyrochlore type phase which was indexed as $Ce_2Zr_2O_7$ but which may have also contained Nd^{+3} ions. It appears that under reducing conditions ceria changes its valency and tends to be more stable in the pyrochlore structure than in solid solution with thoria.

Pellets of the last composition fired under neutral conditions were composed of a thoria phase and a barium cerate phase. Under reducing conditions a third phase appeared which will be called phase X_2. This phase gave an X-ray pattern which did not correspond to any reported phase in the X-ray file index; however, was similar to that given by $BaFeO_{2.9}$, 25-68. The similarity of the patterns indicated that the phase might be a $BaCeO_{2.9}$ type phase or some other hypostoichiometric compound. That such a phase is forming is supported by the fact that the quantity of the $BaCeO_3$ decreased, as indicated by the lower intensity of the X-ray pattern, when the phase X_2 developed. This finding confirms aforementioned results that ceria tends to change its valency state under reducing conditions.

The results of this study agree with those of Koizumi and Satoh[57] in so far that barium zirconate appears to be readily formed and stable up to 1600°C. The latter authors found $(Ba,Sr)UO_3$ phases which developed at temperatures as low as 1150°C and as

TABLE 8.14

Stable Phases Occurring in Oxide Composition of Thoria and Typical Fission Products

Sample No.		Atmosphere	Reaction Products Identified	
			1400°C	1600°C
A	1	Argon	ThO_2 $BaZrO_3$ $Nd_2Zr_2O_7$	$BaZrO_3$ $Nd_2Zr_2O_7$ distorted ThO_2
	1	5% H_2:95% N_2	ThO_2 $BaZrO_3$ $Nd_2Zr_2O_7$	$BaZrO_3$ $Nd_2Zr_2O_7$ ThO_2
B	2	Argon	ThO_2 $BaZrO_3$ Y	$BaZrO_3$ Y Phase X_1
	2	5% H_2:95% N_2	ThO_2 $BaZrO_3$ Y	-
C	3	Argon	-	Mo_2 $BaZrO_3$
	3	5% H_2:95% N_2	-	ThO_2 $BaZrO_3$
D	4	Argon	$BaZrO_3$ ThO_2 Phase 1 ThO_2 Phase 2	$BaZrO_3$ ThO_2 Phase 1 ThO_2 Phase 2
	4	5% H_2:95% N_2	ThO_2 $BaZrO_3$ $Ce_2Zr_2O_7$	ThO_2 $BaZrO_3$ $Ce_2Zr_2O_7$ *
E	5	Argon	ThO_2 $BaCeO_3$	ThO_2 $BaCeO_3$
	5	5% H_2:95% N_2	ThO_2 $BaCeO_3$** + Phase X_2	ThO_2 $BaCeO_3$** + Phase X_2

* Very weak ** Intensity lowered drastically

Phase X_1 probably $Th_2Y_2O_7$ similar to 9-286 $Ce_2Y_2O_7$

Phase X_2 probably $BaCeO_{2.9}$ similar to 25-68 $BaFeO_{2.9}$

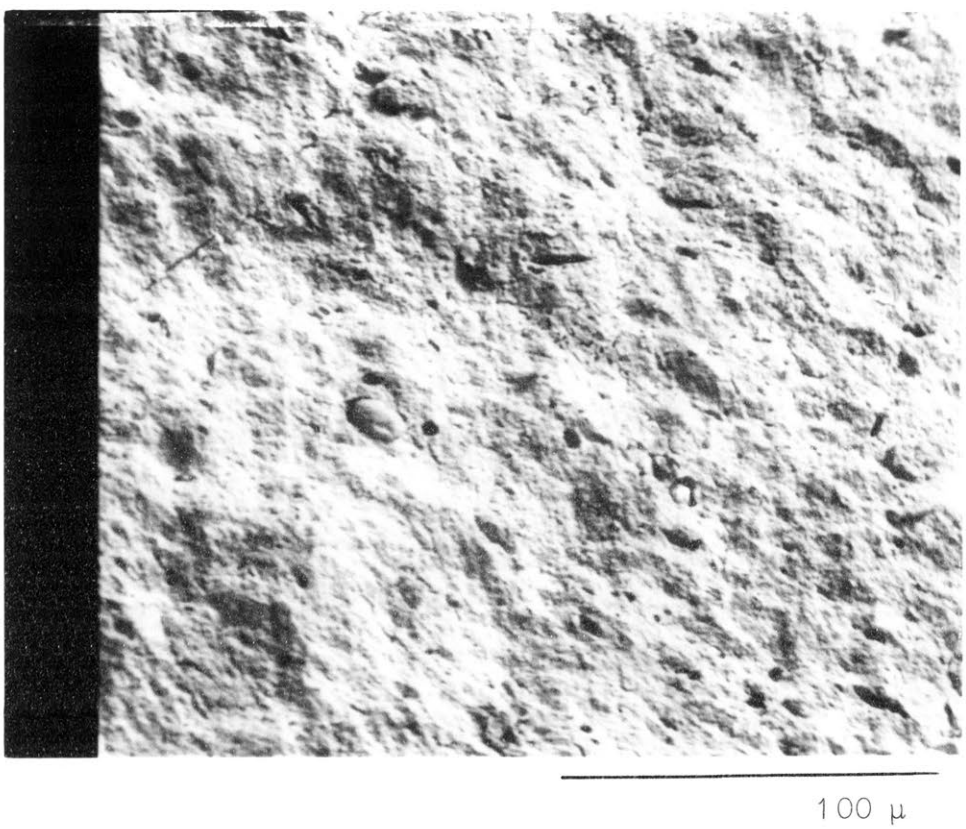

Figure 8.46. Scanning Electron Micrograph of a Fracture Surface of Thoria Containing Fission Products Fired 8 hours at 1600 C

high as 1650°C. They understandably found no pyrochlore phases since none of the compositions in their study included any +3 valent cations.

8.4. Simulation of a Fuel Element after High Burn-up

Simulation of a fuel element has been attempted by several workers as discussed in previous chapters, however, a totally satisfactory simulation was not achieved in those studies. It was the major aim of this work to develop a satisfactory simulation technique and study simulated fuel elements based on thoria as the fuel diluent. The non radioactive solid fission products were added to the thoria in various ways, described in the following sections, reacted and then analyzed to determine the change in microstructure and the development of secondary phases present with thoria.

8.4.1. Study of Hand Mixing Fission Products with ThO_2

The initial study involved mixing a few selected fission products with thoria by means of a mortar and pestle. Calcined thoria was added to the mortar with ethanol to which the pre-weighed fission products were added. In this initial study, only six of the most abundant fission products were added; ZrO_2, CeO_2, Nd_2O_3, MoO_3 and Mo metal. When the resultant mixture was dry enough steric acid-acetone solution was added to make a thick paste which was mixed until dry, whereupon pellets were pressed at 76.6 MPa and fired in oxygen free dry nitrogen to 1600°C for eight hours. The resulting specimens were analyzed in the scanning microscope and included phases with thoria were easily observable. Figure 8.46 shows the fracture surface showing two types of inclusions, one small and highly reflective and one larger and dull.

(A) 10 μ

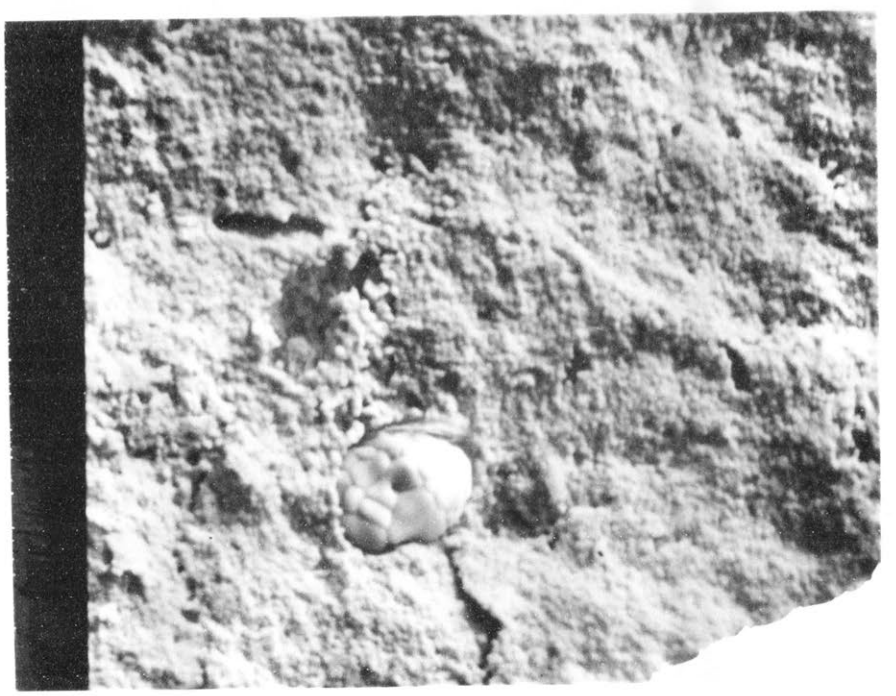

(B) 10 μ

Figure 8.47. Scanning Electron Micrograph of Highly Magnified Inclusions in Thoria Fracture Surface

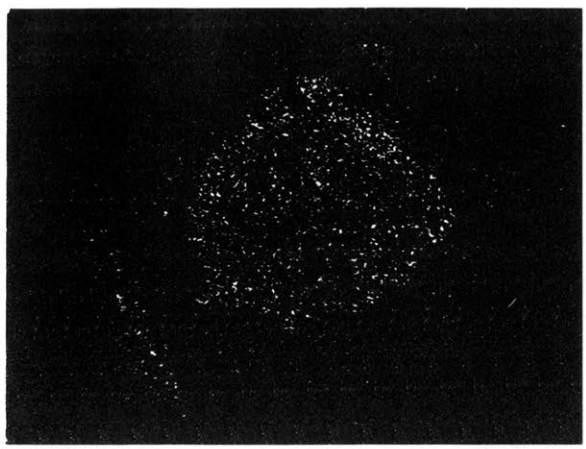

Mo

(A)

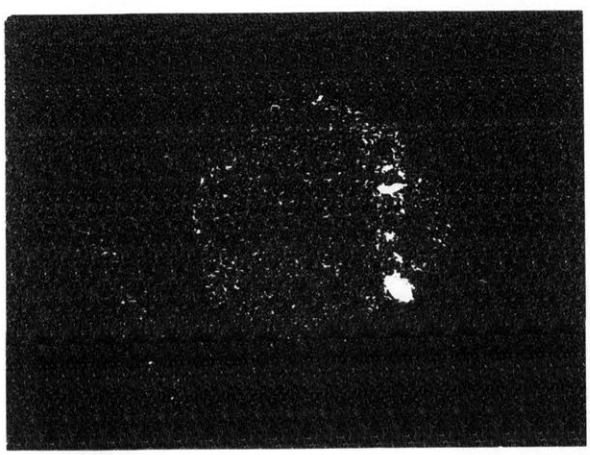

Sr

(B)

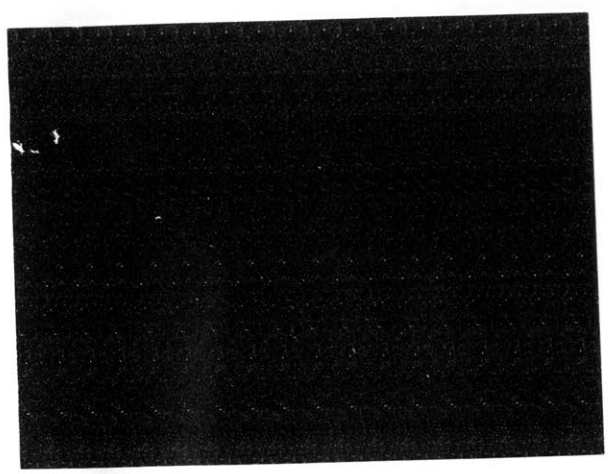

Ce

(C)

Figure 8.48. Microprobe Area Scans of Large Inclusions

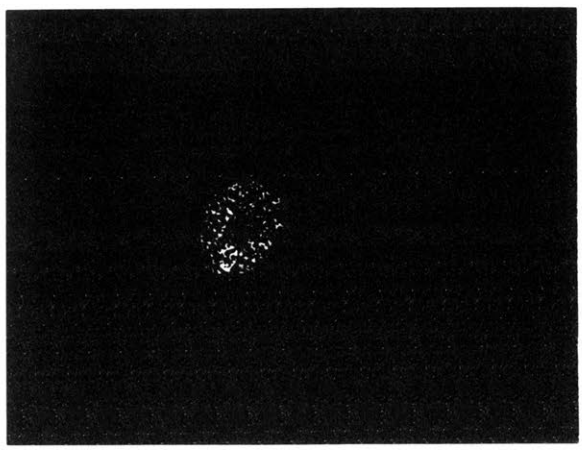

Nd

(A)

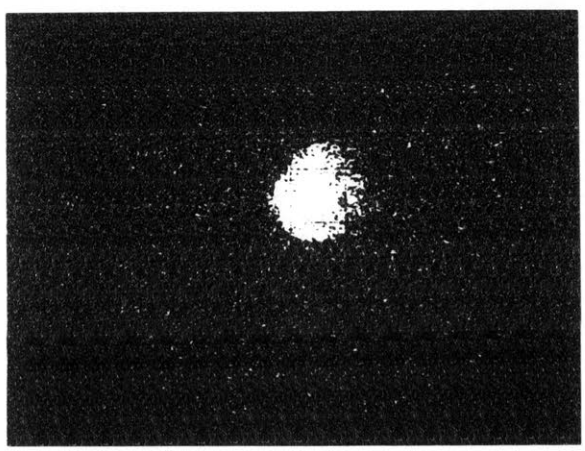

Zr

(B)

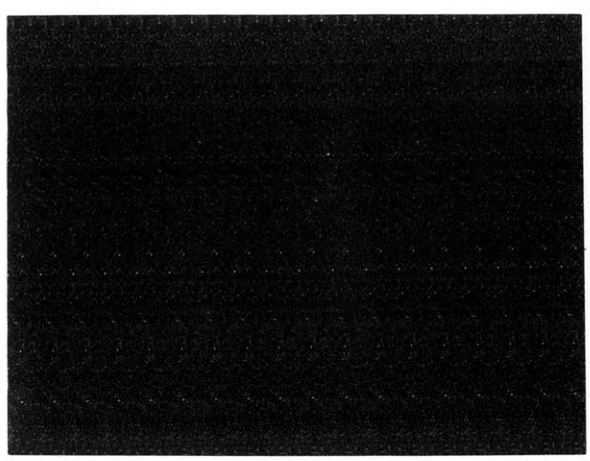

Ce

(C)

Figure 8.49. Microprobe Area Scans of Small Inclusion

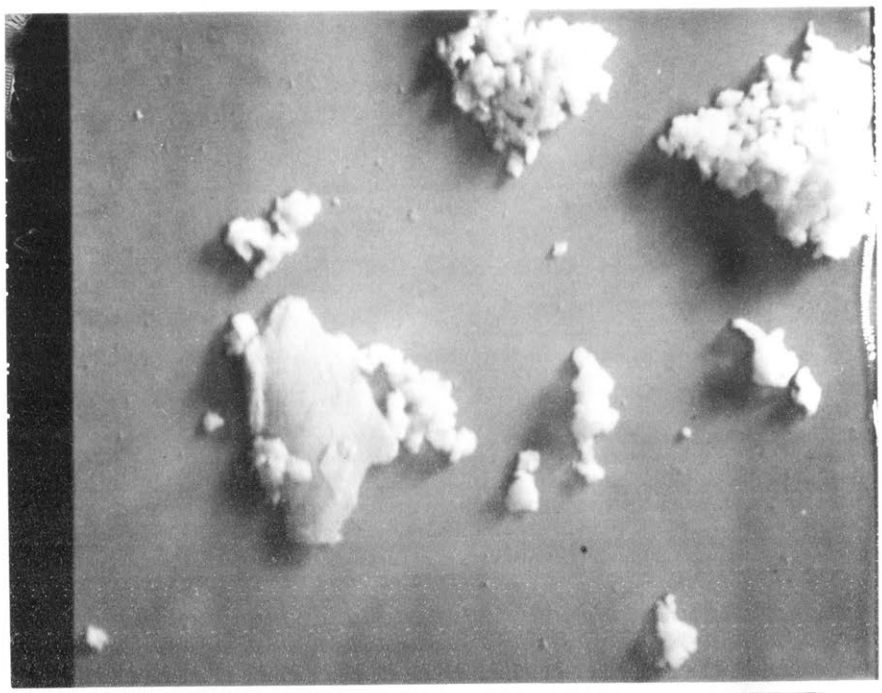

(A) 10 μ

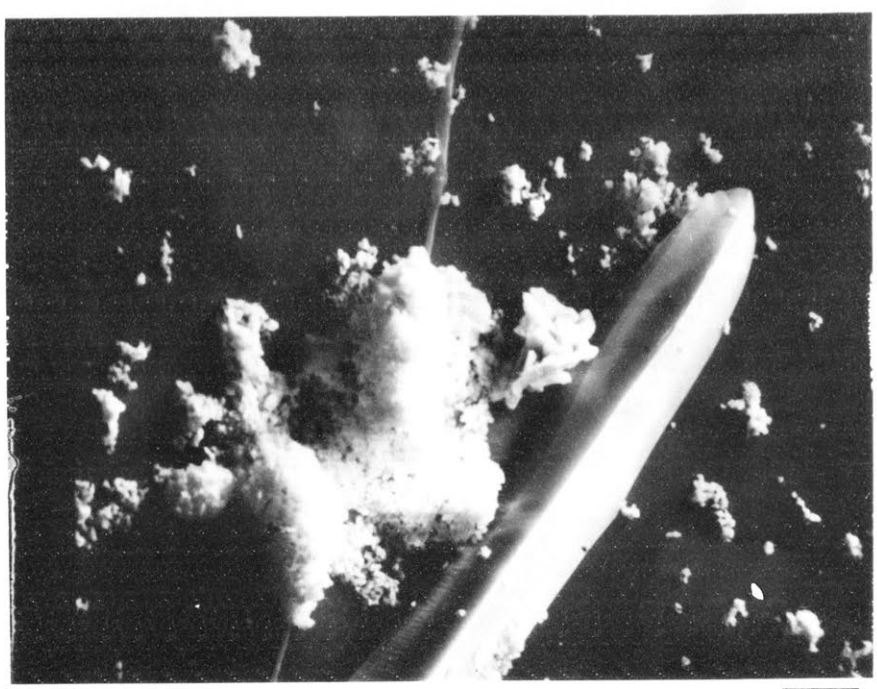

(B) 10 μ

Figure 8.50. Scanning Electron Micrographs of the Thoria-Fission Product Powder Mixture

(A) Thoria with ZrO_2 Particle

(B) Thoria with a SrO Particle

Figures 8.47 A and B show the two inclusions at high magnification. These inclusions were analyzed by the electron microprobe and it was found that the larger inclusion contained molybdenum and strontium and the small inclusion contained cerium, zirconium and neodymium. The area scans for the large and small are shown in Figures 8.48 and 8.49 respectively. Thoria was absent from these inclusions. In order to determine whether these inclusions were found upon firing as a result of solid state diffusion or the result of improper mixing, probe scans of an unfired pellet were made at the same magnification. These results indicated that, in the unfired state, particles of the size of the inclusion found in the fired specimen were present. The tendency to form compositions of two types discovered in the microprobe analysis may truly exist by noting the concentration gradient between Nd and Zr in Figure 8.49, but certainly a great deal of confidence cannot be placed in these results. Scanning micrographs of zirconium and strontium found in the mixed powder are shown in Figure 8.50 which confirms the results from the probe on an unfired pressed pellet. The unfired pellet deteriorated prior to further microprobe analysis making the detailed study impossible, but the scanning micrographs indicate that the detected inclusions were formed by the reaction of large particles of the mixed oxides. Since only two types of inclusions were formed similar compounds may be formed even in well mixed samples.

8.4.2. Intimate Mixing of Fissium with ThO_2

In order to achieve intimate mixing between thoria and fissium, a method of ball milling was devised using a type 6 nylon ball mill and zirconia balls. Zirconia was chosen since contamination by zirconia could be tolerated. The results of the initial

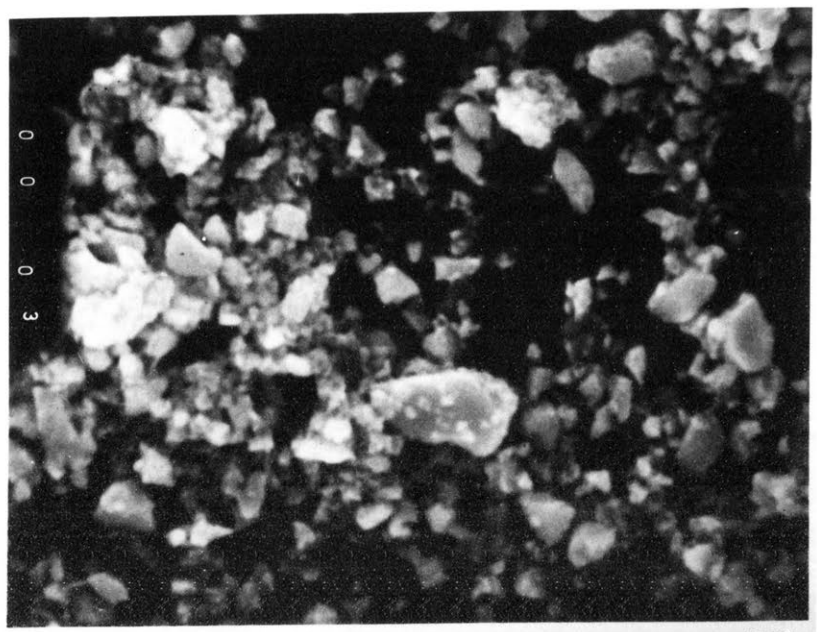

(A) 1 μ

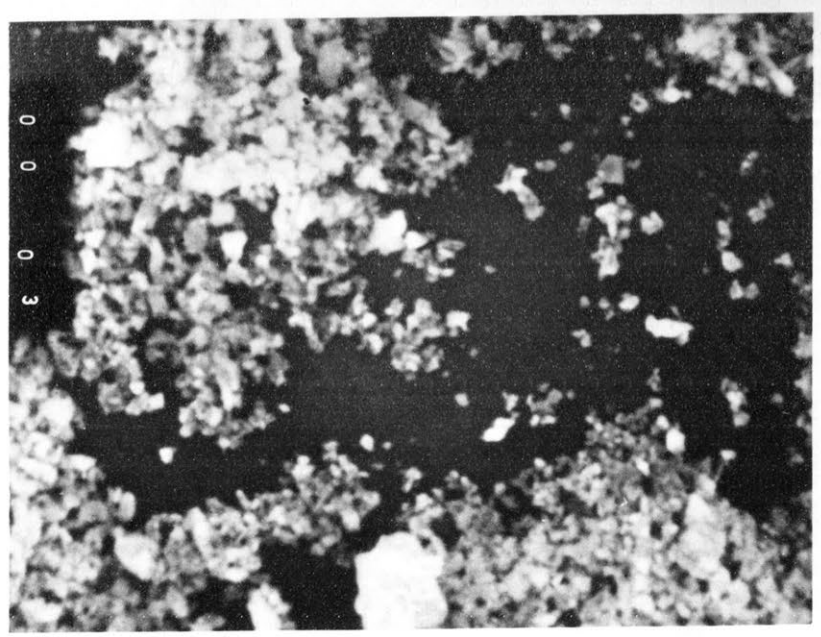

(B) 1 μ

Figure 8.51. Scanning Electron Micrographs of Thoria-Fission Product Mixed Powders
(A) Ball Milled
(B) Precipitated

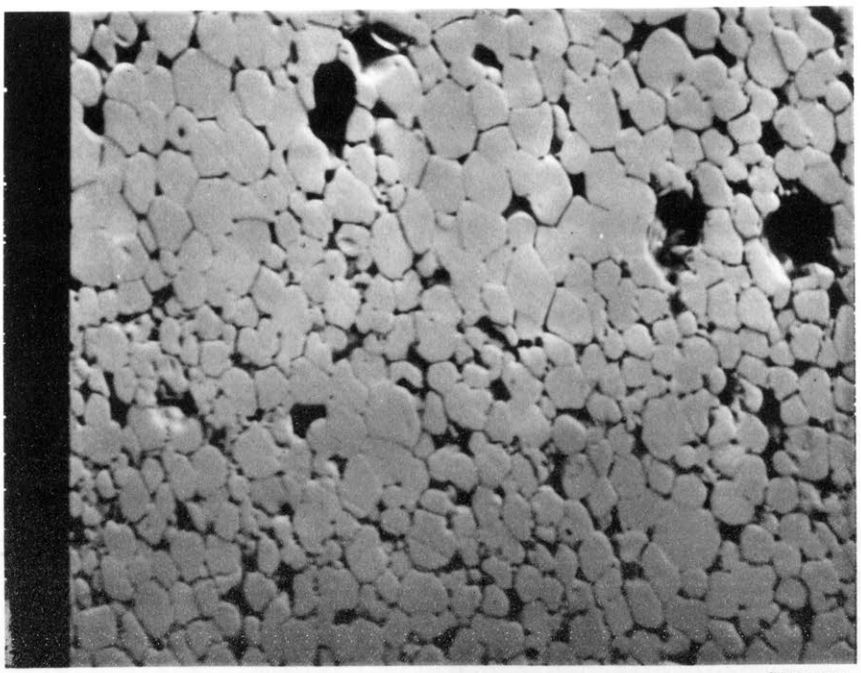

(A) 10 μ

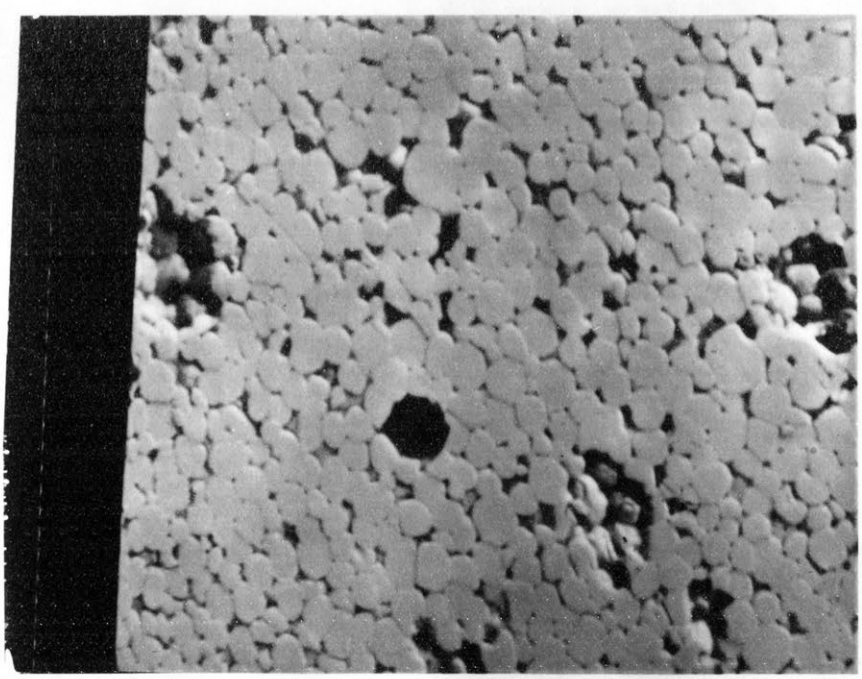

(B) 10 μ

Figure 8.52. Scanning Electron Micrographs of Etched Polished Sections

(A) Thoria Contaning Fission Products made from Ball Milled Powder
(B) Thoria containing Fission Products made from Precipitated Powders

milling produced fine powder but ball wear became significant and contamination occurred causing the fired specimen to bloat. The cause of the bloating was traced to bentonite which was used as a forming and densification aid in the zirconia balls. Thoria balls were therefore obtained from the Atomic Energy Commission for use as grinding media. As well as ball milling the as received oxides, precipitation of the oxalates of the desired fissium was carried out. Powders of mixtures obtained in both ways are shown in Figure 8.51. From powders prepared in each way, pellets were pressed and fired to 1700°C for 72 hours. Figure 8.52 shows scanning micrographs of polished and etched samples. The appearance of the two microstructures is quite similar except the ball milled specimen appears to be more advanced in developing exaggerated grain growth.

Both of these samples were analyzed on the electron microprobe but no concentrations of fission products were detected. It was initially thought that the etching process had removed any second phases at the boundaries. When the sample was repolished and lightly etched areas high in ZrO_2 and Nd_2O_3 and in one case ZrO_2 and BaO were faintly detected. These phases were associated with grain boundaries. As mentioned previously, the low optical magnification of the probe made many of these analyses difficult and, as a result, area scans were used to detect the presence of elements. The low concentration of fissium in thoria, equivalent to ten per cent burn-up, and the possibility of fission product loss by vaporization during firing prompted the firing of simulated fuel elements in a sealed container and increasing the total concentration of fission products in fuel elements to be studied. The results of these changes are discussed in the following section.

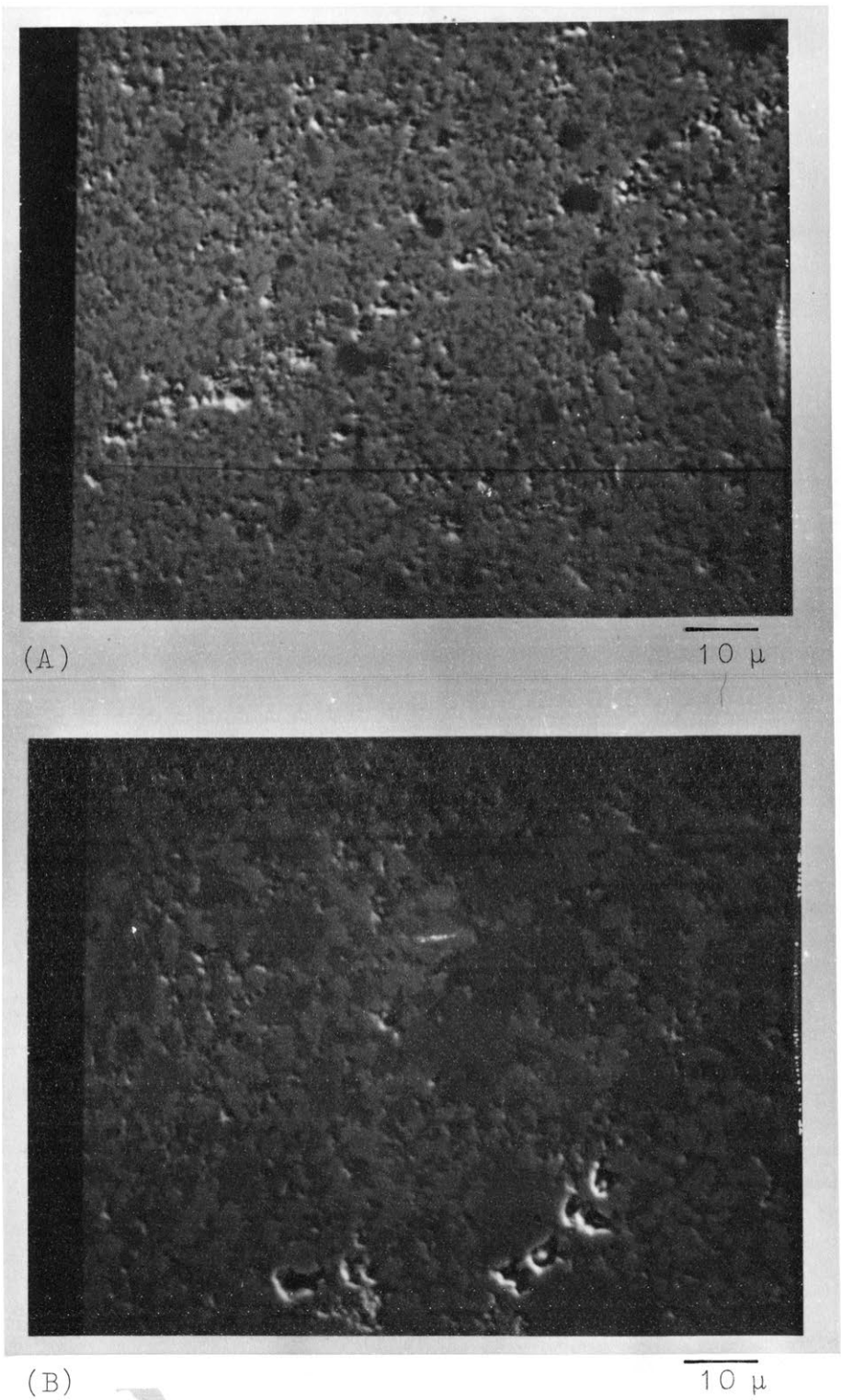

Figure 8.53. Scanning Electron Micrographs of a Polished Section of Thoria Containing Fission Products

(A) Molybdenum added as Dioxide

(B) Molybdenum added as Metal

8.4.3. The Effect of Sealing Simulated Fuel Elements During Firing

In reported experiments on simulated urania based fuels[56] the constituents were sealed in an iridium crucible and fired to 1750°C. Iridium is very difficult to work so thoria pellets containing 35 per cent by weight of fissium were initially sealed in platinum under a helium atmosphere. These samples were fired to 1700°C but, after 16 hours, the capsule had melted. The experiment was repeated using an alumina boat with a diamond ground top to effect a seal. Significant reaction had occurred after 16 hours and the lid had to be broken to remove it. Spectrographic analysis of the lid indicated the presence of Mo, Ba, Zr, Nd and Th.

In view of the extent of vapour phases apparently present at high temperatures which may affect the oxygen partial pressure about the fuel, the sealing experiment was repeated with the following modifications. First temperatures of 1460°C and 1600°C were used instead of 1700°C to prevent attack of the platinum capsule and, secondly, since it is known that the state of molybdenum in the fuel element may control the oxygen partial pressure, molybdenum was introduced as MoO_2 in one set of sealed samples and as Mo metal in the other. Figure 8.53 shows scanning micrographs of the samples after firing at 1460°C for 144 hours. Electron microprobe area scans were conducted for fissium for both samples for all elements which showed detectable levels. The results of scans are shown in Figures 8.54 and 8.55. Although the patterns are fairly weak, it could be concluded that the sample containing molybdenum in the form of the dioxide was composed of

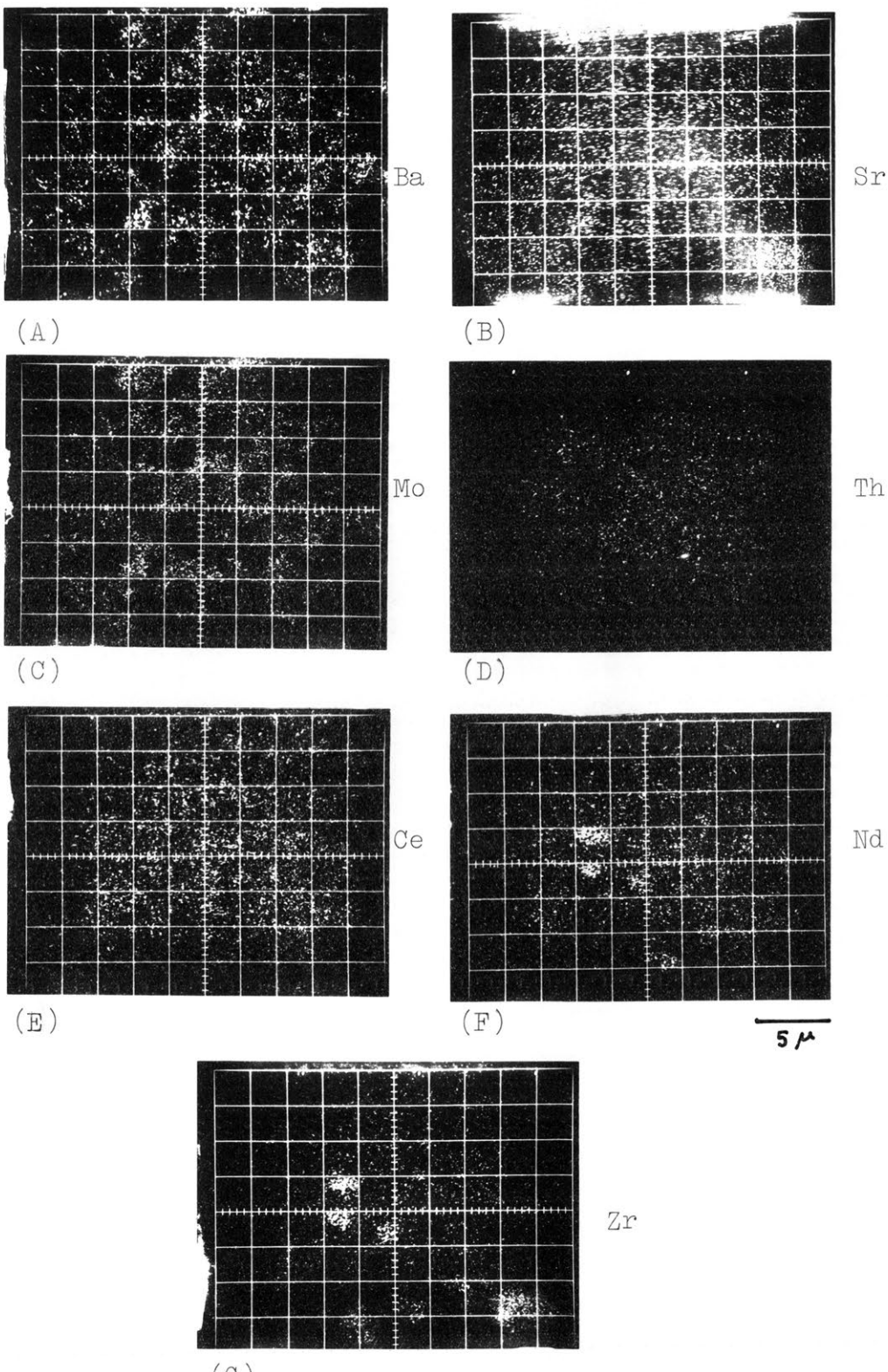

Figure 8.54. Microprobe Area Scans for Elements in Thoria Sample Containing MoO_2

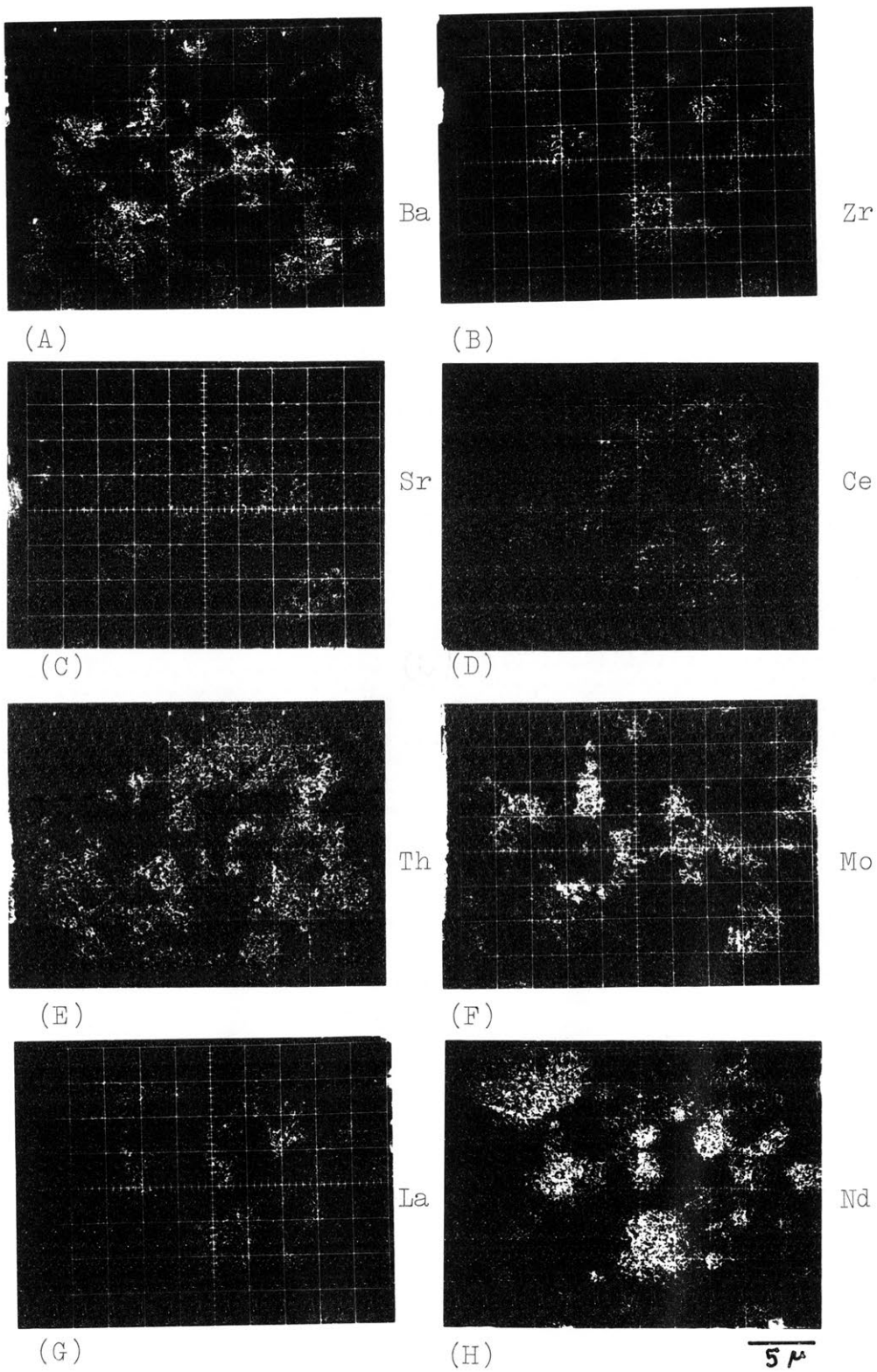

Figure 8.55. Microprobe Area Scan for Elements in Thoria Sample Containing Mo Metal

a thoria matrix containing large amounts of Ce along with smaller concentrations of Zr, Nd, Ba and Mo. The concentrations of Y and La were too low to be detected. The five elements which were associated with thoria were not uniformly distributed. Within the thoria matrix, Nd was found in conjunction with Ce, whereas Ba and Mo occurred where Ce was absent. Zr appeared to be uniformly dispersed at low concentrations. There were inclusions which appeared to contain no Th or Ce. One type contained Ba, Mo and Sr, another Zr, Sr and Ba and yet another consisted mainly of Zr and Nd. The first types probably have, as constituents, $SrMoO_4$ and $BaMoO_4$ or mixtures thereof. The inclusion containing Zr and Nd is probably a solid solution of the type $Zr_2Nd_2O_4$. This confirms findings made in the reaction couple and composite mixtures discussed previously.

The sample which contained Mo metal and no MoO_2 was markedly different from the previous sample in several ways. There was some Ce and Nd in the Th matrix but to a lesser extent. Ba and Mo were not found in the matrix as in the previous sample. Ba, Mo and Sr, as in the former case, formed one type of inclusion while Zr and Nd formed the other type. Along with Zr and Nd were La and Ce. No zirconates of Ba or Sr were found. The greatest difference between the two samples has been the placement of Ce which has been substantially removed from the thoria matrix. This is probably due to its being reduced from the +4 state to the +3 state by the influence of Mo metal. In neither of these samples were metallic inclusions found. When attempts were made to fire specimens to 1600°C, cladding failure occurred similar to that previously mentioned. These findings seem consistent with work previously cited in the couple work and reaction compact work.

That metallic inclusions were not seen does not mean necessarily that metallic components did not exist but that the temperature may not have been sufficient to allow large metallic inclusions to form.

8.4.4. Effect of a Thermal Gradient on a Simulated Fuel Element

Information about compatible phases which exist between thoria and typical solid fission products have been obtained under a variety of atmospheric conditions by analyzing simulated thoria fuel elements which have been held at temperatures for long periods of time. Information regarding the effect of a thermal gradient on the production of these second phases would complete the objective of this study. Several attempts to develop a thermal gradient in thoria specimen were made in order to simulate the temperature profile of a real fuel element. Direct flame impingement was first attempted, then induction heating and, finally, direct electrical heating by means of a current controlling power circuit. The electrical heating method was considered excellent in that the natural tendency was to produce higher internal temperatures than external temperatures on the conducting element which is exactly the condition found in a nuclear reactor fuel element. Freund and Sari[58] had success at developing high thermal gradients and, after only three hours, observed columnar grains. Metallic inclusions of Mo were found and barium and cerium were found to migrate to the grain boundaries. The original device used in this work consisted of a silicon carbide electrode directly sealed on to the doped thoria sample. D.C. current was controlled to four amps. These electrodes proved unsatisfactory and were replaced first by stainless steel and finally by tungsten. The D.C. power supply was replaced by an A.C. current controlling circuit previously

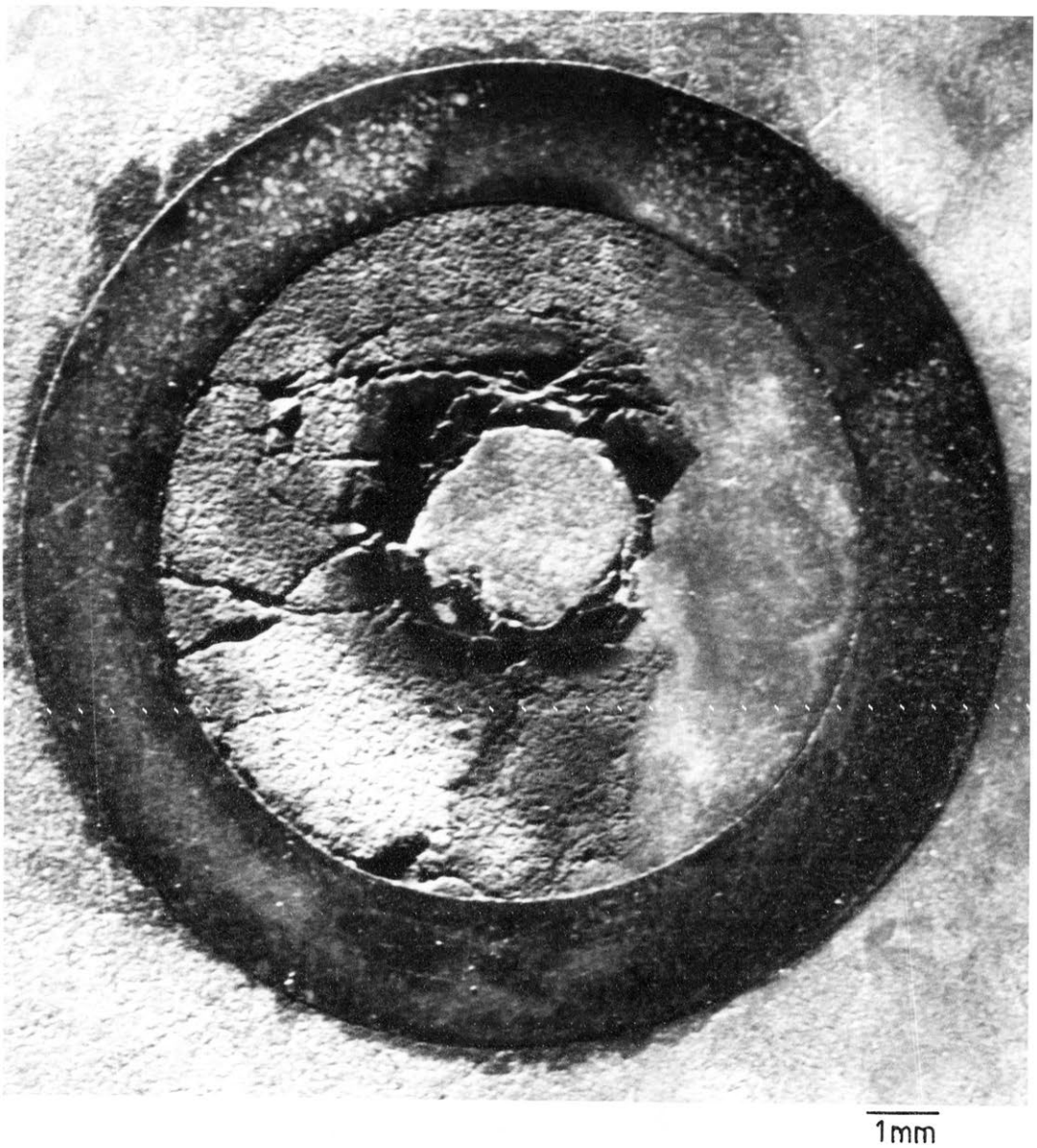

Figure 8.56. Polished Section of Cladded Sample of Thoria Containing Fission Products which was subjected to a Thermal Gradient

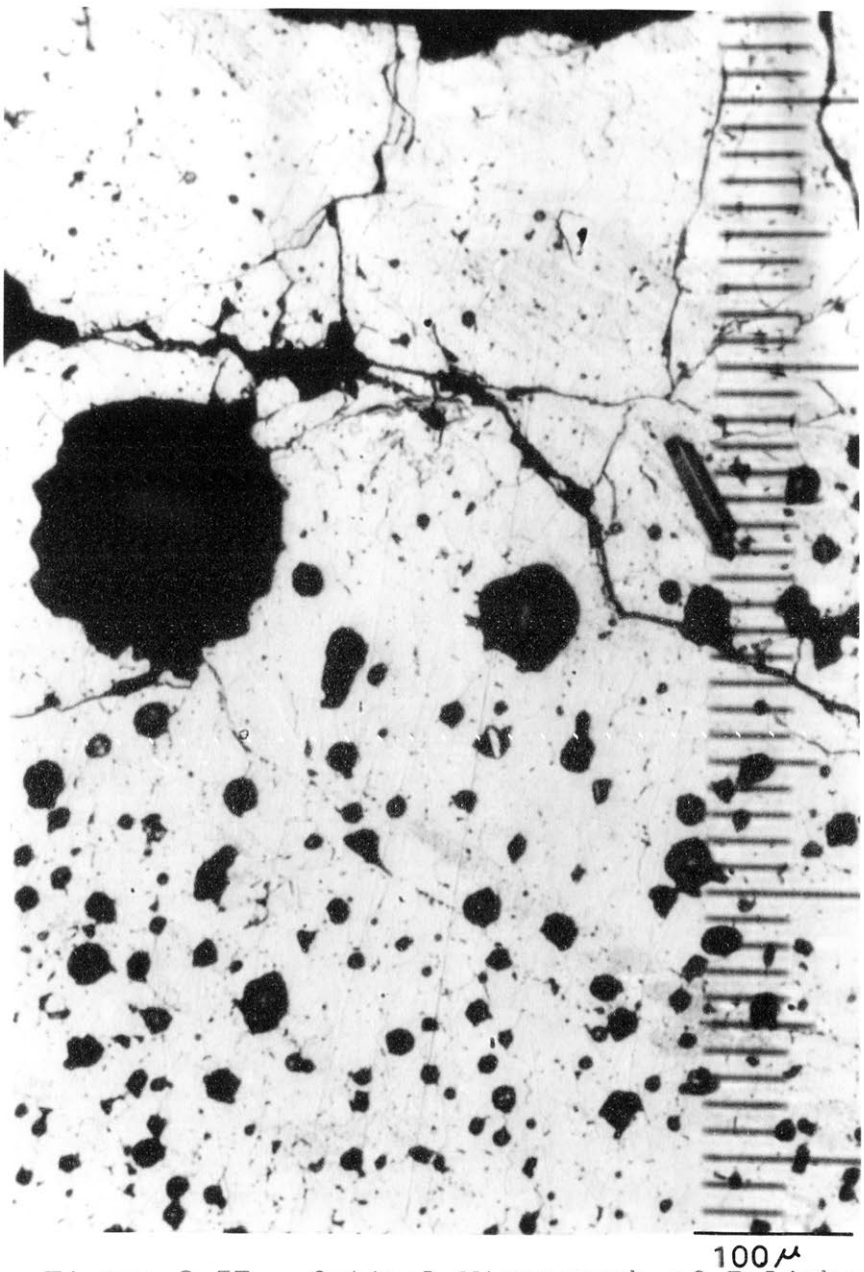

Figure 8.57. Optical Micrograph of Polished Section of Thermal Gradient Specimen

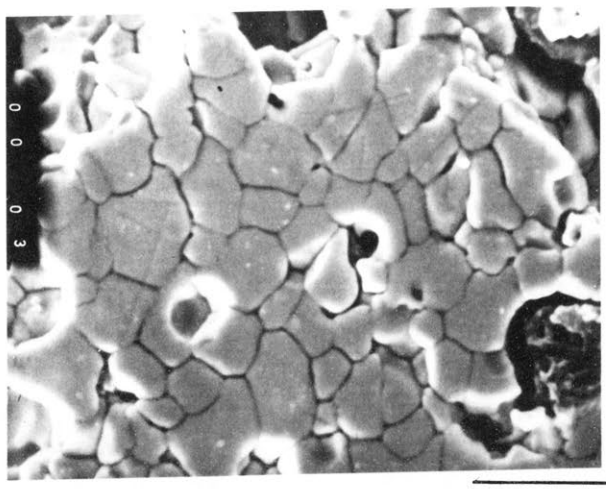

(A) 10 μ

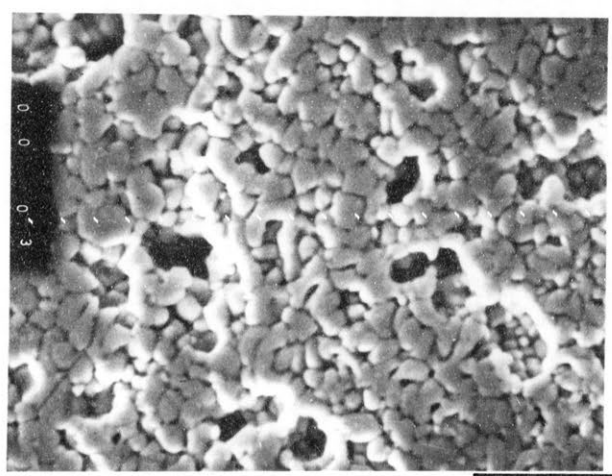

(B) 10 μ

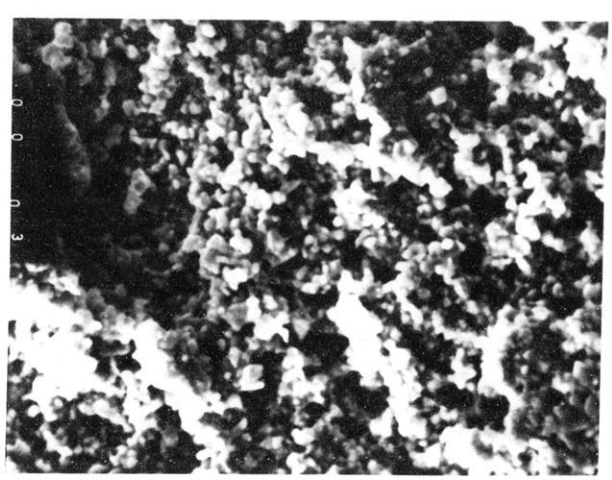

(C) 10 μ

Figure 8.58. Scanning Electron Micrograph of Etched Polished Section of Thermal Gradient Specimen
(A) Area Adjacent to Central Void
(B) Equated Grain Region
(C) Unaffected Region

described which proved more satisfactory. Samples of length one cm were held at three amps for three hours. A photograph of the polished sample is shown in Figure 8.56. This polished section was etched in boiling phosphoric acid and analyzed under the optical and scanning electron microscopes shown in Figures 8.57 and 8.58. Three distinct zones were observed on the surface of the pellet. The area immediately adjacent to the central void shown in Figure 8.58 was characterized by large grains which had begun to undergo exaggerated grain growth. The second region shows equiaxed grains and the final region shows the unaffected area. No columnar grains were observed on any of the runs which were made. No inclusions were observed under either optical microscopy nor under the scanner. The sample was carbon coated and analyzed under the electron microprobe. No inclusions were found nor were any areas enriched in any of the fission products found after exposures up to twenty minutes in duration. High temperatures were reached as shown by the fact that centre core melting had occurred. No columnar grain growth was observed; however this may be due to the shortness of time of the run. Potter and Elyard[95] have shown that under a thermal gradient at 1800°C columnar grains were formed in twenty-five hours and at 2200°C in eight hours. While, in this work, runs only lasted three hours some indication of columnar grains should have been seen. Freund and Sari[58] who heated a urania specimen electrically found columnar grain developing within three hours. The consequences of this observation are that either columnar grains do not develop in pure thoria or that thoria requires much longer times to develop the structure. If columnar grains do not develop in pure thoria, this indicates that the mechanism of columnar grain formation involves the vaporization

condensation mechanism of UO_3 similar to that suggested by MacEwan and Lawson[47] rather than the diffusion mechanism suggested by Potter and Elyard[95]. The absence of observable or detectable inclusions in any of the samples analyzed was disappointing. Either greater times are required to produce inclusions of sufficient size to be detected or the solubility of fissium in thoria is high enough to prevent inclusions from being developed. The former explanation is probably the correct one.

CHAPTER IX

GENERAL DISCUSSION, CONCLUSIONS AND SUGGESTIONS FOR FUTURE WORK

9. General Discussion

The aims of this work were: (1) to establish a technique for simulating a thoria based fuel element after high burn-up in a conceptual heavy water moderated thermal reactor enriched with 2 per cent $U^{233}O_2$, and (2) to determine the effect that solid fission products have on the fuel element after a simulated high burn-up.

Several techniques were employed to this end which involved isothermal heating of compacts containing thoria and fission products under sealed and unsealed conditions, and non-isothermal heating of compacts containing thoria and fission products under high thermal gradients.

Under the former conditions of heating, information about phases which develop between thoria and the solid fission products was obtained. Stable mixed oxide phases were found to depend upon the atmosphere above the reacting chemical species. As has been noted in the case of urania based fuels which have been analyzed after irradiation, the non-metallic phase almost always found in thoria compacts containing fission products was barium-zirconate. Contrary, however, to studies on urania systems, synthetic pyrochlores of the type $Nd_2Zr_2O_7$ appeared to be readily developed in the thoria based systems; and metallic phases were not observed. The latter discovery was not surprising in that

concentrations of metallic components in the compacts were low and the isothermal temperatures used were too low to expect significant alloying of the metal additions. The main effect of atmosphere on the thoria compacts studied in this work was to rearrange variable valency oxides, notably ceria, which appears to take on a lower oxidation state under reducing conditions and in so doing, forms in new phases compatible with its lower valency state.

Under the condition of high thermal gradient heating, physical changes in the thoria-fission product oxide compacts were noted which were similar, with one exception, to microstructural changes observed in urania fuel elements after irradiation. None of the thoria compacts studied showed the columnar grain growth which is common to all irradiated urania fuel elements in the vicinity of the central core. The lack of columnar grain growth may have been due to the absence of a urania phase, which is known to produce volatile $UO_3(g)$. This gaseous product is considered to contribute to the formation of columnar grain growth if not to cause the grain growth. Fuels containing thoria are known to have lower gas release than urania-plutonia fuels and this gas release is often related to the development of columnar grains. This would seem to suggest that addition of thoria inhibits columnar grain growth and in the limiting case, of 100 per cent thoria, prevents the formation of columnar grain growth, which is consistent with the findings in this work.

Compacts subjected to the thermal gradient were analyzed for included phases, however, none were detected, which resulted most probably from the shortness of the heating time compared to the time of duration for the isothermal heating.

Binary systems of thoria and typical fission product oxides studied in this work have shown that thoria has an ability to accommodate a large quantity of foreign cations in the fluorite lattice. All of the oxides investigated in this work formed solid solutions with thoria, surprisingly even baria and strontia. The result of this tendency for thoria to form solid solutions with oxides whose cations are lower in valency than thoria is to produce anion vacancies. Furthermore if the assumption is made that the thoria binary systems form ionic conductors as is known for ThO_2-Y_2O_3 solid electrolytes, then the increased production of anion vacancies should provide an increased number of charge carriers for conduction.

Electrical conductivity measurements of the binaries studied showed that, in all cases, the conductivity was markedly affected by the oxygen partial pressure. The most noteworthy system studied was the thoria neodymia system which showed detectable oxygen dependence at temperatures as low as 260°C. The thoria system containing baria showed much lower conductivity than would be expected assuming that the conductivity was solely dependent upon the numbers of defects; however, the mobility of the defects also contributes to the conduction and in the case of the baria-thoria solid solution the mobility of the defects must be low. This fact may give some insight to the as yet unsettled question regarding the means by which calcia is able to enhance the densification of thoria compacts.

It is known that the grain structure of thoria compacts containing strontia and baria is uniform with no sign of exaggerated grain growth even after 16 hours. Furthermore the

grains are relatively small and extremely uniform in shape. The mobility of the defects in these systems is quite low as shown by electrical conductivity measurements which implies a low diffusion rate. The absence of a second phase as shown by the high solubility limit would tend to imply that the classical grain boundary pinning mechanism is not responsible for the enhanced densification as is suggested for thoria containing calcia. With these points in mind it is suggested that the major contributing factor to the densification observed in thoria compacts containing baria and strontia was the Hedvall effect due to the high temperature decomposition of the barium and strontium carbonates. Upon decomposition the reaction between strontia and thoria would proceed at a very rapid rate with simultaneous formation of many small crystal nuclei. Since the diffusion rate within the newly formed solid solution is slow again based on electrical conductivity, no exaggerated grain growth occurs and the crystal nuclei are allowed to grow at a rate such that defects diffuse to the grain boundary to be eliminated faster than the grains grow. In so doing the nucleated crystals grow uniformly and without producing included defects.

9.2. Suggestions for Future Work

There are areas of study which were raised in this investigation which could not be fully treated but deserve further consideration in future work dealing with simulation of thoria based fuel elements or with thoria compacts containing dissimilar oxide additions.

The two major investigations may be further subdivided into (i) a study involving the introduction of urania to the thoria-fusion product compacts, (ii) a study of the effect that prolonged heating under high thermal gradients has on the stable phases and microstructure formed in the simulated fuel element, (iii) the dependence of electrical conductivity on oxygen partial pressure, temperature and composition for thoria compacts containing +3 valent oxide additions, and (iv) the ultimate solubility limit of divalent oxides such as baria and strontia.

The purpose of the first two studies would be to determine how urania affects the stable phases which have been shown to develop between thoria and typical fission product oxides and whether or not the formation of columnar grains is caused by the co-existence of urania with thoria or is simply a function of the time during which the thermal gradient is maintained. The purpose of the last two studies is to investigate the obviously interesting electrical conduction and structural properties of thoria systems containing foreign oxides, especially systems containing neodymia and strontia.

9.3. Conclusions

It is felt that generally the aims of this thesis have been achieved. While several techniques were required to provide information about the physical and chemical effects of fission products on a thoria based fuel, it is felt that a unique simulation is possible with additional work as suggested in the previous section. The major conclusions from this work may be summarized by the following points:

1. Thoria is an extremely stable oxide and is capable of accommodating large quantities of di-, tri- and tetra valent cations in its fluorite structure.

2. Stable phases which develop between fission product oxides at high concentrations in the thoria matrix are barium zirconate, which is similarly found in urania, and pyrochlore phases of the $Nd_2Zr_2O_7$, type which have not been reported in systems with urania. Thoria phases similar to the barium uranate reported to occur in systems containing urania and some fission product oxides were not found.

3. Microstructures of thoria compacts containing typical fission product oxides which underwent high thermal gradients, were similar to microstructures of urania fuel elements which had undergone irradiation except that columnar grain growth did not occur.

4. Additions to thoria of foreign oxides of lower valency produced an oxygen deficient fluorite structure and compacts so formed have electrical conductivity dependent upon oxygen partial pressure.

Since defects are known to exist in these systems, greater diffusion is expected with increased defect concentrations which in turn should enhance densification if the diffusion mechanism for densification as proposed by Laha[28] is dominant. Some compacts containing +3 valent oxides did not enhance the density of thoria while the addition of +3 neodymia did. The conductivity

results would support the diffusion model for densification; however, in the case of baria additions the mobility, hence the implied diffusion, for defects is low this would refute the diffusion model. The explanation that the Hedvall effect was a major contributor to the increased densification of thoria compacts containing baria and strontia seems reasonable. Also if in the work of Laha[28] and Jorgensen,[29] the calcia added to thoria had been exposed to atmospheric CO_2, calcium carbonate could have formed giving rise to a third possible explanation for the enhanced densification similar to that for compacts containing baria and strontia.

BIBLIOGRAPHY

1. Olsen, A.R. et al., Properties and Prospects of Thoria-Based Nuclear Fuels, Proc. Brit. Ceram. Soc., Nuclear and Engineering Ceramics, Vol. 7, pp. 289-310 (1967).

2. Williams, J., Characteristics and Preparation of Ceramic Powders, Proc. Brit. Ceram. Soc., 3, 1 (1965).

3. Livey, D.T. et al., The Properties of MgO Powders Prepared by the Decomposition of $Mg(OH)_2$, Trans. Brit. Ceram. Soc. 56, 217 (1957).

4. Moorthy, V.K. et al., Relation between the Origin, Powder Characteristics and Sintering Treatments on the Densification and Microstructures of Compacts of Urania and Thoria. Proceedings of the 3rd United Nations International Conference on the Peaceful Uses of Atomic Energy, May 1964.

5. Moorehead, D.R., The Preparation and Sintering Behaviour of Thorium Oxide. Ph.D. Thesis, University of New South Wales, Sydney, Australia, 1971.

6. Leigh , H.D., and McCartney, E.R., Redetermination of Lattice Parameter of ThO_2, J. Am. Ceram. Soc., 57, 4 (1974).

7. Kurnakova, A.G., Shubochkin, L.K., Solubility of $Th(C_2O_4)_2 \cdot 6H_2O$ in Aqueous HNO_3 and $H_2C_2O_4$ at 25°C, Russian J. Inorg. Chemistry, 8, 5, 647 (1963).

8. D'Eye, R.M.W., and Sellman, P.G., The Thermal Decomposition of Thorium Oxalate, J. Inorg. Nucl. Chem., 1, 143-148 (1955).

9. Kinoshita, H., Aoki, S., Takagi, A., and Kobayashi, Y., Fabrication of Thorium Oxide Fuel Element (1) Thermal Decomposition of Thorium Oxalate and Particle Size Growth of Thorium Oxide by Heating, Fapig Tokyo, 30, 378-383 (1964).

10. Jenkins. I.L., Moore, F.H., and Waterman, M.J., X-ray Powder Crystallographic Data on Plutonium and other Oxalates - II. J. Inorg. Nucl. Chem., 27, 81-87 (1965).

11. Srivastava, O.K., and Vasudeva Murthy, A.R., Thermal Decomposition of Oxalates of Lantanthanum and Thorium in Vacuum, J. Indian Inst. Sci., 47, (3), 87 (1965).

12. Bussiere, P., Claudel, B., Renough, P., Trambouze, Y., Prettre, M., Etude des Phase Solides, J. Chim. Physic., 58, 668 (1961).

13. Allred, V.D., Buxton, S.R., and McBride, J.P., Characteristic Properties of Thorium Oxide Particles, J. Phys. Chem., 61, 117 (1957).

14. Beckett, R. and Winfield, M.E., The Thermal Decomposition of Thorium Oxalate, Aust. J. Sci. Res. A., 4, (4), 644 (1951).

15. Warren, D., and Elyard, C.A., The Properties and Sintering Behaviour of Thorium Oxide Produced by Calcination of Thorium Oxalate, Special Ceramics (4), Ed. Popper, P., 57 (1968).

16. Moorthly, U.K., Exwara Prasad, G., and Kulkarni, A.K., Sintering of Thoria Powders. Part IV. Development of Crystallinity in Thoria Powders During Heating and its Influence on their Sintering Behaviour, Trans. Indian Ceram. Soc., 24, (4), 103 (1965).

17. McCorkle, K., Surface Chemistry and Viscosity of Thoria Sols, Thesis, University of Tennessee, July, 1966.

18. Kuczynski, G.C., Self Diffusion in Sintering Metallic Particles, Trans. AIMME, 185, 169 (1949).

19. Kingery, W.D. and Berg, M., Study of Initial Stage of Sintering Solids by Viscous Flow, J. Ap. Chem. Phys., 26, 1205 (1955).

20. Nichols, R.A., and Mullins, W.W., Morphology Changes of a Surface of Revolution due to Capillarity-induced Surface Diffusion, J. Ap. Phys., 36, (6), 1826 (1965).

21. Alexander, B.H., Balluffi, R.W., Mechanisms of Sintering of Copper, Acta. Met., 5, (11), 666-677 (1957).

22. Coble, R.L., Sintering Crystalline Solids: I and II, J. Ap. Phys., 32, (5), 787-799 (1961).

23. Burke, J.E., Role of Grain Boundaries in Sintering, J. Am. Ceram. Soc., 40, (3), 80-85, (1957).

24. Westbrook, J.H., Analysis of the Nature of Grain Boundaries Part I. Ceramic Microstructures; Their Analysis, Significance and Production. Proceedings of the Third International Materials Symposium. Ed. Fulrath, R.M. and Pask, J.A., 231-251 (1968).

25. Burke, J.E., Grain Growth, Part III. Ceramic Microstructures their Analysis Significance and Production. Proceedings of the Third International Materials Symposium, Fulrath R.M., and Pask, J.A., Ed., 681-700 (1968).

26. Coble, R.L., Burke, J.E., Sintering in Ceramics, Prog. Ceram. Sci., 3, 199-249 (1963).

27. Jorgensen, P.J., Modification of Sintering Kinetics by Solute Segregation in Al_2O_3, J. Am. Ceram. Soc., 48, 4, 207-210 (1965).

28. Laha, S.N. and Das, A.R., Isothermal Grain Growth and Sintering in Pure ThO_2-CaO Composition, J. Nucl. Matl., 39, 285-291 (1971).

29. Jorgensen, P.J., and Schmidt, W.G., Final Stage Sintering of ThO_2, J. Am. Ceram. Soc., 53, 1, 24-27 (1970).

30. Bennett, C.E.G., et al., Sintering in Gas Discharges, Nature, 217, 1267-1268 (1968).

31. Im, S.J., Wadsworth, M.E., Shrinkage Measurements of ThO_2 Compacts Containing Added Impurities, O.R.N.L. Report XXXII. (Jan 31 1967).

32. Graham, M.J., Caplan, D., Detection of CO_2 in Cavities in NiO Scale, J. Electro-Chem. Soc., 120, (6), 769-70 (1973).

33. Gallagher, P.K. et al., Thermal Characterization of Iron Oxide Films, Themo Chimica Acta, 8, 141-148 (1974).

34. Thompson, M.A., The Sintering and Electrical Conductivity of 12 mole percent Y_2O_3-ZrO_2. Thesis, University of New South Wales, Sydney, 1973.

35. Fox, A.C., Jackson, E.E., Junkinson, A.R., Wait, E., X-ray Studies of Radiation Damage in Fissile Materials. Part II. Uranium Dioxide, U.K. Report AERE R4267 (1963).

36. Roberts, L.E.J., Brock,P., Findlay, J.R., Frost, B.R.T., Russell, L.E., Sayer, J.B. and Wait, E., The Behaviour of UO_2 and of $(U,Pu)O_2$ Fuel Materials Under Irradiation, 3rd ICPUEA P/155 United Nations (1964).

37. Berman, R.M., Bleiberg, M.L., and Yeniscovich, W., Fission Fragment Damage to Crystal Structures, J. Nucl. Matl., 2, 2, 129 (1960).

38. Bleiberg, M.L., Berman, R.M., and Lustman, B., Effects of High Burnup on Oxide Ceramic Fuels. Radiation Damage in Reactor Materials, 319, IAEA, Vienna (1962).

39. Bates, J.L., Christensen, J.A., and Daniel, J.L., Irradiation Effects in Uranium Dioxide Single Crystals, U.S. Report HW-73959, (1962).

40. Olsen, A.R., Douglas, D.A.,Hiesose, Y., Scott, J.L., Ullmann, J.W., Properties and Prospect of Thoria-based Nuclear Fuels, Proc. Brit. Ceram. Soc. Nucl. Eng. Ceram. 7, 289-310 (1967).

41. Ross, A.M., The Dependence of the Thermal Conductivity of UO_2 on Density, Microstructure Stoichiometry and Thermal Neutron Radiation, Canadian Report AECL-1096 (1960).

42. Bradbury, B.T., Demant, J.T. and Martin, P.M., Solid Fission-products in Irradiated Uranium Dioxide, Proc. Brit. Ceram. Soc. Nucl. Eng. Ceram., 7, 311-329 (1967).

43. Frost, B.R.T. and Wait, E., Irradiation Experiments on Plutonium Fuels for Fast Reactors, Symposium on the use of Pu as a Reactor Fuel, 469-490 (1962).

44. Bain, A.S., Cracking and Bulk Movement in Irradiated Uranium Oxide Fuel Elements. Canadian Report AECL-1827 (1963).

45. de Halas, D.R. and Horn, G.R., Evolution of Uranium Dioxide Structure During Irradiation of Fuel Rods, J. Nucl. Matl., 8, 2, 207 (1963).

46. O'Boyle, D.R., Brown, F.L., Sanecki, J.E., Solid Fission Product Behavior in Uranium-Plutonium Oxide Fuel Irradiated in a Fast Neutron Flux, J. Nucl. Matl., 29, 27-49 (1969).

47. MacEwan, J.R. and Lawson, V.B., Grain Growth in Sintered Uranium Dioxide: II Columnar Grain Growth, J. Am. Ceram. Soc., 45, 1, 42 (1962).

48. Robertson, J.A.L., Bain, A.S., Booth, A.H., Howieson, J., Morrison, W.G., and Robertson, R.E.S., Behaviour of Uranium Oxide as a Reactor Fuel, 2nd ICPUAE, 6, 655, United Nations (1958).

49. Rand, M.H. and Markin, T.L., Some Thermodynamic Aspects of $(U,Pu)O_2$ Solid Solutions and Their Use as Nuclear Fuels, Symposium on Thermodynamics of Nuclear Materials, p.637-650, Vienna, 1967.

50. Field, S.H., Leitz, F.J., McNelly, M.J., and Nelson, R.C., Apparent Boiling of Uranium Oxide in the Centre of a Fuel Pin During Transient Power Generation, Nucl. Sci. Eng., 14, 210 (1962).

51. Katcoff, S., Fission Product Yields from Neutron-Induced Fission, Nuclionics, 18, 11, 201 (1960).

52. Gemmell, W., Clancy, B., Reeve, K.D. Private Communication (1971).

53. Glassner, A., The Thermochemical Properties of Oxides, Fluorides and Chlorides to 2500°K, Argonne National Laboratories Report ANL-5750 (1965).

54. Jeffery, B.M., Microanalysis of Inclusions in Irradiated UO_2, J. Nucl. Matl., 22, 6, 33-40 (1967).

55. Cotton, F.A. and Wilkinson, G., Advanced Inorganic Chemistry, John Wiley and Sons, 1074 (1972).

56. Schmitz, F., Analysis of a Simulation of Irradiated $(U,Pu)O_2$, Ceramic Nuclear Fuels International Symposium, Kruger, O.L., Kaznoff, A.I., Ed., 32-37 (1969).

57. Koizumi, M., and Satoh, M., and Noro, K., Phase Study on Solid Fission Products Ba, Sr, and Zr in Oxide Fuel, J. Nucl. Matl., 51, 90-94 (1974).

58. Freund, D. and Sari, C., A New Simulation Method for Investigations of UO_2 Fuel in a Thermal Gradient Corresponding to Reactor Conditions, International Meeting, Kernforschungszentrum Karlsruhe, 28-30 (1971).

59. Hand ., J.H., Abernathy, L.L., and Bach, J.H., Thoria and Urania Bodies, Am. Ceram. Soc. Bull., 36, 3, 99-100 (1957).

60. Karkhanavala, M.D., Momin, A.C., The Formation of Urania-Thoria Solid Solutions, J. Nucl. Matl., 11, 1, 114-116 (1964).

61. Felton, F.J., Aitken, E.A., The Mechanism and Kinetics of the Formation of $UO_{2.90}.6YO_{1.5}$, J. Inorg. Nucl. Chem., 24, 35 (1962).

62. Anderson, J.S., Edgington, D.N., Roberts, L.E.J., Wait, E., The Oxides of Uranium, Part IV. The System UO_2-ThO_2-O, Chemical Society, 3324-3331 (1954).

63. Roberts, L.E.J., The Oxide of Uranium. Part V. The Chemisorption of Oxygen on UO_2 and on UO_2-ThO_2 Solid Solutions, Chemical Society, 3332-3339 (1954).

64. Duwez, P. and Loh, E., Phase Relationships in the System Zirconia-Thoria, J. Am. Ceram. Soc., 40, 9, 321-4 (1957).

65. Campbell, I.E., High Temperature Technology, John Wiley and Sons, New York (1957).

66. Keller, C., Berndt, U., Engerer, H., and Leitner, L., Phasengleichtgewichte in den Systemen Thoriumoxid-Lanthanidenoxide, J. Solid State Chem., 4, 453-465 (1972).

67. Subbarao, E.C., Sutter, P.H., Hrizo, J., Defect Structure and Electrical Conductivity of ThO_2- Y_2O_3 Solid Solutions, J. Am. Ceram. Soc., 48, 9, 443-446 (1965).

68. Narsy-Szabo, I., Muegyeterni. Kozlemenyek, 1, 30 (1947).

69. Coffeen, W.W., Ceramic and Dielectric Properties of the Stannates, J. Am. Ceram. Soc., 36, 207 (1953).

70. Smith, A.J. and Welch, A.J.E., Some Mixed Metal Oxides of Pervoskite Structure, Acta. Cryst. 13, 653-656 (1960).

71. Fava, J., Le Flem, G., Devalette, M., Rabardel, L., Coutures, J.P., Foex, M., Hagenmuller, P., Mise Au Point D'un Four de Haute Temperatures, Rev. Int. Hautes Temper. et Refract., 8, 305-310 (1971).

72. Hoffmann, A., Z. Phys. Chem., B 28, 65 (1935).

73. Phillips, B., and Chang, L.L.Y., Condensed-Phase Relations in the System Mo-O, Trans. Met. Soc. AIME, 233, 1433-36 (1965).

74. Trunov, V.K., and Kovba, L.M., X-ray Analysis of Thorium Tungstate and Molybdate, Vestn. Mosk. Univ., Ser. Khim., 18, 3, 60-63 (1963).

75. Maayer, P.De, Bruyne, R. De, and Brabers, M.J., Decomposition Temperature of $Th(WO_4)_2$, J. Am. Ceram. Soc., 55, 2, 113 (1972).

76. Spitsyn, V.I., Pokrovskii, A.N., Afonskii, N.S., Trunov, U.K., Study of the ThO_2-Y_2O_3-WO_3 System, Dokl. Akad. Nauk. SSSR, 188, 5, 1065-68 (1969).

77. Swanson, et al., Standard X-Ray Diffraction Powder Patterns, N.B.S. Circular, 539(V), (1955).

78. Foex, Traverse, and Coutures, Compt. Rend., 264C, 1837-40 (1967).

79. Mastromonaco et al, Ann. Chi. (Rome) 59, 465-87 (1969).

80. Padurow, and Schusterivs, Ber. Dent. Keram. Ges., 30, 251 (1953).

81. Casey, J.J. et al., Formation of $Ce_2O_3.2ZrO_2$ in the System $BaCl_2$-$CeCl_3$-$BaZrO_3$, J. Am. Chem. Soc., 77, 2187 (1955).

82. Duwez, P. and Odell, F., Phase Relationships in the System Zirconia-Ceria, J. Am. Ceram. Soc., 33, (9), 274-83 (1950).

83. McCarthy, G.J., and Grooden, C.E., Compound Formation in the System Sr-Mo-O, J. Inorg. Nucl. Chem., 35, 2669-72 (1973).

84. Baly, D., and Plieth, K., Z. Electrochem., 59, 545 (1955).

85. McCarthy, G.J., Divalent Europium Compounds in the System Eu-Mo-O and Eu-W-O, Mat. Res. Bull., 6, 31-40 (1971).

86. McCarthy, G.J. and Fischer, R.D., The System Eu-Fe-O: Compound Formation and its Implications for Systematic Crystal Chemistry, J. Solid State Chem., 4, 340-44 (1972).

87. McCarthy, G.J., Fischer, R.D., and Sanzgiri, J., Crystal Chemistry and Subsolidus Phase Relations in the System Eu-W-O, J. Solid State Chem., 5, 200-6, (1972).

88. Brixner, L.H., X-ray Study and Electrical Properties of the System $Ba_xSr_{(1-x)}MoO_3$, J. Inorg. Nucl. Chem., 14, 225-30 (1960).

89. Coughlin, J.P., Contributions to the Data on Theoretical Metallurgy, U.S. Bureau of Mines Bull, 542 (1951).

90. Kelley, K.K., Contribution to the Data on Theoretical Metallurgy, U.S. Bureau of Mines Bull, 383 (1935).

91. Claudel, B., Perrin, M., and Trambouge, Y., Influence des Produits de Decomposition sur la Thermicite des Reactions Observes por Analyse Thermique Differentielle, Comp. Rend., 252, 107 (1961).

92. Swanson, H.E. and Tatge, E., Standard X-ray Diffraction Powder Patterns, U.S. Nat. Bur. Stand. Cir., 539, (I), 95 (1953).

93. Fullam, H.T., and Mitchell, C.J., Hot Pressing of Rare Earth Oxides, BNWL Report 448 (1967).

94. Harada, Y., Baskin, Y., Handwerk, J.H., Calcination and Sintering Study of Thoria, J. Am. Ceram. Soc., 45, 6, 253-257 (1967).

95. Potter, T.J. and Elyard, C.A., Columnar Grain Growth in UO_2, Proc. Brit. Ceram. Soc., Nuclear and Engineering Ceramics, 7, 273-288 (1967).